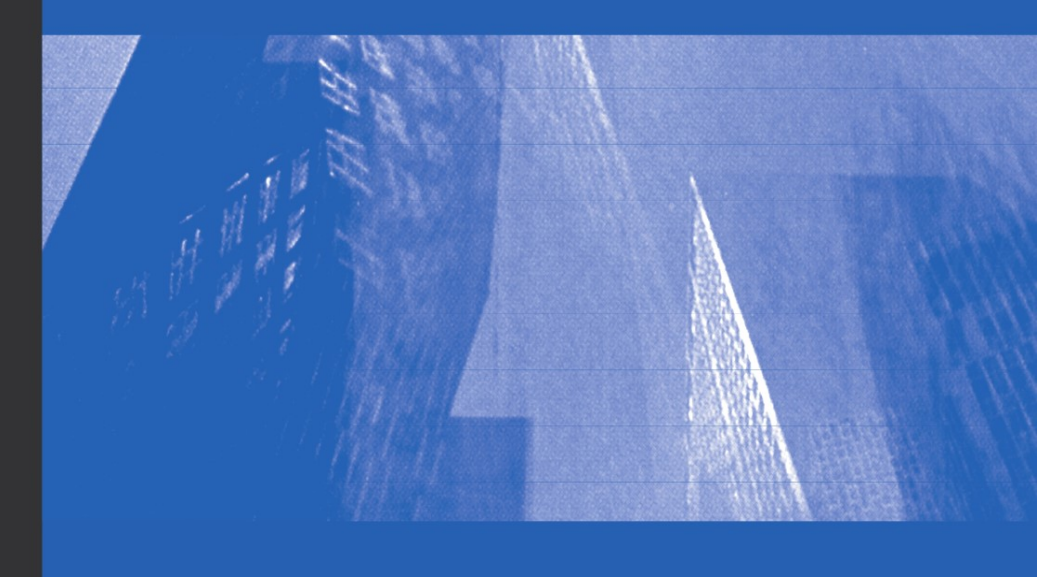


Smart Membrane Materials and Systems

From Flat Membranes to Microcapsule Membranes







ADVANCED TOPICS IN SCIENCE AND TECHNOLOGY IN CHINA

ADVANCED TOPICS IN SCIENCE AND TECHNOLOGY IN CHINA

Zhejiang University is one of the leading universities in China. In Advanced Topics in Science and Technology in China, Zhejiang University Press and Springer jointly publish monographs by Chinese scholars and professors, as well as invited authors and editors from abroad who are outstanding experts and scholars in their fields. This series will be of interest to researchers, lecturers, and graduate students alike.

Advanced Topics in Science and Technology in China aims to present the latest and most cutting-edge theories, techniques, and methodologies in various research areas in China. It covers all disciplines in the fields of natural science and technology, including but not limited to, computer science, materials science, life sciences, engineering, environmental sciences, mathematics, and physics.

Smart Membrane Materials and Systems

From Flat Membranes to Microcapsule Membranes

With 172 figures





Author
Prof. Liang-Yin Chu
School of Chemical Engineering
Sichuan University
Chengdu 610065, China
E-mail: chuly@scu.edu.cn

ISSN 1995-6819 e-ISSN 1995-6827 Advanced Topics in Science and Technology in China

ISBN 978-7-308-08089-7 Zhejiang University Press, Hangzhou

ISBN 978-3-642-18113-9 ISBN 978-3-642-18114-6 (eBook) Springer Heidelberg Dordrecht London New York

Library of Congress Control Number: 2011920973

© Zhejiang University Press, Hangzhou and Springer-Verlag Berlin Heidelberg 2011

This work is subject to copyright. All rights are reserved, whether the whole or part of the material is concerned, specifically the rights of translation, reprinting, reuse of illustrations, recitation, broadcasting, reproduction on microfilm or in any other way, and storage in data banks. Duplication of this publication or parts thereof is permitted only under the provisions of the German Copyright Law of September 9, 1965, in its current version, and permission for use must always be obtained from Springer. Violations are liable to prosecution under the German Copyright Law.

The use of general descriptive names, registered names, trademarks, etc. in this publication does not imply, even in the absence of a specific statement, that such names are exempt from the relevant protective laws and regulations and therefore free for general use.

Printed on acid-free paper

Springer is a part of Springer Science+Business Media (www.springer.com)

Preface

As emerging artificial biomimetic membranes, smart or intelligent membranes that are able to respond to environmental stimuli are attracting ever-increasing interest from various fields. Their surface characteristics and/or permeation properties including hydraulic permeability (pressure-driven convective flow of solvents) and diffusional permeability (concentration-driven molecular diffusion of solutes) can be dramatically controlled or adjusted self-regulatively in response to small chemical and/or physical stimuli in their environments, such as temperature, pH, ionic strength, electrical field, photo irradiation, glucose concentration, oxidoreduction and/or chemical or biological species. Such environmental stimuli-responsive smart membranes could find myriad applications in numerous fields ranging from controlled drug delivery, to chemical separation, to water treatment, to bioseparation, to chemical sensors, to chemical valves, to tissue engineering, etc. The development of these smart or intelligent membranes is of both scientific and technological interest.

The author has been devoted to the development of smart membrane materials and systems since 1999, when he was a research fellow in Prof. Shin-ichi Nakao's group at the Department of Chemical System Engineering at the University of Tokyo. He is currently a professor at Sichuan University where he leads the Membrane Science and Functional Materials Group (http://teacher.scu.edu.cn/ftp_teacher0/cly/) with a diverse and interdisciplinary focus on the development of new membranes for separation and systems for controlled release, especially smart membrane materials and systems. Since 1999, he has successfully developed various environmental stimuli-responsive smart membranes, including thermo-responsive, pH-responsive, glucose-responsive, molecular-recognizable and dual-/multi-stimuli-responsive ones, for different applications from controlled release, to chemical valves, affinity separation, chiral resolution, chemical sensors, etc.

This book is the first one that comprehensively and systematically introduces smart or intelligent membranes with environmental stimuli-responsive functions. The contents range from flat membranes to microcapsule membranes with various response properties, such as thermo-response, pH-response, glucose-response, molecular-recognition and dual-/multi-stimuli-response, and so on. Each chapter is independent, in which the design concept, fabrication strategy and methods,

microstructures and performance of smart membranes are clearly described. Lively schematic illustrations and pictures throughout the text help make the theory and technologies more accessible to readers. The author sincerely hopes that this book will be a valuable reference work for designing and fabricating artificial biomimetic smart membranes for various application purposes and for grasping the current status of smart membrane materials and systems.

The book is composed of 12 chapters. In Chapter 1, a brief introduction of smart or intelligent membranes as emerging artificial biomimetic membranes will be outlined. In Chapter 2, the emphasis is focused on the design, microstructures and performance of thermo-responsive gating membranes, because in many cases the environmental temperature fluctuations can occur naturally and the temperature stimuli can be easily designed and artificially controlled. The contents of this chapter on thermo-responsive gating membranes are also valuable for designing and fabricating other stimuli-responsive gating membranes. In Chapters 3 and 4, smart microcapsules with thermo-responsive gating membranes and with thermoresponsive hydrogel membranes are introduced respectively, which are designed for the purpose of controlled release. In Chapters 5 and 6, the contents are focused on developments of thermo-responsive membranes for chiral resolution and for affinity separation, respectively. In Chapter 7, pH-responsive gating membrane systems with pumping effects for improved controlled release performance are introduced. In Chapter 8, smart microcapsules with pH-responsive hydrogel membranes, which are promising for pH-responsive controlled release, are introduced. In Chapters 9 and 10, the contents are focused on glucose-responsive and molecular-recognizable smart membranes, which have high potential in applications in glucose-responsive self-regulated insulin delivery for diabetes therapy and in specific site-targeted drug delivery and/or chemical sensors. In Chapter 11, dual-/multi-stimuli-responsive smart membranes, which are preferable for more comprehensive systems, are introduced. Finally, perspectives on the development of smart membrane materials and systems are given in Chapter 12.

Most of the contents in this book are the fresh achievements of the author's group on smart membranes since the beginning of this new century. The author gratefully acknowledges financial support for the continuous study of smart membranes from the National Natural Science Foundation of China for Distinguished Young Scholars (Grant No. 20825622), the National Basic Research Program of China (Grant No. 2009CB623407), the National Natural Science Foundation of China (Grant No. 20206019, 50373029, 20674054, 20990220, 21076127), the NSFC-KOSEF Scientific Cooperation Program (Grant Nos. 20511140501), the "Chang Jiang Scholars Program" of the Ministry of Education of China for Distinguished Professors, Sichuan Youth Science and Technology Foundation for Distinguished Young Scholars (Grant Nos. 03ZQ026-41, 08ZO026-042), the Key Project of the Ministry of Education of China (Grant Nos. 106131), the Specialized Research Fund for the Doctoral Program of Higher Education of the Ministry of Education of China (Grant Nos. 20040610042, 200806100038), the Fok Ying Tung Education Foundation (Grant No. 91070), the Scientific and Technological Creation and Innovation Foundation of Sichuan

University (Grant No. 2004CF06), the Trans-Century Training Programme Foundation for Talented Scientists of the Ministry of Education of China (Grant No. 2002-48) and the Scientific Research Foundation for Returned Overseas Chinese Scholars of the Ministry of Education of China (Grant No. 2002-247).

The author is very grateful to Profs. Shin-ichi Nakao and Takeo Yamaguchi at the University of Tokyo in Japan, Profs. Wenmei Chen and Jiahua Zhu at Sichuan University in China and Prof. David A. Weitz at Harvard University in USA, who helped the author carry out investigations in the field of smart membranes. The author would like to thank all his former and current students who contributed to the study on smart membranes, especially Dr. Rui Xie, Dr. Xiaojie Ju, Dr. Yan Li, Dr. Mei Yang, Dr. Pengfei Li, Dr. Tao Meng, Dr. Jianbo Qu, Dr. Haidong Wang, Dr. Changjing Cheng, Wei Wang, Li Liu, Yongchao Chen, Lin Hu, Yijian Liang, Wenchuan Yang, Jianping Yang, Shibo Zhang, Jiyun Wang, Yao Jin, Shuowei Pi, Yalan Yu, Chuanlin Mu, Zhuang Liu, Nannan Deng, Lili Yue, and Jie Wei, for their hard work and creative research on developing smart membrane materials and systems.

Finally, the author is deeply indebted to his family members, especially his wife, Jianjun Qin and his son, Dikai Chu, for their love, encouragement and support.

Liang-Yin Chu Chengdu, China September, 2010

Contents

1	Intr	Introduction1				
	1.1	A Gla	nce at Membranes and Their Developments	. 1		
	1.2	2 Environmental Stimuli-Responsive Gating Model of Biomembranes				
1.3 Environmental Stimuli-			onmental Stimuli-Responsive Smart Materials	.3		
		1.3.1	Thermo-Responsive Smart Materials	.4		
		1.3.2	pH-Responsive Smart Materials	.6		
		1.3.3	Glucose-Responsive Smart Materials	.8		
		1.3.4	Molecular-Recognizable Smart Materials	.9		
	1.4	Bio-In	nspired Design of Environmental Stimuli-Responsive Smart			
		Memb	pranes	3		
		1.4.1	Smart Membranes with Porous Substrates and			
			Stimuli-Responsive Gates	3		
		1.4.2	Smart Membranes with Grafted Stimuli-Responsive Surfaces			
			1	5		
		1.4.3	Stimuli-Responsive Smart Hydrogel Membranes	5		
	Refe	erences.	1	6		
2	Thousand Desponsive Cating Mambuaness Design Misus to the state of					
2		Thermo-Responsive Gating Membranes: Design, Microstructures and Performances				
	Peri	ormano	:es	.9		
	2.1	Design	n of Thermo-Responsive Gating Membranes	9		
	2.2	Formation and Microstructures of Grafted PNIPAM Polymers in				
	Pore-Filling Type Thermo-Responsive Gating Membranes					
		2.2.1	Pore-Filling Type Thermo-Responsive Gating Membranes			
			Fabricated by Plasma-Induced Grafting Polymerization	21		
		2.2.2	Pore-Filling Type Thermo-Responsive Gating Membranes			
			Fabricated by Atom-Transfer Radical Polymerization	27		
	2.3	Effect	of the Grafting Yield on Thermo-Responsive Gating			
		Chara	cteristics of Pore-Filling Type PNIPAM-Grafted Membranes 3	34		

		2.3.1	Substrate Membranes with Regular Straight Pore		
			Microstructures	34	
		2.3.2	Substrate Membranes with Irregular Pore Microstructures	. 38	
	2.4	Effect	of the Length and Density of Grafted Chains on		
		Therm	no-Responsive Gating Characteristics of		
		PNIPA	AM-Grafted Gating Membranes	. 50	
	2.5	Gating	g Characteristics of Thermo-Responsive Membranes with Graft	ed	
		Linear	and Crosslinked PNIPAM Gates	. 52	
	2.6	Therm	no-Responsive Wettability Characteristics of PNIPAM-Grafted		
		Memb	oranes	60	
	2.7	Therm	no-Responsive Gating Membranes with Controllable Response		
		Tempe	erature	61	
	2.8		oranes with Negatively Thermo-Responsive Gating		
		Chara	cteristics	62	
	Refe	rences.		65	
3	Sma	rt Micr	ocapsules with Thermo-Responsive Gating Membranes	. 69	
	3.1	Design	n of Smart Microcapsules with Thermo-Responsive Gating		
		_	oranes	69	
	3.2	Fabrication and Performance of Thermo-Responsive Microcapsules with			
			s Membrane and PNIPAM Gates		
		3.2.1	Fabrication of Hollow Microcapsules with Porous Membrane		
			1		
		3.2.2	Grafting PNIPAM Gates in the Membrane Pores of		
			Microcapsules	. 75	
		3.2.3	Thermo-Responsive Controlled-Release Characteristics		
	3.3	Mono	dispersed Thermo-Responsive Microcapsules with Porous		
		Memb	orane and PNIPAM Gates	. 82	
		3.3.1	Preparation of Monodispersed Microcapsules with Porous		
			Membrane	. 83	
		3.3.2	Monodispersed Microcapsules with Porous Membrane and		
			Grafted PNIPAM Gates	. 92	
		3.3.3	Thermo-Responsive Controlled-Release Characteristics	. 93	
	Refe	rences.	-		
4	Sma	rt Micr	ocapsules with Thermo-Responsive Hydrogel Membranes	. 97	
	4.1	Introd	uction	97	
	4.2		disperse Thermo-Responsive PNIPAM Hollow Microcapsules		
			red with W/O Single Emulsions as Templates	. 98	
		repared with w/o onigie Lineasions as remplates			

		4.2.1	Fabrication Strategy and Microstructure Control	98	
		4.2.2	Thermo-Responsive Characteristics	01	
	4.3	4.3 Monodisperse Thermo-Responsive PNIPAM Hollow Mic			
		Prepar	red with O/W/O Double Emulsions as Templates 1	03	
		4.3.1	Fabrication Strategy and Microstructure Control 1	03	
		4.3.2	Thermo-Responsive Controlled-Release Characteristics 1	06	
	4.4	Mono	disperse Thermo-Responsive PNIPAM Hollow Microcapsules		
		Prepar	pared with W/O/W/O Triple Emulsions as Templates107		
		4.4.1	Thermo-Responsive Squirting Microcapsules for Nanoparticle	2	
			Delivery1	80	
		4.4.2	Thermo-Responsive Trojan-Horse-Like Microcapsules 1	15	
	4.5	Summ	nary and Outlook1	17	
	Refe	rences.		18	
5	The	rmo-Re	sponsive Membranes for Chiral Resolution 1	2.1	
	5.1		uction1		
	5.2		ept and Design of the Thermo-Responsive Membrane for Chiral		
		ution			
	5.3		ration and Componential and Morphological Characterization of		
			oranes		
		5.3.1	Preparation of Thermo-Responsive Chiral Membranes 1	.24	
		5.3.2	Componential and Morphological Characterization of		
		a	Membranes	27	
	5.4	Resolution Performance of Tryptophan Enantiomers with			
			no-Responsive Membranes	31	
		5.4.1	Permeation of <i>D</i> , <i>L</i> -Tryptophan through Grafted		
			Thermo-Responsive Membranes		
		5.4.2	Effects of Grafting Yield and Temperature on Chiral Resolution		
			of <i>D,L</i> -Tryptophan through Membranes		
	5.5		nplexation of Tryptophan Enantiomers from Thermo-Responsiv		
			pranes		
	5.6	, and the second se			
	Refe	rences.		41	
6	Thermo-Responsive Membranes for Affinity Separation				
	6.1	Introd	uction1	45	
	6.2 Thermo-Responsive Affinity Membrane with Nano-Structu				
		Grafte	d PNIPAM Surface I over for Hydrophobic Adsorption 1	16	

		6.2.1	Design of Thermo-Responsive Affinity Membrane with
			Nano-Structured Pores and Grafted PNIPAM Surface Layer
		6.2.2	Preparation and Characterization of Thermo-Responsive
			Membrane with Nano-Structured Pores and Grafted
			PNIPAM Surface Layer
		6.2.3	Thermo-Responsive Adsorption/Desorption Characteristics
		0.2.5	
	6.3	Tempe	erature-Dependent Molecular-Recognizable Membranes for
	0.5	-	ty Separation
		6.3.1	Design and Preparation of Thermo-Responsive Molecular-
		0.5.1	Recognizable Membranes for Affinity Separation
		6.3.2	Morphological Characterization of Membranes
		6.3.3	Thermo-Responsive Adsorption/Desorption Characteristics
		0.5.5	
	6.4	Summ	nary
7	pH-	Respon	sive Gating Membrane Systems with Pumping Effects 169
	7.1	Introd	uction
	7.2	Design	n of the Composite pH-Responsive Gating Membrane System with
		Pumpi	ing Effects
	7.3	Prepai	ration and Characterization of the Composite pH-Responsive
		Memb	orane System
		7.3.1	Preparation and Characterization of pH-Responsive
			PMAA-g-PVDF Gating Membranes
		7.3.2	Preparation and Characterization of Crosslinked pH-Responsive
			PDM Hydrogels175
	7.4	pH-Re	esponsive Controlled-Release Characteristics of the Composite
		Memb	orane System with Pumping Effects
	7.5	Summ	nary
	Refe	rences.	
8	Sma	rt Micr	ocapsules with pH-Responsive Hydrogel Membranes 185
o			
	8.1		uction
	8.2	_	n and Fabrication Strategy of Smart Microcapsules with
		-	esponsive Chitosan Hydrogel Membranes
	8.3	Prepar	ration of Microcapsules with Crosslinked Chitosan Hydrogel
		Memb	oranes

		8.3.1	Microfluidic Device	188			
		8.3.2	Preparation of Microcapsules with Crosslinked Chitosan				
			Hydrogel Membranes	188			
	8.4	Morph	ological Characterization of Chitosan Microcapsules	189			
	8.5	pH-Re	sponsive Property of Microcapsules with Chitosan Hydroge	1			
		Memb	ranes	190			
	8.6	Summ	ary	194			
	Refe	rences		194			
9	Gluc	Glucose-Responsive Gating Membranes197					
	9.1	Introdi	action	197			
	9.2		se-Responsive Flat Gating Membranes				
	> 	9.2.1	Fabrication of Glucose-Responsive Flat Gating Membranes				
		9.2.2	Characterization of Glucose-Responsive Flat Gating Memb	ranes			
				200			
		9.2.3	pH-Responsive Control of the Pore Size of PAAC-Grafted				
			Membranes	200			
		9.2.4	Glucose-Responsive Controlled-Release Characteristics	205			
	9.3	Glucos	se-Responsive Microcapsule Membranes	208			
		9.3.1	Design of Glucose-Responsive Microcapsule Membranes	208			
		9.3.2	Preparation of Glucose-Responsive Microcapsule Membran	nes			
				209			
		9.3.3	Characterization of Glucose-Responsive Microcapsule				
			Membranes				
		9.3.4	Glucose-Responsive Controlled-Release Characteristics of				
			Microcapsules				
	9.4		ary				
	Refe	rences		215			
10	Mole	cular-F	Recognizable Smart Membranes	217			
	10.1	Introdu	action	217			
	10.2 Molecular-Recognizable Smart Membranes with β-CDs		ular-Recognizable Smart Membranes with β-CDs as Host				
		Molect	ules	218			
		10.2.1	Design of Molecular-Recognizable Gating Membranes with	n			
			β-CDs as Host Molecules	218			
		10.2.2	Fabrication of Molecular-Recognizable Gating Membranes	with			
			β-CDs as Host Molecules	219			
		10.2.3	Componential and Morphological Characterization of				
			Membranes	221			

		10.2.4	Molecular-Recognizable Diffusional Permeability and Gating
			Characteristics
	10.3		ular-Recognizable Smart Membranes with Crown Ethers as Host
			ules
		10.3.1	Smart Microcapsules with Molecular-Recognizable Gating
			Membranes
		10.3.2	Smart Microcapsules with Molecular-Recognizable Hydrogel
			Membranes
	10.4	Summa	ary237
	Refer	ences	238
11	Dua	l-/Mult	i-Stimuli-Responsive Smart Membranes241
	11.1	Introd	luction
	11.2	Dual	Stimuli-Responsive Microcapsules with Superparamagnetic
		Porou	is Membrane and Thermo-Responsive Gates
		11.2.1	Strategy for Fabricating Microcapsules with Superparamagnetic
			Porous Membrane and Thermo-Responsive Gates
		11.2.2	2 Preparation of Microcapsules with Superparamagnetic Porous
			Membrane and Thermo-Responsive Gates
		11.2.3	Morphology and Composition Characterization of the
			Microcapsules
		11.2.4	Magnetic Properties of PNIPAM-Grafted Magnetic
			Microcapsules
		11.2.5	Thermo-Responsive Controlled-Release Properties of
			PNIPAM-Grafted Magnetic Microcapsules
	11.3	Super	paramagnetic and Thermo-Responsive Microcapsules with
			ogel Membranes
	11.4	Dual '	Thermo-Responsive and Molecular-Recognizable Membranes
			255
	11.5	Multi	-Stimuli-Responsive Membrane Gates with Hierarchical
		Struct	tures
	11.6	Sumn	nary
	Refe	erences.	
12	Pers	spective	es on Smart Membrane Materials and Systems259
	12.1	Devel	lopment Trend of Smart Membrane Materials and Systems 259
			tial Applications of Smart Membranes
			2/2

Introduction

In this chapter, membranes and their development progress are introduced briefly at the beginning, from which the readers can see that the development of environmental stimuli-responsive smart materials is essential and important. Then, the environmental stimuli-responsive gating model of biomembranes in the natural world and some typical artificial environmental stimuli-responsive smart materials, including thermo-responsive, pH-responsive, glucose-responsive and molecular-recognizable ones, are introduced, to show the original natural model and possible material candidates for designing and fabricating artificial smart membranes. Next, several bio-inspired design concepts are described for artificial biomimetic environmental stimuli-responsive smart membranes. Finally, some potential applications of smart membrane materials and systems are discussed.

1.1 A Glance at Membranes and Their Development

We are living in a membrane world. Our life depends upon membrane technology so much nowadays. In the past several decades, membrane scientists have successfully developed membranes for microfiltration, ultrafiltration, nanofiltration, reverse osmosis, dialysis, electrodialysis, pervaporation, gas separation, controlled release, etc., and membrane technologists have successfully applied the membranes in numerous fields from chemical engineering to biomedical engineering, petrochemical engineering, environmental engineering, mechanical manufacture, food engineering, pharmaceutical engineering, biochemical engineering, the electronics industry, the textile industry, spaceflight, gas separation, water treatment, drug delivery, etc. Membrane technology is playing a more and more important role in modern life and global sustainable development.

Although the achievements in the membrane fields have been very significant up to now, commercialized membranes are still single-function membranes. For example, membrane separation is only achieved by either size difference, or solution-diffusion difference, or electrostatic charge difference, except for some charged ultrafiltration and nanofiltration processes carried out by both size and electrostatic charge differences. The permeability of existing commercial membranes cannot be self-regulatively adjusted by the change in environmental conditions. That means the permeation performances of membranes are not able to respond to environmental stimuli. However, the biomembranes in nature have environmental stimuli-responsive channels across the membranes, [1-3] that means the permeability of biomembranes has environmental stimuli-responsive characteristics.

Bionic technology is endlessly bringing us new ideas, new principles, new approaches and new theories from the natural world for developing the novel high-tech world. Unexceptionally, biomembranes provide original inspiration for membrane scientists and technologists to develop mimetic functional membranes, which are highly attractive for achieving more advanced and comprehensive membrane systems, *e.g.*, composite-function membranes with not only a selectivity factor but also an environmental stimuli-response factor and a gate factor. Since the middle of the 1980s, membrane scientists and technologists have been much devoted to the development of bio-inspired environmental stimuli-responsive smart membranes. Because they have great potential for applications in myriad fields from controlled drug delivery to chemical separation, water treatment, bioseparation, chemical sensors, chemical valves and tissue engineering, such environmental stimuli-responsive smart membranes are attracting ever-increasing attention from various fields.

1.2 Environmental Stimuli-Responsive Gating Model of Biomembranes

Nature gives us endless examples of sophisticated environmental stimuli-responsive smart systems. Ion channels are pore-forming proteins that help establish and control the small voltage gradient across the cell membrane of all living cells, by allowing the flow of ions down their electrochemical gradient. ^[4] In some ion channels of the cell membrane, passage through the pore is governed by a "gate", which may be opened or closed by chemical or electrical signals, temperature or mechanical force, depending on the variety of channels. For example, activated by a membrane voltage or a signaling molecule, a potassium ion channel can switch from a closed to an open state and the process is reversible. Therefore potassium ions can be selectively allowed to cross the membrane (**Fig.1.1**). Such an environmental stimuli-responsive gating function of biomembranes provides an exciting model for membrane scientists and technologists to develop artificial smart membranes.

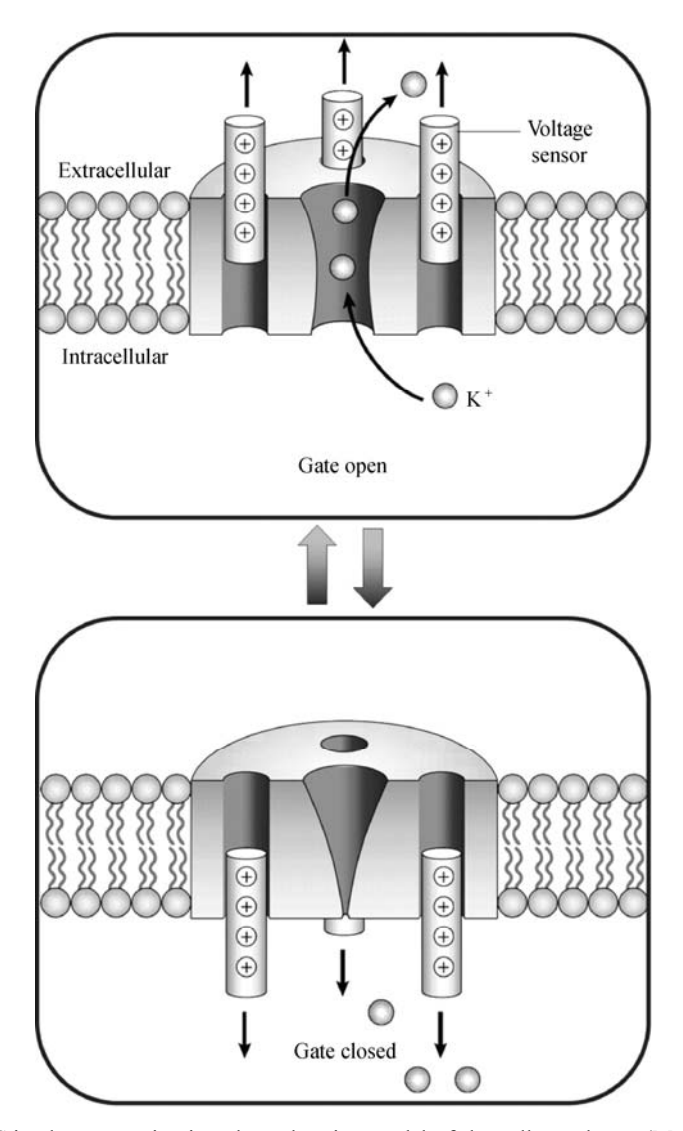


Fig.1.1. Stimulus-responsive ion channel gating model of the cell membrane (Modified with permission from Ref. [3]). Copyright (2004), Nature Publishing Group

1.3 Environmental Stimuli-Responsive Smart Materials

Environmental stimuli-responsive smart materials, or intelligent materials, are the kind of marvelous materials that have the capability to sense their environment signals, process these data and respond. They have one or more properties that can be significantly changed in a controlled fashion by external stimuli, such as

temperature, pH, stress, moisture, electric or magnetic fields. Such smart materials make it possible to design and fabricate artificial biomimetic smart membranes.

In the following sections, thermo-responsive, pH-responsive, glucose-responsive and molecular-recognizable smart materials are introduced.

1.3.1 Thermo-Responsive Smart Materials

Because there are many cases in which environmental temperature fluctuations occur naturally, and in which the environmental temperature stimuli can be easily designed and artificially controlled, much attention has been focused on thermoresponsive materials and systems.

Poly(N-isopropylacrylamide) (PNIPAM), whose chemical structure is shown in Fig.1.2, is a popular thermo-responsive polymer. It shows a distinct and reversible phase transition at the lower critical solution temperature (LCST) around 32 °C. When the environmental temperature is lower than the LCST, the PNIPAM can bind plenty of water molecules on its amide groups through hydrogen-bonding interaction, and thus it is in a swollen and hydrophilic state; however, when the temperature is higher than the LCST, the PNIPAM is dehydrated because of the cleavage of the hydrogen-bonding, and thus it is in a shrunken and hydrophobic state (Fig.1.3).^[5] That is, the conformation change of the PNIPAM can result in volume phase transition of PNIPAM hydrogels from a swollen and hydrophilic state, at temperatures below the LCST, to a shrunken and hydrophobic state at temperatures above the LCST. Figure 1.4 shows the thermo-responsive volume phase transition behavior of monodisperse PNIPAM microgels prepared by the microfluidic method by the author. [6] Such dramatic phase transition characteristics make PNIPAM hydrogels extremely valuable for numerous applications including smart membranes.

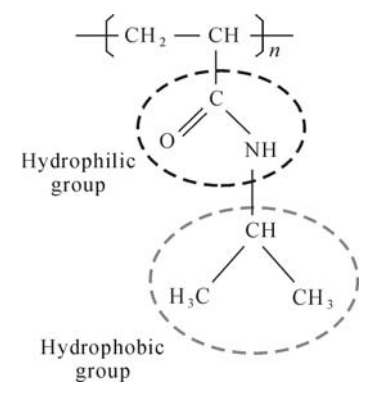


Fig.1.2. Chemical structure of PNIPAM

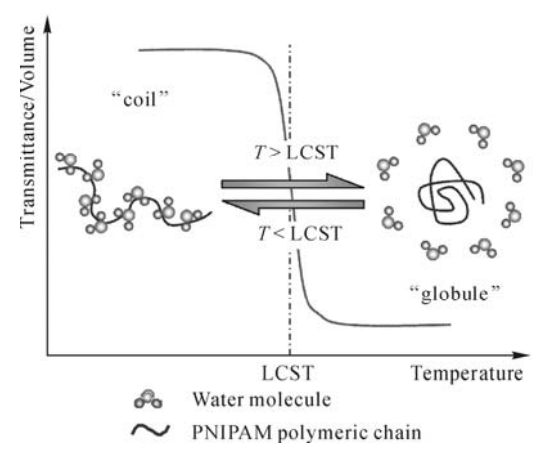


Fig.1.3. Thermo-responsive phase transition characteristics of PNIPAM

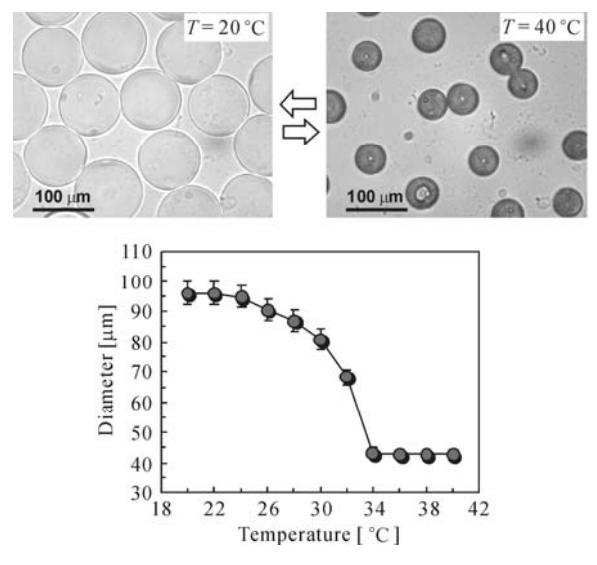


Fig.1.4. Thermo-responsive volume phase transition behavior of monodisperse PNIPAM microgels (Reproduced with permission from Ref. [6]). Copyright (2008), The Royal Society of Chemistry

As mentioned above, PNIPAM shrinks dramatically when the temperature increases to above the LCST. In other words, PNIPAM hydrogels are featured with negatively thermo-responsive characteristics, *i.e.*, the volume of PNIPAM hydrogels decreases with an increase in the environmental temperature. On the contrary, the thermo-responsive interpenetrating polymer networks (IPNs) that are composed of poly(acrylamide) (PAAM) and poly(acrylic acid) (PAAC) are featured with positively thermo-responsive characteristics (Fig.1.5). It is known that PAAM and PAAC form polycomplexes in solution through hydrogen bonding. By the cooperative "zipping" interactions between the molecules that result from hydrogen bonding,

it has been found that the PAAM/PAAC-based IPN hydrogels are featured with a thermo-responsive volume phase transition characteristic that is the reverse of that of PNIPAM, *i.e.*, the hydrogel swelling is induced by an increase rather than a decrease in temperature.^[7] When the environmental temperature is lower than the upper critical solution temperature (UCST) of the PAAM/PAAC-based IPN hydrogel, PAAC forms intermolecular hydrogen bonds with PAAM, and the IPN hydrogels retain a shrinking state by the interaction between two polymer chains or the so-called chain-chain zipper effect; however, when the environmental temperature is higher than the UCST of the IPN hydrogel, PAAC dissociates intermolecular hydrogen bonds with PAAM, and the IPN hydrogels retain a swelling state by the relaxation of the two polymer chains (**Fig.1.5**). Therefore, the PAAM/PAAC-based IPN hydrogels can be used to achieve thermo-responsive functions opposite to that of PNIPAM hydrogels.

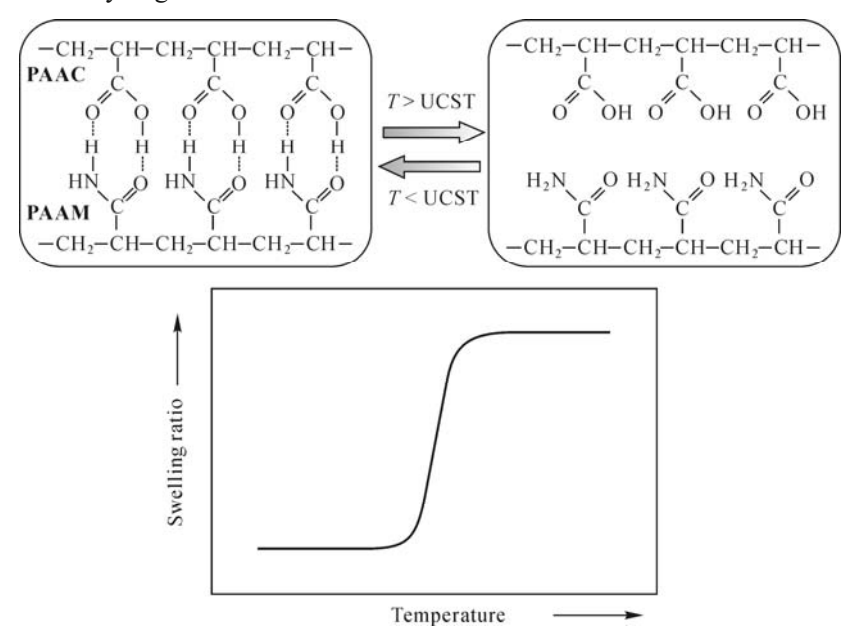


Fig.1.5. Thermo-responsive volume change behavior of PAAC/PAAM-based IPN networks

1.3.2 pH-Responsive Smart Materials

pH is an important environmental parameter for biomedical applications, because the pH change occurs at many specific or pathological body sites, such as the stomach, intestine, endosome, lysosome, blood vessels, vagina and tumor extracellular sites. For example, there is an obvious change in pH along the gastrointestinal tract from the stomach (pH = $1\sim3$) to the intestine (pH = $5\sim8$). Moreover, there are also more subtle changes within different tissues. Certain tumors, as well as inflamed

or wound tissue, exhibit a pH different from 7.4 as it is in circulation. For example, chronic wounds have been reported to have pH values between 7.4 and 5.4, and tumor tissue is also reported to be acidic extracellularly. Besides, pH variation is also very common in chemical reactions and environmental changes. Therefore, pH-responsive smart materials and systems have attracted considerable interest from various fields.

All pH-responsive materials with pH-responsive swelling or shrinking properties contain either acidic or basic groups, which can respond to changes in environmental pH by gaining or losing protons (Fig.1.6). For example, the pH-responsive volume phase transition characteristics of poly (methacrylic acid) (PMAA) and poly(N,N-dimethylaminoethyl methacrylate) (PDM) hydrogels have been verified to be opposite (Fig.1.7). [9] PMAA hydrogels are featured with a positively pHresponsive volume phase transition characteristic, i.e., the hydrogel swelling is induced by an increase in the environmental pH; on the contrary, PDM hydrogels show a negatively pH-responsive volume phase transition characteristic, i.e., the hydrogel swelling is induced by a decrease in the environmental pH. When the environmental pH is higher than the corresponding value of the effective dissociation constant (pKa), the PDM hydrogel shrinks, but the PMAA hydrogel swells. On the other hand, when the ambient pH is decreased to be lower than the corresponding value of pKa, the PMAA hydrogel shrinks, but the PDM hydrogel swells. Therefore, the PMAA hydrogels can be used to achieve pH-responsive functions opposite to that of PDM hydrogels.

R-COOH
$$\stackrel{\text{OH}^-}{\longleftarrow}$$
 R-COO-
R-NH₃ $\stackrel{\text{OH}^-}{\longleftarrow}$ R-NH₂

Fig.1.6. pH-responsive ionization of carboxylic group and amino group by losing or gaining protons

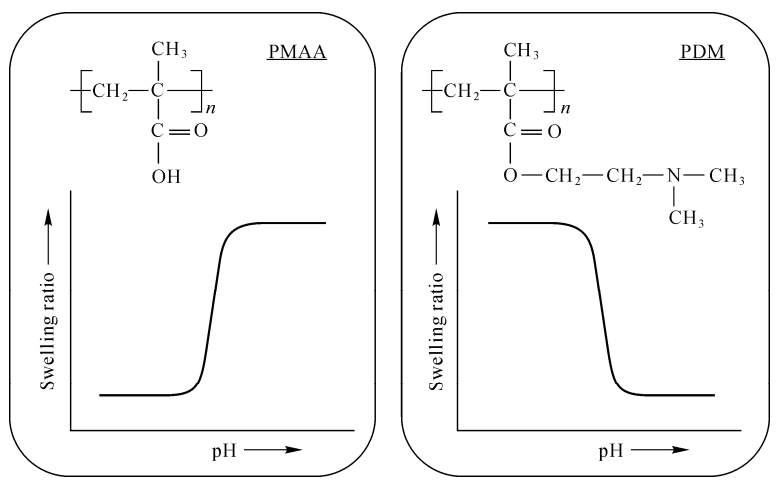


Fig.1.7. pH-responsive volume phase transition characteristics of PMAA and PDM hydrogels

1.3.3 Glucose-Responsive Smart Materials

Glucose-responsive materials and systems are considered to be very important candidates for developing glucose-responsive self-regulated insulin release systems for therapy of diabetes, which is a major cause of death in industrialized countries and is still lacking better ways to administrate insulin delivery.

Up to now, three major kinds of glucose-responsive materials have been developed, with functional moieties involving glucose oxide, concanavalin A and phenylboronic acid (PBA), respectively.^[10,11] By chemically immobilizing glucose oxidase (GOD) onto pH-responsive polymers, the polymeric system could exhibit a glucose-responsive property. The immobilized GOD acts as the glucose sensor and catalyzer, because it is sensitive to glucose and could catalyze the glucose conversion to gluconic acid. Due to the appearance of gluconic acid, the local pH value decreases in the microenvironment as a result. Therefore, the GOD-immobilized pH-responsive polymer could respond to environmental glucose concentration variation. For example, if the GOD is chemically immobilized onto poly(acrylic acid) (PAAC) chains, at neutral pH in the absence of glucose, the carboxyl groups of the PAAC chains are dissociated and negatively charged. Therefore, the repulsion between negative charges makes the PAAC chains extended. However, when the glucose concentration increases, GOD catalyzes the oxidation of glucose into gluconic acid, thereby lowering the local pH in the microenvironment, protonating the carboxylate groups of the PAAC chains. Therefore, the chains shrink due to the reduced electrostatic repulsion between the PAAC chains.

PBA-based systems do not contain any enzyme or protein, and can reversibly form a complex with *cis*-diol such as glucose. [12] In an acid or neutral environment, boronic acid moieties of PBA maintain a plane triangle structure, which hardly form a complex with cis-diol, while in an alkali environment, PBA turns into a boronic anion tetrahedral structure by combining a hydroxyl on the boron, because the pKa of 3-acrylamidophenylboronic acid (AAPBA) moiety in the copolymer of N-isopropylacrylamide (NIPAM) and AAPBA is 8.2. [13,14] When glucose exists, the tetrahedral structure can form a stable complex with glucose, as shown in Fig.1.8. The PBA-based system can be made into many forms by introducing PNIPAM as backbone. As mentioned above, PNIPAM can exhibit reversible volume phase transition as the temperature changes, due to the interaction of hydrophilic and hydrophobic functional groups together with the temperature change. The LCST transition of PNIPAM is driven by an increase in entropy upon heating. At a given temperature, the chemical potential of water in saccharide solution decreases with an increase in saccharide concentration due to the mixing free energy.^[15] That is, adding saccharides and raising the temperature have the same effect of decreasing the chemical potential of water. As a result, the decrease in the chemical potential of water molecules by adding saccharides causes saccharide-induced volume phase transition of poly(NIPAM-co-AAPBA) hydrogels. Decrement of the chemical potential of water by glucose may destabilize the hydration on poly(NIPAM-co-AAPBA) hydrogel chains, resulting in the shrinkage

of the hydrogels.^[15,16] The LCST of PNIPAM-based polymer can be tuned by introducing hydrophilic or hydrophobic components into the polymer. PBA moiety, which is hydrophobic due to its phenyl group, has the ability to combine 1,2-*cis*-diols, such as glucose, reversibly after dissociation to a charged state, at a pH around 9. Therefore, the critical deswelling temperature of the poly(NIPAM-*co*-AAPBA) polymer shifts to a higher temperature in aqueous solution with higher glucose concentration.^[16] Thus, the poly(NIPAM-*co*-AAPBA) polymer exhibits an isothermal glucose-responsive property at fixed temperatures in the range between the two critical deswelling temperatures (**Fig.1.9**).

Fig.1.8. Complexation equilibrium between phenylboronic acid (PBA) moiety grafted on PNIPAM-based polymers and glucose in alkaline environment (Reproduced with permission from Ref. [16]). Copyright (2008), John Wiley and Sons

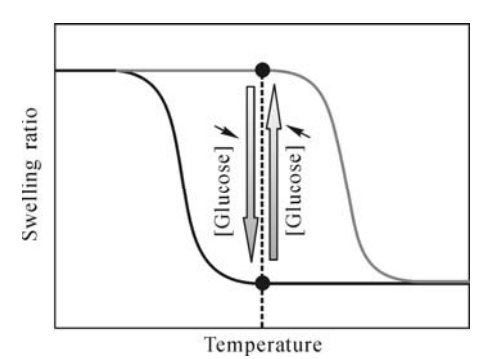


Fig.1.9. Swelling and shrinking behavior of poly(NIPAM-co-AAPBA) hydrogels containing PBA moieties in response to glucose concentration transition (Reproduced with permission from Ref. [16]). Copyright (2008), John Wiley and Sons

1.3.4 Molecular-Recognizable Smart Materials

Molecular-recognizable smart materials that can recognize and respond to specific molecules are highly attractive for developing bio/chemical sensors and actuators.

Crown ethers have remarkable properties of selectively recognizing specific ions and forming stable "host-guest" complexes. If the crown ether groups are

introduced into the thermo-responsive PNIPAM hydrogel, it is possible to prepare an ion-recognition hydrogel that responds to both temperature and specific ion stimuli. A molecular-responsive copolymer of PNIPAM with a pendant crown ether 18-crown-6 groups has been designed and synthesized (**Fig.1.10**). [17-19] PNIPAM acts as an actuator, and benzo-18-crown-6-acrylamide (BCAm), with a crown ether cavity, is used as an ion-signal sensing receptor. When the crown ether receptors capture specific ions, the LCST of the copolymer shifts to a higher temperature due to the enhancement of hydrophilicity of the copolymer when specific ions are captured (**Fig.1.11**). As a result, when the environmental temperature is located between LCST_a and LCST_b in **Fig.1.11**, the copolymer exhibits an isothermal and significant swelling by recognizing special ions.

More recently, a smart polymer demonstrating negative shift of the LCST for phase transition responding specifically to certain alkali metal ions has been developed as poly(N-isopropylacrylamide-co-benzo-15-crown-5-acrylamide) (poly (NIPAM-co-B15C5Am)). [20] The polymer contains pendent crown ether benzo-15-crown-5-acrylamide (B15C5Am) groups as sensors and thermo-responsive PNIPAM groups as actuators (Fig.1.12). Its molecules form hydrogen bonds with water in the polymer aqueous solution, exhibiting an LCST for phase transition (LCST_b in Fig.1.13). The value of the LCST of poly(NIPAM-co-B15C5Am) in aqueous solution is almost the same as that of PNIPAM. Once a certain alkali metal cation such as K⁺ is added to the polymer aqueous solution, the B15C5Am receptors capture the K⁺ and form a well-known 2:1 (ligand: cation) "sandwich" complex, which disrupts the hydrogen bonding between the oxygen atoms in the crown ether and the hydrogen atoms of water. As a result, the hydrophobicity of the polymer is enhanced, and then the LCST for phase transition shifts negatively to a lower value (LCST_a in Fig.1.13). [20] When the environmental temperature is maintained between LCST $_a$ and LCST $_b$, the smart polymer in the aqueous solution changes its physical state abruptly and reversibly from a swollen state to a shrunken state responding to the presence of K⁺. The stimuli-responsive behaviour of the smart polymer induced by alkali metal ions is similar to some phenomena in the natural world, such as the behaviour of Venus flytraps shown in Fig.1.13.

$$\begin{array}{c|c}
-\{CH_2CH\}_{1-X} & \{CH_2CH\}_X \\
C=O & C=O \\
NH & NH \\
CH & O & O \\
O & O & O
\end{array}$$

Fig.1.10. Chemical structure of poly(NIPAM-*co*-B18C6Am)

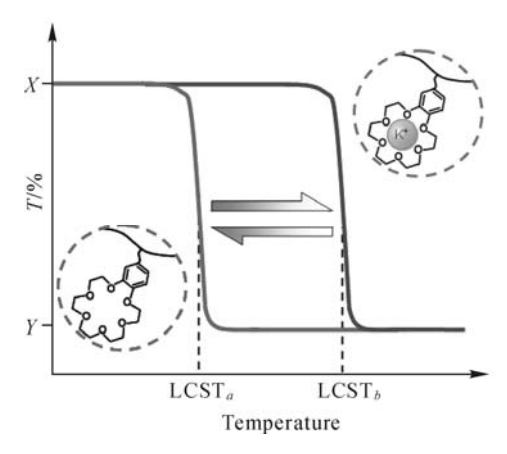


Fig.1.11. Positive shift of LCST of poly(NIPAM-co-B18C6Am) triggered by ion-recognition

Fig.1.12. Chemical structure of poly(NIPAM-*co*-B15C5Am)

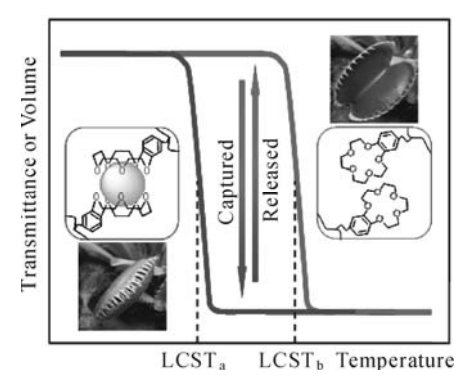


Fig.1.13. Negative shift of LCST of poly(NIPAM-co-B15C5Am) triggered by ion-recognition (Reproduced with permission from Ref. [20]). Copyright (2008), Wiley-VCH Verlag GmbH & Co. KGaA

Beta-cyclodextrin (β -CD), which is composed of cyclic α -1,4-oligoglucopyranosides, possesses a hydrophobic cavity and hydrophilic external surface. Through a series of weak intermolecular forces, such as hydrophobic, electrostatic and hydrogenbonding interactions, β -CD is a well-known host molecule capable of selectively associating with guest molecules having a similar size to its cavity; therefore, β -CD and its derivatives were used widely in molecular recognition systems. Due to the interesting integration of the molecular recognition ability of β -CD and the thermoresponsivity of PNIPAM, certain attention has been drawn to hydrogels and polymers with a combination of NIPAM and β -CD. Recently, a PNIPAM-based thermo-responsive polymer with pendent β -CD groups, poly(N-isopropylacylamideco-glycidyl methacrylate/cyclodextrin) (poly(NIPAM-co-CD), Fig.1.14), was successfully synthesized and the molecular-recognition induced phase-transition behavior of fabricated polymers was reported. [21] The poly(NIPAM-co-CD) polymers could significantly recognize the guest 8-anilino-1-naphthalenesulfonic acid ammonium salt (ANS) molecules, and their LCSTs in the ANS aqueous solutions were lower than that in blank aqueous solution because of the hydrophobic phenyl group of ANS out of the cavity after CD/ANS complexation. However, the guest 2-naphthalenesulfonic acid (NS) molecules had an opposite influence on the LCSTs of poly(NIPAM-co-CD) polymers, because the complexation between CD and NS slightly enlarged the hydrophilic moiety of polymers, due to the dissociation of NS molecules in the water. Therefore, the poly(NIPAM-co-CD) polymers isothermally shrink when recognizing certain guest molecules with a hydrophobic side group (e.g., ANS) at T_1 , but isothermally swell when recognizing different guest molecules with a hydrophilic side group or without side group (e.g., NS) at T_2 (Fig.1.15). [21]

Fig.1.14. Chemical structure of poly(NIPAM-co-CD)

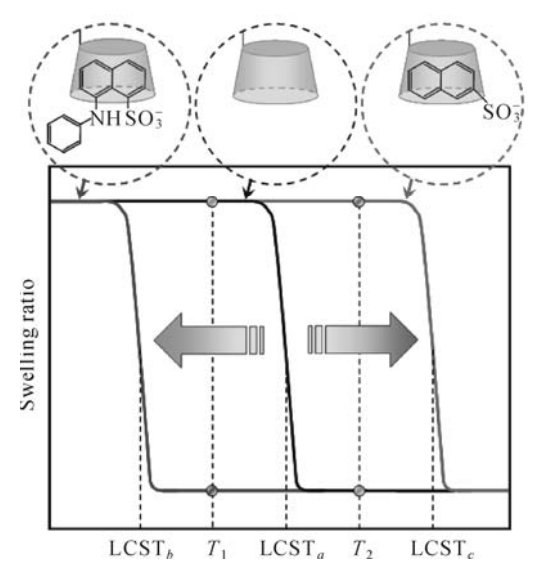


Fig.1.15. Negative and positive shifts of the LCST of poly (NIPAM-co-CD) triggered by recognizing different guest molecules

1.4 Bio-Inspired Design of Environmental Stimuli-Responsive Smart Membranes

Inspired by the stimuli-responsive ion channels across the cell membranes and according to the existing smart materials, artificial environmental stimuli-responsive smart membranes can be designed as smart membranes with porous substrates and stimuli-responsive gates, smart membranes with grafted stimuli-responsive surfaces, and stimuli-responsive smart hydrogel membranes.

1.4.1 Smart Membranes with Porous Substrates and Stimuli-Responsive Gates

Smart membranes with porous substrates and stimuli-responsive gates, are those prepared by grafting or coating smart materials onto the porous membrane substrate by certain chemical or physical methods. The pore size or the permeability of such membranes can be adjusted by self-regulation by the stimuli-responsive volume phase transition behavior of the grafted or coated smart material gates in the membrane pores (**Fig.1.16**). The grafted or coated smart materials in the membrane pores can act as smart valves that respond to environmental stimuli.

14 1 Introduction

By applying the same principle from flat membranes to microcapsule membranes, we can design and fabricate environmental stimuli-responsive smart microcapsules with porous membranes and responsive gates (**Fig.1.17**). Such microcapsules are highly valuable for achieving stimuli-responsive and self-regulated controlled release and drug delivery.

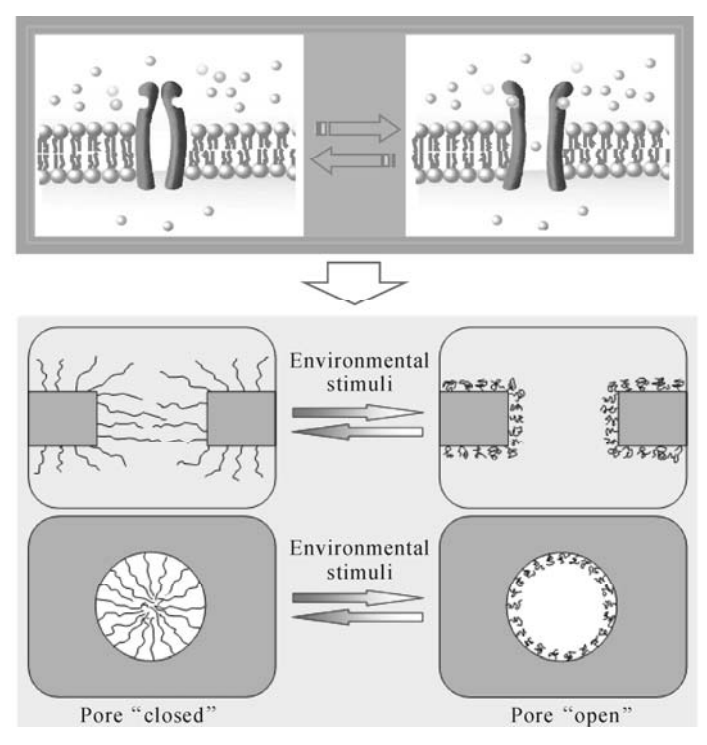


Fig.1.16. Environmental stimuli-responsive smart gating membrane with porous substrate and responsive gate

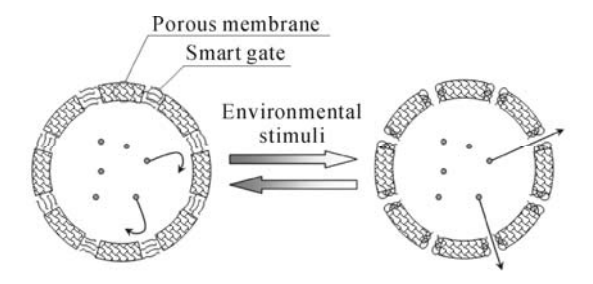


Fig.1.17. Environmental stimuli-responsive smart microcapsule with porous membrane and responsive smart gate

1.4.2 Smart Membranes with Grafted Stimuli-Responsive Surfaces

Smart membranes, with grafted stimuli-responsive surfaces, are those prepared by grafting or coating smart materials onto the membrane surface by certain chemical or physical methods. The surface characteristics and/or the permeability of such membranes can be adjusted by self-regulation by the stimuli-responsive volume phase transition behavior of the grafted or coated smart materials on the membrane surfaces (**Fig.1.18**). As mentioned above, the thermo-responsive conformation change of PNIPAM can result in phase transition of PNIPAM from a swollen and hydrophilic state, at temperatures below the LCST, to a shrunken and hydrophobic state, at temperatures above the LCST. Thus, if PNIPAM is grafted on the membrane surface, the membrane surface layer exhibits a loose and hydrophobic state at temperatures below the LCST; however, it switches to a dense and hydrophobic state at temperatures above the LCST.

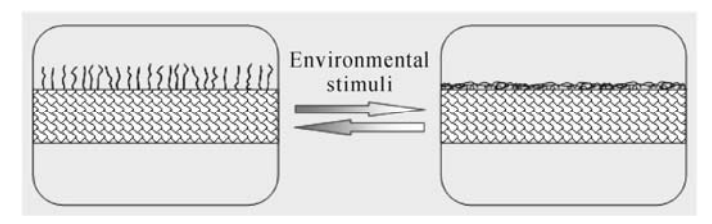


Fig.1.18. Environmental stimuli-responsive smart membrane with grafted responsive surface

1.4.3 Stimuli-Responsive Smart Hydrogel Membranes

Stimuli-responsive smart hydrogel membranes are those prepared with the whole membrane made of stimuli-responsive smart hydrogels. The permeability of such membranes can be adjusted by self-regulation by the stimuli-responsive volume phase transition behavior of the smart hydrogels that construct the whole membrane (**Fig.1.19**). For example, if PNIPAM is the membrane material, the whole membrane exhibits a loose and hydrophilic state at temperatures below the LCST; however, it switches to a dense and hydrophobic state at temperatures above the LCST. As a result, the permeability can be controlled by self-regulation by the environmental temperature change.

Just like smart membranes with porous substrates and stimuli-responsive gates, the principles underlying the creation of both smart membranes with grafted stimuli-responsive surfaces and stimuli-responsive smart hydrogel membranes can also be applied to smart microcapsule membrane systems.

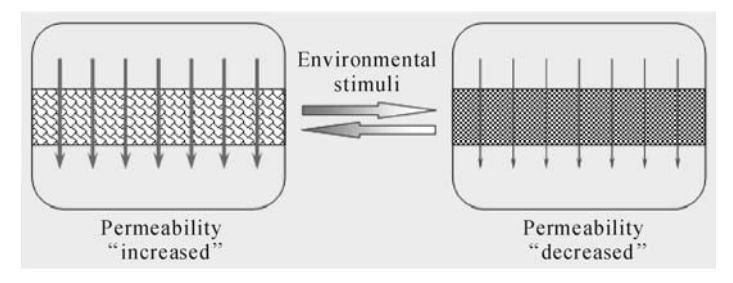


Fig.1.19. Environmental stimuli-responsive smart hydrogel membrane

References

- [1] Dutzler R, Campbell E B, MacKinnon R. Gating the selectivity filter in ClC chloride channels. *Science*, **2003**, *300*: 108-112.
- [2] Jiang Y, Lee A, Chen J, Cadene M, Chait B T, MacKinnon R. The open pore conformation of potassium channels. *Nature*, **2002**, *417*: 523-526.
- [3] The Nature Reviews Drug Discovery Ion Channel Questionnaire Participants. The state of ion channel research in 2004. *Nature Reviews Drug Discovery*, **2004**, *3*: 239-278.
- [4] Hille B. *Ion Channels of Excitable Membranes (3rd ed.)*. Sunderland, Mass: Sinauer Associates, **2001**.
- [5] Schild H G. Poly(*N*-isopropylacrylamide): experiment, theory and application. *Progress in Polymer Science*, **1992**, *17*: 163-249.
- [6] Shah R K, Kim J W, Agresti J J, Weitz D A, Chu L Y. Fabrication of monodisperse thermosensitive microgels and gel capsules in microfluidic devices. *Soft Matter*, **2008**, *4*: 2303-2309.
- [7] Ilmain F, Tanaka T, Kokufuta E. Volume transition in a gel driven by hydrogen bonding. *Nature*, **1991**, *349*: 400-401.
- [8] Ju X J, Xie R, Yang L, Chu L Y. Biodegradable "intelligent" materials in response to chemical stimuli for biomedical applications. *Expert Opinion on Therapeutic Patents*, **2009**, *19*: 683-696.
- [9] Qu J B, Chu L Y, Yang M, Xie R, Hu L, Chen W M. A pH-responsive gating membrane system with pumping effects for improved controlled-release. *Advanced Functional Materials*, **2006**, *16*: 1865-1872.
- [10] Kost J, Langer R. Responsive polymeric delivery systems. *Advanced Drug Delivery Reviews*, **2001**, *46*: 125-148.
- [11] Miyata T, Uragami T, Nakamae K. Biomolecule-sensitive hydrogels. *Advanced Drug Delivery Reviews*, **2002**, *54*: 79-98.
- [12] Zhang Y J, Guan Y, Zhou S Q. Synthesis and volume phase transitions of glucose-sensitive microgels. *Biomacromolecules*, **2006**, 7: 3196-3201.
- [13] Matsumoto A, Yoshida R, Kataoka K. Glucose-responsive polymer gel bearing phenylborate derivative as a glucose-sensing moiety operating at the physiological

- pH. Biomacromolecules, 2004, 5: 1038-1045.
- [14] Matsumoto A, Ikeda S, Harada A, Kataoka K. Glucose-responsive polymer bearing a novel phenylborate derivative as a glucose-sensing moiety operating at physiological pH. *Biomacromolecules*, **2003**, *4*: 1410-1416.
- [15] Kawasaki H, Sasaki S, Maeda H. Saccharide-induced volume phase transition of poly(*N*-isopropylacrylamide) gels. *Journal of Physical Chemistry*, **1996**, *100*: 16282-16284.
- [16] Zhang S B, Chu L Y, Xu D, Zhang J, Ju X J, Xie R. Poly(*N*-isopropylacrylamide)-based comb-type grafted hydrogel with rapid response to blood glucose concentration change at physiological temperature. *Polymers for Advanced Technologies*, **2008**, *19*: 937-743.
- [17] Irie M, Misumi Y, Tanaka T. Stimuli-responsive polymers-chemical-induced reversible phase-separation of an aqueous-solution of poly(*N*-isopropylacrylamide) with pendent crown-ether groups. *Polymer*, **1993**, *34*: 4531-4535.
- [18] Ju X J, Chu L Y, Liu L, Mi P, Lee Y M. A novel thermo-responsive hydrogel with ion-recognition property through supramolecular host-guest complexation. *The Journal of Physical Chemistry B*, **2008**, *112*: 1112-1118.
- [19] Ju X J, Liu L, Xie R, Niu C H, Chu L Y. Dual thermo-responsive and ion-recognizable monodisperse microspheres. *Polymer*, **2009**, *50*: 922-929.
- [20] Mi P, Chu L Y, Ju X J, Niu C H. A smart polymer with ion-induced negative shift of the lower critical solution temperature for phase-transition. *Macromolecular Rapid Communications*, **2008**, *29*: 27-32.
- [21] Yang M, Chu L Y, Xie R, Wang C. Molecular-recognition induced phase-transition of two thermo-responsive polymers with pendent beta-cyclodextrin groups. *Macromolecular Chemistry & Physics*, **2008**, *209*: 204-211.

Thermo-Responsive Gating Membranes: Design, Microstructures and Performances

As there are many cases in which environmental temperature fluctuations occur naturally, and in which the environmental temperature stimuli can be easily designed and artificially controlled, much attention has recently focused on thermoresponsive smart membrane materials and systems. In this chapter, the emphasis is focused on the design, microstructures and performances of thermo-responsive gating membranes, which are also valuable for designing and fabricating other stimuli-responsive gating membranes. Firstly, the design of thermo-responsive gating membranes is introduced. Secondly, the formation and microstructures of grafted PNIPAM polymers in pore-filling type thermo-responsive gating membranes, fabricated by both plasma-induced grafting polymerization and atom-transfer radical polymerization, are discussed. Then, effects of the grafting yield, the length and density of grafted chains on thermo-responsive gating characteristics of pore-filling type PNIPAM-grafted membranes are discussed systematically. Next, the gating characteristics of thermo-responsive membranes with grafted linear and crosslinked PNIPAM gates and the thermo-responsive wettability characteristics of PNIPAMgrafted membranes are described. Finally, thermo-responsive gating membranes with controllable response temperature and membranes with negatively thermoresponsive gating characteristics are introduced.

2.1 Design of Thermo-Responsive Gating Membranes

As mentioned in Chapter 1, one of the main types of smart membrane is the type with porous substrate and a stimuli-responsive gate, which is called a gating membrane and can be prepared by grafting or coating smart materials onto the porous membrane substrate by certain chemical or physical methods. A convenient way of preparing such thermo-responsive gating membranes is to graft thermo-responsive polymers (*e.g.*, PNIPAM in **Fig.1.2**) onto the pore surface of porous membrane substrates. The substrate provides mechanical strength and dimensional

stability, while the grafted thermo-responsive polymers provide the environmental thermo-responsive characteristics, *i.e.*, altering their conformation and physical structure as the environmental temperature varies. As a result, the permeability of such gating membranes can be controlled or adjusted by the grafted gates according to the external temperature. Two main advantages can be gained from grafting techniques in preparing gating membranes. One is that the grafted chains are chemically bonded to the membrane substrate compared with those prepared by physical coating techniques, so that they will not be dissolved as the solvent permeates through the membrane. The other is that the grafted chains have freely mobile ends, so that the prepared membranes respond faster to the environmental stimuli when compared with hydrogels with typical crosslinked network structures.

Up to now, various grafting techniques, including chemical grafting, plasma-induced grafting and radiation-induced grafting and so on, have been introduced to prepare environment-responsive membranes by grafting different functional polymers either onto the external membrane surface or onto both the external surface and the inside surface of the pores. According to the location of grafted polymers on the porous membrane substrates, thermo-responsive gating membranes can be classified as pore-covering models^[1,2] (**Fig.2.1a**) and pore-filling models^[3-10] (**Fig.2.1b**). Usually, the pore-covering model of gating membranes is prepared by UV radiation-induced grafting polymerization,^[1,2] while the pore-filling model of gating membranes is prepared by plasma-induced grafting or chemical grafting polymerizations. [3-10] **Fig.2.1c** illustrates the thermo-responsive microgel-coated gating membrane model. [11]

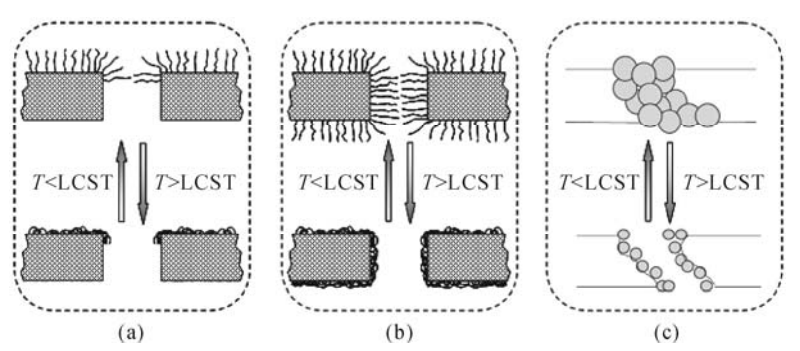


Fig.2.1. Thermo-responsive gating membranes with different gating models. (a) Pore-covering model with grafted thermo-responsive polymeric chains; (b) Pore-filling model with grafted thermo-responsive polymeric chains; (c) Pore-filling model with coated thermo-responsive polymeric microgels

In **Fig.2.1**, the thermo-responsive materials are assumed to be PNIPAM-based polymers because PNIPAM is the most popular thermo-responsive polymer. When the grafting yield is in the proper range, the grafted PNIPAM chains or microgels on the pore surface are in a swollen state at temperatures below the lower critical solution temperature (LCST), so the pores in the membrane are closed by the PNIPAM gates. In contrast, the grafted PNIPAM chains or microgels on the pore

surface are in a shrunken state at temperatures above the LCST, and therefore the pores in the membrane are in an open state. As a result, from the thermo-responsive "closed/open" switching of the gates in the membrane pores, the hydraulic permeability (pressure-driven convective flow of solvents) or the diffusional permeability (concentration-driven molecular diffusion of solutes) across the membranes can be controlled by self-regulation by the environmental temperature.

2.2 Formation and Microstructures of Grafted PNIPAM Polymers in Pore-Filling Type Thermo-Responsive Gating Membranes

In pore-filling type thermo-responsive gating membranes, the grafted functional polymers are assumed to be distributed throughout the whole membrane thickness. As a result, the thermo-responsive gating performance should be more stable than that of the pore-covering type, and the grafted chains have freely mobile ends so that the prepared membranes respond faster to the environmental stimuli when compared with crosslinked microgels. Therefore, in this chapter, most of the contents are focused on the fabrication and performance of pore-filling type thermo-responsive gating membranes with linear grafted chains.

2.2.1 Pore-Filling Type Thermo-Responsive Gating Membranes Fabricated by Plasma-Induced Grafting Polymerization

Plasma-induced grafting polymerization is usually used to prepare pore-filling type thermo-responsive gating membranes. In this section, the preparation, microstructure and performance of pore-filling type thermo-responsive gating membranes fabricated by plasma-induced grafting polymerization will be introduced.

2.2.1.1 Brief Introduction to Plasma-Induced Pore-Filling Graft Polymerization Method

Plasma treatment is well-known as a surface treatment technique. In the 1990s, it was found that a grafted polymer could be formed in pores of porous substrates by controlling plasma and graft polymerization conditions, [12] and a method named plasma-graft pore-filling polymerization has been successfully developed for the preparation of pore-filling functional membranes. [12,13] This technique has been reported to be able to graft a linear polymer onto the inner pore surface in a porous substrate and results in a fast response of the grafted functional polymer to stimuli. By adopting the plasma-graft pore-filling polymerization technique, [3,14] stimuli-responsive separating membrane systems with a fast response have been developed,

in which a fast response molecular recognition ion gating membrane system was featured with a response time within 30 s.^[14]

Plasma-graft pore-filling polymerization for grafting linear functional chains both on the surface and into the pores of porous membrane substrates is usually operated as follows. [3-10,14] Briefly, the porous substrate membrane is placed in a transparent glass tube, which is then filled with argon gas. The tube is then evacuated to a pressure of 10 Pa, and the porous substrate membrane is subjected to a radio-frequency plasma operating at 13.56 MHz and delivering at about 10 to 30 W for about 60 s. After that, the membrane is immersed into the monomer solution and the graft polymerization takes place in a shaking constant-temperature bath (usually at 30 °C for PNIPAM grafting) for a predetermined length of time. The polymerization time is usually from several tens of minutes to several tens of hours. A typical schematic illustration of the equipment for plasma-induced grafting polymerization is shown in **Fig.2.2.** The grafted membrane is then rinsed in well-deionized water under vibration in a constant-temperature bath for more than 24 h to remove any non-reacted monomer and homopolymer, and finally the membrane is dried in an oven at 50 °C overnight.

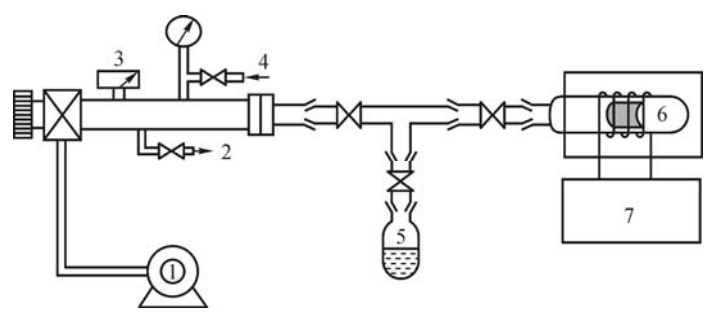


Fig.2.2. Schematic illustration of typical equipment for plasma-induced grafting polymerization. (1) Vacuum pump; (2) Air outlet; (3) Vacuum gauge; (4) Air inlet; (5) Monomer tube; (6) Substrate membrane tube; (7) Plasma generator

2.2.1.2 Formation and Microstructures of Thermo-Responsive Gating Membranes Prepared by Plasma-Induced Pore-Filling Graft Polymerization

To verify the formation of grafted polymers inside the porous membranes, the grafted polymer formation profile of the flat porous substrate was measured using the microscopic Fourier transform infrared (FT-IR) mapping method (MAGNA-IR 560 with Nic-Plan, Nicolet, USA). The PNIPAM-grafted polyethylene (PNIPAM-g-PE) membrane sample was sliced using a microtome, and the sliced sample was scanned by FT-IR. The spectra were collected in up to 10-μm steps along the membrane axial thickness. The aperture size of each measurement was 10×50 μm². The profile of the grafted polymer formation was obtained by measuring the ratio of the characteristic PNIPAM peak (amide II peak, 1,550 cm⁻¹) to the characteristic

polyethylene substrate peak (methylene peak, 1,450 cm⁻¹). **Fig.2.3a** compares the IR spectra of a polyethylene porous membrane before and after the plasma-graft pore-filling polymerization of PNIPAM. ^[10] The polyethylene substrate exhibits a characteristic methylene peak at 1,450 cm⁻¹. After grafting PNIPAM onto the PE substrate, two characteristic peaks of PNIPAM, the amide I peak (1,650 cm⁻¹) and the amide II peak (1,550 cm⁻¹), appear beside the methylene peak.

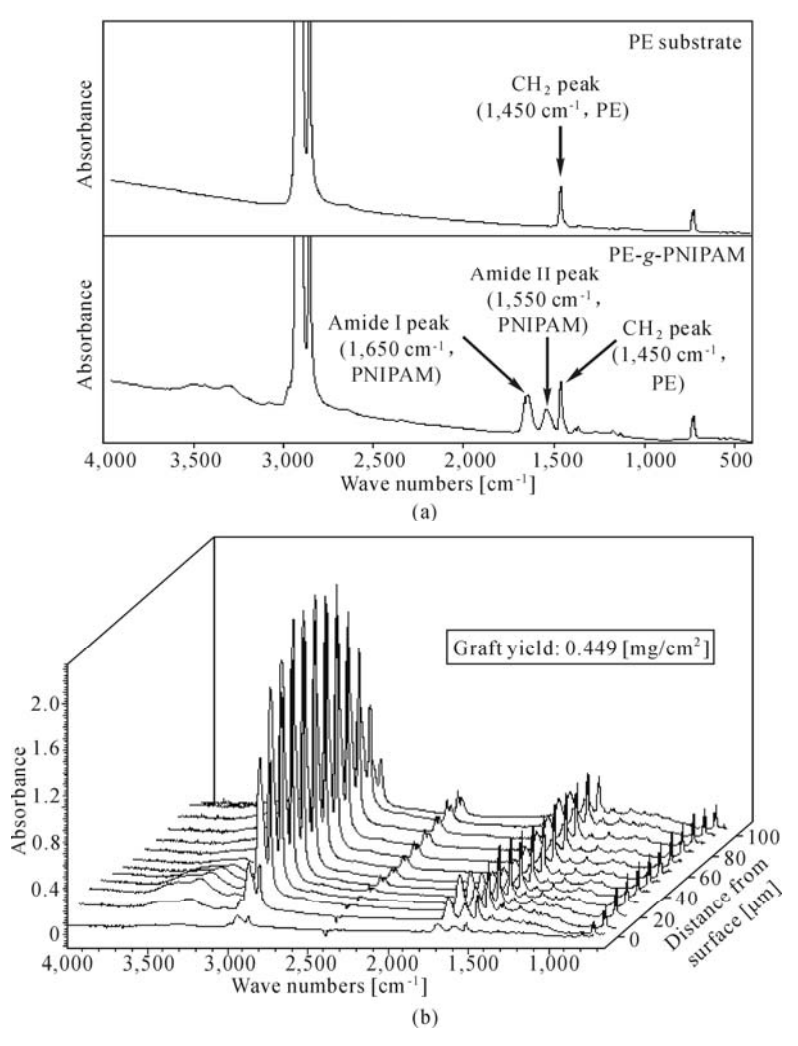


Fig.2.3. (a) IR spectra of a polyethylene porous membrane before and after the plasma-graft pore-filling polymerization of PNIPAM; (b) A typical IR-mapping spectrum across the thickness of the PNIPAM-g-PE membrane (the degree of grafting = 0.449 mg/cm², step distance = 10 μ m) (Reproduced with permission from Ref. [10]). Copyright (2003), John Wiley and Sons

Therefore, the grafted polymer formation profile could be determined by measuring the height ratio of the PNIPAM characteristic peak to the polyethylene substrate characteristic peak. **Fig.2.3b** shows a typical IR-mapping spectrum across the PNIPAM-*g*-PE membrane thickness.^[10] The PNIPAM peaks exist throughout the entire membrane thickness. That implies that the PNIPAM chains were grafted onto the inner surfaces of the pores throughout the entire thickness of the porous membrane. The height ratio of the characteristic PNIPAM peak (amide II peak) to the characteristic polyethylene substrate peak was used to quantitatively characterize the grafting composition of PNIPAM across the membrane thickness. **Fig.2.4a** shows a profile of the FT-IR absorbance ratio of the amide II peak to the polyethylene peak in the PNIPAM-grafted membranes.^[10] The absorbance ratio was plotted against the distance from the membrane surface. The results show that a roughly homogeneous graft was formed throughout the entire thickness of the membrane. The height ratio of the amide II peak to the characteristic polyethylene peak was found to be directly proportional to the graft yield of PNIPAM, indicating that the grafted polymer formed homogeneously in the pores of the membranes (as illustrated in **Fig.2.4b**).

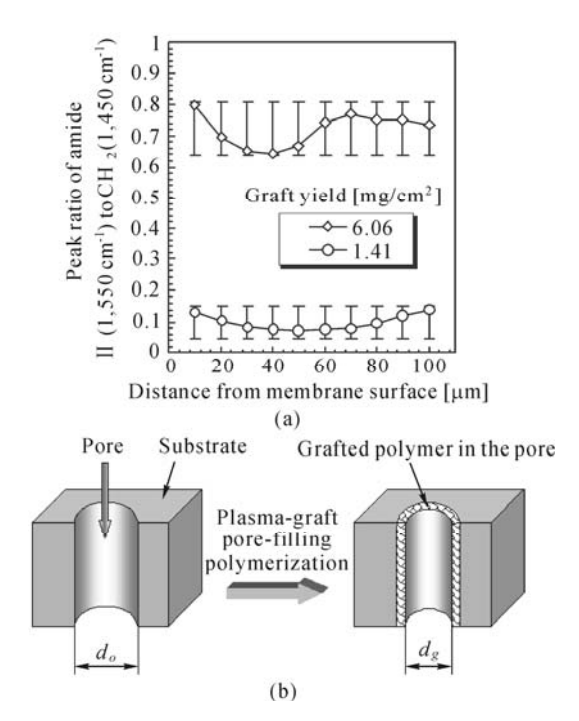


Fig.2.4. (a) Grafted polymer formation profile on a cross-section of PNIPAM-g-PE membrane; (b) A schematic illustration of the membrane pore before and after grafting PNIPAM onto the inner pore surfaces (Reproduced with permission from Ref. [10]). Copyright (2003), John Wiley and Sons

Polycarbonate track-etched (PCTE) membranes are considered as excellent substrates to study the microstructures of PNIPAM-grafted membranes because of their standard cylindrical and straight pores and narrow pore size distribution. To observe microstructures of thermo-responsive gating membranes more directly, the PNIPAM was grafted on PCTE porous membrane substrates by using a plasma-graft pore-filling polymerization method, and the microscopic configuration of the PNIPAM-g-PCTE membranes were systematically investigated by employing scanning electron microscope (SEM, JSM-5900LV, Hitachi Com., Japan). ^[7] To observe the cross-sections, membrane samples were put into liquid nitrogen for enough time, fractured mechanically and stuck to the sample holder.

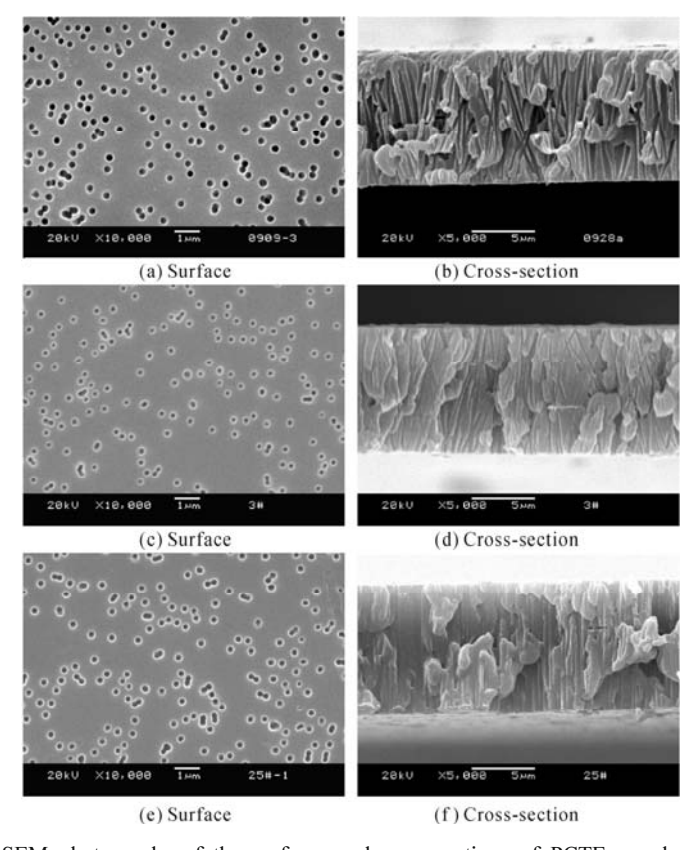


Fig.2.5. SEM photographs of the surfaces and cross-sections of PCTE membranes. (a, b) Ungrafted PCTE membrane; (c, d, e, f) PNIPAM-g-PCTE membranes with pore-filling ratio of 57.0% (c, d) and 76.1% (e, f) respectively (Reproduced with permission from Ref. [7]). Copyright (2005), Elsevier

Fig.2.5 shows SEM images of the surfaces and cross-sections of ungrafted and PNIPAM-grafted PCTE membranes.^[7] Before grafting, uniform pore geometry and cylindrical and straight pores could be clearly seen in the ungrafted membranes, as shown in **Figs.2.5a** and **2.5b**. After grafting, both surface and cross-sectional micrographs show that the membrane pore size decreased. From the surface SEM images shown in **Figs.2.5a**, **2.5c** and **2.5e**, it can be seen that the surface pores of PNIPAM-grafted membranes are smaller and the pore outlines are more obscure

when compared with those of the ungrafted membranes, but there is not a dense PNIPAM layer formed on the membrane surface even at a pore-filling ratio as high as 76.1%. From the cross-sectional SEM images shown in **Figs.2.5b**, **2.5d** and **2.5f**, it can obviously be seen that the grafted PNIPAM polymers were formed inside the pores throughout the entire membrane thickness, and the PNIPAM polymers were filled in the membrane pores gradually with the increase in the pore-filling ratio. An interesting finding is that the membrane thickness did not change significantly after the PNIPAM grafting, even at a high pore-filling ratio (e.g., F=76.1%). It is because the grafted PNIPAM layer was very thin and the membrane thickness variation was not apparently observable. The above results verified again that, by introducing the plasma-graft pore-filling polymerization method, functional polymer PNIPAM could be grafted on both the outer surfaces of the membrane and the inner surfaces of the membrane pores, just as illustrated in **Fig.2.4b**.

An atomic force microscope (AFM, SPA400, SII. Com., Japan) was used to investigate the pore shape and depth changes of PNIPAM-g-PCTE membrane in a dry state and in deionized water. Tapping mode and Si $_3$ N $_4$ cantilevers (DF3) were employed to obtain DFM (dynamic atomic force microscopy) images. **Fig.2.6** shows AFM images of the surfaces of ungrafted and PNIAPM-grafted PCTE membranes and corresponding measured depths of membrane pores. The AFM micrographs describe the variation of the pore size and measured pore depth of ungrafted and PNIPAM-grafted PCTE membranes, both in a dry state and in water. In a dry state, the pore size only changed a little after grafting PNIPAM onto the PCTE membrane, which can be seen from **Figs.2.6a** and **2.6b**. On the other hand, when the PNIPAM-grafted PCTE membrane was immersed in water at $T \approx 30$ °C, the pore size became smaller and the measured pore depth became significantly shallower, when compared with those in a dry state, as shown in **Fig.2.6c**.

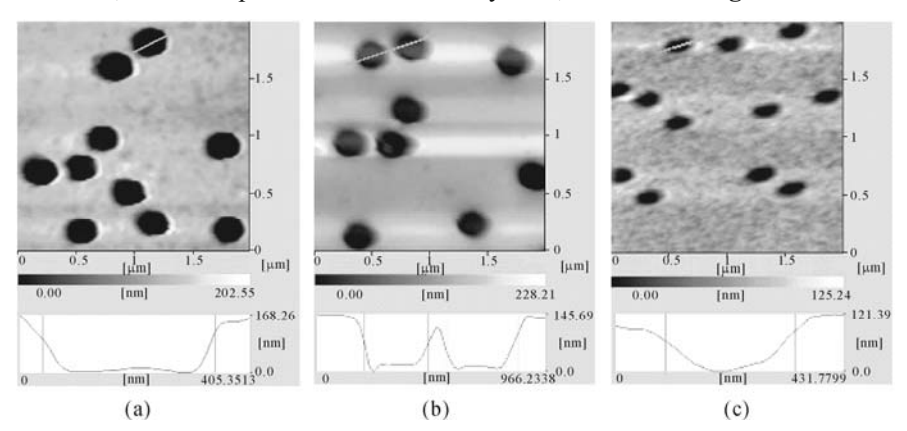


Fig.2.6. AFM photographs of surfaces of PCTE membranes and cross-sectional plots showing the depths of the pores along the green lines in the AFM photographs. (a) Ungrafted membrane in dry state; (b, c) PNIPAM-grafted membranes with pore-filling ratio of 67.0% in dry state (b) and in water at about 30 °C (c) respectively (Reproduced with permission from Ref. [7]). Copyright (2005), Elsevier

2.2.2 Pore-Filling Type Thermo-Responsive Gating Membranes Fabricated by Atom-Transfer Radical Polymerization

Atom-transfer radical polymerization is used to prepare pore-filling type thermoresponsive gating membranes with more controllable grafted chains. In this section, the preparation, microstructure and performance of pore-filling type thermoresponsive gating membranes fabricated by atom-transfer radical polymerization will be introduced.

2.2.2.1 Brief Introduction to Atom-Transfer Radical Polymerization Method

The atom-transfer radical polymerization (ATRP) method has been proven to be valid when initiating polymerization for a wide range of monomers and water can be used as the solvent for ATRP. [15-22] Moreover, the ATRP method is simple, with good repeatability, because there is no need to add external power such as UV light, γ -ray, or thermal energy and the deoxygenating condition in ATRP is not so strict compared with the plasma-induced grafting method. [23] Therefore, the ATRP method could provide an effective way of preparing PNIPAM-grafted gating membranes with grafted PNIPAM chains of controllable length and density in the pores.

Recently, PNIPAM-grafted anodic aluminum oxide (PNIPAM-g-AAO) gating membranes were prepared by grafting linear PNIPAM chains onto the pore surfaces of porous AAO substrate membranes with the ATRP method at room temperature. [24] Because the porous inorganic AAO membrane possesses a simple chemical composition and narrowly-distributed straight pores, it is convenient to verify the graft polymerization by Fourier transform infrared (FT-IR) or scanning electron microscope (SEM). Furthermore, there are abundant hydroxyl groups on the AAO membrane surface and the pore surface so that the AAO substrate membrane could be easily modified. As shown in Fig.2.7, the ATRP initiator (-Br) must be introduced onto the AAO membrane before grafting PNIPAM. The immobilization of -Br onto the AAO substrate membrane included two steps: silanization and acylation. In the first step, the hydroxyl groups on the AAO substrate membrane were activated by 3-aminopropyl trimethoxysilane (ATMS). The AAO substrate membrane was immersed in a mixture of 0.5 ml of ATMS and 79.5 ml of toluene and treated ultrasonically for 30 s to remove the bubbles in the membrane pores. The silanization reaction was terminated after a certain period of time (within 30 min) by rinsing the membrane with ethanol for 24 h. The resultant membrane with -NH₂ groups was then treated ultrasonically for 10 s to remove the ATMS which was physically adsorbed on the membrane. The membrane was then dried at 50 °C for 8 h. In the second step, the amino groups on the membrane reacted with 2-bromoisobutyryl bromide (BIBB). The membrane with -NH₂ groups was firstly put into 97 ml of dry dichloromethane containing dry triethylamine (2 vol%). Afterwards, 1 ml of BIBB was added dropwise into the solvent for

10 min with an ice bath. The membrane was treated ultrasonically for 30 s to make sure that the $-NH_2$ groups in the membrane pores could contact the BIBB solution sufficiently.

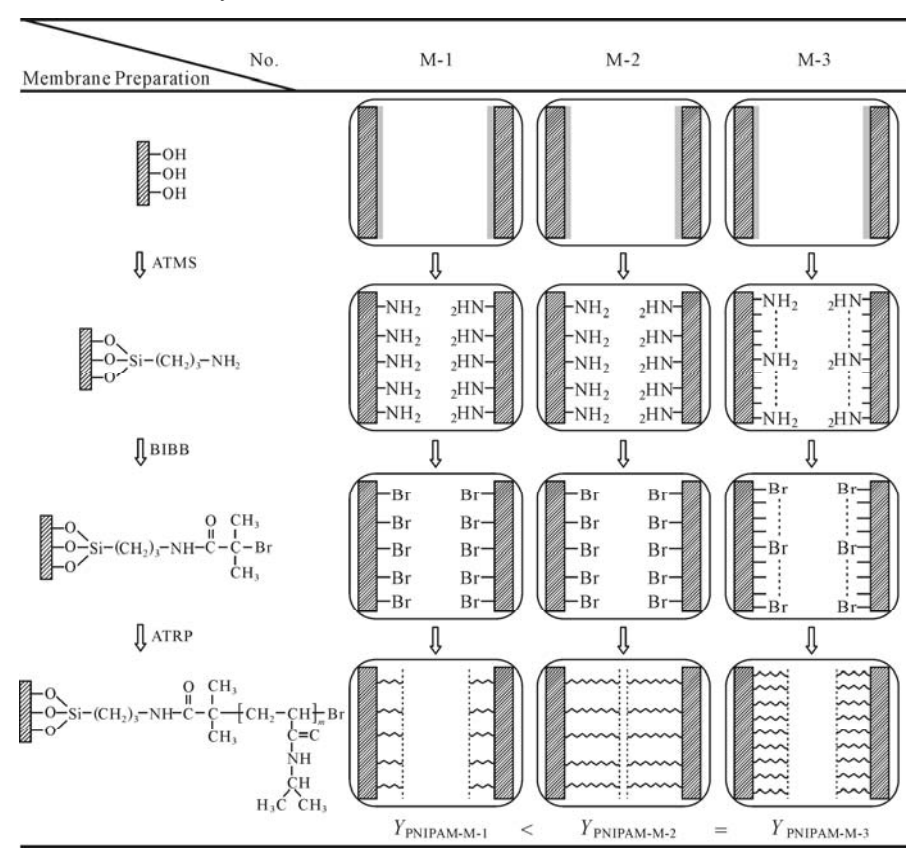


Fig.2.7. Schematic illustration of preparation of PNIPAM-g-AAO membranes with controllable length and density of grafted PNIPAM chains by ATRP method. Membranes No. M-1 and M-2 are controlled to have almost the same density of $-NH_2$ and -Br, and the density of $-NH_2$ and -Br on the membrane No. M-3 is controlled to be larger than that on No. M-1 and M-2. The grafting yields (Y_{PNIPAM}) of membranes M-1, M-2 and M-3 are controlled to be $Y_{PNIPAM-M-1} < Y_{PNIPAM-M-2} = Y_{PNIPAM-M-3}$. As a result, the dens8ities of the grafted PNIPAM chains on M-1 and M-2 are the same but both are smaller than that on M-3, and the length of the grafted PNIAPM chains on M-2 is the longest (Reproduced with permission from Ref. [24]). Copyright (2009), Elsevier

The reaction was carried out for 4 h at room temperature. The resultant membrane with –Br groups was then washed with ethanol for 24 h and dried at 50 °C for 8 h. The thermo-responsive PNIPAM-g-AAO membrane was fabricated by reacting the –Br groups on the membrane with NIPAM monomers during the subsequent ATRP. The membrane with –Br groups was immersed in a degassed solution of NIPAM for several hours (*i.e.*, 2 to 12 h). The degassed NIPAM solution was a mixture of 12.5 ml H₂O and 7.5 ml of methanol containing 0.016 g

of CuBr, 0.005 g of CuBr₂ and 0.14 ml of 1,1,4,7,7-pentamethyl diethylenetriamine (PMDTA), wherein CuBr and CuBr₂ were used as catalysts and PMDTA was used as ligand. After the polymerization, the PNIPAM-g-AAO membrane was washed by immersing in deionzed water for 8 h, which was subsequently decanted to remove the residual unreacted components. The washing process was repeated at least 3 times, and then the PNIPAM-g-AAO membrane was dried at 50 °C for 12 h.

During the fabrication process of the membrane with -Br groups, the densities of $-NH_2$ and -Br on the membrane were defined as the mass change ratio of membranes after and before generating $-NH_2$ or -Br groups, which can be calculated as in Eqs. (2.1) and (2.2):^[24]

$$NH_{2}\% = \frac{m_{NH_{2}} - m_{0}}{m_{0}} \times 100\% \times 0.186$$
 (2.1)

Br% =
$$\frac{m_{\text{Br}} - m_{\text{NH}_2}}{m_{\text{NH}_3}} \times 100\% \times 0.533$$
 (2.2)

where NH₂% and Br% are the densities of $-NH_2$ and -Br on the membranes, respectively [wt%]; m_0 , m_{NH_2} and m_{Br} are the masses of substrate membrane, membrane with $-NH_2$ groups and membrane with -Br groups, respectively [g]; The coefficients, 0.186 and 0.533, are the mass ratio of $-NH_2$ to $-(CH_2)_3NH_2$ groups and that of -Br to $-(C=O)C(CH_3)_2Br$ group, respectively [-]. Because PNIPAM chains grafted on the PNIPAM-g-AAO membrane were fabricated from the -Br active sites, the density of grafted PNIPAM chains on the PNIPAM-g-AAO membrane was equal to the -Br density before grafting PNIPAM.

The grafting yield of PNIPAM on the PNIPAM-g-AAO membrane was defined as the mass increase ratio after grafting PNIPAM and calculated by Eq.(2.3), [24] which reflected the length and density of PNIPAM chains grafted on the membrane pores.

$$Y_{\text{PNIPAM}} = \frac{m_{\text{PNIPAM}} - m_{\text{Br}}}{m_{\text{Br}}} \times 100\%$$
 (2.3)

where Y_{PNIPAM} stands for the grafting yield of PNIPAM on PNIPAM-g-AAO membrane [wt%], and m_{PNIPAM} is the mass of the PNIPAM-g-AAO membrane [g].

In order to investigate the effects of preparation conditions in ATRP polymerization on the density and length of grafted PNIPAM chains, a series of PNIPAM-*g*-AAO membranes were prepared by changing the grafting temperature, grafting time, concentration of NIPAM monomer and the density of –Br on the membrane, in turn. When one parameter changed, the other parameters remained unchanged. First, the effect of grafting temperature on the grafting yield of PNIPAM chains was studied by using the grafting temperature as the only variable while keeping the other three factors constant. Specifically, the –Br densities on the series of membranes were fixed in the narrow range of 0.08 – 0.09 wt% and the feed concentration of NIPAM monomer and grafting time were kept constant at 0.05 g/ml and 120 min, respectively. Considering the LCST of PNIPAM is ~32 °C, the grafting temperature varied from 25 °C to 60 °C. As the grafting temperature

increases, the grafting yield $Y_{\rm PNIPAM}$ of PNIPAM-g-AAO membranes increases linearly (**Fig.2.8a**). This result is not exceptional; the higher the grafting temperature is, the higher the reactivity of the catalyst and the monomers, and as a result the higher the grafting yield $Y_{\rm PNIPAM}$ is. When the –Br density is the same, higher $Y_{\rm PNIPAM}$ results in a longer length of grafted PNIPAM chains. That is to say, the PNIPAM-g-AAO membranes with controllable length of grafted PNIPAM chains can be achieved by varying the grafting temperature if the –Br density and the grafting time are fixed.

The effect of grafting time on the $Y_{\rm PNIPAM}$ of PNIPAM-g-AAO membranes is shown in Fig.2.8b. The –Br density of membranes is fixed in the range of 0.09 – 0.13 wt%, the grafting temperature is fixed at 25 °C, and the feed concentration of the NIPAM monomer is 0.05 g/ml, in this case. The $Y_{\rm PNIPAM}$ rapidly increases with grafting time when the grafting time is within 480 min; however, it increases slowly with increasing grafting time when the grafting time is beyond 480 min. This phenomenon is similar to that in several surface-initiated ATRP researches. [22,25] The reason might be that the –Br terminal groups lose due to the radical coupling and disproportionation reactions when the grafting time is beyond 480 min. Because the –Br groups are active sites for radical polymerization of NIPAM monomers, the reaction is gradually terminated when the –Br groups lose. The results show that the length of grafted PNIPAM chains on PNIPAM-g- AAO membranes can be regulated by varying the grafting time when the –Br density and grafting temperature are fixed.

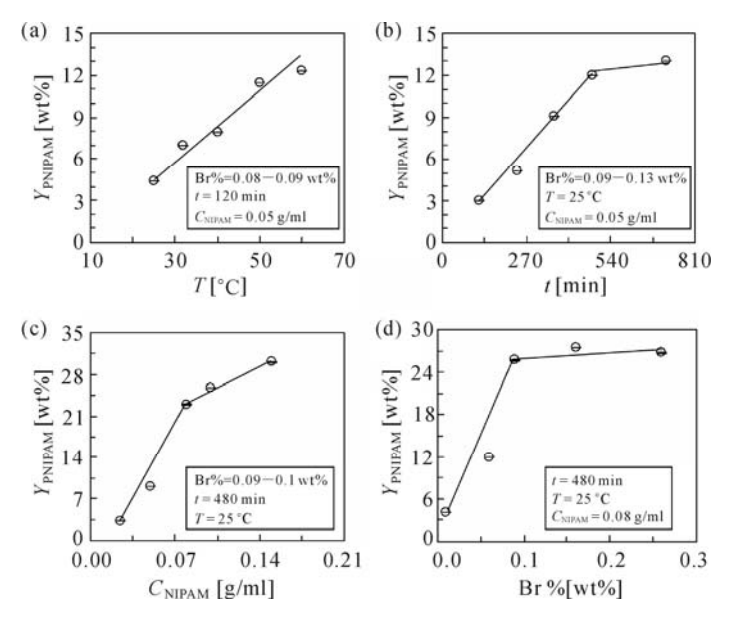


Fig.2.8. Effects of (a) grafting temperature (T), (b) grafting time (t), (c) feed concentration of NIPAM monomer (C_{NIPAM}) and (d) density of –Br on membrane (Br%) on the grafting yield of PNIPAM of PNIPAM-g-AAO membranes (Y_{PNIPAM}) in the ATRP grafting polymerization (Reproduced with permission from Ref. [24]). Copyright (2009), Elsevier

The effect of the concentration of the NIPAM monomer on the grafting yield of the PNIPAM-g-AAO membrane is shown in Fig.2.8c. In the ATRP, the -Br density is fixed in the range of 0.09 - 0.1 wt\%, the grafting temperature is fixed at 25 °C, and the grafting time is fixed as 480 min. Generally, Y_{PNIPAM} increases with an increase in the NIPAM concentration of monomer solution. Y_{PNIPAM} goes up more sharply with an increase in the NIPAM concentration when the NIPAM concentration is less than 0.08 g/ml than it does when the NIPAM concentration is higher than 0.08 g/ml. At the beginning of ATRP, NIPAM monomers are initiated to polymerize at the active sites (i.e., -Br groups) both on the membrane surface and inside pores. When the NIPAM concentration is less than 0.08 g/ml, the length of grafted PNIPAM chains is not long enough to prevent the NIPAM monomers from entering the membrane pores throughout the whole polymerization reaction. Therefore, all the -Br groups on both the membrane surface and the inner surfaces of pores contribute to the polymerization from beginning to end. However, when the NIPAM concentration is higher than 0.08 g/ml, the length of grafted PNIPAM chains could be so long that NIPAM monomers are prevented from entering the membrane pores in the later period of the polymerization reaction. As a result, the Y_{PNIPAM} only increases slowly with an increase in the NIPAM concentration when the NIPAM concentration is higher than 0.08 g/ml.

The effect of –Br density on the Y_{PNIPAM} of PNIPAM-g-AAO membranes is shown in Fig.2.8d. During ATRP, the grafting temperature is fixed at 25 °C, the concentration of the NIPAM monomer and the grafting time are fixed at 0.08 g/ml and 480 min, respectively. In general, higher -Br density on the membrane leads to higher grafting yield Y_{PNIPAM} of the PNIPAM-g-AAO membrane. The membranes with different densities of -NH2 groups on the membrane are controllably prepared by changing the reaction time during the preparation of membranes with -NH₂ groups. Longer reaction time leads to higher density of the -NH₂ groups on the membrane and, as a result, more -Br groups introduced on the membrane. When the –Br density is lower than 0.09 wt%, Y_{PNIPAM} increases linearly with an increase in the -Br density. However, Y_{PNIPAM} only increases slightly when the -Br density increases from 0.09 to 0.28 wt%. When the -Br density is lower than 0.09 wt%, the NIPAM content in the monomer solution is excessive for radical polymerization, the Y_{PNIPAM} of the PNIPAM-g-AAO membrane increases linearly with an increase in the –Br density. However, when the –Br density is higher than 0.09 wt%, because of the limit of NIPAM content in the monomer solution, the Y_{PNIPAM} of the PNIPAM-g-AAO membrane could only increase slowly with an increase in the –Br density.

To summarize, with the ATRP method, precise control over the length and density of grafted PNIPAM chains on the PNIPAM-g-AAO membranes can be achieved by adjusting the grafting temperature, grafting time, NIPAM concentration of monomer solution and the density of –Br groups.

2.2.2.2 Formation and Microstructures of Thermo-Responsive Gating Membranes Prepared by ATRP Method

FT-IR was used to characterize the chemical formation of PNIPAM-*g*-AAO membranes at different preparation stages in ATRP polymerization. **Fig.2.9** illustrates the FT-IR spectra of AAO substrate membrane, membrane with –NH₂ groups, membrane with –Br groups and PNIPAM-*g*-AAO membrane.^[24] Compared with that of the AAO substrate membrane (**Fig.2.9a**), an additional peak of methylene group (–CH₂) appears at 2,931 cm⁻¹ in the FT-IR spectrum of the membrane with –NH₂ groups (**Fig.2.9b**). This peak of the methylene group is a characteristic peak of ATMS. In **Fig.2.9c**, the peaks of carbonyl group (–C=O) at 1,641 cm⁻¹ and the methyl group (–CH₃) at 2,990 cm⁻¹ are the characteristic peaks of BIBB, which show that the –Br groups have been successfully introduced onto the membrane by silanization and acylation. In **Fig.2.9d**, the characteristic peaks of PNIPAM, especially newly-emerged isopropyl group (–CH(CH₃)₂) at 1,368 and 1,388 cm⁻¹ are clearly observed in the spectrum of the PNIPAM-*g*-AAO membrane, which indicates that the PNIPAM-*g*-AAO membrane has been successfully fabricated by the ATRP method.

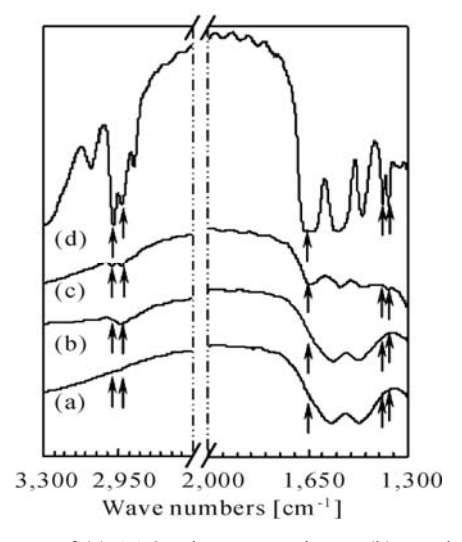


Fig.2.9. The FT-IR spectra of (a) AAO substrate membrane, (b) membrane with $-NH_2$ groups $(NH_2\% = 0.15 \text{ wt\%})$, (c) membrane with -Br groups (Br% = 0.06 wt%) and (d) PNIPAM-g-AAO membrane $(Y_{PNIPAM} = 11.9 \text{ wt\%})$ (Reproduced with permission from Ref. [24]). Copyright (2009), Elsevier

The morphologies of membranes and membrane pores are characterized using SEM. **Fig.2.10** shows SEM micrographs of surfaces and cross-sections of AAO substrate membrane and PNIPAM-g-AAO membrane with $Y_{PNIPAM} = 11.9 \text{ wt}\%$. [24] Compared with the AAO substrate membrane, the PNIPAM-g-AAO membrane has significantly different microstructures. As shown in **Figs.2.10a** to **2.10d**, the

AAO substrate membrane is obviously featured with a uniform straight pore structure with a different pore size on the upper and lower surfaces. After grafting PNIPAM into the membrane pores, the pore size of the PNIPAM-g-AAO membrane becomes smaller (as shown in Figs.2.10a' and 2.10c'). According to the SEM images, the grafted PNIPAM layer inside the pores of the PNIPAM-g-AAO membranes is uniform and no pore is blocked (Figs.2.10b' and 2.10d'). The SEM micrographs show that PNIPAM can be homogeneously grafted in the pores of porous AAO substrate membranes by employing the ATRP method.

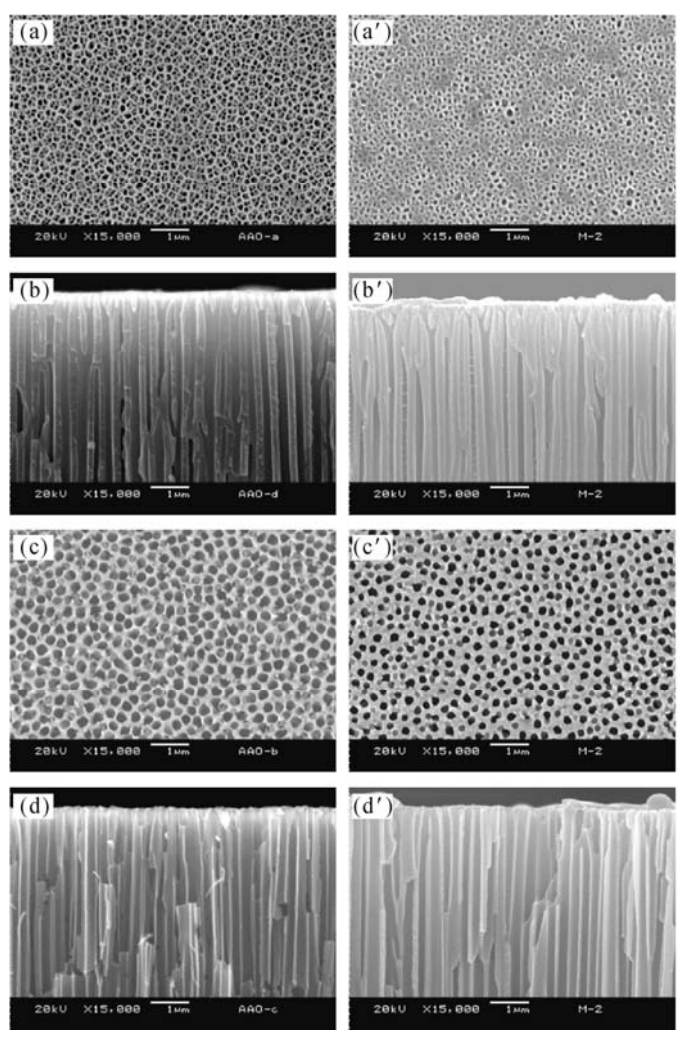


Fig.2.10. SEM mirographs of AAO substrate membrane (a, b, c, d) and PNIPAM-g-AAO membranes with $Y_{PNIPAM} = 11.9$ wt% (a', b', c', d'). (a, a') Top surfaces, (b, b') top cross-sections, (c, c') bottom surfaces and (d, d') bottom cross-sections (Reproduced with permission from Ref. [24]). Copyright (2009), Elsevier

2.3 Effect of the Grafting Yield on Thermo-Responsive Gating Characteristics of Pore-Filling Type PNIPAM-Grafted Membranes

The grafting yield has significant influence on the thermo-responsive gating characteristics of pore-filling type gating membranes. In this section, the effect of the grafting yield on thermo-responsive gating characteristics of pore-filling type PNIPAM-grafted membranes will be introduced.

2.3.1 Substrate Membranes with Regular Straight Pore Microstructures

According to the above-mentioned results, the PNIPAM chains can be considered to be grafted homogeneously, not only on the surface of the membrane but also in the pores by plasma-graft pore-filling polymerization. A schematic illustration of a PNIPAM-grafted PCTE membrane is shown in **Fig.2.11**. If porous substrate membranes with regular straight pore microstructures (*e.g.*, above-mentioned PCTE or AAO membrane) are used as substrates to fabricate PNIPAM-grafted membranes, a coefficient called the pore-filling ratio (*F*) can be used to characterize the grafting yield of the grafted membrane:^[7]

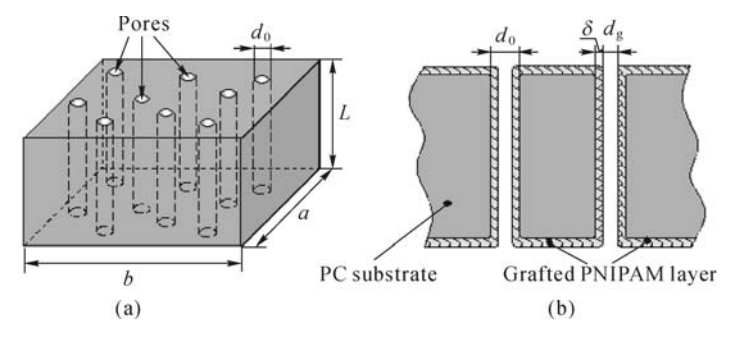


Fig.2.11. Schematic illustration of (a) three-dimensional microstructure of ungrafted PCTE membrane and (b) cross-section of PNIPAM-g-PCTE membrane (Reproduced with permission from Ref. [7]). Copyright (2005), Elsevier

$$F = \frac{V_{p,g}}{V_p} = 1 - \left(\frac{d_g}{d_0}\right)^2 = 1 - \left(1 - \frac{2\delta}{d_0}\right)^2$$
 (2.4)

where $V_{\rm p,g}$ is the volume of the grafted PNIPAM polymer in the pore (cm³), $V_{\rm p}$ is the volume of the pore before grafting PNIPAM (cm³), d_0 and $d_{\rm g}$ stand for the average pore diameters before and after grafting PNIPAM respectively (μ m), and δ is the uniform thickness of the grafted PNIPAM layer (μ m). According to the

above presumption, δ can be estimated by the ratio of the total volume of the grafted PNIPAM layer to the total grafting area. The total volume of the grafted PNIPAM layer can be obtained from the measured weight increase of the membrane after grafting and the PNIPAM density. The total grafting area, including both the outer surface area of the membrane and the inner surface area of all the pores, can be calculated by the length, width, thickness, porosity or pore density and the pore diameter of the membrane.

The effect of the pore-filling ratio on the water flux and pore diameter ratio of PNIPAM-*g*-PCTE membranes at 25 °C and 40 °C is shown in **Fig.2.12**.^[7]

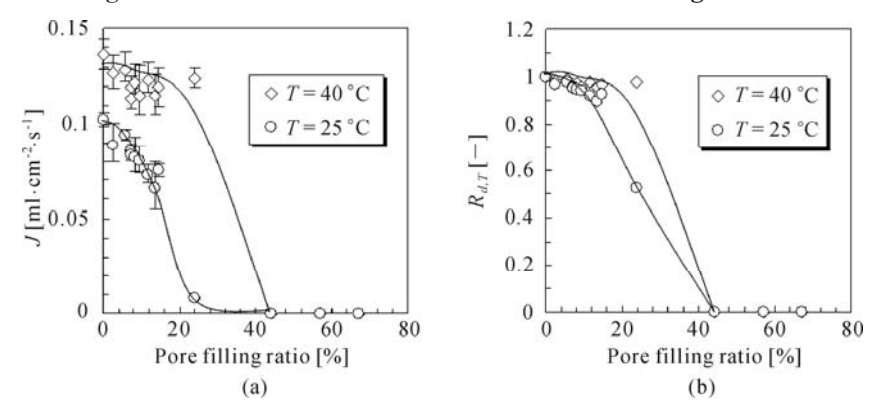


Fig.2.12. Effect of pore-filling ratios on water flux (a) and on pore diameter ratio (b) of PNIPAM-g-PCTE membranes (Reproduced with permission from Ref. [7]). Copyright (2005), Elsevier

The water flux of ungrafted PCTE membrane (F = 0) was always larger than that of PNIPAM-grafted PCTE membranes, no matter whether at 25 °C or at 40 °C, because the grafted PNIPAM layer made the pore diameters smaller. With an increase in the pore-filling ratio, the water flux of PNIPAM-grafted membranes decreased at 25 °C, as well as at 40 °C. For the grafted membranes with F < 44.2%, the water flux at 40 °C was always larger than that at 25 °C. There are two reasons for this. Firstly, the viscosity of water decreased with an increase in temperature. Secondly, the conformation of grafted PNIPAM changed when the environmental temperature changed across the LCST of PNIPAM (about 32 °C). The PNIPAM chains grafted in the membrane pores shrunk when the environmental temperature was higher than the LCST, which made the pores "open", and then the water flux was larger, while the grafted PNIPAM chains swelled when the temperature was lower than LCST, which made the pores became smaller or even "closed" and therefore the water flux was smaller. However, when the pore-filling ratio was too high (larger than 44.2%), the water flux became zero, no matter what the environmental temperature was. The pores were choked completely by the grafted PNIPAM chains at this time, and the grafted membranes did not have thermoresponsive gating characteristics any longer. It is interesting that this result is close to that of bubble-point experiments, [10] which was when the pore-filling ratio of PNIPAM-grafted polyethylene membrane was larger than 32.8% and the pores could not be blown open by the pressurized gas employing the bubble-point method at $28 \sim 29$ °C. [10]

To eliminate the effect of water viscosity on the water flux of the membrane, a coefficient called the pore diameter ratio is introduced. The pore diameter ratio $(R_{d,T})$ is defined as the ratio of the pore mean diameter of the grafted membrane to that of the ungrafted membrane at the same temperature. The water flux of a skinless porous membrane can be calculated by the Hagen-Poiseuille equation^[6,7]

$$J = \frac{n\pi d^4 p}{128nl} \tag{2.5}$$

where J is the water flux (ml·cm⁻²·s⁻¹) of the membrane, n is the number of pores per unit membrane area (cm⁻²), d is the membrane pore mean diameter (cm), p is the trans-membrane pressure (Pa), η is liquid viscosity (Pa·s) and l is the thickness of the membrane (cm).

From Eq.(2.5), the mean diameter of a skinless porous membrane can be expressed as

$$d = \sqrt[4]{\frac{128\eta lJ}{n\pi p}} \tag{2.6}$$

Therefore, the pore diameter ratio $(R_{d,T})$ can be calculated according to the following equation

$$R_{d,T} = \frac{d_{\rm g}}{d_{\rm o}} = \sqrt[4]{\frac{J_{\rm g,T}}{J_{\rm 0,T}}}$$
 (2.7)

where d_0 and $d_{\rm g}$ are the same as those in Eq.(2.4) (cm), $J_{0,\rm T}$ and $J_{\rm g,T}$ are the water fluxes of the ungrafted and PNIPAM-grafted membrane at T °C respectively (ml·cm⁻²·s⁻¹). The value of $R_{\rm d,T}$ is always smaller than 1.0, owing to the pore size of the PNIAPM-grafted membrane always being smaller than that of the ungrafted membrane.

The effect of the pore-filling ratio on the pore diameter ratio of PNIPAM-g-PCTE membranes at both 25 °C and 40 °C is shown in **Fig.2.12b**. ^[7] For the PNIPAM-grafted membranes with F < 44.2%, the values of both $R_{\rm d,40}$ and $R_{\rm d,25}$ decreased with the pore-filling ratios increasing. In addition, $R_{\rm d,40}$ was always larger than $R_{\rm d,25}$, because of the volume change of grafted PNIPAM chains in the pores at a temperature above and below the LCST. The larger the difference between $R_{\rm d,40}$ and $R_{\rm d,25}$, the more significant the thermo-responsive characteristics of the PNIPAM-g-PCTE membranes. When the pore-filling ratio was larger than 44.2%, both $R_{\rm d,40}$ and $R_{\rm d,25}$ became zero, *i.e.*, the PNIAPM-grafted membranes did not show thermo-responsive gating characteristics any longer.

Fig.2.13 shows the thermo-responsive characteristics of an ungrafted membrane and a PNIPAM-g-PCTE membrane with F=23.9%. [7] For the ungrafted membrane, the water flux just increased simply with an increase in the environmental temperature, which was due to the decrease in water viscosity with an increase in temperature. On the other hand, under the same experimental conditions, the temperature-dependent

water flux characteristic of the PNIPAM-g-PCTE membrane with F=23.9% was quite different. The water flux of the PNIPAM-g-PCTE membrane in the temperature range 25 °C to 30 °C was much lower than that in the temperature range 34 °C to 40 °C. A sharp transition in the water flux occurred on going from 30 °C to 34 °C, which corresponded to the LCST of PNIPAM (around 32 °C). Below the LCST, the grafted PNIPAM on the inner pore surface was in a swollen state and the pores in the membrane were "closed" by the PNIPAM gate; as a result the water flux was low. In contrast, the grafted PNIPAM on the inner pore surface was in a shrunken state at temperatures above the LCST, and therefore the pores in the membrane were "open" and a higher water flux was the result.

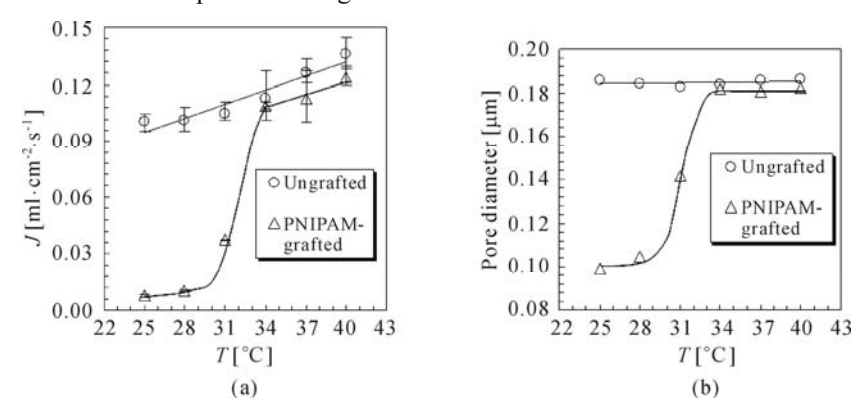


Fig.2.13. Temperature-dependent characteristics of water flux (a) and pore size (b) of ungrafted membrane and PNIPAM-g-PCTE membrane with F=23.9% (Reproduced with permission from Ref. [7]). Copyright (2005), Elsevier

According to Hagen-Poiseuille's law, the mean diameter of membrane pores can be evaluated by Eq.(2.6). As seen in **Fig.2.13b**, the pore diameter of the ungrafted membrane remained unchanged when the temperature increased from 25 °C to 40 °C, while the pore size of the PNIPAM-g-PCTE membrane changed dramatically when the temperature changed from 28 °C to 34 °C, and remained unvaried at temperatures lower than 28 °C and/or higher than 34 °C. The pore diameter of the PNIPAM-g-PCTE membrane at 40 °C was almost twice that at 25 °C.

According to the schematic illustration shown in **Fig.2.11**, the pore diameter of the PNIPAM-g-PCTE membrane in dry state can also be evaluated by using the pore-filling ratio (F) as follows:

$$d_{g} = d_{0}\sqrt{1 - F} \tag{2.8}$$

Fig.2.14 shows the comparison of the average pore size of PNIPAM-*g*-PCTE membranes in a dry state (calculated by using Eq.(2.8)) and in a wet state at 40 °C (calculated by using Eq.(2.6)).^[7] When the pore-filling ratio was smaller than 23.9%, the two calculated results were close to each other. However, with the pore-filling ratio $F \ge 44.2\%$, the situation was quite different. The pore diameter of

the membrane in a dry state, calculated from Eq.(2.8), still decreased gradually with the increase in the pore-filling ratio, while the pore diameter of the membrane with $F \ge 44.2\%$ in a wet state at 40 °C, calculated from Eq.(2.6), became zero. When the PNIPAM-g-PCTE membranes were immersed in water, the volume of the grafted PNIAPM polymers in the membrane pores might be much larger than that in a dry state because of the volume expansion of PNIPAM polymers in water, even though the PNIPAM polymers were in a shrunken state at 40 °C. Therefore, when the PNIPAM-grafted membrane was used in water filtration, *i.e.*, the membrane was immersed in water, the membrane pores could be choked by the grafted PNIPAM polymers, even though the calculated pore-filling ratio (in a dry state) was still much smaller than 100% (*e.g.*, 44.2%). From the above-mentioned experimental results, the critical pore-filling ratio for choking the pores of PNIPAM-g-PCTE membranes in water at temperatures above the LCST of PNIPAM was in the range of 30% to 40%.

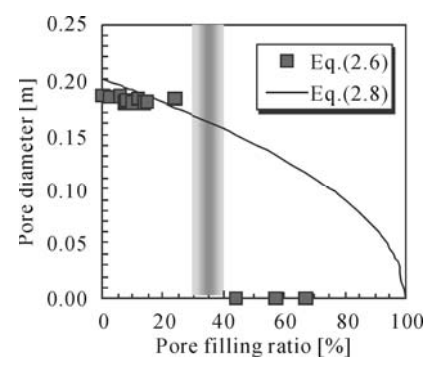


Fig.2.14. Comparison of the average pore size of PNIPAM-g-PCTE membranes in dry state (—) and in wet state at 40 °C (\blacksquare) (Reproduced with permission from Ref. [7]). Copyright (2005), Elsevier

2.3.2 Substrate Membranes with Irregular Pore Microstructures

When porous substrate membranes with irregular pore microstructures (*e.g.*, porous polyamide, polyethylene (PE) or poly(vinylidene fluoride) (PVDF) membranes) are used as substrates to fabricate PNIPAM-grafted membranes, it is difficult and accurate to calculate the above-mentioned pore-filling ratio. In this case, a more convenient coefficient called the grafting yield can be used to characterize the grafting degree of the grafted membrane, which is defined as the weight increase of the membrane after the grafting and can be calculated according to the following equation: [6,26,27]

$$Y = \frac{W_g - W_0}{W_0} \times 100\% \tag{2.9}$$

where Y(%) stands for the grafting yield of PNIPAM on the membrane substrate,

and $W_{\rm g}$ and $W_{\rm 0}$ (g) for the mass of the membrane after and before grafting respectively.

2.3.2.1 PNIPAM-grafted Nylon6 and PVDF Membranes with Irregular Pore Microstructures

Both hydrophilic Nylon6 and hydrophobic PVDF porous membranes with average pore size of 0.22 µm have been used as the porous membrane substrates for preparing PNIPAM-grafted thermo-responsive gating membranes by the plasma-graft pore-filling polymerization method. [27]

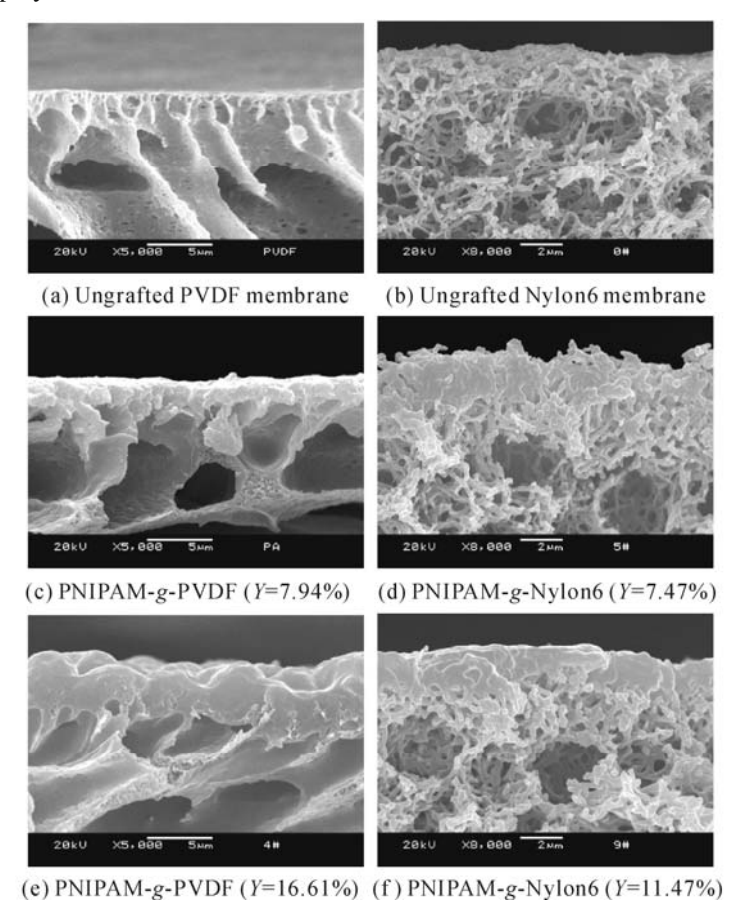


Fig.2.15. SEM micrographs of cross-sections of ungrafted and PNIPAM-grafted membranes with different substrates (Reproduced with permission from Ref. [27]). Copyright (2006), Wiley-VCH Verlag GmbH & Co. KGaA

Fig.2.15 shows SEM photographs of the cross-sections of ungrafted and PNIPAM-grafted membranes with different substrates. [27] The ungrafted PVDF

and Nylon6 substrates were both obviously constructed with a thin functional porous top layer; however, the PVDF substrate was featured with closely-packed finger-like large cavities below the skin layer, while the Nylon6 substrate was featured with honeycombed porous structures below the skin layer. After grafting, the cross-sectional structures of membranes were significantly different from those of ungrafted substrates. For both PVDF and Nylon6 membranes, grafted PNIPAM polymers were found not only on the membrane outer surface but also on the inner surfaces of the pores throughout the entire membrane thickness. With an increase in the grafting yield, the cross-sections of PNIPAM-grafted membranes became denser. The results showed that although the microstructures of the porous substrates were different, the grafting positions of PNIPAM were almost the same, *i.e.* PNIPAM could be grafted on both the membrane outer surface and the inner surfaces of membrane pores by the plasma-graft pore-filling polymerization method.

2.3.2.2 Thermo-Responsive Gating Characteristics Determined by Hydraulic Permeability

The thermo-responsive characteristics of water flux through PNIPAM-grafted membranes with different substrates are shown in Fig.2.16. [27] At the same temperature, the water flux through the ungrafted PVDF substrate was lower than that through the Nylon6 substrate, due to the hydrophilic property of Nylon6. For both ungrafted PVDF and ungrafted Nylon6 membrane substrates, the water flux increased slowly with an increase in the environmental temperature from 25 to 40 °C, which was due to the decrease in liquid viscosity resulting from the temperature increase. Under the same experimental conditions, the hydraulic permeability of the PNIPAM-g-PVDF membrane (with grafting yield of 0.19%) and the PNIPAM-g-Nylon6 membrane (with grafting yield of 7.47%) were quite different. The water fluxes through the PNIPAM-grafted membranes in a temperature range from 25 to 30 °C were much lower than those in a temperature range from 34 to 40 °C. A dramatic transition in the water flux occurred, going from 30 to 34 °C, which corresponded to the LCST of PNIPAM (around 32 °C). When the environmental temperature was below the LCST, the grafted PNIPAM chains on the inner pore surfaces were in a swollen state and the pore size decreased or pores were "closed" by the PNIPAM gates. As a result, the water flux was low. In contrast, when the environmental temperature was above the LCST, the grafted PNIPAM chains on the inner pore surfaces were in a shrunken state and therefore the pore size increased or pores were "opened" and a larger water flux was the result. The grafted PNIPAM chains in the membrane pores acted as thermo-responsive chemical gates.

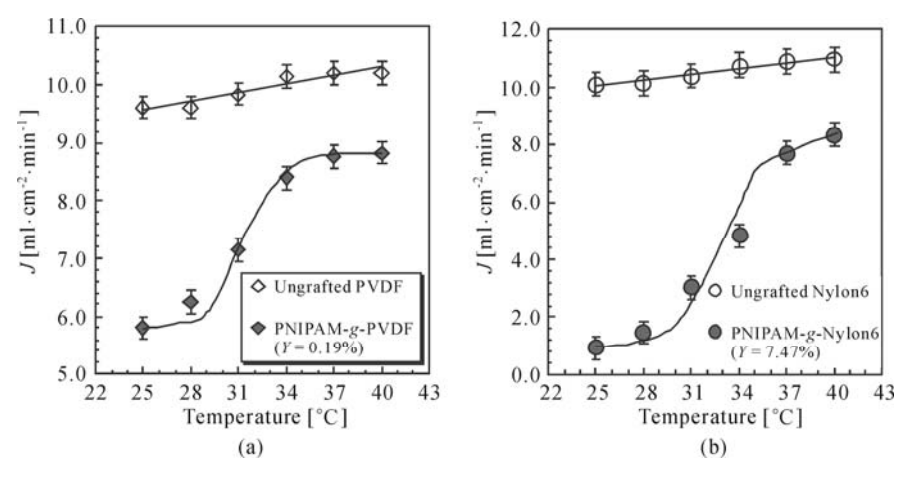


Fig.2.16. Thermo-responsive characteristics of water flux through PNIPAM-grafted membranes with different substrates: (a) PVDF substrates, (b) Nylon6 substrates (Reproduced with permission from Ref. [27]). Copyright (2006), Wiley-VCH Verlag GmbH & Co. KGaA

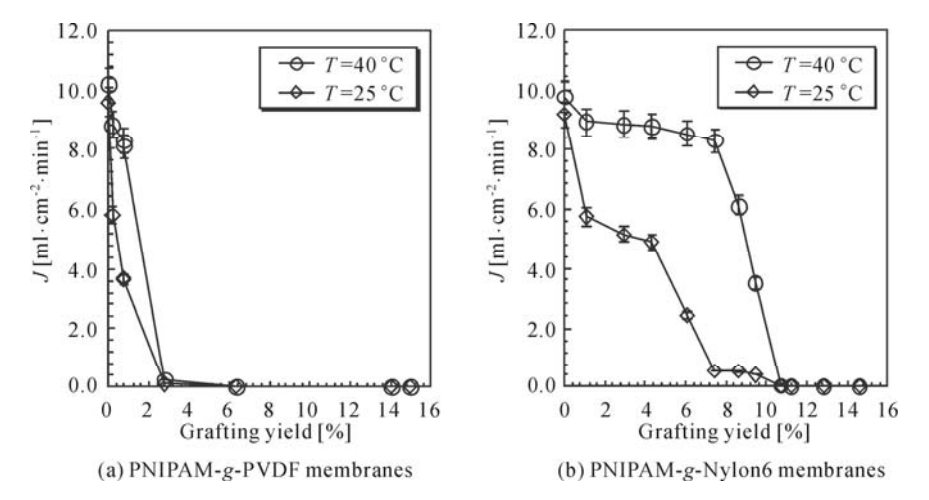


Fig.2.17. Effect of grafting yield on the water flux through PNIPAM-grafted membranes with different substrates (Reproduced with permission from Ref. [27]). Copyright (2006), Wiley-VCH Verlag GmbH & Co. KGaA

The effect of the grafting yield on the water flux through PNIPAM-grafted membranes with different substrates is shown in Fig.2.17. For both PNIPAM-grafted PVDF and Nylon6 membranes, the water fluxes decreased at both 25 °C and 40 °C with the increase in the grafting yield, because the length and density of the grafted PNIPAM chains increased with an increase in the grafting yield and then the pore sizes became smaller. On the other hand, the water flux at 40 °C was always larger than that at 25 °C because of the swelling/shrinking property of grafted PNIPAM gates. The grafted PNIPAM chains in the pores swelled at 25 °C,

and then the pore size decreased by the PNIPAM gates. Therefore the water flux was lower. However, the grafted PNIPAM chains shrunk at 40 °C and then the pore size increased. Consequently the water flux was larger. Another interesting finding was that, when the environmental temperature and grafting yield were the same, the water flux of the PNIPAM-g-Nylon6 membrane was always much larger than that of the PNIPAM-g-PVDF membrane (excepting those conditions in which the grafting yields were so large that all the water fluxes became zero). The reason was that the hydrophilic property of Nylon6 resulted in a larger water flux, while the hydrophobic property of PVDF resulted in a much lower water flux. That means the hydrophilicity of the porous substrates affected not only the water flux of the ungrafted membrane substrate but also that of the PNIPAM-grafted membrane.

The effect of the grafting yield on the thermo-responsive gating characteristics of PNIPAM-grafted membranes with different substrates is shown in **Fig.2.18**, in which the thermo-responsive gating coefficient R_J is defined as follows:^[27]

$$R_J = \frac{J_{40}}{J_{25}} \tag{2.10}$$

where J_{40} and J_{25} are the measured water fluxes at an environmental temperature of 40 °C and 25 °C, respectively (m³·m⁻²·s⁻¹). If the water fluxes are the same at 25 °C and 40 °C, the flux responsiveness coefficient R_J is defined as 1.0. That means the PNIPAM-grafted membrane has no gating function in that case.

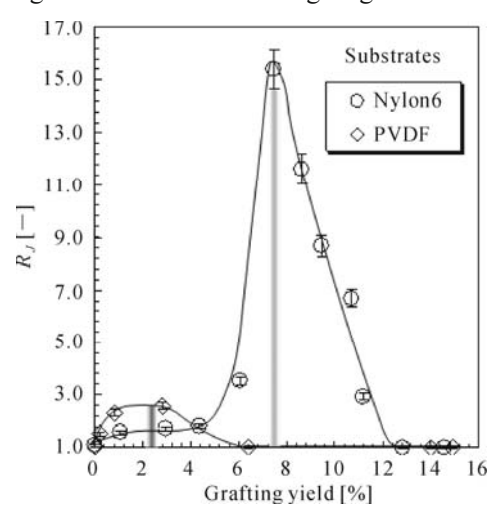


Fig.2.18. Effect of grafting yield on the thermo-responsive gating characteristics of PNIPAM-grafted membranes with different substrates (Reproduced with permission from Ref. [27]). Copyright (2006), Wiley-VCH Verlag GmbH & Co. KGaA

For the PNIPAM-g-Nylon6 membranes, only when the grafting yield was less than 12.84% could the grafted PNIPAM chains in the membrane pores act as thermo-responsive gates, *i.e.*, the membranes had no gating function in the

filtration experiments when the grafting yield was larger than 12.84%. When the grafting yield was larger than 12.84%, the length and density of the grafted PNIPAM chains were too long and large, resulting in the pores being choked by the grafted polymers. Therefore, the water flux through the PNIPAM-grafted membranes tended to zero at both 25 °C and 40 °C, and then the thermo-responsive gating coefficient tended to 1.0. When the grafting yield was 7.47%, the thermoresponsive gating coefficient R_J was the largest one (as large as 15.41). When the grafting yield was less than 7.47%, the thermo-responsive gating coefficient increased with an increase in the grafting yield. However, the situation was the opposite when the grafting yield was larger than 7.47% and the gating coefficient R_J tended to 1.0 when the grafting yield approached 12.84%. On the other hand, for the PNIPAM-g-PVDF membranes, the situation was quite different. The critical grafting yield of PNIPAM for choking the membrane pores was as low as 6.38%, and the optimum grafting yield for thermo-responsive gating was 2.81%, with the largest gating coefficient R_J merely 2.54. That means the thermoresponsive gating coefficient R_J of the PNIPAM-g-Nylon6 membrane was much larger than that of the PNIPAM-g-PVDF membrane. The phenomena should result from the difference in the physical and chemical properties, such as the hydrophilicity and microstructure of the porous substrates.

Because of the hydrophilic property of Nylon6, the porous Nylon6-based membranes are featured with the capability of saving up water or the property of retaining water, which is depended on the micro pores, the capillary interspaces between the fibers and the environmental humidity. When the humidity is more than 99%, or the fibers have already been completely saturated with water, the micro pores and capillary interspaces in the Nylon6-based membranes can be filled with water. In the experiments, the membranes were all immersed in well-deionized water for six hours before the filtration operation. The PNIPAM-g-Nylon6 membranes, which were very wet due to the hydrophilicity of Nylon6 substrates, could let the water easily get through the pores. On the other hand, the PNIPAM-g-PVDF membranes were just slightly wet due to the hydrophobicity of PVDF substrates, and then the permeation of water through the membranes was prevented to some extent. As a result, the water flux and the largest thermoresponsive gating coefficient R_J of PNIPAM-g-Nylon6 membranes were larger than those of the PNIPAM-g-PVDF membranes.

Another interesting phenomenon was that, when the thermo-responsive gating coefficient R_J was at its peak, the corresponding optimum grafting yield of PNIPAM for the PNIPAM-g-Nylon6 membranes was much larger than that of the PNIPAM-g-PVDF membranes. For the PNIPAM-g-Nylon6 membranes, the optimum grafting yield of PNIPAM corresponding to the largest R_J was 7.47%, while that for the PNIPAM-g-PVDF membranes was just 2.81%. A reasonable explanation for this phenomenon could be described as the effect of the difference in the microstructures of the porous substrates.

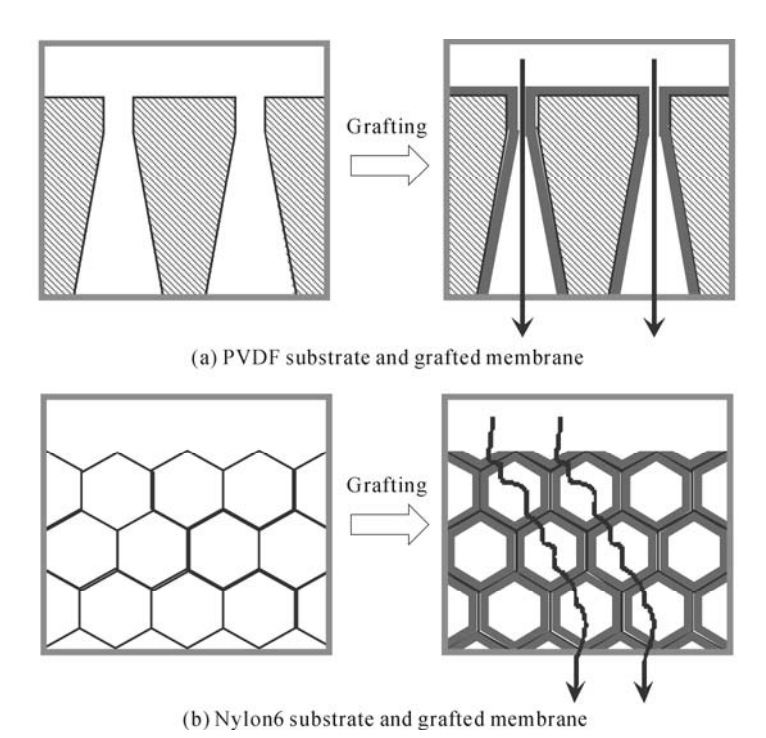


Fig.2.19. Schematic illustration of the microstructures of cross-sections of PNIPAM-grafted membranes with different porous substrates prepared by plasma-graft pore-filling polymerization (Reproduced with permission from Ref. [27]). Copyright (2006), Wiley-VCH Verlag GmbH & Co. KGaA

Fig.2.19 shows the schematic illustration of the microstructures of cross-sections of PNIPAM-grafted membranes with different porous substrates prepared by plasma-graft pore-filling polymerization. [27] From the SEM images shown in Fig.2.15, the grafted PNIPAM polymers have been found to be formed not only on the membrane outer surface but also on the inner surfaces of the pores throughout the entire membrane thickness. The PVDF membranes were featured with finger-like pores with a thin functional top layer. After grafting PNIPAM, only the grafted PNIPAM in the functional top layer with the controlling pore size could play the role of thermo-responsive gates, while the pore size in the membrane sub-layer was much larger than that in the top controlling layer, and the PNIPAM swelling there could not affect the water flux. Therefore, those PNIPAM polymers grafted on the inner surfaces of those large pores in the membrane sub-layer could not act as the thermo-responsive gates when the environmental temperature changed. On the other hand, for the Nylon6 membranes with a honeycombed porous structure, the pore sizes were almost the same, and then the grafted PNIPAM polymers in the pores all through the membrane thickness could work effectively. Because of the difference in the porous structures of PVDF and Nylon6 substrates, the total area of the inner surfaces of pores inside the Nylon6

membrane per unit membrane volume should be much larger than that of the PVDF membrane. As a result, when the grafting yield of PNIPAM was the same, the thickness of the grafted PNIPAM polymer layer on the inner pore surface of Nylon6 membranes should be much thinner than that of PVDF membranes. Besides, in the grafting process, the grafted polymers seemed to be formed more easily in the top layer near the membrane outer surface rather than in the membrane sub-layer (as shown in **Fig.2.15**), because of the monomer diffusion effects. Therefore, for the PNIPAM-g-PVDF membranes, a smaller grafting yield of PNIPAM could achieve the largest thermo-responsive gating coefficient. However, for the PNIPAM-g-Nylon6 membranes, to achieve the largest thermo-responsive gating coefficient, a larger grafting yield was necessary.

To describe quantitatively the effect of the grafting yield on the pore gating behavior of the PNIPAM-grafted membranes, a special thermo-responsive gating factor of pore size, which is named pore size thermo-responsivity, is defined as follows:^[6]

$$N_{d,40/25} = \frac{d_{g,40}}{d_{g,25}} \tag{2.11}$$

where $N_{\rm d,40/25}$ is the pore size thermo-responsivity of the membrane, and $d_{\rm g,40}$ is the effective pore diameter of the PNIPAM-grafted membrane at 40 °C.

The effect of the grafting yield on the pore size thermo-responsivity of PNIPAMg-PVDF membranes and the schematic illustration of the thermo-responsive control of the pore size is shown in Fig.2.20. For the membrane substrate, the pore size does not change with a variation in the environmental temperature. For the PNIPAM-grafted membranes, the thermo-responsivity of the pore size is heavily affected by the grafting yield. When the grafting yield is too small, the grafted PNIPAM chains are too short, resulting in small responsivity of the membrane pore size. With an increase in the grafting yield, the length of grafted PNIPAM chains increases, consequently the thermo-responsivity of the pore size also increases. However, when the grafting yield increases too much, the grafted PNIPAM chains become too long, and the conformational change of the PNIPAM chains cannot bring any obvious change to the pore size any more. That means the membrane pores have been "choked" by the grafted polymers. The influences of the behavior of the grafting yield on the thermo-responsive gating coefficient, calculated by water flux, and on the thermo-responsivity of pore size are similar to each other. This verifies again that the thermo-responsive flux change of the PNIPAM-grafted membranes is controlled by the thermo-responsivity of the pore size.

To sum up, it is very important to choose a proper grafting yield to obtain an ideal "on/off" gating response. Furthermore, if the microstructures and physicochemical properties of the porous membrane substrates are different, the optimum grafting yields should be adjusted accordingly.

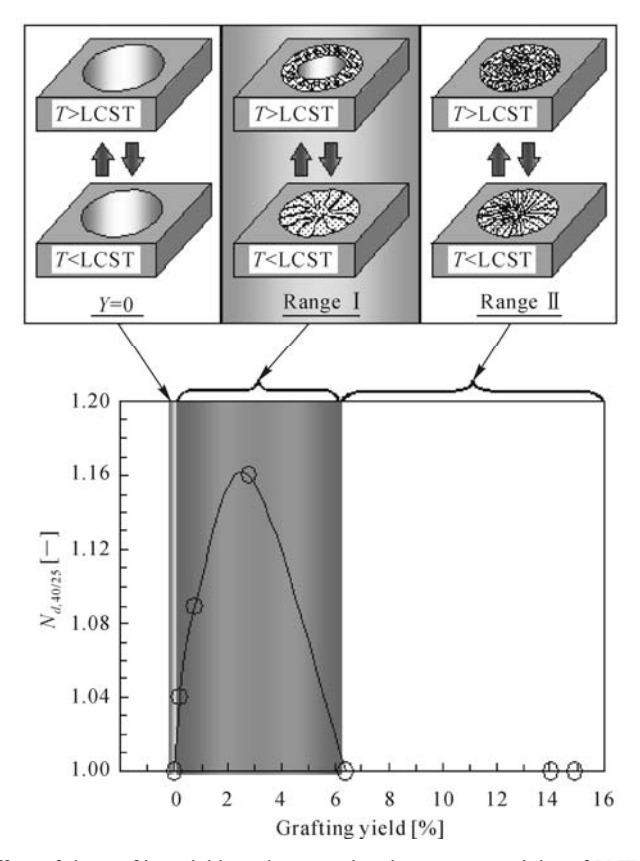


Fig.2.20. Effect of the grafting yield on the pore size thermo-responsivity of PNIPAM-g-PVDF membranes and schematic illustration of the thermo-responsive control of pore size (Reproduced with permission from Ref. [6]). Copyright (2004), American Chemical Society

2.3.2.3 Thermo-Responsive Gating Characteristics Determined by Diffusional Permeability

Due to the thermo-responsive "open/closed" switching function of PNIPAM-grafted membrane pores, such PNIPAM-grafted gating membranes can be used to control the diffusional permeability by varying the environmental temperature across the LCST. The diffusional permeability of solute molecules through the membranes can be measured using a standard side-by-side diffusion cell located in a constant-temperature incubator, and calculated with a model derived from Fick's first law of diffusion. [26] In developing the diffusion model the following assumptions have been made: (i) The diffusion on the donor side is much faster than diffusion through the membrane wall; therefore a uniform concentration on the donor side could be assumed. (ii) The solubility of the diffusing species on the receptor side is equal to its solubility on the donor side (partition coefficient equal to one).

(iii) The solution on the receptor side is well mixed; therefore the concentration on the receptor side is uniform (no concentration gradients exist). (iv) Diffusivity of the diffusing species through the membrane is constant, with respect to the membrane structure and the concentration. (v) A linear concentration gradient exists across the membrane and (vi) pseudo steady-state diffusion through the membrane is established immediately and is maintained throughout. A schematic illustration of the diffusion of solute from the donor side into the receptor side is shown in Fig.2.21.

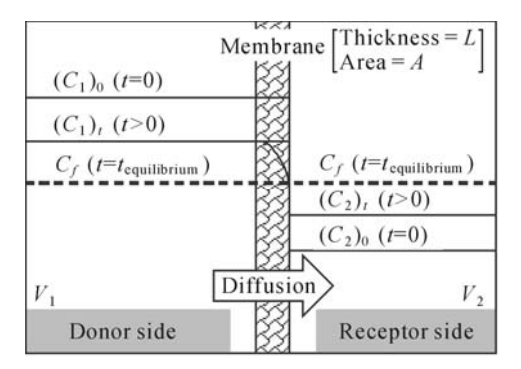


Fig.2.21. Schematic illustrations of the diffusion of solutes through the membrane

The permeating rate of diffusing species from the donor side to the receptor side can be described by Fick's first law of diffusion as follows: [28]

$$\frac{\mathrm{d}M}{\mathrm{d}t} = -AD\left(\frac{\partial C}{\partial r}\right) = AD\left(\frac{\Delta C}{L}\right) \tag{2.12}$$

where dM/dt is the rate of change of solute on the receptor side, A is the effective diffusion area of the membrane, D is the diffusion coefficient in the membrane and $\partial C/\partial r$ is the solute concentration gradient at the membrane-solution interface on the receptor side. ΔC is the solute concentration difference between the receptor side and donor side and L is the thickness of the membrane.

The rate of change in the solute concentration on the receptor side, $d(C_2)/dt$, can be obtained by dividing the total change in the amount of solute by the solution volume on the receptor side:

$$\frac{\mathrm{d}(C_2)_t}{\mathrm{d}t} = \frac{1}{V_2} \frac{\mathrm{d}M}{\mathrm{d}t} = \frac{DA}{V_2} \left(\frac{\Delta C}{L}\right) \tag{2.13}$$

where V_2 is the volume of the solution on the receptor side.

From the conservation of the total amount of solute in the system

$$(C_2)_0 V_2 + (C_1)_0 V_1 = (C_2)_t V_2 + (C_1)_t V_1 = C_t (V_1 + V_2)$$
 (2.14)

where $(C_1)_0$ and $(C_1)_t$ are the initial and intermediary concentrations (at time t) of the solute in the donor compartment, respectively; $(C_2)_0$ and $(C_2)_t$ are the initial and intermediary concentrations (at time t) of the solute in the receptor cell respectively; V_1 and V_2 are the volumes of the solutions in the donor cell and in the

receptor cell, respectively.

The diffusion driving force reads

$$\Delta C = (C_1)_t - (C_2)_t = \frac{C_f (V_1 + V_2) - (C_2)_t V_2}{V_1} - (C_2)_t = (C_f - (C_2)_t) \frac{V_1 + V_2}{V_1}$$
(2.15)

Then Eq.(2.13) upon substitution of Eq.(2.15) becomes

$$\frac{d(C_2)_t}{dt} = \frac{DA}{L} \frac{(V_1 + V_2)}{V_1 V_2} (C_f - (C_2)_t)$$
(2.16)

Integrating Eq.(2.16), the diffusion coefficient across the membrane can be derived as follows:

$$D = \frac{L}{A} \frac{V_1 V_2}{(V_1 + V_2)} \frac{1}{t} \ln \frac{C_f - (C_2)_0}{C_f - (C_2)_t}$$
(2.17)

Because it is difficult to measure the membrane thickness exactly, the diffusional permeability coefficient P, instead of diffusion coefficient D, is usually used as follows:

$$P = \frac{V_1 V_2}{A(V_1 + V_2)t} \ln \frac{C_f - (C_2)_0}{C_f - (C_2)_t}$$
(2.18)

That means that if the effective diffusion area of the membrane and the solution volumes of both the donor side and receptor side are known, the diffusional permeability of solute molecules across the membrane can be calculated by measuring the change in the solute concentration of the solution in the receptor cell over time.

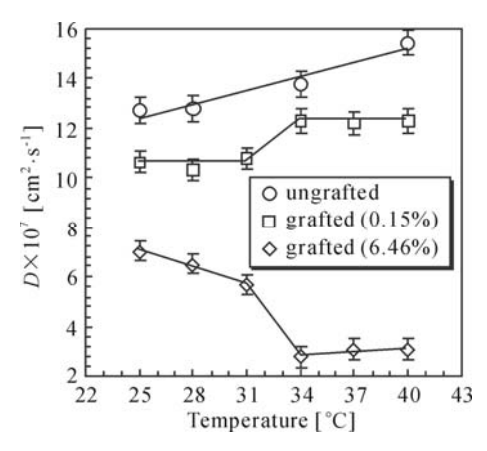


Fig.2.22. Effect of the grafting yield on thermo-responsive diffusional permeation (Reproduced with permission from Ref. [6]). Copyright (2004), American Chemical Society

Fig.2.22 shows the thermo-responsive diffusional permeability through PNIPAM-*g*-PVDF membranes with different grafting yields. ^[6] When the grafting yield is zero (*i.e.*, the substrate membrane), the diffusional coefficient of solute across the membrane increases slightly with an increase in environmental temperature in the

range of 25 to 40 °C, because the diffusivity of the solute increases with the increase in temperature. After grafting PNIPAM, the diffusional coefficient of the solute across the membrane changes dramatically at temperatures around the LCST of PNIPAM, which is due to the conformational change of the PNIPAM chains grafted in the membrane pores. As seen from Fig.2.22, the temperature has an opposite effect on the diffusional coefficients of solutes across the membranes with low grafting yield, as opposed to those with high grafting yield. A schematic illustration of the diffusional permeability through PNIPAM-grafted membranes with different grafting yields is shown in Fig.2.23. When the grafting yield was low, the diffusional coefficient of solute across the membrane was higher at temperatures above the LCST than those below the LCST, owing to the pores of the membrane being controlled open/closed by the shrinking/swelling mechanism of the grafted PNIPAM gates. And when the grafting yield was high, the diffusional coefficient was lower at temperatures above the LCST than those below the LCST, owing to the hydrophilic/hydrophobic phase transition of the grafted PNIPAM gates. Because the solute used in the experiments was water-soluble, any solute diffusion within the membranes occurred primarily within the water-filled regions in the spaces delineated by the grafted PNIPAM chains. Therefore, it is easier for the solute to find water-filled regions in the membranes with hydrophilic PNIPAM gates rather than in the membranes with hydrophobic PNIPAM gates.

Therefore, it is also very important to choose a proper graft yield to obtain a desired thermo-responsive diffusional permeability of solute molecules across the PNIPAM-grafted gating membranes.

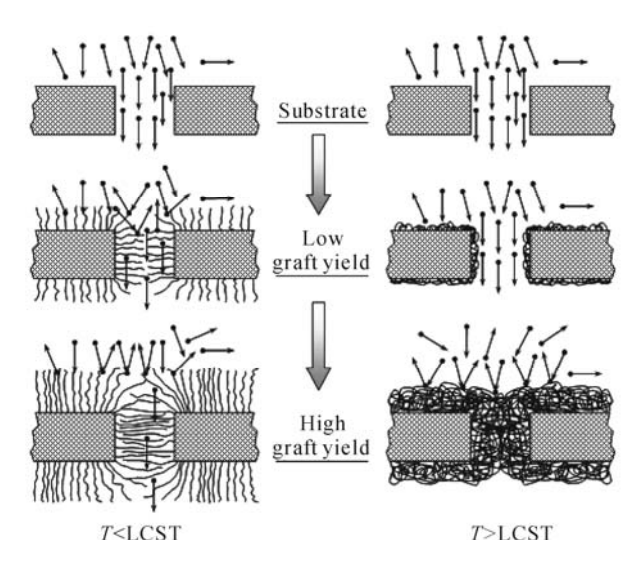


Fig.2.23. Schematic illustration of thermo-responsive diffusional permeability through PNIPAM-grafted membranes with different grafting yields (Reproduced with permission from Ref. [6]). Copyright (2004), American Chemical Society

2.4 Effect of the Length and Density of Grafted Chains on Thermo-Responsive Gating Characteristics of PNIPAM-Grafted Gating Membranes

To systematically study the effects of the length and density of grafted PNIPAM chains on the thermo-responsive gating characteristics of PNIPAM-*g*-AAO membranes prepared by the ATRP method, three PNIPAM-*g*-AAO membranes with different lengths and densities of grafted PNIPAM chains in the membrane pores were prepared (No. M-1, M-2 and M-3 in **Fig.2.7**).^[24] To quantify the thermo-responsive diffusional permeability of Vitamin B12 (VB12) molecules across the PNIPAM-*g*-AAO membranes, we define a coefficient called the thermo-responsive factor, which is calculated as the ratio of the diffusional coefficient at 40 °C to that at 25 °C: ^[24]

$$R_D = \frac{D_{40}}{D_{25}} \tag{2.19}$$

where R_D is the thermo-responsive factor and D_{40} and D_{25} (cm²·s⁻¹) are the diffusional coefficients at 40 and 25 °C, respectively.

Fig.2.24 shows the thermo-responsive factors of the AAO substrate membrane and three PNIPAM-g-AAO membranes with different lengths and densities of grafted PNIPAM chains, and the schematic illustration of the thermo-responsive change of membrane pores at temperatures above and below the LCST of PNIPAM. [24] The diffusional coefficient of the solute across the substrate membrane increases slightly with an increase in the environmental temperature for the decreased viscosity of water, according to the Stokes-Einstein equation, $^{[10]}$ and thus the R_D value of the AAO substrate membrane is slightly larger than 1.0 (i.e., 1.47). This R_D value measured by experiments is close to that calculated from the Stokes-Einstein equation (1.45). Clearly, the pore size of the AAO substrate membrane does not change with variation in the environmental temperature, as shown in the top left illustration of Fig.2.24. As illustrated in Fig.2.7, PNIPAM-g-AAO membranes No. M-1 and No. M-2 have the same density of grafted PNIPAM chains on the membranes, but the length of grafted PNIPAM chains of membrane No. M-1 is shorter than that of membrane No. M-2. The thermo-responsive factor of membrane No. M-2 $(R_D = 8.1)$ is much larger than that of membrane No. M-1 $(R_D = 1.58)$, as shown in Fig.2.24. At 40 °C, the PNIPAM chains grafted in the membrane pores are in a "shrunken" state and the pores are in an "open" state. At this temperature, the pore size of membrane No. M-2 is smaller than that of membrane No. M-1 due to the longer length of grafted PNIPAM chains on membrane No. M-2. As a result, the D_{40} of membrane No. M-1 is twice that of membrane No. M-2. At 25 °C, the grafted PNIPAM chains are in a "swollen" state, which make the membrane pore sizes become smaller. At this temperature, the longer the length of grafted PNIPAM chains, the smaller the membrane pore sizes. As a result, the D_{25} of membrane No. M-1 is 10 times higher than that of membrane No. M-2. Therefore, the thermoresponsive factor R_D (the ratio of D_{40} to D_{25}) of membrane No. M-2 is significantly

larger than that of membrane No. M-1. Compared with the AAO substrate membrane, the PNIPAM-g-AAO membrane No. M-1 has a slightly larger R_D value, but the difference is not so significant. The results indicate that the proper length of grafted PNIPAM chains in the membrane pores is a key factor in obtaining the desired thermo-responsive characteristics of PNIPAM-grafted membranes.

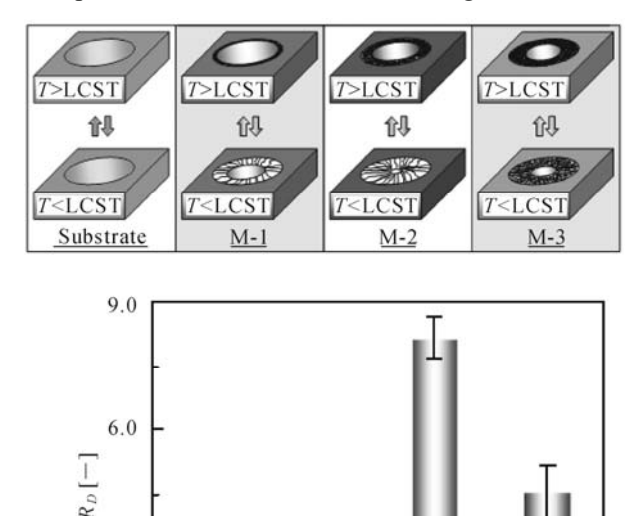


Fig.2.24. Thermo-responsive gating characteristics of PNIPAM-*g*-AAO membranes with different lengths and densities of grafted PNIPAM chains. Nos. M-1, M-2 and M-3 are the same as those illustrated in **Fig.2.7** (Reproduced with permission from Ref. [24]). Copyright (2009), Elsevier

M-1

M-2

M-3

3.0

0.0

Substrate

To study the effect of the density of grafted PNIPAM chains on the thermoresponsive performance of PNIPAM-g-AAO membranes, we compare the R_D values of membranes No. M-1 and No. M-3. The density of grafted PNIPAM chains on the membrane No. M-3 is 1.67 times higher than that on membrane No. M-1, and the grafting yield Y_{PNIPAM} of membrane No. M-3 is 2.18 times more than that of membrane No. M-1. [24] Therefore, the length of grafted PNIPAM chains on membrane No. M-3 is 1.3 times longer than that on membrane No. M-1 (**Fig.2.7**). The thermo-responsive factor of membrane No. M-3 ($R_D = 4.4$) is more than two times larger than that of membrane No. M-1 ($R_D = 1.58$) (**Fig.2.24**). Compared with membrane No. M-1, the larger R_D value of membrane No. M-3 results from both the higher density and the longer length of grafted PNIPAM chains. At 40 °C, the pore size of membrane No. M-3 is smaller than that of membrane No. M-1, because the length of grafted PNIPAM chains in the pores of membrane No. M-3

is 1.3 times longer than that in the pores of membrane No. M-1, and also the density of grafted PNIPAM chains on the membrane No. M-3 is 1.67 times higher than that on membrane No. M-1. As a result, the D_{40} of the membrane No. M-1 is about 7 times larger than that of membrane No. M-3. At 25 °C, the pore size of membrane No. M-3 is still slightly smaller than that of membrane No. M-1 and the "swollen" PNIPAM chains in the pores of membrane No. M-3 are still denser than those of membrane No. M-1. Due to the swollen state of PNIPAM chains at a temperature below the LCST, the size effect of the solute diffusion through the membrane pores is more significant. As a result, the D_{25} of the membrane No. M-1 is about 22 times as large as that of membrane No. M-3. Therefore, the thermoresponsive factor R_D of membrane No. M-3 is larger than that of membrane No. M-1. The results demonstrate that the density of grafted PNIPAM chains in the membrane pores is another key factor for achieving desired thermo-responsive characteristics of PNIPAM-g-AAO membranes.

For membranes No. M-2 and No. M-3, the length of grafted PNIPAM chains in the pores of membrane No. M-2 is longer than that in the pores of membrane No. M-3, but the density of grafted PNIPAM chains on membrane No. M-3 is larger than that on membrane No. M-2 (**Fig.2.7**). ^[24] By comparing the R_D values of membranes No. M-2 and No. M-3, it is clear that the thermo-responsive factor membrane No. M-2 ($R_D = 8.1$) is larger than that of membrane No. M-3 ($R_D = 4.4$) (**Fig.2.24**). That is to say, the length of grafted PNIPAM chains in the membrane pores has a more significant effect on the thermo-responsive characteristics of PNIPAM-g-AAO membranes than the density of grafted PNIPAM chains.

2.5 Gating Characteristics of Thermo-Responsive Membranes with Grafted Linear and Crosslinked PNIPAM Gates

Most of the smart gating membranes have usually been prepared by grafting linear stimuli-responsive polymer chains onto the substrate membranes. However, the linear grafted smart membranes are usually considered to be weak to endure high operating pressures because the linear grafted gates might be easily collapsed at high operating pressures. Furthermore, for thermo-responsive membranes with grafted PNIPAM gates, different grafting temperatures in the grafting polymerization reaction may lead to different conformations of grafted polymers, because PNIPAM exhibits a thermo-sensitive phase transition as the temperature varies across the LCST. In order to provide valuable guidance for designing, fabricating and operating thermo-responsive gating membranes with desirable performances, the influences of the operating pressure and grafting temperature on the gating characteristics of thermo-responsive membranes with both linear and crosslinked grafted PNIPAM gates have been investigated recently in the author's group.^[29]

Because a crosslinked polymeric network structure is considered to be mechanically stronger than a linear polymeric chain structure, membranes with grafted crosslinked PNIPAM gates are introduced to endure high operating pressures. Thermo-responsive membranes with both linear and crosslinked grafted PNIPAM gates are prepared on Nylon6 porous substrates at temperatures above and below the LCST of PNIPAM by using a plasma-induced grafting polymerization method. As listed in Table 2.1, [29] the linear PNIPAM-grafted membranes prepared at 25 °C and 40 °C are respectively coded as LM-LT and LM-HT for short, and the crosslinked PNIPAM-grafted membranes prepared at 25 °C and 40 °C are respectively coded as CM-LT and CM-HT. In order to compare the gating characteristics of the CM-HT, CM-LT, LM-HT and LM-LT membranes, the membranes are prepared with the same grafting yield.

Table 2.1. Definition of the code for PNIPAM-*g*-N6 membranes (Reproduced with permission from Ref. [29]). Copyright (2009), Wiley-VCH Verlag GmbH & Co. KGaA

Membrane code	Preparation Conditions	
	Monomer/Crosslinker	Grafting temperature (°C)
LM-HT	NIPAM/none	40
LM-LT	NIPAM/none	25
CM-HT	NIPAM/MBA	40
CM-LT	NIPAM/MBA	25

Fig.2.25 shows the effect of the operating pressure on the flux of water through both linear and crosslinked PNIPAM-grafted membranes at 25 °C. [29] When the operating pressure increases from 0.02 to 0.28 MPa, the flux of water through the CM-LT membrane simply increases, whereas the water flux of the LM-LT membrane shows a dramatic change under an operating pressure from 0.12 to 0.14 MPa. When the operating pressure is lower than 0.12 MPa, the flux of water through the LM-LT membrane at 25 °C is equal to 0, while the water flux abruptly increases to 0.0017 ml·cm⁻²·s⁻¹ when the operating pressure increases to 0.14 MPa, which is due to the flexibility of the linear grafted PNIPAM chains in the membrane pores. Fig.2.26 schematically illustrates the conformations of grafted linear and crosslinked PNIPAM gates in the membrane pores under different operating pressures at temperatures below the LCST. Because of the addition of a crosslinker, the grafted layers in the crosslinked PNIPAM-grafted membranes are network structures rather than linear chains in the linear PNIPAM-grafted membranes. With the same grafting yield, the thickness of the grafted layer in the crosslinked PNIPAM-grafted membrane is slightly thinner than that in the linear PNIPAM-grafted membrane, because of the addition of a crosslinker. Therefore, the effective pore of a CM-LT membrane exhibits a larger effective size than that of an LM-LT membrane, and thus the flux of water through a CM-LT membrane is larger than that through an LM-LT membrane under the same operating pressure (Fig.2.25). On the other hand, the crosslinked network structure of a grafted PNIPAM layer in a CM-LT membrane is mechanically stronger than the linear chain structure in an LM-LT membrane under high operating pressure. As a result, the grafted crosslinked PNIPAM gates can endure high operating pressure, whereas the linear grafted PNIPAM gates cannot. When

the operating pressure increases across 0.12 MPa, the effective membrane pore size of a CM-LT membrane does not change (**Fig.2.26a**); however, the membrane pore of a LM-LT membrane changes from the "fully closed" state at pressures lower than 0.12 MPa to the "slightly opened" state at operating pressures higher than 0.12 MPa, which results from the collapse of the linear grafted PNIPAM chains under high operating pressure (**Fig.2.26b**). The result demonstrates that the crosslinked PNIPAM gates in the membranes are more stable than the linear grafted ones under high operating pressures at temperatures below the LCST.

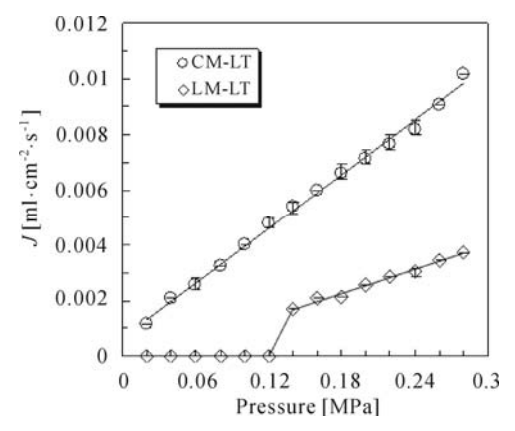


Fig.2.25. Effect of operating pressure on the flux of water through linear and crosslinked PNIPAM-grafted membranes at 25 °C (Reproduced with permission from Ref. [29]). Copyright (2009), Wiley-VCH Verlag GmbH & Co. KGaA

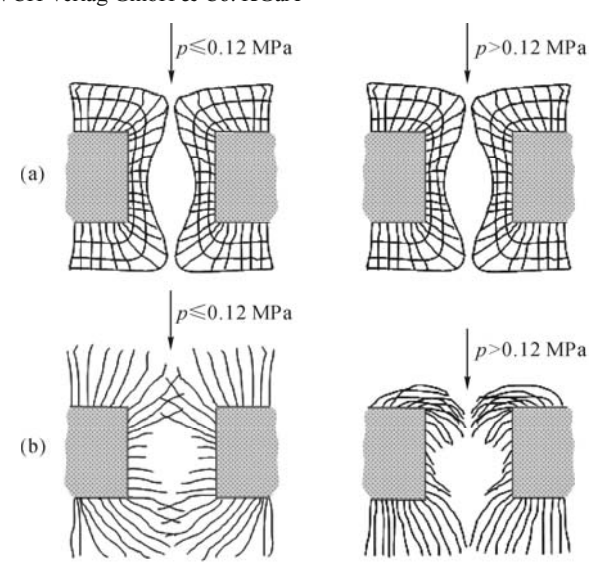


Fig.2.26. Schematic illustrations of linear and crosslinked PNIPAM-*g*-N6 membranes operated under different pressures at 25 °C. (a) CM-LT; (b) LM-LT (Reproduced with permission from Ref. [29]). Copyright (2009), Wiley-VCH Verlag GmbH & Co. KGaA

Thermo-responsive gating coefficients of the ungrafted membrane (UM) and PNIPAM-grafted membranes under different pressures are shown in Fig.2.27, [29] in which the thermo-responsive gating coefficient d_{40}/d_{25} is calculated according to Eq.(2.6). For the ungrafted membrane, the thermo-responsive gating coefficients under different operating pressures are always equal to 1.0, that means the ungrafted membrane does not have any thermo-responsive characteristics. For all the PNIPAM-grafted membranes, the thermo-responsive gating coefficients under different operating pressures remain unchanged when each operating pressure is higher than a certain critical pressure value. The critical pressures for LM-LT, LM-HT, CM-LT and CM-HT membranes are 0.14, 0.06, 0.06 and 0.04 MPa, respectively. It reveals that the thermo-responsive gating performances of LM-LT, LM-HT, CM-LT and CM-HT membranes are all stable and independent of operating pressures when the operating pressures are higher than the above-mentioned critical values.

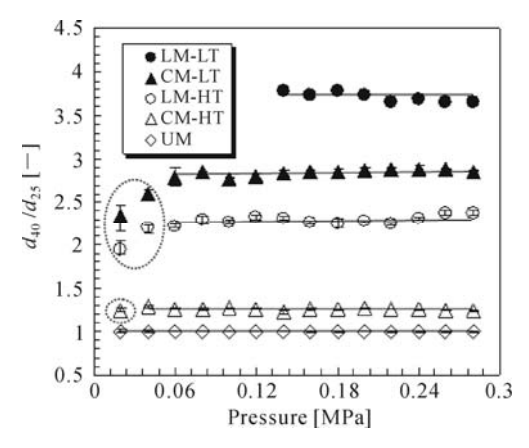


Fig.2.27. Thermo-responsive gating coefficients of different membranes operated under different pressures (Reproduced with permission from Ref. [29]). Copyright (2009), Wiley-VCH Verlag GmbH & Co. KGaA

For CM-LT and LM-HT membranes, the thermo-responsive gating coefficients under operating pressures below 0.06 MPa are slightly lower than those under operating pressures above 0.06 MPa. This phenomenon is ascribed to the hydrophilic/hydrophobic change of the PNIPAM layer grafted on the surface and in the pores of the membrane. When the environmental temperature is below the LCST of PNIPAM, the grafted PNIPAM layer on the surface and in the pores of the membrane is hydrophilic and water can pass through the small pores easily by virtue of capillarity at a low trans-membrane pressure. However, when the environmental temperature is above the LCST of PNIPAM, the grafted layer PNIPAM on the membrane surface and in the membrane pores is hydrophobic and water cannot pass through the small pore with hydrophobic surface easily at a low operating pressure because of the low interfacial tension between the membrane pore surface and water. Therefore, the calculated thermo-responsive gating coefficients

under low operating pressures are not accurate enough, because the surface wettability of the pores affects the water flux heavily under low trans-membrane pressures but it is not taken into account in the calculation with Hagen-Poiseuill's law. When the operating pressures are higher than 0.06 MPa, the thermo-responsive gating coefficients become stable and independent of operating pressures, because the influence of interfacial tension on the water flux goes down with an increase in the trans-membrane pressure.

For the CM-HT membrane, the above-mentioned critical operating pressure decreases to 0.04 MPa. Because the CM-HT membrane is prepared at 40 °C, the effective pore size is slightly larger than that of LM-LT, LM-HT, CM-LT membranes, which will be explained in detail in the next section. Because of a larger effective membrane pore size, the effect of interfacial tension on the flux of water through the membrane pores of a CM-HT membrane is less than that of CM-LT and LM-HT membranes, and thus the above-mentioned critical operating pressure decreases.

With the same grafting yield, the different thermo-responsive gating coefficients of the four PNIPAM-grafted membranes are attributed to the different grafting temperatures as well as to the existence of a crosslinker in the membrane preparation. The effects of grafting temperatures on microstructures of pores of linear and crosslinked PNIPAM-grafted membranes are schematically illustrated in Fig.2.28. [29] In general, the PNIPAM-grafted membranes prepared at temperatures higher than the LCST of PNIPAM have more uniform grafted layers in the membrane pores than those prepared at temperatures lower than the LCST. Taking the LM-LT membrane as an example, at the beginning of the grafting polymerization, NIPAM molecules can easily get into the membrane pores and polymerize into linear chains. As the grafting polymerization reaction goes on, because the PNIPAM chains are in a swollen state at a grafting temperature lower than the LCST of PNIPAM, the effective membrane pore size becomes smaller and smaller and the PNIPAM chains on the membrane surface and at the pore entrance will provide more and more resistance to the transfer of NIPAM molecules into the membrane pores. Therefore, there is a lack of NIPAM molecules in the middle of the membrane pores, and thus PNIPAM chains grafted on the membrane surface and near the pore entrance are longer than those in the middle of the membrane pores (Fig.2.28a). On the other hand, for the LM-HT membrane, because the grafted PNIPAM chains are in a shrunken state at a grafting temperature higher than the LCST during the grafting polymerization, the grafted PNIPAM layer at the pore entrance provides less resistance to the transfer of NIPAM molecules into the pores than that in the preparation of the LM-LT membrane. Consequently, NIPAM molecules can get into membrane pores more easily and then the grafted PNIPAM layer of the LM-HT membrane is more homogeneous throughout the membrane pore length (Fig.2.28b). Therefore, when the grafting yields are the same, the effective pore size of the LM-LT membrane is smaller than that of the LM-HT membrane at the same temperature (Figs.2.28a and 2.28b). Like the LM-LT membrane, the thickness of the grafted layer on the surface and at the pore entrance of the CM-LT membrane is thicker than that in the middle of the

membrane pore (**Fig.2.28c**). On the other hand, just like the LM-HT membrane, a more homogeneous grafted layer can be fabricated throughout the pore length of the CM-HT membrane (**Fig.2.28d**).

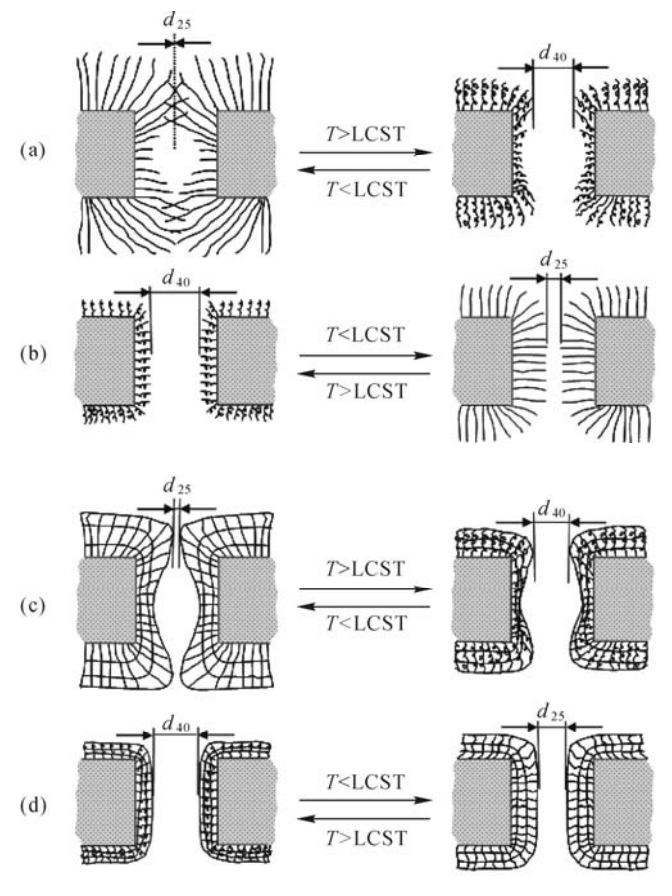


Fig.2.28. Schematic illustrations of thermo-responsive microstructural changes of linear and crosslinked PNIPAM-*g*-N6 membranes prepared at 25 °C and 40 °C, respectively. (a) LM-LT; (b) LM-HT; (c) CM-LT; (d) CM-HT (Reproduced with permission from Ref. [29]). Copyright (2009), Wiley-VCH Verlag GmbH & Co. KGaA

Because the crosslinked network structures of grafted PNIPAM layers of CM-LT and CM-HT membranes should be more compact than the linear PNIPAM chains with free ends of LM-LT and LM-HT membranes, the effective pore sizes of crosslinked PNIPAM-grafted membranes should be slightly larger than those of linear PNIPAM-grafted membranes when the grafting yields are the same (LM-LT vs CM-LT, and LM-HT vs CM-HT). For the CM-HT membrane, because the grafted PNIPAM networks are crosslinked in the shrunken state, the crosslinked structure prevents the PNIPAM networks from fully swelling, even at temperatures below the LCST of PNIPAM. Therefore, the effective pore size of

the CM-HT membrane at 25 °C is the largest among the four grafted membranes and, as a result, the thermo-responsive gating coefficient of the CM-HT membrane is the lowest one.

In a word, the grafting temperature is an important factor that affects the microstructure of the grafted PNIPAM layer in the membrane pore. When the grafting temperature is below the LCST of PNIPAM, the thickness of the grafted PNIPAM layer on the surface and at the pore entrance of the membrane is thicker than that in the middle of the membrane pore. On the other hand, when the grafting temperature is above the LCST of PNIPAM, a more homogeneous grafted layer is formed throughout the membrane pore length. Therefore, with the same grafting yield, the effective pore size of a membrane prepared at 25 °C is smaller than that of a membrane prepared at 40 °C.

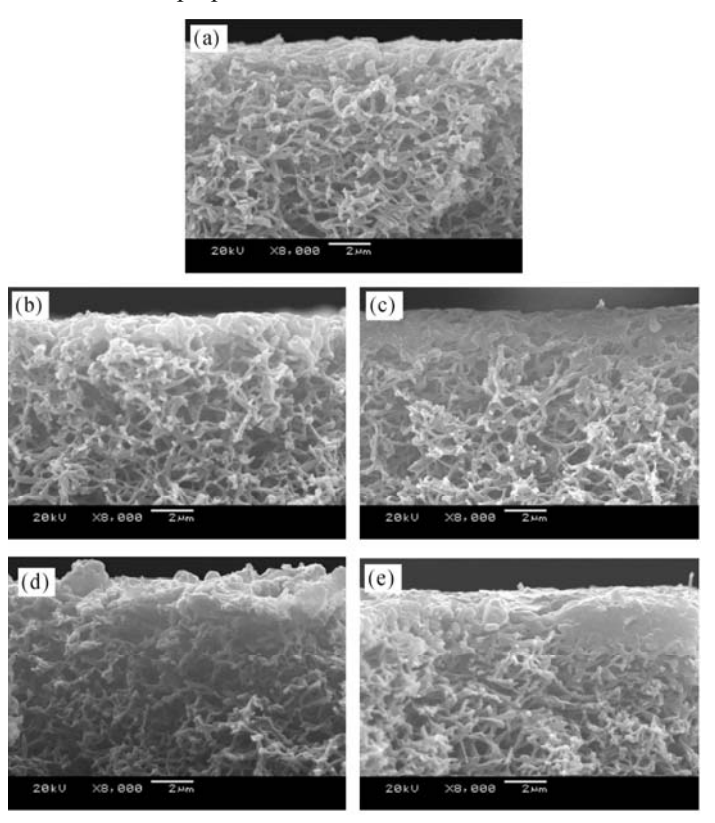


Fig.2.29. SEM micrographs of cross-sections of ungrafted, linear and crosslinked PNIPAMg-N6 membranes. (a) Ungrafted membrane; (b) LM-HT; (c) LM-LT; (d) CM-HT; (e) CM-LT (Reproduced with permission from Ref. [29]). Copyright (2009), Wiley-VCH Verlag GmbH & Co. KGaA

The distributions of grafted polymers in the PNIPAM-grafted membranes prepared at different temperatures with the same grafting yield are verified by

SEM micrographs of the membrane cross-sections (**Fig.2.29**). After grafting, the cross-sectional structures of the membranes are significantly different from those of the membrane substrate. For both linear and crosslinked PNIPAM-grafted membranes, the pores near the membrane surface are apparently filled with grafted polymers to some extent. Compared with those on LM-HT and CM-HT membranes, the grafted polymers on LM-LT and CM-LT membranes are denser near the membrane surfaces. It verifies that the grafted polymer locates mainly on the surface and at the pore entrance of the membrane when the grafting temperature is 25 °C and the grafted polymer distributes more homogeneously throughout the entire membrane thickness when the grafting temperature is 40 °C.

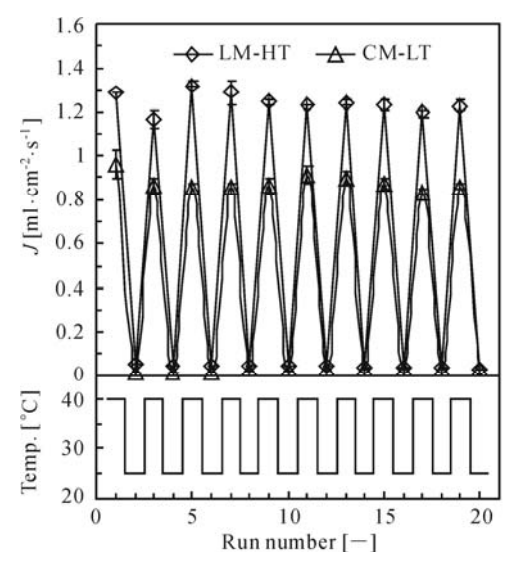


Fig.2.30. Repeatability of "open-closed" switch of linear and crosslinked grafted PNIPAM gates in the membrane pores under the test pressure of 0.26 MPa (Reproduced with permission from Ref. [29]). Copyright (2009), Wiley-VCH Verlag GmbH & Co. KGaA

To examine the stability of the grafted PNIPAM gates in the membrane pores in long-term operations, the repeatability of the thermo-responsive "open-closed" gating switch of grafted membranes is investigated and the results are shown in Fig.2.30.^[29] Among the four kinds of grafted membranes in Fig.2.27, the gating coefficient of the CM-HT membrane is very low and only slightly higher than that of an ungrafted membrane, and the gating coefficient of the LM-LT membrane is unavailable when the operating pressure is lower than 0.12 MPa. Therefore, the LM-HT and CM-LT membranes are chosen for repeatability experiments. Both LM-HT and CM-LT membranes exhibit stable gating characteristics within 20 runs of operation. The water fluxes of the LM-HT and CM-LT membranes at 40 °C and 25 °C hardly change when the environmental temperature returns to 40 °C from 25 °C or returns to 25 °C from 40 °C in the cycles. That means both linear and crosslinked PNIPAM gates grafted in LM-HT and CM-LT membranes

demonstrate satisfactory repeatability of thermo-responsive "open-closed" switch performance under an operating pressure of 0.26 MPa, because the grafted linear or crosslinked PNIPAM gates in LM-HT and CM-LT membranes can return to their original shrunken state at 40 °C and their swollen state at 25 °C, even after a lot of operating cycles. In a word, both linear and crosslinked PNIPAM gates grafted in the membranes possess stable and repeatable thermo-responsive gating characteristics.

To obtain desired and satisfactory thermo-responsive gating characteristics of PNIPAM-grafted membranes, it is quite important and essential to design the grafted gates with proper structures (linear chains or crosslinked networks), to fabricate the PNIPAM-grafted gates at a proper temperature (higher or lower than the LCST of PNIPAM), and to operate the membrane under a proper pressure (should be higher than a critical value).

2.6 Thermo-Responsive Wettability Characteristics of PNIPAM-Grafted Membranes

The temperature-dependent contact angle (θ) variations of ungrafted and PNIPAMgrafted PCTE membranes are shown in Fig.2.31.^[7] According to the AFM observation results, the surface roughness of the ungrafted and PNIPAM-grafted PCTE membranes were very close to each other. Therefore, the effect of surface roughness on the contact angles was neglected here. The contact angle of the ungrafted PCTE membrane decreased somewhat (from 67.5° to 63.1°) when the temperature increased from 25 °C to 40 °C, because it has been known that the liquid surface tension between liquid and air decreases with an increase in the temperature, [30] and the decrease in liquid surface tension causes a decrease in the contact angle.^[31] On the other hand, the contact angle of the PNIPAM-g-PCTE membrane showed a reverse change tendency. When the temperature changed from 25 °C to 40 °C, the contact angle increased greatly, from 58.5° to 87.9°. This was due to the hydrophilic/hydrophobic change in the grafted PNIPAM layer on the PNIPAM-g-PCTE membrane surface when the temperature varied across the LCST of PNIPAM (around 32 °C). Because the PNIPAM chains grafted on the membrane surface became hydrophobic when the temperature was 40 °C (above the LCST of PNIPAM), the contact angle became much larger (than that of the ungrafted membrane) although the decrease in liquid surface tension at a higher temperature made the contact angle smaller. When the temperature was 25 °C (below the LCST of PNIPAM), the PNIPAM layer grafted on the membrane surface became hydrophilic. As a result, the contact angle of the PNIPAMg-PCTE membrane became smaller than that of the ungrafted membrane at the same temperature. A hydrophilic membrane surface and a hydrophilic pore surface should be helpful in increasing the water flux of a membrane rather than a hydrophobic membrane surface and a hydrophobic pore surface. However, the experimental results in **Figs.2.12 and 2.13** showed that the water flux of the PNIPAM-g-PCTE membrane was mainly dependent on the change in pore size. That means the influence of the pore size change on the membrane water flux was more significant than that of the variation in membrane/pore surface hydrophilicity.

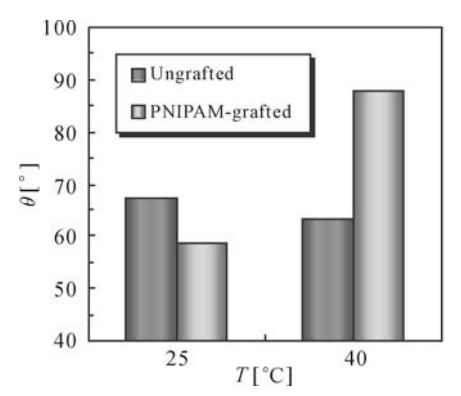


Fig.2.31. Temperature-dependent variations of contact angles (θ) of ungrafted PCTE membrane and PNIPAM-*g*-PCTE membrane with F = 76.1% (Reproduced with permission from Ref. [7]). Copyright (2005), Elsevier

2.7 Thermo-Responsive Gating Membranes with Controllable Response Temperature

Up to now, most of the functional gates for thermo-responsive membranes were constructed from the well-known thermo-responsive PNIPAM. Therefore, the response temperature of these membranes is always around 32 °C, which is determined by the LCST of PNIPAM. In most applications, however, higher or lower response temperatures of the thermo-responsive membranes are preferred. It has been reported that the addition of hydrophilic monomer in the NIPAM-based copolymer could result in a shift of the LCST to a higher temperature, and the addition of hydrophobic monomer results in a lower LCST of the copolymer. [32,33] Thermo-responsive gating membranes with controllable response temperature have been recently prepared with a plasma-induced grafting polymerization method by adding hydrophilic monomer acrylamide (AAM) or hydrophobic monomer butyl methacrylate (BMA) into the NIPAM monomer solution in the fabrication of the thermo-responsive gates. [29]

The response temperature of the thermo-responsive membrane was defined as the temperature at which the water flux across the membrane changed dramatically. **Fig.2.32a** shows the effect of the molar ratio of [AAM] to [NIPAM+AAM] in *co*-monomer solution on the response temperature of poly(NIPAM-*co*-AAM)-grafted membranes and **Fig.2.32b** shows the effect of the molar ratio of [BMA] to

[NIPAM+BMA] in monomer solution on the response temperature of poly(NIPAM-co-BMA)-grafted membranes. [29] Obviously, the response temperatures of the grafted membranes linearly increased with an increase in the molar ratio of AAM in co-monomer solution and linearly decreased with an increase in the molar ratio of BMA in co-monomer solution, respectively. The response temperatures of poly(NIPAM-co-AAM)-grafted PVDF membranes were 34, 36, 38 and 40 °C, respectively, while those of poly(NIPAM-co-BMA)-grafted N6 membranes were 26.5, 23.5, 20.5 and 17.5 °C, respectively. That is to say, the response temperature of the grafted membrane could be effectively controlled or manipulated by simply adjusting the content of AAM or BMA in the NIPAM co-monomer solution in the preparation of thermo-responsive membranes. The response temperature of the poly(NIPAM-co-AAM)-g-PVDF membrane could be raised to about 40 °C when 7 mol.% of AAM was added into the NIPAM co-monomer solution, and that of the poly(NIPAM-co-BMA)-g-N6 membrane could be reduced to about 17.5 °C when 10 mol.% of BMA was added into the NIPAM co-monomer solution.

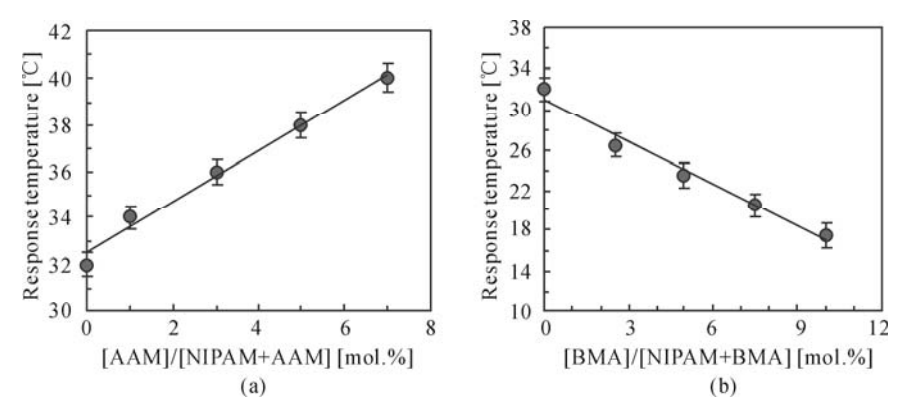


Fig.2.32. Effects of the molar ratio of [AAM] to [NIPAM+AAM] and that of [BMA] to [NIPAM+BMA] in monomer solutions on the response temperature of PNA-grafted (a) and PNB-grafted (b) membranes (Reproduced with permission from Ref. [8]). Copyright (2007), Elsevier

2.8 Membranes with Negatively Thermo-Responsive Gating Characteristics

Up to now, almost all of the thermo-responsive gating membranes have been featured with positively thermo-responsive gating characteristics, *i.e.*, the membrane permeability increases with an increase in the environmental temperature, because almost all of the thermo-responsive functional gates were constructed from PNIPAM, and therefore the membrane pores changed from a "closed" situation into an "open" situation when the environmental temperature increased from a lower one than the LCST of PNIPAM to a higher one above the LCST, due to the swelling/shrinking

conformational change of PNIPAM. In certain applications however, an inverse mode of the thermo-responsive gating behavior for the membranes is preferred. Recently, a novel family of thermo-responsive gating membranes featured with negatively thermo-responsive gating characteristics, *i.e.*, the membrane pores' "opening" is induced by a decrease rather than an increase in temperature, has been developed.^[34]

The concept of the proposed negatively thermo-responsive gating membrane with functional gates and the fabrication procedure are schematically illustrated in Fig.2.33.^[34]

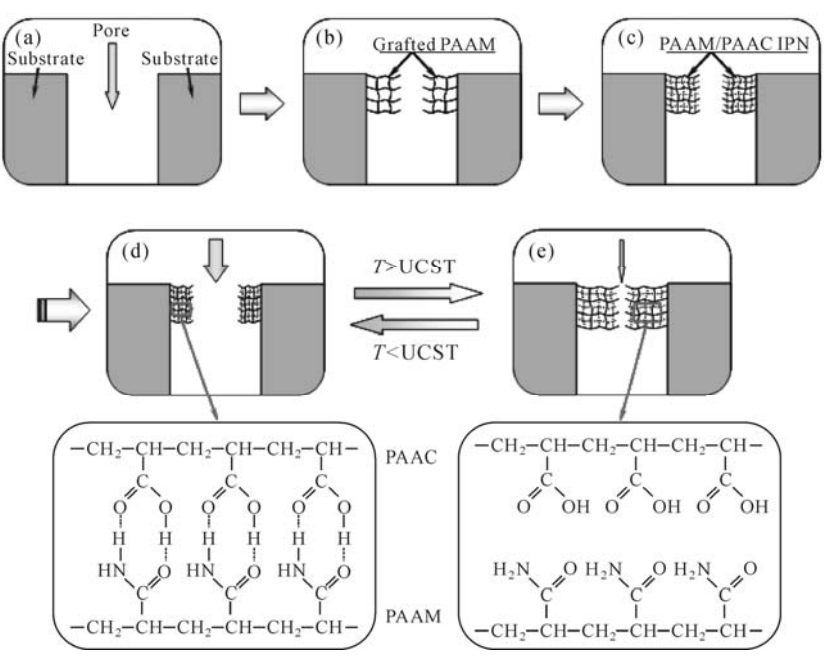


Fig.2.33. Schematic illustration of the concept of the negatively thermo-responsive gating membrane with functional gates and the fabrication procedure (Reproduced with permission from Ref. [34]). Copyright (2005), Wiley-VCH Verlag GmbH & Co. KGaA

The functional gates of the membrane are constructed from thermo- responsive interpenetrating polymer networks (IPNs) that are composed of poly (acrylamide) (PAAM) and poly(acrylic acid) (PAAC). It is known that PAAM and PAAC form polycomplexes in solution through hydrogen bonding. By cooperative "zipping" interactions between the molecules that result from hydrogen bonding, it has been found that the PAAM/PAAC-based IPN hydrogels are featured with a thermoresponsive volume phase transition characteristic that is the reverse of that of PNIPAM, *i.e.*, the hydrogel swelling is induced by an increase rather than a decrease in temperature. When the environmental temperature is lower than the upper critical solution temperature (UCST) of the PAAM/PAAC-based IPN gel, PAAC forms intermolecular hydrogen bonds with PAAM, and the IPN hydrogels retain a shrinking state by the interaction between two polymer chains or so-called

chain-chain zipper effect. On the other hand, when the environmental temperature is higher than the UCST of the IPN gel, PAAC dissociates intermolecular hydrogen bonds with PAAM and the IPN hydrogels retain a swelling state by the relaxation of the two polymer chains. Therefore, the membrane gates shrink at temperatures below the UCST, due to the complex formation by hydrogen bonding, and swell at temperatures above the UCST, due to PAAM/PAAC complex dissociation by the breakage of hydrogen bonds. As a result, the membrane pores change from an "open" situation into a "closed" situation when the temperature increases from one that is below the UCST to one that is above the UCST.

The thermo-responsive membranes with PAAM/PAAC-based IPN gates were prepared by a method of sequential IPN synthesis, in which crosslinked PAAM that was grafted in the pores of porous nylon 6 (N6) membranes and PAAC gels were synthesized as initial gel matrix and secondary gels, respectively. Firstly, plasma-graft pore-filling polymerization was employed to graft crosslinked PAAM gates in the pores of the porous N6 membrane substrates. Next, the PAAM-grafted N6 membranes were immersed in 20 vol% formic acid aqueous solution to swell for 2 h, and then repetitively washed with well-deionized water until pH equaled 7. Then, the treated PAAM-grafted membranes were immersed in aqueous AAC solution containing potassium persulfate (KPS) and methylenebisacrylamide (MBA) as initiator and crosslinker respectively for 24 h at 4 °C, and the monomer AAC was subsequently polymerized and crosslinked within the initial grafted PAAM matrix gels in the pores of the membranes for 24 h at 50 °C in a nitrogen environment to form PAAM/PAAC-based IPN gates.

Fig.2.34a shows the temperature dependence of hydraulic permeability through the prepared membrane with PAAM/PAAC-based IPN gates. The membranes with PAAM/PAAC-based IPN gates exhibited negatively thermo-responsive characteristics, i.e., the membrane permeability decreases with an increase in the environmental temperature. The water flux of the membrane with PAAM/PAAC-based IPN gates in the temperature range of 10 °C to 15 °C was much larger than that in the temperature range of 30 °C to 40 °C. A sharp transition in the hydraulic permeability occurred on going from 20 °C to 25 °C, which corresponded to the UCST of PAAM/PAACbased IPN hydrogels. [35,36] Below the UCST, PAAM/PAAC intermolecular complexes formed by hydrogen bonding, the chain-chain zipper effect made the IPN shrink, and the pores in the membrane were open. As a result, the hydraulic permeability was large. In contrast, the IPN gates were in a swollen state at temperatures above the UCST due to PAAM/PAAC complex dissociation by the breakage of hydrogen bonds. Therefore, the pores in the membrane were closed by the IPN gates and a smaller hydraulic permeability resulted (as illustrated in Fig.2.33). The thermoresponsive gating characteristics of the prepared membranes were just the opposite of those of the thermo-responsive gating membranes constructed with PNIPAM gates.

To verify the reversibility of the PAAM/PAAC-based IPN gates fabricated on the inner surfaces of the pores in the membranes, pressure-driven filtration experiments were carried out by alternatively changing the environmental temperature across the UCST. The temperature was alternately kept at 10 °C and 40 °C. The reversible

environmental thermo-responsive gating characteristics of the membrane with PAAM/PAAC-based IPN gates are shown in **Fig.2.34b**. The thermo-responsive permeability of the membrane with PAAM/PAAC-based IPN gates was found to be satisfactorily reversible and reproducible, suggesting that the fabricated PAAM/PAAC-based IPN gates retained their thermal swelling/shrinking properties intact, even though they underwent repeated temperature changes across the UCST. That is to say, a repeatable thermo-responsive permeation was effectively achieved. Such negatively thermo-responsive gating membranes provide a new mode of the phase transition behavior for thermo-responsive smart or intelligent membrane actuators, which is highly attractive for targeting drug delivery systems, chemical separations and sensors and so on.

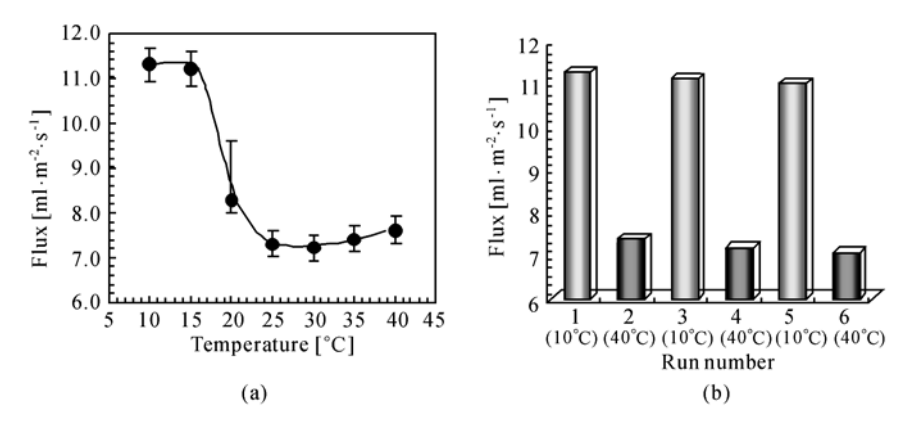


Fig.2.34. Temperature dependence (a) and reversible thermo-responsive gating (b) characteristics of hydraulic permeability through membranes with PAAM/PAAC-based IPN gates. $Y_{PAAM} = 5.01\%$ and $Y_{PAAC} = 4.64\%$ (Reproduced with permission from Ref. [34]). Copyright (2005), Wiley-VCH Verlag GmbH & Co. KGaA

References

- [1] Iwata H, Oodate M, Uyama Y, Amemiya H, Ikada Y. Preparation of temperaturesensitive membranes by graft-polymerization onto a porous membrane. *Journal* of Membrane Science, **1991**, *55*: 119-130.
- [2] Yang B, Yang W T. Thermo-sensitive switching membranes regulated by pore-covering polymer brushes. *Journal of Membrane Science*, **2003**, *218*: 247-255.
- [3] Choi Y J, Yamaguchi T, Nakao S. A novel separation system using porous thermosensitive membranes. *Industrial & Engineering Chemistry Research*, **2000**, *39*: 2491-2495.
- [4] Chu L Y, Yamaguchi T, Nakao S. A molecular-recognition microcapsule for environmental stimuli-responsive controlled release. *Advanced Materials*, **2002**, *14*: 386-389.

- [5] Chu L Y, Park S H, Yamaguchi T, Nakao S. Preparation of thermo-responsive core-shell microcapsules with a porous membrane and poly(*N*-isopropylacrylamide) gates. *Journal of Membrane Science*, **2001**, *192*: 27-39.
- [6] Li Y, Chu L Y, Zhu J H, Wang H D, Xia S L, Chen W M. Thermo-responsive gating characteristics of poly(*N*-isopropylacrylamide)-grafted porous polyvinylidene fluoride membranes. *Industrial & Engineering Chemistry Research*, **2004**, *43*: 2643-2649.
- [7] Xie R, Chu L Y, Chen W M, Xiao W, Wang H D, Qu J B. Characterization of microstructure of poly(*N*-isopropylacrylamide)-grafted polycarbonate tracketched membranes prepared by plasma-graft pore-filling polymerization. *Journal of Membrane Science*, **2005**, *258*: 157-166.
- [8] Xie R, Li Y, Chu L Y. Preparation of thermo-responsive gating membranes with controllable response temperature. *Journal of Membrane Science*, **2007**, 289(1-2): 76-85.
- [9] Qu J B, Chu L Y, Yang M, Xie R, Hu L, Chen W M. A pH-responsive gating membrane system with pumping effects for improved controlled release. *Advanced Functional Materials*, **2006**, *16*: 1865-1872.
- [10] Chu L Y, Niitsuma T, Yamaguchi T, Nakao S. Thermo-responsive transport through porous membranes with grafted PNIPAM gates. *AIChE Journal*, **2003**, *49*: 896-909.
- [11] Zhang K, Wu X Y. Temperature and pH-responsive polymeric composite membranes for controlled delivery of proteins and peptides. *Biomaterials*, **2004**, *25*: 5281-5291.
- [12] Yamaguchi T, Nakao S, Kimura S. Plasma-graft filling polymerization: Preparation of a new type of pervaporation membrane for organic liquid mixtures. *Macromolecules*, **1991**, *24*: 5522-5527.
- [13] Yamaguchi T, Nakao S, Kimura S. Evidence and mechanisms of filling polymerization by plasma-induced graft polymerization. *Journal of Polymer Science, Polymer Chemistry Edition*, **1996**, *34*: 1203-1208.
- [14] Yamaguchi T, Ito T, Sato T, Shinbo T, Nakao S. Development of a fast response molecular recognition ion gating membrane. *Journal of American Chemical Society*, **1999**, *121*: 4078-4079.
- [15] Xu F J, Zhao J P, Kang E T, Neoh K G, Li J. Functionalization of nylon membranes via surface-initiated atom-transfer radical polymerization. *Langmuir*, **2007**, *23*: 8585-8592.
- [16] Lokuge I, Wang X, Bohn P W. Temperature-controlled flow switching in nanocapillary array membranes mediated by poly(*N*-isopropylacrylamide) polymer brushes grafted by atom transfer radical polymerization. *Langmuir*, **2007**, *23*: 305-311.
- [17] Fulghum T M, Estillore N C, Vo C D, Armes S P, Advincula R C. Stimuliresponsive polymer ultrathin films with a binary architecture: combined layer-by-layer polyelectrolyte and surface-initiated polymerization approach. *Macromolecules*, **2008**, *41*: 429-435.
- [18] Friebe A, Ulbricht M. Controlled pore functionalization of poly(ethylene terephthalate) track-etched membranes via surface-initiated atom transfer

- radical polymerization. Langmuir, 2007, 23: 10316-10322.
- [19] Alem H, Duwez A S, Lussis P, Lipnik P, Jonas A M, Demoustier-Champagne S. Microstructure and thermo-responsive behavior of poly(*N*-isopropylacrylamide) brushes grafted in nanopores of track-etched membranes. *Journal of Membrane Science*, **2008**, *308*: 75-86.
- [20] Matyjaszewski K, Xia J H. Atom transfer radical polymerization. *Chemical Review*, **2001**, *101*: 2921-2990.
- [21] Edmondson S, Osborne V L, Huck W T S. Polymer brushes via surface-initiated polymerizations. *Chemical Society Reviews*, **2004**, *33*: 14-22.
- [22] Huang W X, Kim J B, Bruening M L, Baker G L. Functionalization of surfaces by water-accelerated atom-transfer radical polymerization of hydroxyethyl methacrylate and subsequent derivatization. *Macromolecules*, **2002**, *35*: 1175-1179.
- [23] Verma H, Tharanikkarasu K. Synthesis and characterization of novel polystyrene-block-polyurethane-block-polystyrene tri-block copolymers through atom transfer radical polymerization. *Polymer International*, **2008**, *57*: 226-232.
- [24] Li P F, Xie R, Jiang J C, Meng T, Yang M, Ju X J, Yang L, Chu L Y. Thermo-responsive gating membranes with controllable length and density of poly(*N*-isopropylacrylamide) chains grafted by ATRP method. *Journal of Membrane Science*, **2009**, *337*: 310-317.
- [25] Matyjaszewski K, Shipp D A, Wang J L, Grimaud T, Patten T E. Utilizing halide exchange to improve control of atom transfer radical polymerization. *Macromolecules*, **1998**, *31*: 6836-6840.
- [26] Chu L Y, Zhu J H, Chen W M, Niitsuma T, Yamaguchi T, Nakao S. Effect of graft yield on the thermo-responsive permeability through porous membranes with plasma-grafted poly(*N*-isopropylacrylamide) gates. *Chinese Journal of Chemical Engineering*, **2003**, *11*: 269-275.
- [27] Yang M, Chu L Y, Li Y, Zhao X J, Song H, Chen W M. Thermo-responsive gating characteristics of poly(*N*-isopropylacrylamide)-grafted membranes. *Chemical Engineering and Technology*, **2006**, *29*: 631-636.
- [28] Crank J. *The Mathematics of Diffusion (2nd ed.)*. Clarendon Press, Oxford, **1975**.
- [29] Chen Y C, Xie R, Yang M, Li P F, Zhu X L, Chu L Y. Gating characteristics of thermo-responsive membranes with grafted linear and crosslinked poly(*N*-isopropylacrylamide) gates. *Chemical Engineering and Technology*, **2009**, *32*: 622-631.
- [30] Henn A R. The surface tension of water calculated from a random network model. *Biophysical Chemistry*, **2003**, *105*: 533-543.
- [31] Extrand C W, Kumagai Y. An experimental study of contact angle hysteresis. *Journal of Colloid and Interface Science*, **1997**, *191*: 378-383.
- [32] Chee C K, Rimmer S, Shaw D A, Soutar I, Swanson L. Manipulating the thermoresponsive behavior of poly(*N*-isopropylacrylamide). 1. on the conformational behavior of a series of *N*-isopropylacrylamide-styrene statistical copolymers. *Macromolecules*, **2001**, *34*: 7544-7549.
- [33] Barker I C, Cowie J M G, Huckerby T N, Shaw D A, Soutar I, Swanson L.

- Studies of the "smart" thermoresponsive behavior of copolymers of *N*-isopropylacrylamide and *N*,*N*-dimethylacrylamide in dilute aqueous solution. *Macromolecules*, **2003**, *36*: 7765-7770.
- [34] Chu L Y, Li Y, Zhu J H, Chen W M. Negatively thermoresponsive membranes with functional gates driven by zipper-type hydrogen-bonding interactions. *Angewandte Chemie International Edition*, **2005**, *44*: 2124-2127.
- [35] Ilmain F, Tanaka T, Kokufuta E. Volume transition in a gel driven by hydrogen bonding. *Nature*, **1991**, *349*: 400-401.
- [36] Xiao X C, Chu L Y, Chen W M, Wang S, Li Y. Positively thermo-sensitive monodisperse core-shell microspheres. *Advanced Functional Materials*, **2003**, *13*: 847-852.

Smart Microcapsules with Thermo-Responsive Gating Membranes

On the basis of the knowledge of thermo-responsive gating membranes, introduced in Chapter 2, the design, fabrication and performance of smart microcapsules with thermo-responsive gating membranes for controlled release are described in this chapter. Firstly, the design of smart microcapsules with thermo-responsive gating membranes is introduced. Next, the fabrication, microstructure control and controlled-release performance of thermo-responsive microcapsules with a porous membrane and PNIPAM gates are described systematically. Then, the fabrication and microstructure control of small-sized monodispersed thermo-responsive microcapsules are introduced.

3.1 Design of Smart Microcapsules with Thermo-Responsive Gating Membranes

On the basis of the knowledge of thermo-responsive gating membranes described in Chapter 2, it is possible to design smart microcapsules with thermo-responsive gating membranes for controlled release. The target of a controlled drug delivery system is for an improved drug treatment (outcome) through rate-and time-programmed and site-specific drug delivery. [1] Environmental stimuli-responsive controlled-release systems have been developed specifically for this purpose. These environmental stimuli-responsive release systems can release specified chemicals or drugs at a particular site where an environmental condition, such as temperature, pH or other information, is different from that at other sites. As there are many cases in which environmental temperature fluctuations occur naturally, and in which the environmental temperature stimuli can be easily designed and artificially controlled, in recent years much attention has been focused on thermo-responsive controlled-release systems. [2-5] In developing environmental stimuli-responsive controlled-release systems, especially pulsated release systems with an

on-off switching response, one of the important parameters is to reduce the response time of the release rate to stimuli. As the release rate from microcapsules is generally controlled by the rate of diffusion of solute molecules across the thin microcapsule membrane, an increase in the release rate in response to stimuli may be expected when compared to gels and microspheres. Therefore, microcapsules with a thin membrane are suitable for stimuli-responsive controlled-release systems.

Recently, a thermo-responsive microcapsule with a porous membrane and grafted PNIPAM gates has been developed by applying the plasma-graft pore-filling polymerization method to graft a linear thermo-responsive polymer inside the porous membrane of a hollow microcapsule. [6] The concept of the proposed system is schematically illustrated in **Fig.3.1**. [6] At a low graft yield, due to the thermo-responsive "open-closed" switching function of the grafted PNIPAM in the membrane pores, the system behaves as a positive thermo-response controlled-release type, i.e., the release rate increases with temperature, while, at a high graft yield, due to the thermo-responsive "hydrophilic-hydrophobic" switching property of the grafted PNIPAM in the membrane pores, the system acts as a negative thermo-response release type, i.e., the release rate decreases with an increase in temperature.

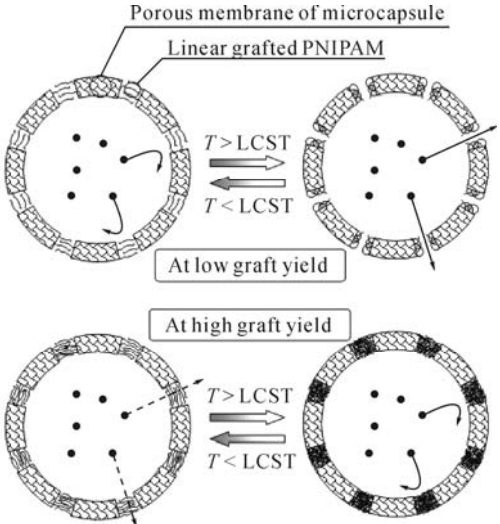


Fig.3.1. A schematic representation of the thermo-responsive release principle of hollow microcapsules with a porous membrane and thermo-responsive polymeric gates (Reproduced with permission from Ref. [6]). Copyright (2001), Elsevier

3.2 Fabrication and Performance of Thermo-Responsive Microcapsules with Porous Membrane and PNIPAM Gates

The schematic illustration of the preparation process route and the controlled-

release behavior of the proposed thermo-responsive microcapsule with low graft yield (**Fig.3.1**) is shown in **Fig.3.2**.^[7] Briefly, the preparation of the thermo-responsive microcapsule includes three main steps as follows. Firstly, oil-in-water (O/W) emulsions are prepared by emulsification. Then, hollow microcapsules with a porous membrane are prepared by interfacial polymerization, using the emulsions as templates. Finally, linear PNIPAM chains are grafted into the pores of the microcapsule membrane by using the plasma-graft pore-filling polymerization method.

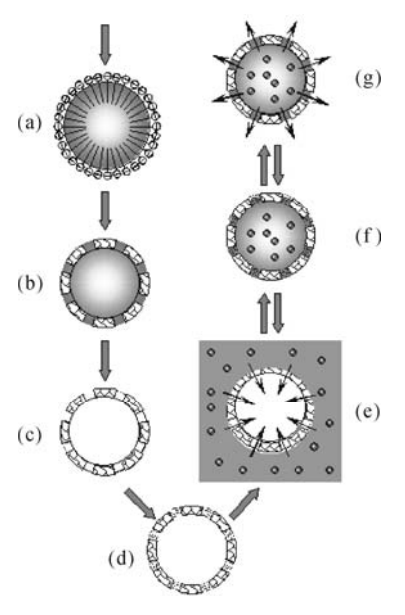


Fig.3.2. Schematic illustration of the preparation process route and the controlled-release behavior of the proposed thermo-responsive microcapsule with low graft yield. (a) Oil-in-water (O/W) emulsions prepared by emulsification; (b) Hollow microcapsules with a porous membrane prepared by interfacial polymerization; (c) Spherical hollow reservoirs with a porous shell prepared by freeze-drying the microcapsules; (d) Spherical reservoirs with PNIPAM gates prepared using a plasma-graft pore-filling polymerization to graft linear PNIPAM chains into the pores of the shell; (e) Loading drug/chemicals into the microcapsule by controlling the environmental temperature to "open" the gates; (f) Drug-/chemical-loaded microcapsule with gates "closed" by changing the environmental temperature across the LCST, and then keeping the temperature constant; (g) Releasing the drug/chemicals from the microcapsules by changing the environmental temperature across the LCST (Reproduced with permission from Ref. [7]). Copyright (2002), American Chemical Society

3.2.1 Fabrication of Hollow Microcapsules with Porous Membrane

To achieve the designed thermo-responsive microcapsules by grafting NIPAM into the pores in the porous membrane of hollow microcapsules using plasma-

graft pore-filling polymerization, it is first necessary to prepare hollow microcapsules with a porous membrane. For this, a porous microcapsule membrane with a large permeability coefficient is the preferred option, because the quickest release rate in response to a stimulus is the most desirable for stimuli-responsive microcapsules.

3.2.1.1 Fabrication of Porous Polyamide Microcapsules

Porous polyamide microcapsules were prepared from ethylenediamine (EDA) and terephthaloyl dichloride (TDC) by interfacial polymerization. [6] First, 10 ml of the organic phase containing 0.5 mol·L⁻¹ terephthaloyl dichloride, was added to 160 ml of the water phase containing 1.0 wt% sodium dodecyl sulfate (SDS) as an emulsifier. Four types of mixed organic solvents were used: chloroform/cyclohexane (1:4 [v/v]); chloroform/cyclohexane (1:3 [v/v]); chloroform/cyclohexane (3:1 [v/v]); and benzene/xylene (2:1 [v/v]). Then the mixture was mechanically agitated for 10 min with a stirring speed of 800 r/min to yield an oil-in-water emulsion. The stirring speed was then reduced to 200 r/min and both the buffer (20 ml water containing 1.18 mol·L⁻¹ sodium carbonate) and 15 ml of monomer ethylene diamine were added to the emulsion and the mixture further stirred. During emulsification and interfacial polymerization, the temperature was kept at a constant 10 °C using a thermostatic unit. The experimental recipe for the preparation of the microcapsules is given in **Table 3.1**. [6] The microcapsules were separated by centrifugation, and washed three times using deionized water in order to remove any emulsifier and remnants of the monomer. These were then dialyzed against deionized water and freeze-dried. After freeze-drying, all the organic phase inside the microcapsules had been removed.

Table 3.1. Experimental parameters for the emulsification and interfacial polymerization in the preparation of porous microcapsules (Reproduced with permission from Ref. [6]). Copyright (2001), Elsevier

No.	Organic phase solvent [v/v]	Polymerization time [min]
MC6221	Chloroform/cyclohexane (1:4)	60
MC6222	Chloroform/cyclohexane (1:3)	60
MC6285	Chloroform/cyclohexane (3:1)	60
MC6223	Benzene/xylene (2:1)	60
MC6281	Benzene/xylene (2:1)	5
MC6282	Benzene/xylene (2:1)	30
MC6283	Benzene/xylene (2:1)	30
MC6284	Benzene/xylene (2:1)	180

3.2.1.2 Microstructures of Porous Polyamide Microcapsules

All the mean diameters of the as-prepared microcapsules were in the range 36.7 to $43.1 \mu m$. When the chloroform and cyclohexane mixture was used as the organic solvent, the mean diameters of microcapsules prepared with the ratios of chloroform

to cyclohexane of 1:4 [v/v] and 1:3 [v/v] were almost the same as those prepared using benzene/xylene (2:1 [v/v]) as the organic solvent. The mean diameter of the microcapsule decreased slightly when the ratio of chloroform to cyclohexane was 3:1 [v/v]. When the benzene and xylene mixture was used as organic solvent, the mean diameter of the microcapsule increased slightly with increasing interfacial polymerization time. These results indicate that the size of the microcapsule is principally decided by the emulsion size.

Scanning electron micrographs (SEM) of the outer and inner surfaces of the microcapsules, and cross-sectional views, are shown in Figs.3.3 and 3.4. [6] The hollow polyamide microcapsules were shown to have asymmetrical and porous membrane structures; the outer surface (the water side in the interfacial polymerization) was smooth, and the inner surface (the organic side) was rough. This reflects the fact that the interfacial polymerization proceeds by the diffusion of the amine compounds from the aqueous to the organic phase. When the chloroform and cyclohexane mixture was used as the solvent, the microcapsule membrane became more porous, and the thickness increased with the increasing ratio of chloroform to cyclohexane in the solvent. Compared with those membranes prepared using the chloroform and cyclohexane mixture, the membranes of the microcapsules prepared with the benzene and xylene mixture were more porous. This indicates that the porous structure of the microcapsule membrane depends on the solubility of the solvent in water and also, to some extent, on the solubility of water in the solvent. When the interfacial polymerization time increased, the thickness of the microcapsule membrane increased and, during interfacial polymerization, a thin membrane layer on the water side became more dense.

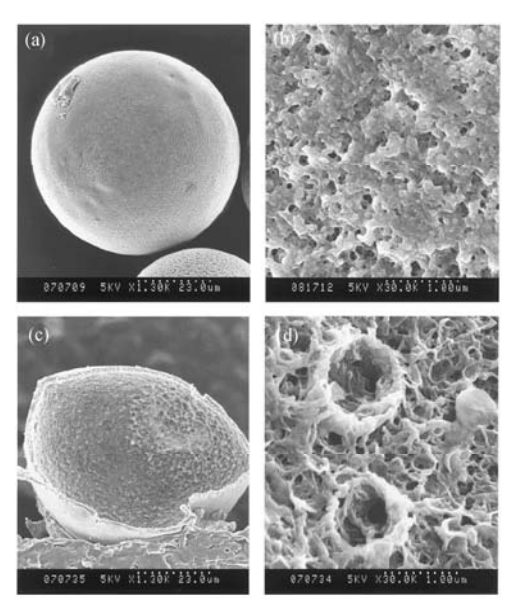


Fig.3.3. FE-SEM micrographs of microcapsule MC6281. (a, b) Outer surface; (c) Cross-section; (d) Inner surface (Reproduced with permission from Ref. [6]). Copyright (2001), Elsevier

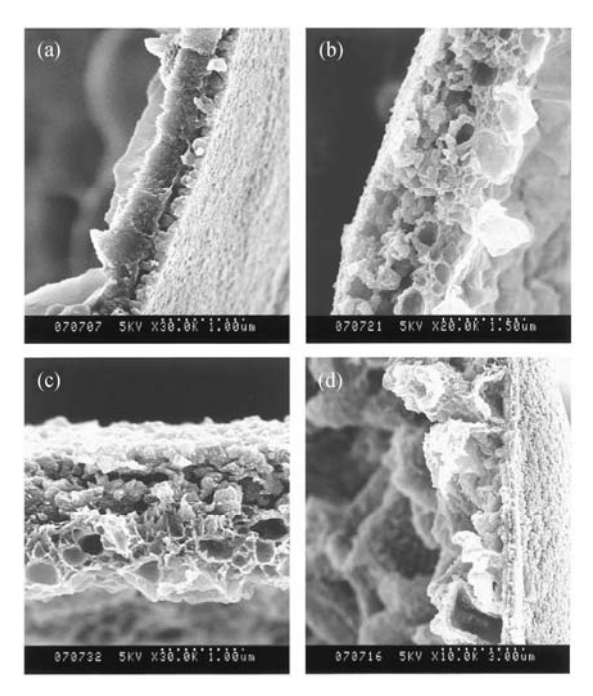


Fig.3.4. FE-SEM micrographs of the cross-sectional structures of the microcapsules. (a) MC6222; (b) MC6285; (c) MC6281; (d) MC6223 (Reproduced with permission from Ref. [6]). Copyright (2001), Elsevier

3.2.1.3 Permeability of Solutes across Porous Polyamide Microcapsule Membranes

The permeability coefficients of NaCl across the prepared microcapsules at 25 °C are shown in Fig.3.5.^[6] When the chloroform and cyclohexane mixture was used as organic solvent, the permeability coefficient increased with an increase in the ratio of chloroform to cyclohexane. When the organic solvent was replaced by the benzene and xylene mixture, the rate of release increased even more. The permeability coefficient of NaCl across the microcapsule membrane decreased with increasing interfacial polymerization time. These results indicate that the more porous the microcapsule membrane, the larger the permeability coefficient of NaCl across the microcapsule membrane.

From the above results on both microstructure and permeability of the microcapsules, microcapsule MC6281 was selected for subsequent grafting of PNIPAM gates.

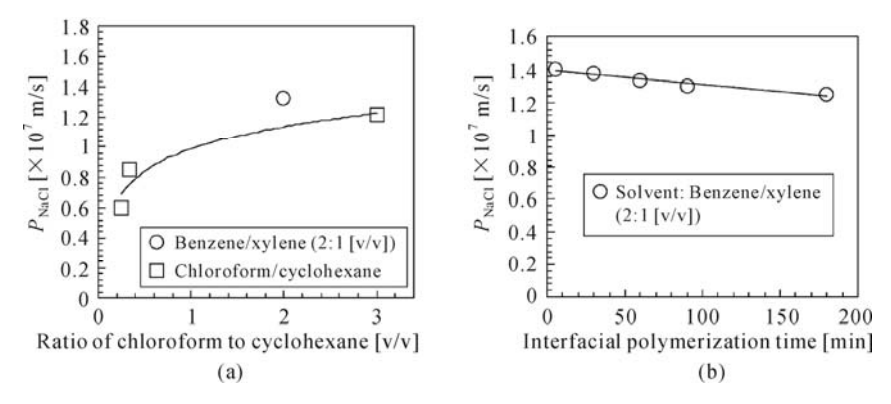


Fig.3.5. The NaCl permeability coefficients across the microcapsule membranes at 25 °C. (a) The effect of solvent composition on the permeability of the microcapsule; (b) The effect of interfacial polymerization time on the permeability of the microcapsule (Reproduced with permission from Ref. [6]). Copyright (2001), Elsevier

3.2.2 Grafting PNIPAM Gates in the Membrane Pores of Microcapsules

To prepare thermo-responsive gating membranes, how to graft thermo-responsive gates in the membrane pores is the most important issue.

3.2.2.1 Grafting PNIPAM Gates into Porous Microcapsule Membranes with Plasma-Graft Pore-Filling Polymerization

Plasma-graft pore-filling polymerization was employed to graft linear PNIPAM into the pores in the microcapsule membrane according to the method described previously for the preparation of a flat separating membrane. [6] Briefly, the freeze-dried microcapsules were put into a transparent glass tube, which was then filled with argon gas. The tube was then evacuated to a pressure of 10 Pa, and the microcapsules were subjected to a radio-frequency plasma operating at 13.56 MHz and delivering at 30 W for 60 s. Then, under inert atmospheric conditions, the microcapsules were immersed into NIPAM monomer solution and the graft polymerization was carried out in a shaking constant-temperature bath (30 °C) for a fixed time. A schematic illustration of the process of plasma-graft pore-filling polymerization for the hollow microcapsule with a porous membrane is shown in **Fig.3.6**. [6] The experimental parameters of the plasma-graft pore-filling polymerization are shown in **Table 3.2**. [6] The PNIPAM-grafted microcapsules were separated centrifugally and washed three times with deionized water. These were then dialyzed against deionized water.

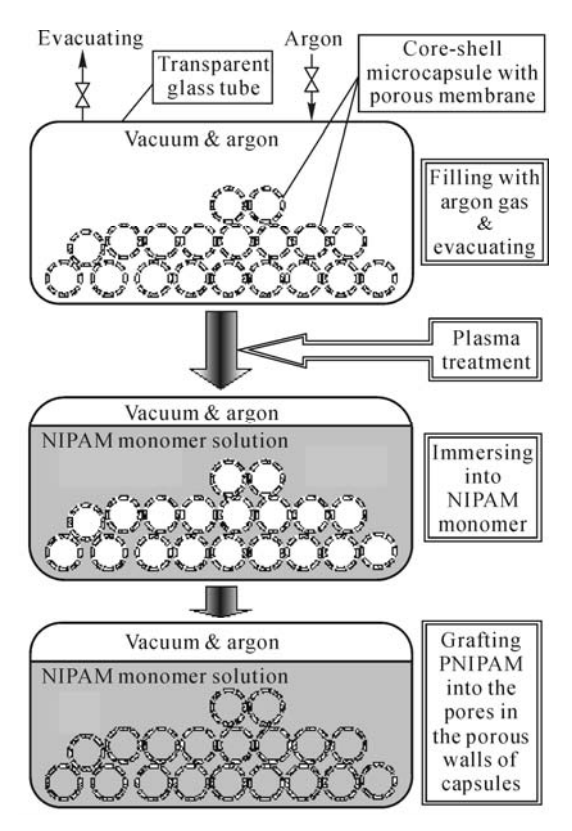


Fig.3.6. A schematic illustration of the process of plasma-graft pore-filling polymerization for the hollow microcapsule with a porous membrane (Reproduced with permission from Ref. [6]). Copyright (2001), Elsevier

Table 3.2. Experimental parameters in the plasma-graft pore-filling polymerization for grafting PNIPAM gates in the porous microcapsule membranes (Reproduced with permission from Ref. [6]). Copyright (2001), Elsevier

	NIPAM monome	Graft		
No.	Solvent	NIPAM concentration [wt%]	polymerization time [min]	
MC6281g05W20	Water	0.5	20	
MC6281g05WM20	water/methanol (1:1 [v/v])	0.5	20	
MC6281g10W20	Water	1.0	20	
MC6281g30W20	Water	3.0	20	
MC6281g30W60	Water	3.0	60	
MC6281g30W120	Water	3.0	120	
MC6281g30W180	Water	3.0	180	
MC6281g30W240	Water	3.0	240	

3.2.2.2 Microstructures of the PNIPAM-Grafted Microcapsules

Fig. 3.7 shows FE-SEM micrographs of the outer surfaces and cross-sectional views of the PNIPAM-grafted microcapsules. ^[6] Comparing these micrographs with those shown in **Figs. 3.3b** and **3.4c**, the un-grafted and PNIPAM-grafted microcapsules are seen to have significantly different structures. After grafting PNIPAM onto the inner pore surface in the porous membrane of the microcapsule, the pore size became smaller. The porous structure across the cross-section of the microcapsule was covered by the grafted polymer throughout the entire membrane thickness. This coverage appears to increase in density in the membrane of the PNIPAM-grafted microcapsules from samples MC6281g10W20, MC6281g30W20 and MC6281g30W120 to MC6281g30W240. This indicates that the graft yield increased with increasing monomer concentration and with increasing grafting time.

The SEM micrographs show that a homogeneous graft of PNIPAM in the porous membrane of the microcapsule is the result of the plasma-graft pore-filling polymerization. As shown in Fig.3.6, [6] the microcapsule was evacuated before being immersed into the NIPAM monomer solution. When the microcapsule was immersed into the NIPAM monomer solution, the monomer solution was forced to pass through the pores in the membrane and enter into the intra-capsular space because of the vacuum inside the microcapsule. Therefore, all of the pores in the microcapsule membrane were supplied with enough NIPAM monomer. Consequently, the graft polymerization of PNIPAM onto the inner pore surface occurred homogeneously throughout the porous membrane of the microcapsule. These results verify that the plasma-graft pore-filling polymerization method is efficient for grafting polymers into the pores in the porous membranes of hollow particles.

3.2.3 Thermo-Responsive Controlled-Release Characteristics

In order to measure the permeability through the microcapsule membrane, $^{[6]}$ the freeze-dried microcapsules and the PNIPAM-grafted microcapsules were dialyzed against aqueous NaCl or vitamin B_{12} (VB₁₂) with a known concentration for more than 3 days. The dialysis was carried out alternately in shaking constant-temperature baths kept at 25 °C and 40 °C. The permeability of NaCl from the microcapsules was measured by determining the increase in the electrical conductance of the surrounding medium with time. This was carried out using an electrical conductivity meter, after mixing a certain volume of microcapsule dispersion, with a known NaCl concentration, with the same volume of deionized water. During measurement, the liquid temperature was kept constant using a thermostat unit. The concentration of VB₁₂ was analyzed spectrophotometrically at 360 nm using a UV-visible recording spectrophotometer.

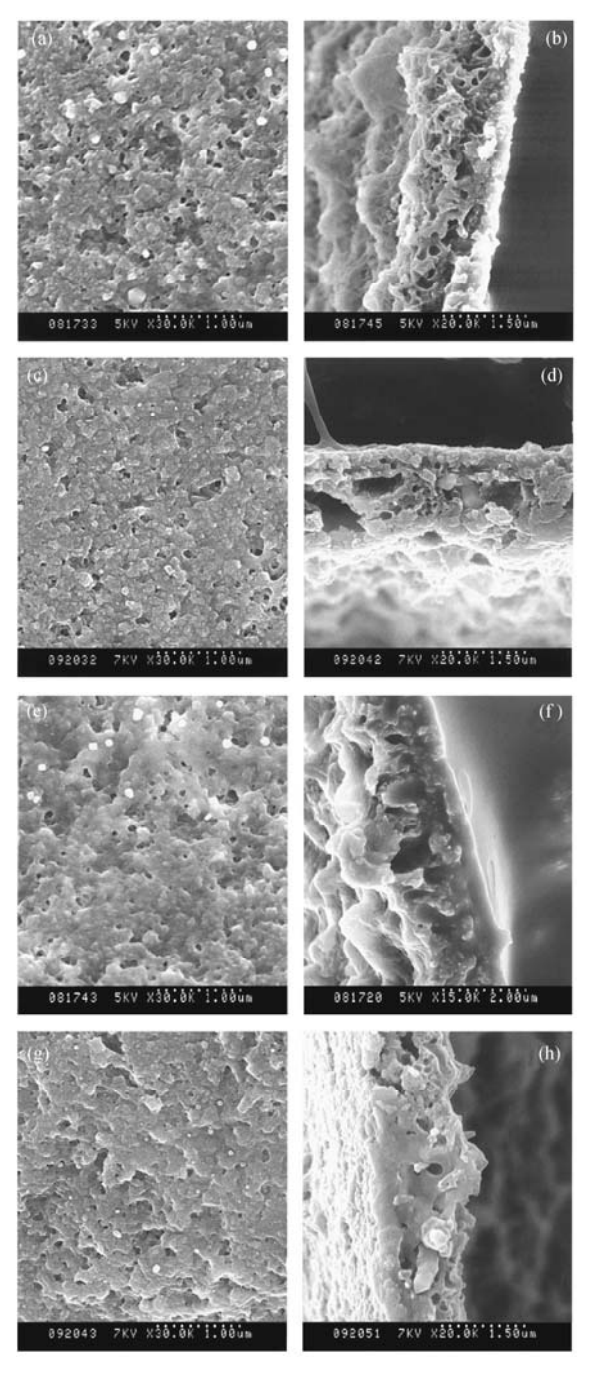


Fig.3.7. FE-SEM micrographs of the outer surfaces and cross-sections of the PNIPAM-grafted microcapsules. (a, b) MC6281g10W20; (c, d) MC6281g30W20; (e, f) MC6281g30W120; (g, h) MC6281g30W240 (Reproduced with permission from Ref. [6]). Copyright (2001), Elsevier

The permeability coefficient, *P*, could be calculated using the following equation derived from Fick's first law of diffusion (please see **Section 2.3.2.3** for detailed deduction):^[6]

$$P = \frac{V_{s}V_{m}}{A(V_{s} + V_{m})t} \ln \frac{C_{f} - C_{i}}{C_{f} - C_{t}} = \frac{V_{s}V_{m}}{A(V_{s} + V_{m})t} \ln \frac{S_{f} - S_{i}}{S_{f} - S_{t}}$$
(3.1)

where C_i , C_t , and C_f are the initial, intermediary (at time t) and final concentrations of solute in the surrounding medium, respectively. The parameters V_m and A are, respectively, the total volume and the total surface area of microcapsules, V_s is the volume of the surrounding medium and S_i , S_t , and S_f are the initial, intermediary and final specific conductance for NaCl, or absorbance at 360 nm for VB₁₂ of the surrounding medium, respectively.

In all the experiments, a plot of $\ln[(S_f - S_i)/(S_f - S_t)]$ (from Eq.(3.1)) against time, t, showed a straight line. From this, the permeability coefficient could be calculated using the following equation:

$$P = K \frac{V_{\rm s} V_{\rm m}}{A (V_{\rm s} + V_{\rm m})} \tag{3.2}$$

where *K* is the gradient of the line from the $\ln[(S_f - S_i)/(S_f - S_t)]$ versus *t* plots.

3.2.3.1 Thermo-Responsive Release of Solutes across the PNIPAM-Grafted Microcapsule Membranes

The permeability coefficient of NaCl release from un-grafted and PNIPAMgrafted microcapsules was investigated in the temperature range 25 to 40 °C, and the results are shown in Figs.3.8 and 3.9. [6] Fig.3.8 shows the positive thermo-response release of NaCl from PNIPAM-grafted microcapsules with low graft yields. The release of NaCl from the PNIPAM-grafted microcapsule was slow in the temperature range 25 to 31 °C, and fast in the temperature range 34 to 40 °C. A sharp transition of the permeability coefficient occurred going from 31 to 34 °C, which corresponded to the LCST of PNIPAM (around 32 °C). On the other hand, the un-grafted microcapsule did not show such a sharp transition of the permeability coefficient between 31 and 34 °C under the same experimental conditions. Below the LCST, the linear grafted PNIPAM on the inner pore surface was in a swollen state and the pores in the membrane were closed by the PNIPAM gate; as a result the permeability coefficient was low. In contrast, the grafted PNIPAM on the inner pore surface was in a shrunken state at temperatures above the LCST. Therefore, the pores in the membrane were open and a higher permeability coefficient was the result (as illustrated in Fig.3.1). The slight changes in the release rate of the PNIPAM-grafted microcapsules upon changing the temperature from 25 to 31 °C, and from 34 to 40 °C, and the increase in the permeability coefficient of the un-grafted microcapsules in the temperature range from 25 to 40 °C, are due to the increasing diffusivity of NaCl with increasing temperature.

Fig.3.9 shows the results of the negative thermo-response release of NaCl from PNIPAM-grafted microcapsules with high graft yields. ^[6] At a high graft yield, because there is too much grafted polymer in the pores of the membrane, the pores cannot reopen even at high temperatures (above the LCST), *i.e.*, the pore is choked. However, the grafted-PNIPAM is still highly hydrophilic and water-soluble below the LCST, and dramatically becomes hydrophobic and insoluble in water above the LCST, undergoing a phase transition. As the solute is water-soluble, any solute diffusion within the membrane occurs primarily within the water-filled regions in the spaces delineated by the polymer chains. It is easier for the solute to find water-filled regions in the membrane with hydrophilic PNIPAM gates rather than in the membrane with hydrophobic PNIPAM gates. Therefore, the release rate of the solute from PNIPAM-grafted microcapsules at low temperatures (below the LCST) is higher than that at high temperatures (above the LCST).

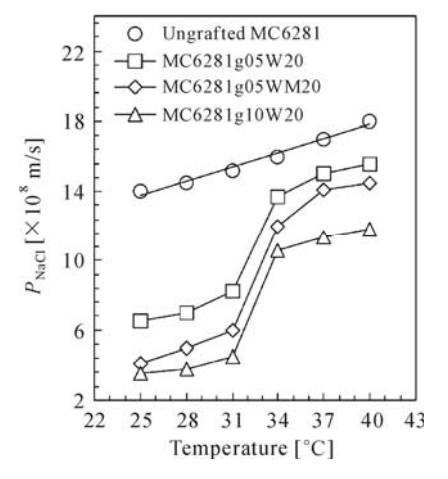


Fig. 3.8. Positive thermo-response release of NaCl from PNIPAM-grafted microcapsules with low graft yields (Reproduced with permission from Ref. [6]). Copyright (2001), Elsevier

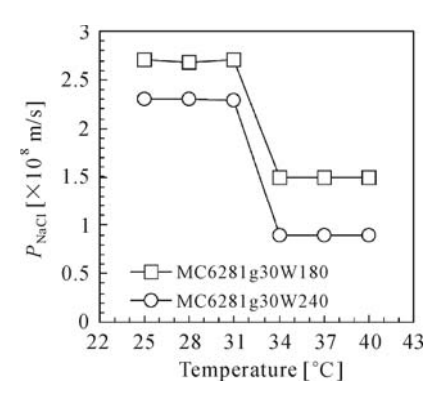


Fig.3.9. Negative thermo-response release of NaCl from PNIPAM-grafted microcapsules with high graft yields (Reproduced with permission from Ref. [6]). Copyright (2001), Elsevier

The thermo-responsive release characteristics of VB_{12} from un-grafted and PNIPAM-grafted microcapsules with different graft yields are illustrated in Fig.3.10. [6] For VB_{12} , the dual-responsive release property of the PNIPAM-grafted microcapsules was also obtained. At low graft yields, the PNIPAM-grafted microcapsules show a positive thermo-response release, while at high graft yields they show a negative thermo-response release. Compared with the release rate of NaCl, the "on/off" ratio of the release rate of VB_{12} from the PNIPAM-grafted microcapsules with low graft yield is much larger. Above the LCST, the pores in the membrane of the PNIPAM-grafted microcapsules with low graft yield are open, and solute diffusion occurs within the pores with openings larger than the solute size. Below the LCST the pores are closed and solute diffusion occurs within the PNIPAM hydrogels. As the size of a solute increases, in general the diffusivity of a solute through a hydrogel decreases remarkably. [8,9] The size of the VB_{12} molecule is larger than that of NaCl and therefore the diffusivity of VB_{12} through the PNIPAM hydrogel is much lower than that of NaCl.

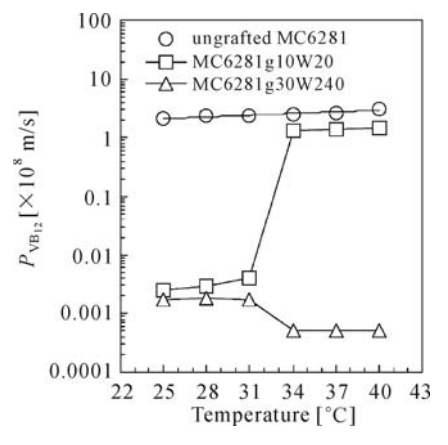


Fig.3.10. Thermo-responsive release of vitamin B₁₂ from PNIPAM-grafted microcapsules with different graft yields (Reproduced with permission from Ref. [6]). Copyright (2001), Elsevier

3.2.3.2 Reversible Thermo-Responsive Release Characteristics

To verify the reversibility of the PNIPAM gates grafted on the surface of the pores in the microcapsule membrane, release experiments were carried out by alternatively changing the environmental temperature across the LCST. The chosen route was: $40~^{\circ}\text{C} \rightarrow 25~^{\circ}\text{C} \rightarrow 37~^{\circ}\text{C} \rightarrow 28~^{\circ}\text{C} \rightarrow 34~^{\circ}\text{C} \rightarrow 31~^{\circ}\text{C} \rightarrow 40~^{\circ}\text{C} \rightarrow 25~^{\circ}\text{C}$. To ensure that there was enough solute inside the microcapsules for release during the entire release experiment, solute (VB₁₂) was reloaded into the inner space of the microcapsules after each run. The reversible thermo-responsive release characteristics of the PNIPAM-grafted microcapsules are shown in **Fig.3.11**. The thermo-responsive release of the PNIPAM-grafted microcapsules was found to be satisfactorily reversible and reproducible, suggesting that the grafted PNIPAM gates retained

their thermal swelling/shrinking and hydrophilic/hydrophobic properties intact, even though they underwent repeated temperature changes across the LCST. That is to say, a repeatable thermo-responsive release can be effectively achieved.

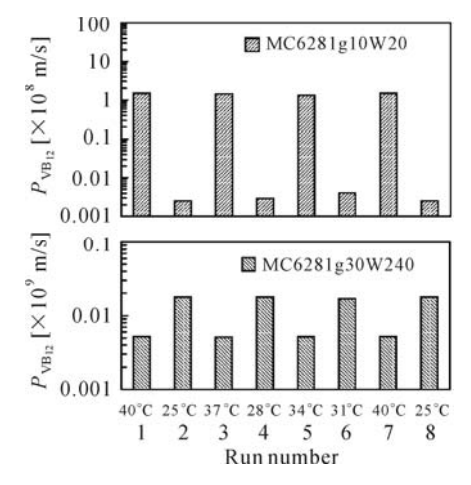


Fig.3.11. Reversible thermo-responsive release characteristics of vitamin B_{12} (VB₁₂) through the PNIPAM-grafted microcapsules with different graft yields (Reproduced with permission from Ref. [6]). Copyright (2001), Elsevier

3.3 Monodispersed Thermo-Responsive Microcapsules with Porous Membrane and PNIPAM Gates

For drug delivery systems (DDS), monodispersed small-size microcapsules are preferable to polydispersed large-size microcapsules. A uniform microcapsule particle size is important, because the distribution of the microcapsules within the body and the interaction with biological cells is greatly affected by the particle size. [10] In addition, if monodispersed microcapsules are available, the drug release kinetics can be manipulated, thereby making it easier to formulate more sophisticated systems. For DDS, there is a size limit for particles to traverse certain organs, [11] and a small particle size minimizes any potential irritant reaction at the injection site. [12] Environmental stimuli-responsive controlled-release systems have been developed, with the aim of achieving site-specific and time-programmed drug delivery, and this is one of the targets of future controlled-DDS. [11] Therefore, the fabrication of small-sized monodispersed stimuli-responsive microcapsules (or hollow reservoirs) that enable the encapsulation of various materials is of both scientific and technological interest.

3.3.1 Preparation of Monodispersed Microcapsules with Porous Membrane

Several methods have been developed to fabricate monodispersed microcapsules. In this section, the preparation of monodispersed microcapsules with porous membrane will be introduced.

3.3.1.1 Fabrication of Small-Sized Monodispersed O/W Emulsions

Because O/W emulsion droplets are the templates for fabricating porous microcapsules as mentioned above, small-sized monodispersed emulsions will result in small-sized monodispersed stimuli-responsive microcapsules. Recently, Shirasu porous glass (SPG) membrane emulsification was introduced to control the size of emulsion droplets during their formation, and to narrow the size distribution of the resulting microcapsules. [7] SPG membrane emulsification is based on injecting a disperse phase through a porous membrane, with the resulting droplets forming at the end of pores on the membrane surface after coming into contact with the continuous phase. [13-15] Thus, using this technique, it is easier to control the droplet size and size distribution.

The SPG membrane emulsification procedure was carried out using an SPG membrane emulsification kit (Kiyomoto Iron Works Co., Ltd., Miyazaki, Japan) as shown in Fig.3.12.^[7] The SPG membrane (SPG Technology Co., Ltd., Miyazaki, Japan) was tube-shaped with an outer diameter of 10 mm. Three different SPG membrane pore sizes of 4.8, 2.5, and 1.2 µm were used in the experiments and the relative transmembrane pressures were 10, 20, and 40 kPa, respectively. The disperse phase, 10 ml of organic solvent containing monomer Terephthaloyl dichloride (TDC), was stored in a pressure-tight vessel and allowed to permeate through the SPG membrane under a certain pressure into the continuous phase. Three types of mixed organic solvents were used: benzene/xylene (2:1 [v/v]), chloroform/cyclohexane (1:4 [v/v]) and benzene/xylene/liquid paraffin (1:1:2 [v/v/v]). Three different concentrations of monomer TDC of 0.1, 0.5 and 1.5 mol·L⁻¹ were used. The continuous phase, 150 ml water containing an emulsifier and a stabilizer, was forced to pass through the SPG membrane surface by magnetic stirring. SDS with concentrations of 0, 17.34, 34.68, 69.36 mmol·L⁻¹ and polyoxyethylene (20) sorbitan monooleate (Tween 80, average molecular weight 1.21×10³) with concentrations of 0, 4.12, 8.24 mmol·L⁻¹, were used as the emulsifiers individually. Three concentrations of stabilizer polyvinyl alcohol (PVA, average molecular weight 1.23×10⁵, 86% - 90% hydrolysis) of 0, 40.59, 81.17 μmol·L⁻¹ were used. The stirring speed was 500 r/min. During emulsification, the temperature was kept at a constant 10 °C using a thermostatic unit.

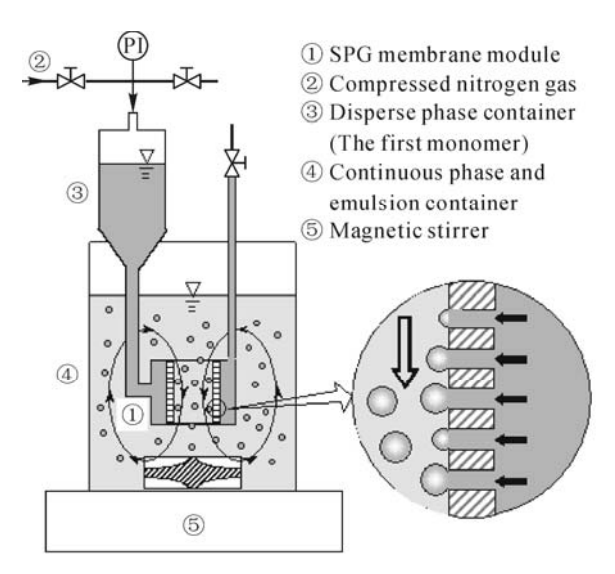


Fig.3.12. Schematic illustration of the SPG membrane emulsification process (Reproduced with permission from Ref. [7]). Copyright (2002), American Chemical Society

The optical micrographs and size distributions of the emulsions prepared with different disperse phase and different emulsification times are shown in **Fig.3.13**,^[7] in which d_{em} is the mean diameter of emulsions and the particle size dispersal coefficient δ is defined as

$$\delta = \frac{D_{90} - D_{10}}{D_{50}} \tag{3.3}$$

where D_n (n = 10, 50, and 90) denotes the cumulative number percentage of particles with diameter up to D_n equal to n%. The smaller the value of δ , the narrower the size distribution.

At relatively long emulsification times in Figs.3.13a~3.13d, the mean diameter of the emulsion droplets decreases, and the particle size dispersal coefficient increases with an increase in the solubility of the disperse phase in water. However, for the disperse phase with a higher solubility in water (on comparing Figs.3.13(e, f) with Figs.3.13(c, d)), a satisfactory monodispersity of the emulsions could be obtained by adopting a shorter emulsification time. If the solubility of the disperse phase in water is marked, the size of the emulsion droplets becomes smaller with time because of the solvation of the disperse phase. Therefore, if the emulsification time for the SPG membrane emulsification process is long, the monodispersity of the droplet sizes at the end of the emulsification period will not be satisfactory. For the preparation of the desired thermo-responsive microcapsules, a porous structure of the hollow microcapsule membrane is essential. It has been found that the microcapsule membranes become more porous with increasing solubility of the solvent of the disperse phase in water, and *vice versa*. [6] Liquid paraffin inside the microcapsule was very difficult to remove by freeze-drying. Therefore, it was

not appropriate to use liquid paraffin as the solvent of the disperse phase in preparing hollow microcapsules with porous membranes. A mixture of benzene and xylene (2:1 [v/v]) was selected as the organic solvent of the disperse phase for fabricating porous microcapsules. [6] Therefore, a shorter emulsification time was selected to obtain a satisfactory monodispersity of the emulsion droplets (*e.g.*, shorter than 60 min).

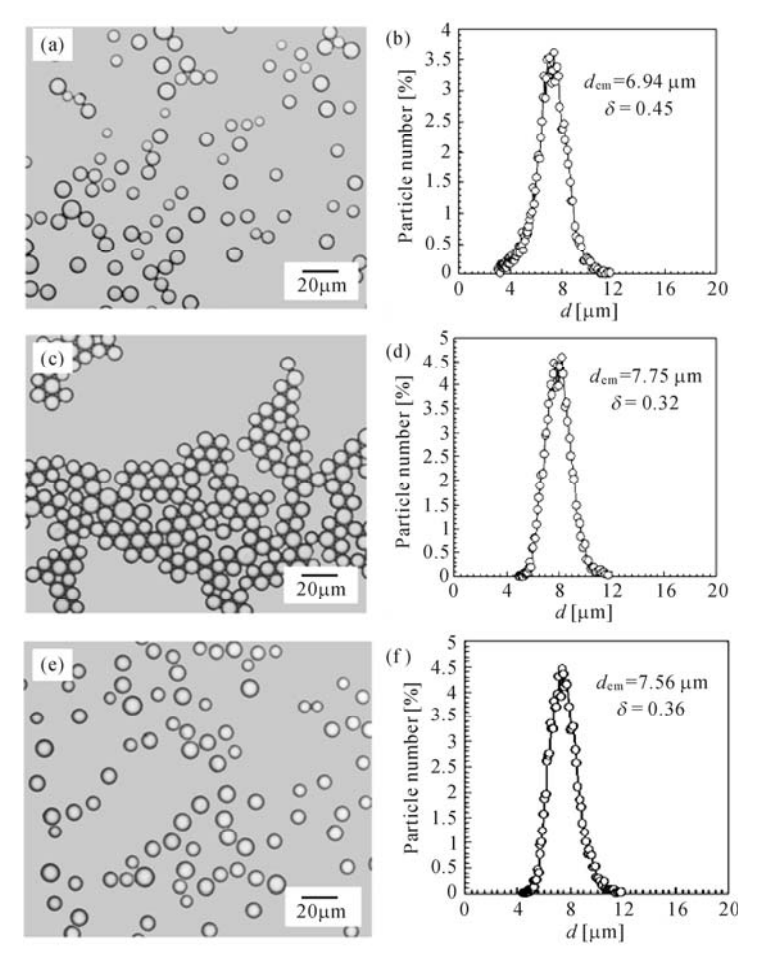


Fig.3.13. Optical micrograph and the size distribution of the emulsions; (a, b) Prepared with chloroform/cyclohexane (1 : 4 [v/v]) as the solvent for the disperse phase, SPG membrane pore size $d_p = 2.5 \, \mu \text{m}$, [TDC] = 0.1 mol·L⁻¹, [SDS] = 17.34 mmol·L⁻¹, [PVA] = 81.17 μmol·L⁻¹ and emulsification time $t_e = 270 \, \text{min}$; (c, d) Prepared with benzene/xylene/liquid paraffin (1 : 1 : 2 [v/v/v]) as the solvent for the disperse phase, SPG membrane pore size $d_p = 2.5 \, \mu \text{m}$, [TDC] = 0.1 mol·L⁻¹, [SDS] = 17.34 mmol·L⁻¹, [PVA] = 81.17 μmol·L⁻¹ and emulsification time $t_e = 270 \, \text{min}$; (e, f) Prepared with benzene/xylene (2 : 1 [v/v]) as the solvent for the disperse phase, SPG membrane pore size $d_p = 2.5 \, \mu \text{m}$, [TDC] = 0.5 mol·L⁻¹, [SDS] = 17.34 mmol·L⁻¹, [PVA] = 40.59 μmol·L⁻¹ and emulsification time $t_e = 60 \, \text{min}$ (Reproduced with permission from Ref. [7]). Copyright (2002), American Chemical Society

The effects of the surfactant and the stabilizer in the continuous phase on the SPG membrane emulsification are shown in **Table 3.3**. [7] When only SDS was used as the surfactant and no stabilizer was added to the continuous phase, emulsion droplets could not be obtained when small membrane pore sizes were used (e.g., = 1.2 μ m), and only crystal-like solid particles existed in the continuous phase. If the solubility of the disperse phase in water is large and the membrane pore size very small, then the amount of solvent in the disperse phase, that gradually dissolved into the continuous phase by diffusion and solution and finally disappeared into the air by volatilization, could be as large as the feed amount from the disperse phase. In such a case no emulsion droplets could be obtained, as the solvent is totally lost by the above-mentioned solution, diffusion and volatilization. However, the monomer used, TDC, was not soluble in water and not volatilizable in the air, and therefore only crystal-like TDC solid particles were observed in the continuous phase.

Table 3.3. Effect of the surfactant and the stabilizer on the SPG membrane emulsification (Reproduced with permission from Ref. [7]). Copyright (2002), American Chemical Society

No.	Continuous pha	se (150 ml) ⁽¹⁾	Membrane pore size [μm]/Pressure [kPa]			
	Surfactant	Stabilizer	4.8/10	2.5/20	1.2/40	
E-1	SDS 17.34 mmol·L	None	$O^{(2)}$	$O(30 \min) \rightarrow *^{(3)}$	*	
E-2	SDS 34.68 mmol·L ⁻¹	None	O	O (15 min)→*	*	
E-3	Tween80 4.12 mmol·L ⁻¹	None		×		
E-4	None	PVA 81.17 μmol·L ⁻¹		×		
E-5	SDS 17.34 mmol·L ⁻¹	PVA 40.59 μmol·L ⁻¹	O	O	O (60 min) $\rightarrow \times^{(4)}$	
E-6	SDS 17.34 mmol·L ⁻¹	PVA 81.17 μmol·L ⁻¹	O	O	O (35 min)→×	
E-7	SDS 17.34 mmol·L ⁻¹ Tween80 8.24 mmol·L ⁻¹	PVA 40.59 μ mol·L ⁻¹		×		

- *Note*: (1) Disperse phase: 10 ml benzene/xylene (2:1 [v/v]) containing 1.5M TDC;
 - (2) Key to symbols: "O": monodispersed emulsions (δ <0.4); "×": polydispersed emulsions (δ >0.4); "*": only crystal-like solid particles and no emulsion droplets; and "--": experiment was not carried out.
 - (3) Monodispersed emulsions initially, but the emulsions disappeared after 30 minutes and only crystal-like solid particles existed.
 - (4) Monodispersed emulsions initially, but large emulsion droplets appeared 60 minutes later and the emulsions became polydispersed.

To improve the stability of the emulsions in the SPG membrane emulsification process, partially hydrolyzed PVA was introduced as a stabilizer. On adding the PVA stabilizer, small-sized monodispersed emulsions were obtained within a relatively short emulsification time using the SPG membrane emulsification technique with a small membrane pore size. The addition of the PVA stabilizer improved the stability of the emulsions for two main reasons: (i) the PVA polymer chains provide repulsive forces between the droplets and so improve the emulsion stability by steric stabilization;^[16-18] and (ii) the addition of PVA increases the viscosity of the continuous phase and therefore the diffusion and solvation of the disperse phase in the continuous phase will be restrained,^[19] resulting in improved emulsion stability.

However, when PVA stabilizer but no surfactant was used, the resulting emulsions were polydispersed in the SPG membrane emulsification process.

The addition of the non-ionic surfactant Tween80 in the continuous phase always resulted in polydispersed emulsion products. To obtain monodispersed oil-in-water (O/W) emulsion droplets using SPG membrane emulsification, the best choice for the surfactant in the continuous phase would be an anionic surfactant, because of the existence of silanol groups on the surface of the SPG.

3.3.1.2 Preparation of Monodispersed Microcapsules with Porous Membrane

The microcapsules were prepared by the interfacial polymerization method as described above. [6] The dosage ratio of Ethylene diamine (EDA) to TDC was selected as 15:1 ml/g. 20 ml water containing 1.18 mol·L⁻¹ sodium carbonate was used as the buffer solution. The stirring speed used was 250 r/min. The temperature was kept at a constant 10 °C using a thermostatic unit and the polymerization time was 10 min. The addition of PVA stabilizer increased the stability of the emulsions and improved the monodispersity of the emulsions in the SPG membrane emulsification process. However, with a certain quantity of PVA in the continuous phase, the microcapsules aggregated/flocculated immediately after the addition of the buffer and the second monomer to initiate the interfacial polymerization. After the interfacial polymerization, the aggregated/flocculated microcapsules could not be well separated again, even when ultrasonification was used. [7] The effect of surfactant concentration and stabilizer concentration on the dispersion condition of the microcapsules is shown in Table 3.4.[7] From the results in Table 3.4, some conclusions can be drawn regarding the aggregation phenomena of the microcapsules in the interfacial polymerization: (i) aggregation occurs only when enough PVA exists in the continuous phase at a given surfactant concentration; (ii) aggregation occurs only after the addition of sodium hydroxide buffer solution and the second monomer (EDA) into the continuous phase (the emulsion droplets are stable and well dispersed before this); and (iii) aggregation can be prevented by adding an appropriate amount of Tween80 or SDS into the emulsion dispersion before starting the interfacial polymerization process. This indicates that aggregation results from the interaction between the PVA chains and the ions, and that aggregation can be prevented by adding enough low molecular weight surfactant before starting the interfacial polymerization process.

Fig.3.14 shows FE-SEM micrographs of both the aggregated and the well-dispersed microcapsules. ^[7] For the aggregated microcapsules, adjacent microcapsules were found to be connected to each other by a polymeric substance, as shown in **Figs.3.14a** and **3.14b**. The aggregation phenomenon here seems to be similar to that of a bridging flocculation, but the bridging substance was not a polymer flocculant. The polymeric substance arose during interfacial polymerization. In contrast, **Figs.3.14c** and **3.14d** show that adjacent microcapsules were bridging-free when prepared with the addition of an appropriate quantity of Tween 80 before starting the interfacial polymerization process.

No.	In the		Emulsion	Addition of	In the interfacial		Microcapsule	
	emulsification		droplet	surfactant before	polymerization process		dispersal	
	process		dispersal	starting the			situation	
	SDS	PVA	situation	interfacial	SDS	Tween80	PVA	
	[mmol	[µmol		polymerization	[mmol	[mmol	[µmol	
	$\cdot L^{-1}$]	·L 1]			·L ⁻¹]	·L ⁻¹]	·L 1]	
P-1	17.34	0	Dispersed	No	17.34	0	0	Dispersed
P-2	34.68	0	Dispersed	No	34.68	0	0	Dispersed
P-3	17.34	40.59	Dispersed	No	17.34	0	40.59	Aggregated
P-4	17.34	40.59	Dispersed	Yes (Tween80)	17.34	0.5	40.59	Aggregated
P-5	17.34	40.59	Dispersed	Yes (Tween80)	17.34	4.0	40.59	Dispersed
P-6	17.34	40.59	Dispersed	Yes (SDS)	43.45	0	40.59	Dispersed
P-7	34.68	40.59	Dispersed	No	34.68	0	40.59	Dispersed

Table 3.4. Effect of the concentration of the surfactant and the stabilizer on the microcapsule aggregation (Reproduced with permission from Ref. [7]). Copyright (2002), American Chemical Society

Note: SPG membrane emulsification: $d_p = 4.8 \ \mu m$; $P = 10 \ kPa$; continuous phase = 150 ml; disperse phase = 10 ml benzene/xylene (2:1 [v/v]) containing 1.5M TDC; $T = 10 \ ^{\circ}$ C

A schematic representation of the aggregation behavior, and the prevention of aggregation by adding enough low molecular weight surfactant, is illustrated in Fig.3.15.^[7] PVA has been reported to form a molecular compound with sodium hydroxide arising from a polymer-ion complex. [20] At certain concentrations, a combination of SDS and PVA can result in both SDS molecules and PVA chains being adsorbed onto the surfaces of the emulsion droplets (case a1). After sodium hydroxide buffer solution and the second monomer are added to the continuous phase, the PVA chains will undergo both intra-chain and inter-chain cross-linkages due to the polymer-ion complex formation.^[21] Owing to the inter-chain crosslinking between the adsorbed PVA chains in the narrow areas between the adjacent emulsion droplets, there will be an attractive force between the PVA chains and some PVA chains may be pulled out to some extent by this attractive force (a2). This would be accompanied by a certain amount of monomer TDC being emitted from the emulsion droplets by the PVA chains. By this mechanism, a "bridging" polymer between the adjacent microcapsules results from the interfacial polymerization (a3). Consequently, the prepared microcapsules would be aggregated.

In contrast, when an appropriate quantity of low molecular weight surfactant is added to the emulsion dispersion before the interfacial polymerization, the adsorbed PVA chains on the surfaces of the emulsion droplets will be totally displaced by the surfactant molecules (b1). This is due to the competitive adsorption of the low molecular weight surfactant and the PVA onto the particle surfaces. It has been proven that low molecular weight substances can be used to displace adsorbed polymers from particle surfaces. [22-26] If a low molecular weight surfactant is added during or after the adsorption of a polymer, then the higher adsorption energy per surfactant molecule may exceed that of a single polymer segment. This results in a displacement of the polymer segments from the particle surface and, above a given

concentration of the surfactant, complete desorption of the polymer molecule may take place. [22] Therefore, the phenomena occurring in case (a2) will not happen, as there are no PVA chains adsorbed on the emulsion surfaces (b2). As a result, the prepared microcapsules will not be aggregated but will be dispersed (b3).

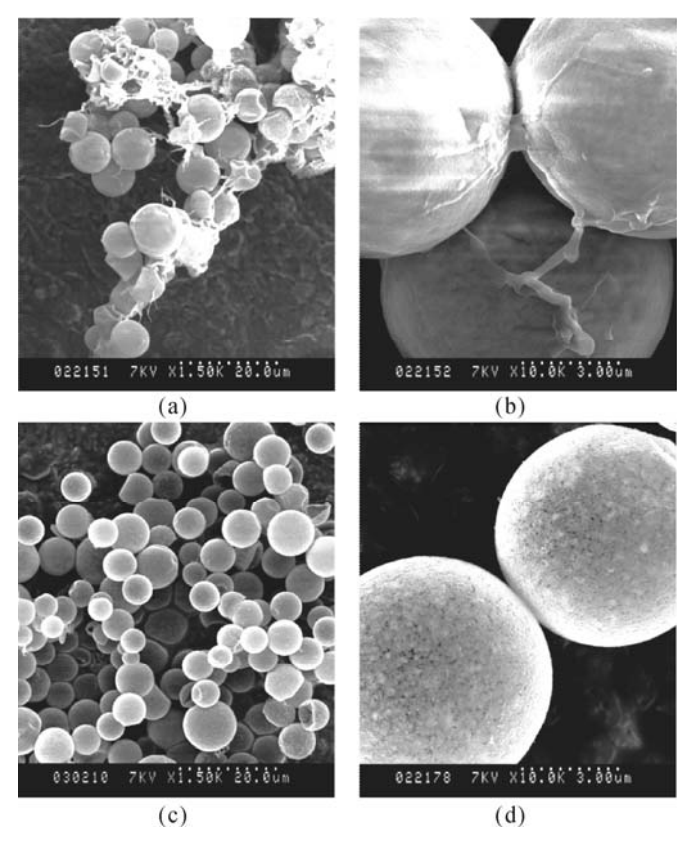


Fig.3.14. FE-SEM micrographs of the aggregated microcapsules (a, b) and well-dispersed microcapsules (c, d). (Reproduced with permission from Ref. [7]). Copyright (2002), American Chemical Society

In summary, the optimum SDS concentration and the optimum PVA concentration in the SPG membrane emulsification process could be selected by solely considering the monodispersity of the emulsion droplets. However, before commencing the interfacial polymerization process, these two concentrations need to be checked to avoid any aggregation of the microcapsules. If necessary, enough SDS or Tween80 needs to be added to prevent the microcapsules from aggregating in the interfacial polymerization process.

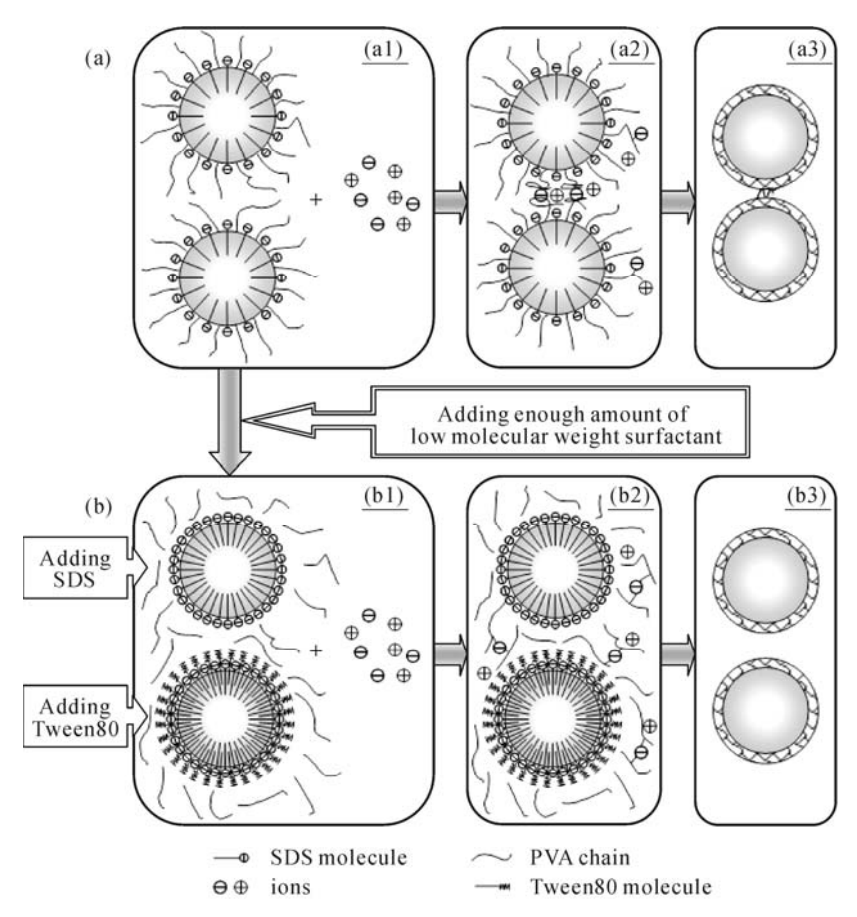


Fig.3.15. A schematic representation of the aggregation behavior (a) and the prevention of aggregation (b) by the addition of an appropriate quantity of low molecular weight surfactant. (Reproduced with permission from Ref. [7]). Copyright (2002), American Chemical Society

FE-SEM micrographs of the outer surfaces and cross-sectional view of the microcapsules prepared with an SPG membrane pore size of 2.5 μm and a disperse phase with TDC concentration of 1.5 mol·L¹ are shown in **Fig.3.16.**^[7] **Figs.3.16b** and **3.16c** show that the microcapsules have a hollow structure with a thin, porous membrane. This type of microcapsule is suitable for environmental stimuli-responsive controlled-release to obtain a fast responsiveness. **Fig.3.17** shows FE-SEM micrographs of the hollow microcapsules prepared with an SPG membrane pore size of 1.2 μm and a disperse phase with TDC concentration of 1.5 mol·L¹ [7] **Fig.3.17a** shows that the microcapsules are highly monodispersed with a mean diameter of around 4 μm. **Fig.3.17b** shows that the ungrafted microcapsules also have an obviously porous membrane structure. In subsequent experiments,

including plasma-graft pore-filling polymerization experiments and release experiments, the monodispersed microcapsules used were all of this type with a mean diameter of about 4 μm .

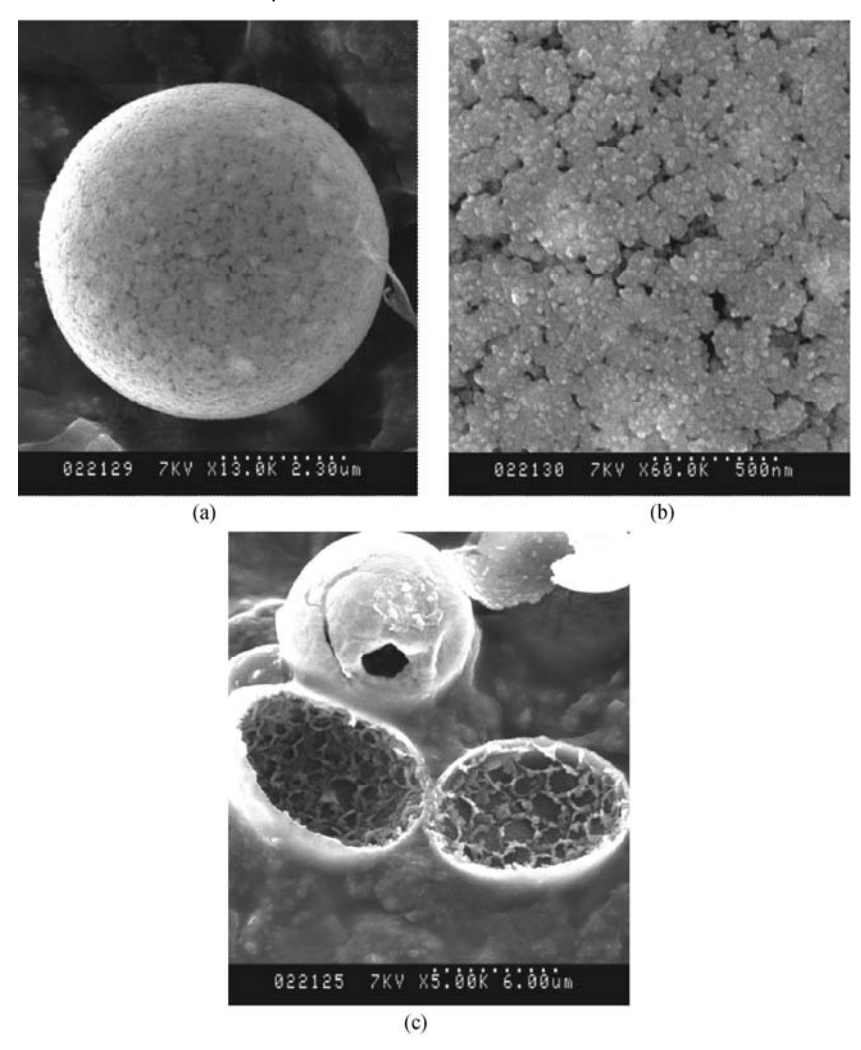


Fig. 3.16. FE-SEM micrographs of the hollow microcapsules prepared with SPG membranes with pore size of 2.5 μm and a disperse phase with TDC concentration of 1.5 mol·L⁻¹ [SDS] = 17.34 mmol·L⁻¹, [PVA] = 40.59 μmol·L⁻¹, emulsification time t_e = 50 min and after the emulsification Tween80 was added to let [Tween80] = 4.12 mmol·L⁻¹. (a, b) Outer surface; (c) Cross-section (Reproduced with permission from Ref. [7]). Copyright (2002), American Chemical Society

3.3.2 Monodispersed Microcapsules with Porous Membrane and Grafted PNIPAM Gates

Plasma-graft pore-filling polymerization was used to graft linear PNIPAM chains into the pores of the microcapsule membrane according to the above-mentioned method. **Fig.3.17c** shows that the pores in the microcapsule membrane become smaller after the plasma-graft pore-filling polymerization of PNIPAM.^[7]

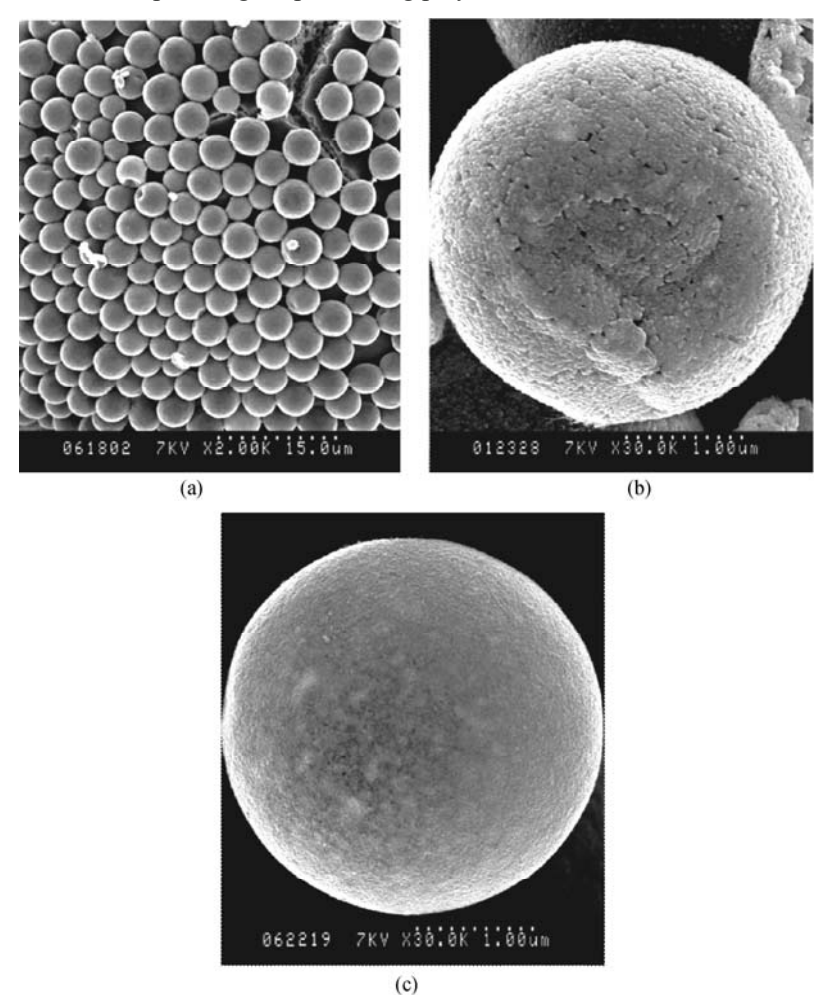


Fig.3.17. FE-SEM micrographs and size distribution of well-dispersed hollow microcapsules prepared with SPG membranes with pore size of 1.2 μm and a disperse phase with TDC concentration of 1.5 mol·L $^{-1}$. [SDS] = 17.34 mmol·L $^{-1}$, [PVA] = 40.59 μmol·L $^{-1}$, emulsification time t_c = 50 min and after the emulsification Tween80 was added to let [Tween80] = 4.12 mmol·L $^{-1}$. (a, b) Ungrafted microcapsules; (c) PNIPAM-grafted microcapsule (Reproduced with permission from Ref. [7]). Copyright (2002), American Chemical Society

3.3.3 Thermo-Responsive Controlled-Release Characteristics

Fig.3.18 shows the thermo-response release of NaCl from PNIPAM-grafted monodispersed microcapsules with a mean diameter of about 4 µm. [7] The NaCl concentration of the bulk solution increased slowly at 25 °C and rapidly at 40 °C; that means the release of NaCl from the PNIPAM-grafted microcapsules was slow at 25 °C and was fast at 40 °C. The lower critical solution temperature (LCST) of PNIPAM is around 32 °C. At temperatures below the LCST, the linear-grafted PNIPAM chains in the pores of the microcapsule membrane were swollen and the pores of the membranes were closed by the PNIPAM gates. As a result, the release of NaCl molecules across the microcapsule membranes was slow. In contrast, at temperatures above the LCST, the linear-grafted PNIPAM chains in the membrane pores were shrunk and therefore the pores of the microcapsule membranes were open, resulting in a faster release rate of the NaCl molecules across the microcapsule membranes. Therefore, the release rate of the solute molecules from these kinds of PNIPAM-grafted microcapsules at higher temperatures (above the LCST) is greater than that at lower temperatures (below the LCST). The thermo-responsive release of solute from the PNIPAM-grafted small-sized monodispersed microcapsules was also satisfactorily reversible and reproducible.

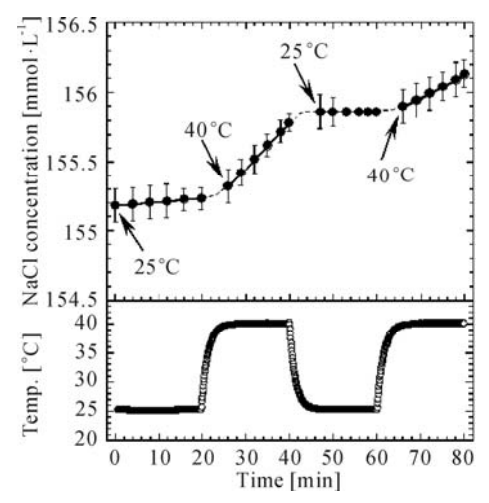


Fig.3.18. Thermo-responsive release of NaCl from the PNIPAM-grafted monodispersed microcapsules with a mean diameter of about 4 μ m (Reproduced with permission from Ref. [7]). Copyright (2002), American Chemical Society

By using the methods described in this chapter, it is possible to fabricate other signal-receptive monodispersed and small-sized hollow microcapsules easily, by introducing other stimuli-responsive functional polymers to prepare linear-grafted functional polymeric gates of the pores of the microcapsule membranes.

References

- [1] Breimer D D. Future challenges for drug delivery. *Journal of Controlled Release*, **1999**, *62*: 3-6.
- [2] Okano T, Bae Y H, Jacobs H, Kim S W. Thermally on-off switching polymers for drug permeation and release. *Journal of Controlled Release*, **1990**, *11*: 255-265.
- [3] Yoshida Y, Kaneko Y, Sakai K, Okano T, Sakurai Y, Bae T H, Kim S W. Positive thermosensitive pulsatile drug release using negative thermosensitive hydrogels. *Journal of Controlled Release*, **1994**, *32*: 97-102.
- [4] Cammas S, Suzuki K, Sone C, Sakurai Y, Kataoka K, Okano T. Thermoresponsive polymer nanoparticles with core-shell micelle structure as site-specific drug carriers. *Journal of Controlled Release*, **1997**, 48: 157-164.
- [5] Chung J E, Yokoyama M, Okano T. Inner core segment design for drug delivery control of thermo-responsive polymeric micelles. *Journal of Controlled Release*, **2000**, *65*: 93-103.
- [6] Chu L Y, Park S H, Yamaguchi T, Nakao S. Preparation of thermoresponsive core-shell microcapsules with a porous membrane and poly(*N*-isopropylacrylamide) gates. *Journal of Membrane Science*, **2001**, *192*: 27-39.
- [7] Chu L Y, Park S H, Yamaguchi T, Nakao S. Preparation of micron-sized monodispersed thermo-responsive core-shell microcapsules. *Langmuir*, **2002**, *18*: 1856-1864.
- [8] Peppas N A. *Hydrogels in Medicine and Pharmacy*. CRC Press, Boca Raton, FL, USA, **1987**.
- [9] Amsden B. Solute diffusion within hydrogels. Mechanisms and models. *Macromolecules*, **1998**, *31*: 8382-8395.
- [10] Shiga K, Muramatsu N, Kondo T. Preparation of poly(*D*,*L*-lactide) and copoly(lactide-glycolide) microspheres of uniform size. *Journal of Pharmacy Pharmacology*, **1996**, *48*: 891-895.
- [11] Thews G, Mutschler E, Vaupel P. *Anatomie*, *Physiologie*, *Pathophysiologie des Manschen*. Wissenschaftl. Verlagsges, Stuttgart, **1980** (in German).
- [12] Little K, Parkhouse J. Tissue reactions to polymers. *Lancet*, **1962**, *II*(7261): 857-861.
- [13] Nakashima T, Shimizu M, Kukizaki M. Membrane emulsification by microporous glass. *Key Engineering Materials*, **1991**, *61&62*: 513-516.
- [14] Kandori K, Kishi K, Ishikawa T. Preparation of monodispersed W/O emulsions by Shirasu-porous-glass filter emulsification. *Colloids and Surfaces*, **1991**, *55*: 73-78.
- [15] Chu L Y, Xie R, Zhu J H, Chen W M, Yamaguchi T, Nakao S. Study on SPG membrane emulsification processes for the preparation of monodispersed core-shell microcapsules. *Journal of Colloid and Interface Science*, **2003**, *265*: 187-196.
- [16] Bachtsi A R, Boutris C J, Kiparissides C. Production of oil-containing

- crosslinked poly(vinyl alcohol) microcapsules by phase separation: effect of process parameters on the capsule size distribution. *Journal of Applied Polymer Science*, **1996**, *60*: 9-20.
- [17] Chatzi E G, Kiparissides C. Drop size distributions in high holdup fraction dispersion systems: effect of the degree of hydrolysis of PVA stabilizer. *Chemical Engineering Science*, **1994**, *49*(*24B*): 5039-5052.
- [18] Kim I T, Luckham P F. The viscoelastic properties of polystyrene latex particles bearing an adsorbed layer of polyvinyl alcohol. *Journal of Colloid Interface Science*, **1991**, *144*: 174-184.
- [19] Hong P D, Chou C M, He C H. Solvent effects on aggregation behavior of polyvinyl alcohol solutions. *Polymer*, **2001**, *42*: 6105-6112.
- [20] Nagano M, Yoshioka Y. Kobunshi Kagaku, 1952, 9: 117-119 (in Japanese).
- [21] Salamone J C (ed.). *Polymer Materials Encyclopedia*. CRC Press, New York, **1996**.
- [22] Rachas I, Tadros Th F, Taylor P. The displacement of adsorbed polymer from silica surfaces by the addition of a nonionic surfactant. *Colloids and Surface A: Physicochemical Engineering Aspects*, **2000**, *161*: 307-319.
- [23] Cohen Stuart M A, Fleer G J, Scheutjens J M H M. Displacement of polymers. I. Theory. Segmental adsorption energy from polymer desorption in binary solvents. *Journal of Colloid Interface Science*, **1984**, *97*: 515-525.
- [24] Kling J A, Ploehn H J. Desorption of adsorbed poly(ethylene oxide) from colloidal polystyrene particles. *Journal of Colloid Interface Science*, **1998**, 198: 241-248.
- [25] Kawaguchi M, Chikazawa M, Takahashi A. Displacement of polymers by displacers. I. Polystyrene at the silica surface. *Macromolecules*, **1989**, *22*: 2195-2199.
- [26] Van der Beek G P, Cohen Stuart M A, Fleer G J, Holfman J E. Segmental adsorption energies for polymers on silica and alumina. *Macromolecules*, **1991**, *24*: 6600-6611.

Smart Microcapsules with Thermo-Responsive Hydrogel Membranes

Besides smart microcapsules with porous substrates and stimuli-responsive gates as described in Chapter 3, smart microcapsules can also be designed with the whole membranes consisting of stimuli-responsive smart hydrogels. In this chapter, the design, fabrication and performance of monodisperse smart microcapsules with thermo-responsive hydrogel membranes are introduced. For different application purposes, smart microcapsules with thermo-responsive PNIPAM hydrogel membranes are designed and fabricated with either water-in-oil (W/O) single emulsions, oil-in-water-in-oil (O/W/O) double emulsions, or water-in-oil-in-water-in-oil (W/O/W/O) triple emulsions as synthesis templates. The thermo-responsive PNIPAM hollow microcapsules, prepared with W/O single emulsions as templates, show reversible thermo-responsive swelling/shrinking volume phase transition behavior as the temperature changes across the lower critical solution temperature (LCST). The thermo-responsive PNIPAM hollow microcapsules, prepared with O/W/O double emulsions and W/O/W/O triple emulsions as templates, demonstrate thermo-induced burst squirting property for controlled release.

4.1 Introduction

As mentioned in Section 1.4, besides smart membranes with porous substrates and stimuli-responsive gates, smart membranes can be designed with the whole membranes made of stimuli-responsive smart hydrogels. The permeability of such membranes can be self-regulatively adjusted by the stimuli-responsive volume phase transition behavior of the smart hydrogels. **Fig.4.1** shows a schematic illustration of thermo-responsive hollow microcapsules with a crosslinked PNIPAM hydrogel membrane. The crosslinked PNIPAM microcapsule membrane exhibits a swollen and hydrophilic state at temperatures below the LCST; however, it switches to a shrunken and hydrophobic state at temperatures above the LCST. As a result,

thermo-responsive controlled release performance can be achieved with such microcapsules.

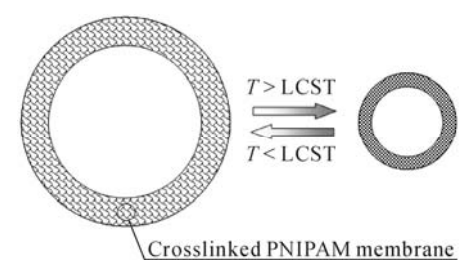


Fig.4.1. A schematic illustration of thermo-responsive hollow microcapsules with crosslinked PNIPAM hydrogel membrane

4.2 Monodisperse Thermo-Responsive PNIPAM Hollow Microcapsules Prepared with W/O Single Emulsions as Templates

Stimuli-responsive polymeric hollow microcapsules have attracted widespread interest in the last decade due to their potential applications in numerous fields, including controlled drug delivery systems, sensors, vesicles for enzymes and chemicals, and so on. As there are many cases in which temperature fluctuations occur naturally, and in which the temperature stimuli can be easily designed and artificially controlled, in recent years much attention has been focused on thermoresponsive microcapsules.

4.2.1 Fabrication Strategy and Microstructure Control

To fabricate hollow thermo-responsive microcapsules with whole PNIPAM membranes, the templating method is one of the most common. The templating method is relatively complicated, because the preparation process must be accompanied by removing the chemically-soluble or degradable cores. Therefore, the application of this approach is considered to be limited. Recently, the author's group reported on a simple method for preparation of monodisperse hollow PNIPAM microcapsules via Shirasu-porous-glass (SPG) membrane emulsification and UV-initiated polymerization at the interface of W/O single emulsions at a temperature below the LCST of PNIPAM.^[1] The preparation approach is illustrated in **Fig.4.2**.^[1] First, monomer and crosslinker are encapsulated in monodisperse W/O emulsions according to the membrane emulsification process.^[2,3] SPG membrane emulsification is based on injecting a disperse phase through a porous

membrane, with the resulting droplets forming at the end of pores on the membrane surface after coming into contact with the continuous phase. Thus, using this technique, it is easier to control the droplet size and size distribution. Next, an oil-soluble photo-initiator is added into the continuous phase of W/O emulsions. Then, hollow PNIPAM microcapsules are synthesized by free-radical polymerization initiated with UV irradiation at 20 °C.

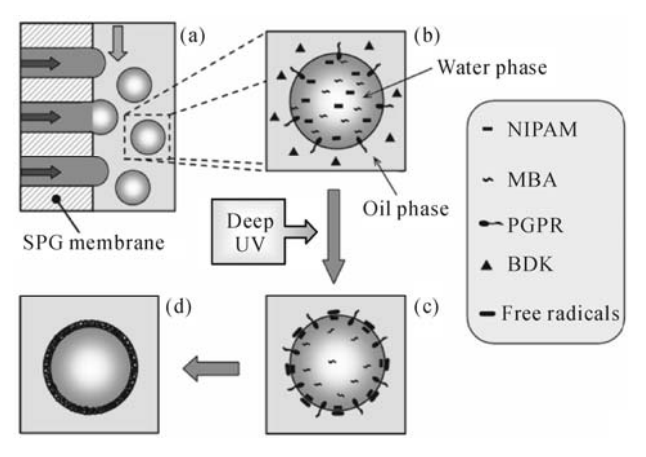


Fig.4.2. Fabrication approach of monodisperse thermo-responsive hollow microcapsules via SPG membrane emulsification and UV-initiated polymerization (Reproduced with permission from Ref. [1]). Copyright (2007), Elsevier

In a typical SPG membrane emulsification process, [1] 10 ml aqueous solution containing 1.13 g monomer NIPAM and 0.077 g crosslinker N,N'-methylenebisacrylamide (MBA) was used as the disperse phase (water phase), and 160 ml kerosene solution containing 5 wt% surfactant polyglycerol polyricinoleate (PGPR) was used as the continuous phase (oil phase). SPG membrane emulsification module (Kiyomoto Iron Works Co. Ltd., Miyazaki, Japan) was used to prepare monodisperse monomercontained W/O emulsions. Before the emulsification process, the SPG membrane has been hydrophobically modified with silicane resin polymethylsilsesquioxane (GRT-350).^[2] In detail, SPG membranes were firstly washed by alcohol and deionized water, then dried in a vacuum at a temperature of 80 ~ 100 °C, and then subsequently soaked in alcohol containing GRT-350 (2.5 wt%) for over 24 h after ultrasonic treatments. After wiping, the solutions remained on the membrane surface, the membrane tubes were dried in a vacuum for over 5 h at $100 \sim 120$ °C. The modified SPG membrane was then wetted by the continuous phase, ultrasonically vibrated for several minutes to remove the bubbles in the membrane pores and then installed into the SPG membrane module. The disperse phase stored in a pressure-tight vessel was pressed to permeate into the continuous phase through the SPG membrane under a pressure of 1.0 to 2.0 kPa. The continuous phase was stirred with a magnetic bar at a stirring speed of about 400 r/min to generate a

rotating flow so that the continuous phase could pass through the membrane surface continuously. The uniform monomer-contained W/O emulsion droplets were then obtained and suspended in the continuous phase. The emulsification was carried out at room temperature.

A 250-W UV lamp with an illuminance spectrum of 250 nm to 450 nm was employed to initiate the polymerization. [1] Before the polymerization, the prepared W/O emulsions and 10 ml kerosene containing 20 mg 2,2-dimethoxy-2phenylacetophenone (BDK) were poured into a self-made cylindrical quartz vessel (6 cm in diameter and 9 cm in height) equipped with nitrogen inlet and outlet, and then bubbled with purified nitrogen for about 10 min to remove oxygen dissolved in the continuous phase. UV irradiation polymerization lasted for 40 min at 20 °C under a nitrogen atmosphere. During the polymerization process, the mixture in the quartz vessel was gently stirred with a magnetic bar to avoid the coagulation of particles. After the polymerization, the polymerized microcapsules were separated from the oil phase by centrifugation at 2,000 r/min for 10 min, and then washed more than 5 times by centrifugation (2,500 r/min, 20 min for each time) with detergent- contained aqueous solution and pure water. Finally, the cleaned microcapsules were redispersed in deionized water at room temperature for further characterization. Cleaned samples were dyed with 0.4 mg/ml rhodamine B (Rd B) aqueous solutions for 2 d before microscope observation.

The optical microscope, confocal laser scanning microscope (CLSM) and scanning electron microscope (SEM) micrographs of PNIPAM hollow microcapsules are shown in Figs.4.3a~4.3c.[1] The hollow structure of PNIPAM microcapsules with thin membranes can be obviously observed in Fig.4.3b. In the SEM image of dried PNIPAM microcapsules (Fig.4.3c), collapsed and crinkled structures resulted from the drying process with oil surrounding. Under the UV irradiation, BDK dissociates to generate a great deal of active free radicals in continuous phase. [4-7] The free radicals then diffuse across the oil/water interface to the water phase of W/O emulsions.^[7] At the same time, monomer NIPAM molecules dissolved in the water phase also diffuse towards the water/oil interface and are initiated to polymerize by the active radicals.^[7] Subsequently, a crosslinked PNIPAM layer forms at the interface because of the function of crosslinker MBA within the emulsion droplets. When the crosslinked PNIPAM layer at the interface becomes thicker and thicker, fewer and fewer active free radicals can diffuse across it and enter into the aqueous phase. As a result the rate of polymerization becomes slower and slower. [4-7] Finally, when the PNIPAM shell becomes too thick for the free radicals to diffuse across it, the polymerization reaction stops and hollow PNIPAM microcapsules result. The mean shell thickness of the microcapsules is about 800 nm at 20 °C. It can be seen from Figs.4.3a and 4.3c that the shell thicknesses of microcapsules are uniform.

Because the polymerization is carried out at a low temperature (20 °C), the emulsions are stable during the reaction process, and therefore the monodispersity of the hollow PNIPAM microcapsules is almost the same as that of the emulsions, as shown in **Fig.4.3d.**^[1] Before and after the polymerization, the particle size

dispersal coefficient δ is maintained at about 0.27. That means monodisperse hollow microcapsules are effectively prepared by the proposed synthesis approach. In **Fig.4.3d**, the mean size of the PNIPAM microcapsules dispersed in water at 20 °C is slightly larger than that of monomer-contained W/O emulsions. The reason is that the washed PNIPAM microcapsules exhibit a highly swollen state in water at 20 °C (**Fig.4.3a**), because water molecules around the isopropyl groups within the PNIPAM molecules are ordered and form an iceberg structure to minimize the number of contacts with the hydrophobic groups, as the environmental temperature is below the LCST of PNIPAM (about 32 °C).

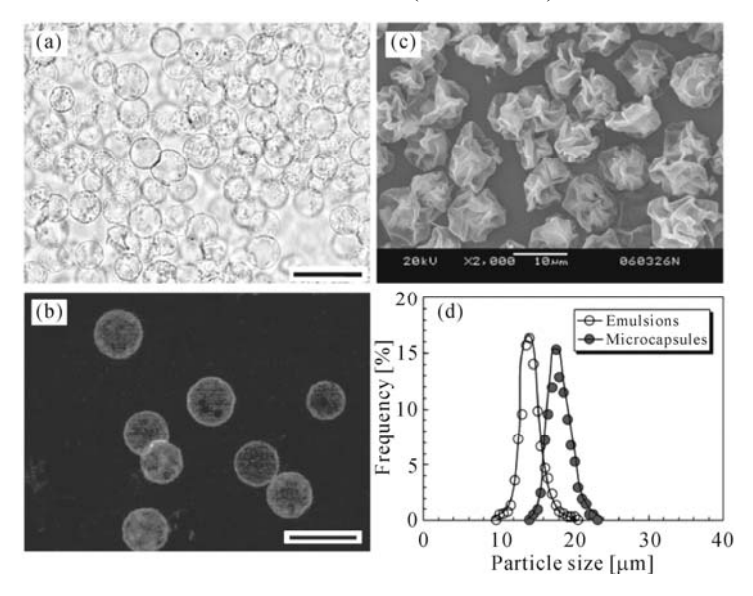


Fig.4.3. (a) Optical microgram of PNIPAM hollow microcapsules; (b) CLSM image of PNIPAM microcapsules dyed with Rd B; (c) SEM image of dried PNIPAM microcapsules. The measuring temperature for optical microscope and CLSM observation is 20 °C; (d) Size distributions of W/O emulsions and resultant PNIPAM microcapsules dispersed in water. T = 20 °C. $\delta_{\text{emulsions}} = 0.274$ and $\delta_{\text{microcapsules}} = 0.289$. Scale bar: (a) = 40 μm, (b) = 30 μm and (c) = 10 μm (Reproduced with permission from Ref. [1]). Copyright (2007), Elsevier

4.2.2 Thermo-Responsive Characteristics

Temperature-dependent phase-transition behavior and dynamic volume-change of the resultant microcapsules were studied by optical microscope equipped with a thermostatic stage system and a CCD camera. [1] In order to investigate the equilibrium swelling/shrinking characteristics of the prepared microcapsules, the microcapsules were kept in the aqueous solution for 15 min at each temperature so that they could reach the equilibrium state. To study the response kinetics of the microcapsules to environmental temperature, microcapsules were first equilibrated

in deionized water at temperature of 20 °C. The temperature was then increased to 40 °C within about 30 s, and the time-dependent shrinkage behavior of the microcapsules was recorded by the CCD camera mounted on the optical microscope.

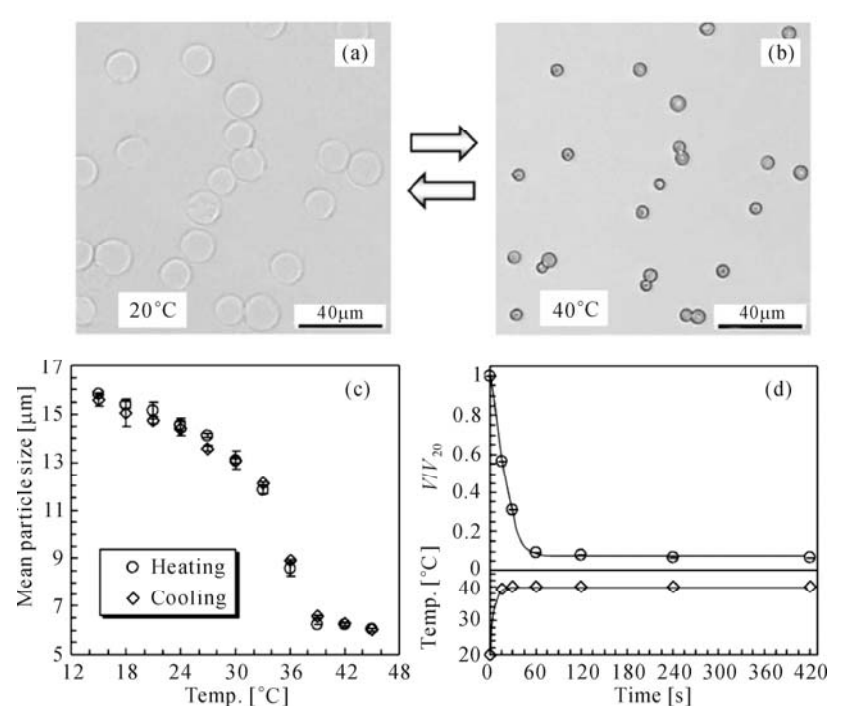


Fig.4.4. (a, b) Optical micrograms of PNIPAM microcapsules in water at 20 °C and 40 °C, respectively. Scale bar = 40 μ m; (c) Temperature-dependent equilibrium diameter-change of PNIPAM microcapsules; (d) Time-dependent volume-change of PNIPAM microcapsules when the temperature increases from 20 °C to 40 °C within 30 s, where V is the measured volume of the microcapsule at each point and V_{20} is the equilibrium volume of the microcapsule at 20 °C (Reproduced with permission from Ref. [1]). Copyright (2007), Elsevier

The prepared PNIPAM hollow microcapsules exhibit a reversibly excellent thermo-sensitivity and fast response to environmental temperature. **Figs.4.4a** and **4.4b** show the optical micrograms of PNIPAM microcapsules in water at 20 °C and 40 °C, respectively. At 20 °C (below the LCST of PNIPAM), the PNIPAM is in a swollen state. Therefore the size of microcapsule is large. On the contrary, the PNIPAM is in a shrunken state at 40 °C (above the LCST of PNIPAM) and as a result the size of the microcapsule becomes small. When the temperature is changed from 45 °C to 15 °C and from 15 °C to 45 °C repeatedly, the prepared hollow PNIPAM microcapsules show good reversibility in the swelling/shrinking volume changes. **Fig.4.4c** shows the temperature-dependent equilibrium volume-change of resultant hollow PNIPAM microcapsules. The volume of microcapsules decreases significantly with an increase in the temperature near the LCST, but no

significant volume change occurs anymore when the temperature is above 38 °C. The equilibrium volume of a microcapsule at 20 °C is about 17 times larger than that at 40 °C. **Fig.4.4d** shows the time-dependent volume-change of the PNIPAM microcapsules when the temperature increases from 20 °C to 40 °C within 30 s. Microcapsules shrink rapidly within 60 s and then reach their equilibrium swelling/shrinking states. The results indicate that the prepared PNIPAM hollow microcapsules are featured with fast response to environmental temperature, which is just what is needed for most potential applications of microgels.

4.3 Monodisperse Thermo-Responsive PNIPAM Hollow Microcapsules Prepared with O/W/O Double Emulsions as Templates

In biomedical fields, microcapsules are widely investigated as effective drug delivery carriers for the treatment of deadly diseases such as cancer. Because most anticancer drugs have harmful side effects on normal tissues, the most ideal delivery carriers should be able to transport and release the anticancer drugs specifically to the targeted tumor site without drug leakage during the transport process. Up to now, numerous studies have been conducted on using an external magnetic field for targeted drug delivery by incorporating magnetic nanoparticles into drug delivery carriers. Some stimuli-responsive carriers, such as core/shell microparticles and microcapsules functionalized with magnetic nanoparticles, have been designed for magnetic-guided drug delivery and subsequent controlled drug release by an external trigger such as temperature, [8,9] pH, [10,11] ultrasonic [12] and high frequency magnetic field. [13,14] Most of the carriers mentioned above were designed for hydrophilic drugs. However, it is worth noting that currently available anticancer drugs such as paclitaxel and carmustine are usually lipophilic molecules. Therefore, design of carriers for lipophilic drugs is of great importance and necessity. Recently, the author's group reported on a novel type of monodisperse thermo-induced self-bursting microcapsule with oil core for encapsulating lipophilic substances.[15]

4.3.1 Fabrication Strategy and Microstructure Control

Fig.4.5 schematically illustrates the concept of the as-proposed thermo-induced self-bursting microcapsule with magnetic-targeting property and its fabrication procedure. The proposed microcapsules are monodisperse and each of them has a core/shell structure comprising an oil core and a thermo-responsive membrane composed of crosslinked PNIPAM hydrogel and homogeneously embedded superparamagnetic Fe₃O₄ nanoparticles (**Fig.4.5a**). The expected oil-core/polymer-

shell structure and monodispersity can be achieved by using a microfluidic fabrication technique. $^{[16]}$ The oil core can be used to encapsulate lipophilic drug molecules. In the PNIPAM hydrogel membrane, the embedded Fe_3O_4 nanoparticles contribute a magnetic-response property to the microcapsule and the PNIPAM network makes the shell thermo-responsive. As a result, the $Fe_3O_4/PNIPAM$ shell enables the microcapsule to undergo magnetic-guided targeting delivery, have no unintended drug leakage during microcapsule transport, and exhibit thermo-triggered drug release.

Because the microcapsules are fabricated at temperatures below the LCST, the as-prepared microcapsules are initially in a swollen and hydrophilic state. Because the encapsulated oil phase and loaded lipophilic chemicals inside the microcapsule are immiscible with, or insoluble in, aqueous solutions, there is no way for them to pass through the hydrophilic PNIPAM membrane via solution/diffusion when the temperature is below the LCST, although the concentration gradient exists between inside and outside of the microcapsule. Therefore, when the microcapsules are stored, transported, or delivered at temperatures below the LCST, there is no leakage of encapsulated lipophilic substances from the microcapsules. After the microcapsules reach the desired site via magnetic guide, a burst release of their encapsulated lipophilic substances can be triggered by an external thermal stimulus, e.g., local heating. When the environmental temperature is increased from one below the LCST to another one above the LCST, the PNIPAM membrane shrinks rapidly. During the membrane shrinkage process, internal pressure in the oil core gradually increases because the oil phase is incompressible. When the internal pressure reaches a certain critical value, the PNIPAM membrane ruptures due to its limited mechanical strength. Such dramatic shrinkage and final rupture of the PNIPAM membrane squeeze the oil core out from the microcapsule with a strong boost to the environment. In such a release process, the loaded lipophilic drug molecules are released, together with the ejecting burst of the encapsulated oil phase from the microcapsule, which leads to not only rapid release but also complete release (**Fig.4.5**). [15]

The fabrication procedure of the microcapsules consists of three major steps as follows. Briefly, the first step is to prepare superparamagnetic Fe₃O₄ nanoparticles and modify them with a silane-coupling reagent to introduce polymerizable groups (**Fig.4.5b**),^[17,18] the second step is to prepare monodisperse oil-in-water-in-oil (O/W/O) double emulsions as templates for subsequent core/shell microcapsule preparation (**Figs.4.5c** and **4.5d**), and the third step is to synthesize the PNIPAM microcapsule membrane via photo-initiated polymerization. Since the aqueous solution containing NIPAM monomer and well-dispersed Fe₃O₄ nanoparticles with polymerizable groups was used as the middle aqueous phase, a superparamagnetic and thermo-responsive PNIPAM hydrogel membrane can be obtained after polymerization of the middle aqueous phase initiated by UV irradiation (**Fig.4.5e**).

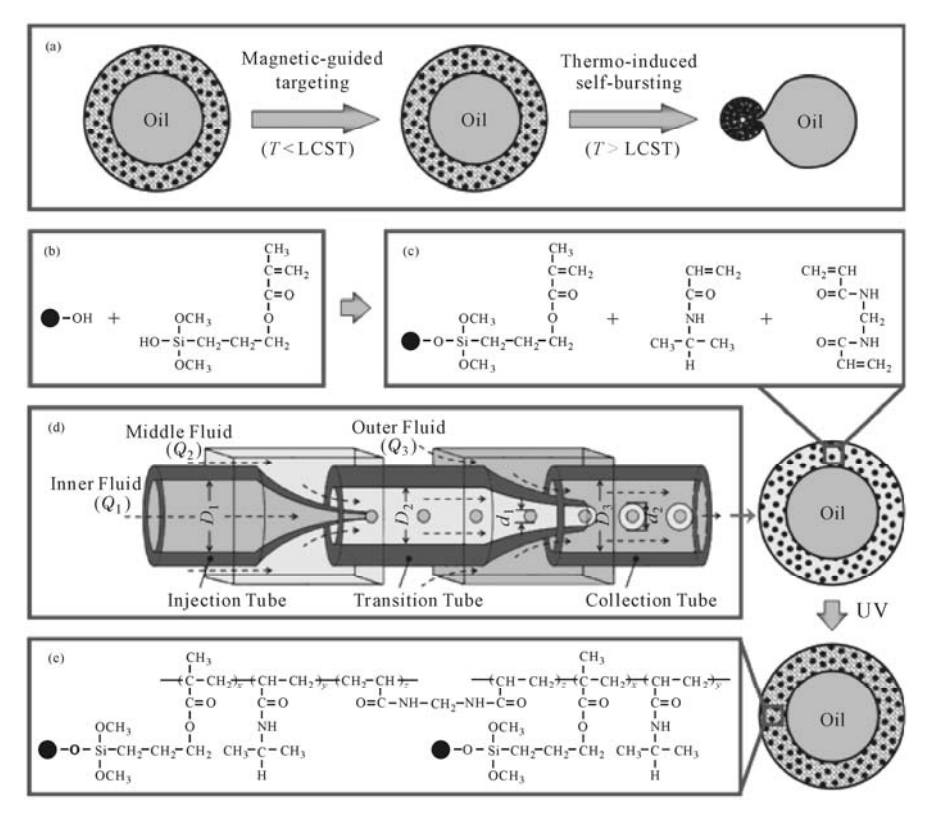


Fig.4.5. Schematic illustration of the concept of the proposed thermo-induced self-bursting microcapsule with magnetic-targeting property (a) and its fabrication procedure. (b) The Fe_3O_4 nanoparticles with hydroxyl groups and silane-coupling reagent. (c) Aqueous phase containing MPTMS-modified Fe_3O_4 nanoparticles, NIPAM monomer and MBA crosslinker for fabricating microcapsule membrane. (d) Capillary microfluidic device used to prepare monodisperse O/W/O double emulsions. (e) The chemical structure of the microcapsule membrane after UV-initiated polymerization (Reproduced with permission from Ref. [15]). Copyright (2009), Wiley-VCH Verlag GmbH & Co. KGaA

The polymerized microcapsules are featured with oil-core/PNIPAM-shell structure (**Fig.4.6a**).^[15] Sudan III, an oil soluble industrial dye, is used as a model chemical to demonstrate the ability of these microcapsules to load lipophilic chemicals or drugs. In microcapsules loaded with Sudan III, the inner oil cores exhibit a red color (**Fig.4.6b**), which is different from the color of the pure oil cores shown in **Fig.4.6a**. The lipophilic Sudan III molecules dissolved in the inner oil core are protected by the membrane and could not permeate through the PNIPAM membrane of the microcapsule at temperatures below the LCST because no solution/diffusion of lipophilic substance in the hydrophilic membrane is available. Since the PNIPAM membrane could protect the inner oil core against various instability processes, such as aggregation and coalescence, the oil-corecontaining microcapsules is a better microcarrier than emulsions, which are

usually employed as delivery systems for lipophilic drugs but are intrinsically thermodynamically unstable.

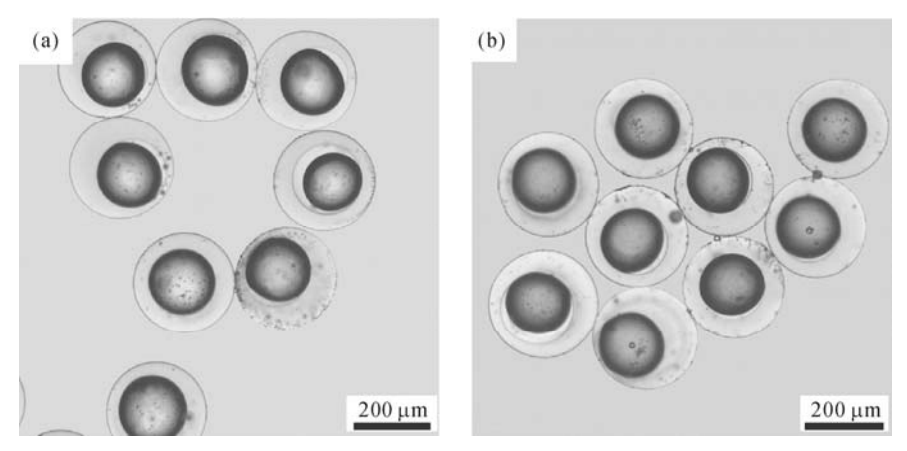


Fig.4.6. Optical micrographs of monodisperse microcapsules with pure oil core (a) and with Sudan III-loaded oil core (b) in water at 20 °C (Reproduced with permission from Ref. [15]). Copyright (2009), Wiley-VCH Verlag GmbH & Co. KGaA

4.3.2 Thermo-Responsive Controlled-Release Characteristics

Owing to the shrinkage of the thermo-responsive PNIPAM microcapsule membrane upon heating, a thermo-induced self-bursting release performance can be achieved by increasing the environmental temperature across the LCST. Fig.4.7a illustrates the burst release of the inner oil core from the microcapsule when temperature is increased from 20 °C to 60 °C. [15] With an increase in the temperature, the thermo-responsive PNIPAM membrane of the microcapsule shrinks dramatically. Since the inner oil core is incompressible but the internal pressure in the oil core keeps increasing, due to the membrane shrinkage, the PNIPAM membrane finally ruptures because of the limited mechanical strength, which results in a burst release of the inner oil core (Figs.4.7a3 to 4.7a4). With the shrinkage and rupture of the PNIPAM membrane, the inner oil phase is squeezed out of the microcapsule within a very short time, and spreads fast into the surrounding environment. As a result, the release from such a microcapsule is complete, leaving just a hollow cavity without any leftovers inside the microcapsule (Fig.4.7b). Such a rapid and complete burst release of the encapsulated oil phase and lipophilic chemicals means that a high local drug concentration can be rapidly achieved. To determine the release rate of the inner oil core, we investigated the burst release behavior during the first 3.2 s after the PNIPAM membrane ruptures (Fig.4.7c). The optical microscope snapshots show that the encapsulated oil phase shoots out very quickly due to the strong boost resulting from shrinkage and the squeeze function of the microcapsule membrane. In addition, the radius of the circular edge of the

released oil phase increases by $\sim\!250~\mu m$ within 3.2 s. This spread speed is much faster than that in diffusion-driven release systems. Such a quick release and spread rate may make our microcapsules be of specific interest and significance, especially in certain cases where released substances need to cross some media with high viscosity or low permeability.

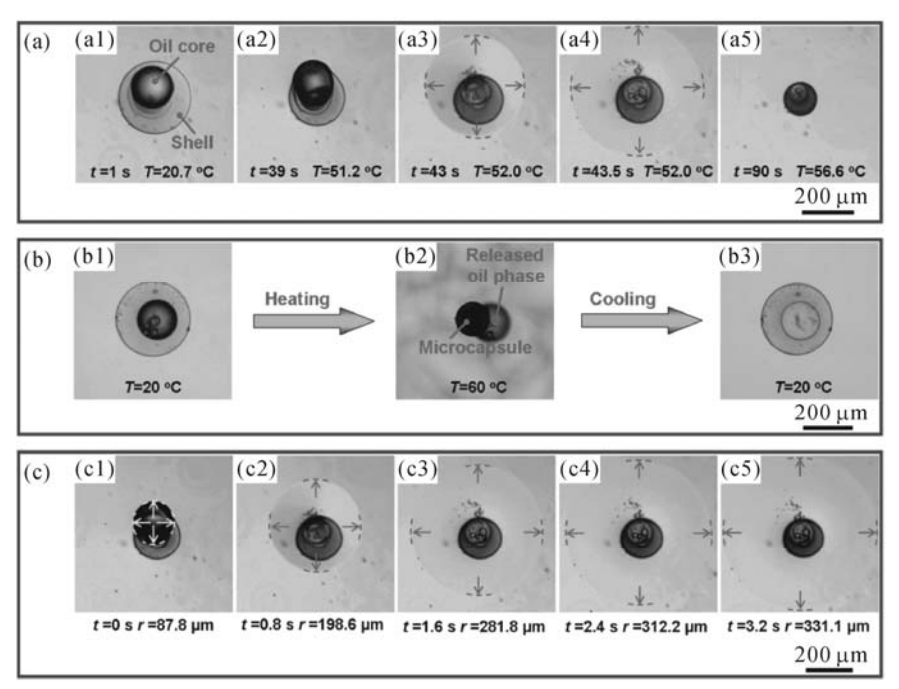


Fig.4.7. Optical microscope snapshots of the thermo-induced self-bursting behavior (a) and complete release performance (b) of the as-prepared microcapsules. (c) Thermo-induced burst-release process of inner oil core from the microcapsule (shown in (a)) during the first 3.2 s of release, in which time-dependent increase of the radius (*r*) of the circle edge of released oil phase is used to valuate the release rate (Reproduced with permission from Ref. [15]). Copyright (2009), Wiley-VCH Verlag GmbH & Co. KGaA

4.4 Monodisperse Thermo-Responsive PNIPAM Hollow Microcapsules Prepared with W/O/W/O Triple Emulsions as Templates

In this section, monodisperse thermo-responsive PNIPAM hollow microcapsules prepared with W/O/W/O triple emulsions as templates will be introduced.

4.4.1 Thermo-Responsive Squirting Microcapsules for Nanoparticle Delivery

Nowadays, nanoparticles are becoming more and more prevalent in the fields of disease diagnosis and therapy.^[19] However, several challenges still remain for their practical applications, such as how to protect nanoparticles from premature degradation^[20] or unwanted interaction with biological molecules before reaching the targeted site, [21] how to selectively deliver nanoparticles only to diseased tissue, [22] and how to achieve a wide distribution of nanoparticles at the targeted site. [23] Some promising nanoparticle candidates for drug delivery systems, such as protein nanoparticles, liposomes, micelles, usually exhibit low physical and chemical stability. [24] Besides, micelles disassemble if they are diluted below the critical micelle concentration. Thus, nanoparticle delivery carriers are wanted to protect the stability of encapsulated nanoparticles and prevent them from degrading prematurely before delivery, and to deliver them only at the targeted site. For stimuli-triggered site-targeting delivery, the delivery triggered by physical contact may not be practicable in the human body, [25] and delivery triggered remotely is more preferable. [26] Furthermore, some biological tissues present diffusion obstacles for nanoparticles and/or their surrounding media are quite viscous. [27] in which situations a higher initial momentum for the nanoparticle delivery is very important.

Some interesting delivery behaviour can be found in some plants in the natural environment when they eject seeds from fruits for the widest possible distribution. For example, the ripe fruit of ecballium elaterium (Fig.4.8a), also called squirting cucumber or exploding cucumber, is highly turgid. When it is ripe or is disturbed by sniffing animals or whatsoever, the ripe fruit squirts a stream of mucilaginous liquid containing its seeds into the air over a considerable distance by a sudden contraction of the wall of the fruit (Fig.4.8b). Inspired by the squirting cucumber, the author's group recently developed a novel thermo-triggered squirting capsule for nanoparticle delivery. [28] The proposed microcapsule is composed of a crosslinked PNIPAM hydrogel membrane and encapsulates water-based nanoparticles by dispersing the aqueous phase that contains nanoparticles into its oil phase core (Fig.4.8c). Because the encapsulated nanoparticles exist in the water phase of the W/O emulsion core inside the microcapsule, the swollen and hydrophilic PNIPAM hydrogel membrane of the microcapsule can protect the encapsulated nanoparticles when the temperature is below the LCST (Fig.4.8c). To eject the encapsulated nanoparticles, what we need to do is just apply a heat stimulus to increase the local environmental temperature above the LCST. Upon heating, the PNIPAM hydrogel membrane shrinks rapidly, which results in a sudden increase in the liquid pressure inside the microcapsule, because both the continuous oil phase and the dispersed water phase in the capsule are incompressible. When the internal pressure increases to a critical value, the PNIPAM hydrogel membrane ruptures suddenly due to its limited mechanical strength. At the same time, the encapsulated nanoparticles are squirted out from

the microcapsule together with the oil phase stream into the environment with great momentum (**Fig.4.8d**), just like the seed-ejection of a ripe squirting cucumber.

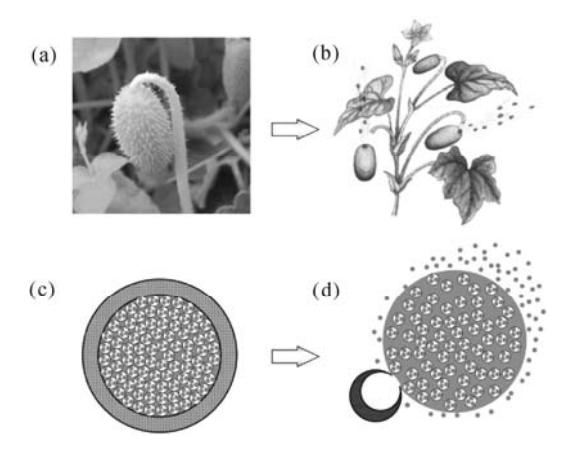


Fig.4.8. (a) A picture of squirting cucumber; (b) Schematic illustration of squirting cucumbers ejecting seeds together with a stream of mucilaginous liquid; (c) A microcapsule with crosslinked PNIPAM hydrogel membrane containing nanoparticles in the inner water phase of W/O emulsion core at temperature below the LCST; (d) Nanoparticles being squirted out from the microcapsule together with the oil phase stream due to the dramatic shrinkage and sudden rupture of PNIPAM hydrogel membrane triggered by an increase in the environmental temperature above the LCST (Reproduced with permission from Ref. [28]). Copyright (2010), The Royal Society of Chemistry

4.4.1.1 Fabrication Strategy and Microstructure Control

Primary W/O Emulsions Containing Nanoparticles: [28] 3 ml of water containing 0.2% yellow-green fluorescent (505/515) carboxylate-modified FluoSphere® polystyrene beads (200 nm, Invitrogen F8811) was employed as the water phase, and 7 ml of soybean oil containing 0.56 g polyglycerol polyricinoleate (PGPR 90, Danisco) as surfactant was employed as the oil phase. The two phases were mixed by magnetic agitation for 10 min and then homogenized (16,000 r/min, 1 min) by a BRT homogenizer (B25 10 mm head).

Microfluidic Preparation of (W/O)/W/O Emulsions:^[28] The microfluidic device for fabrication of (W/O)/W/O emulsions is illustrated in **Fig.4.9**. The prepared W/O primary emulsion containing nanoparticles was employed as inner fluid. The middle fluid was monomer aqueous solution containing surfactant Pluronic F127 (1% (w/v), Sigma-Aldrich), monomer NIPAM (1 mol·L⁻¹, Kohjin), crosslinker *N,N*'-methylenebisacrylamide (MBA) (0.02 mol·L⁻¹) and initiator 2,2'-azobis(2-amidinopropane) dihydrochloride) (0.005 mol·L⁻¹). Soybean oil containing 8% (w/v) PGPR was employed as the outer fluid. The inner, middle and outer fluids were separately pumped into the injection, transition and collection tubes of the microfluidic device. (W/O)/W/O emulsions generated in a collection tube were collected in soybean oil containing 2% (w/v) 2,2-dimethoxy-

2-phenylacetophenone (BDK) as photo initiator.

The CLSM images of the primary emulsion show that the nanoparticle aqueous suspension forms droplets with a size ranging from 570 nm to 920 nm and disperse well in the emulsion without coalescence (**Figs.4.10a** and **4.10b**). The optical micrograph of a typical (W/O)/W/O emulsion droplet is shown in **Fig.4.10c**. [28]

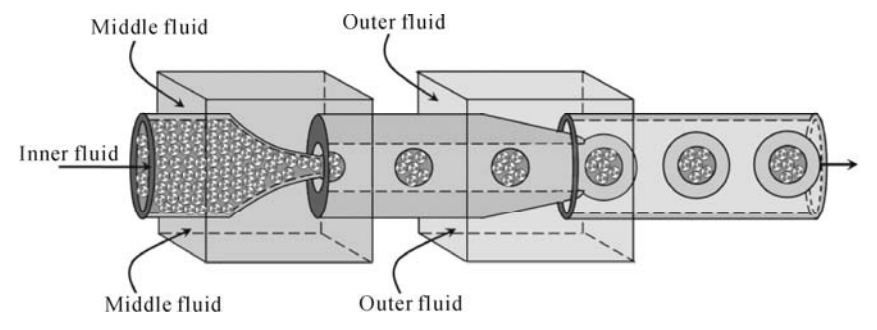


Fig. 4.9. Schematic illustration of the microfluidic device (Reproduced with permission from Ref. [28]). Copyright (2010), The Royal Society of Chemistry

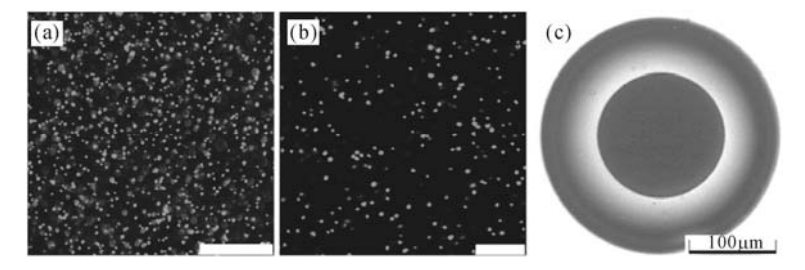


Fig.4.10. (a, b) CLSM images of primary W/O emulsion containing nanoparticles in the inner water phase at different magnification. Scale bars: (a) $25 \mu m$; (b) $10 \mu m$. To see the emulsion droplets more clearly, the emulsion shown here is diluted with soybean oil to one third of the original concentration before CLSM observation. (c) Optical microscope image of prepared (W/O)/W/O emulsions containing nanoparticles in the innermost water phase. Scale bar is $100 \mu m$ (Reproduced with permission from Ref. [28]). Copyright (2010), The Royal Society of Chemistry

UV-initiated Polymerization of PNIPAM Microcapsule Membrane: $^{[28]}$ The collected (W/O)/W/O emulsions were converted into microcapsules by polymerization with UV irradiation for 10 min in an ice-water bath. Under UV light, the activated photo-initiator BDK diffused to the interface between the outer oil phase and middle aqueous phase, where it initiated the polymerization of the NIPAM monomer and MBA crosslinker in the middle aqueous phase to build the hydrogel membrane of the microcapsules. A 250-W UV lamp with an illuminance spectrum of 250 \sim 450 nm was employed to produce UV light. An ice-water bath was introduced to ensure the polymerization was carried out at a temperature below the LCST of PNIPAM. The microcapsules were separated from oil by adding deionized

water into the container. When the oil phase and water phase had separated completely, the capsules settled into the bottom water layer and the upper oil layer was removed. The microcapsules were washed with deionized water several times and then dispersed in deionized water.

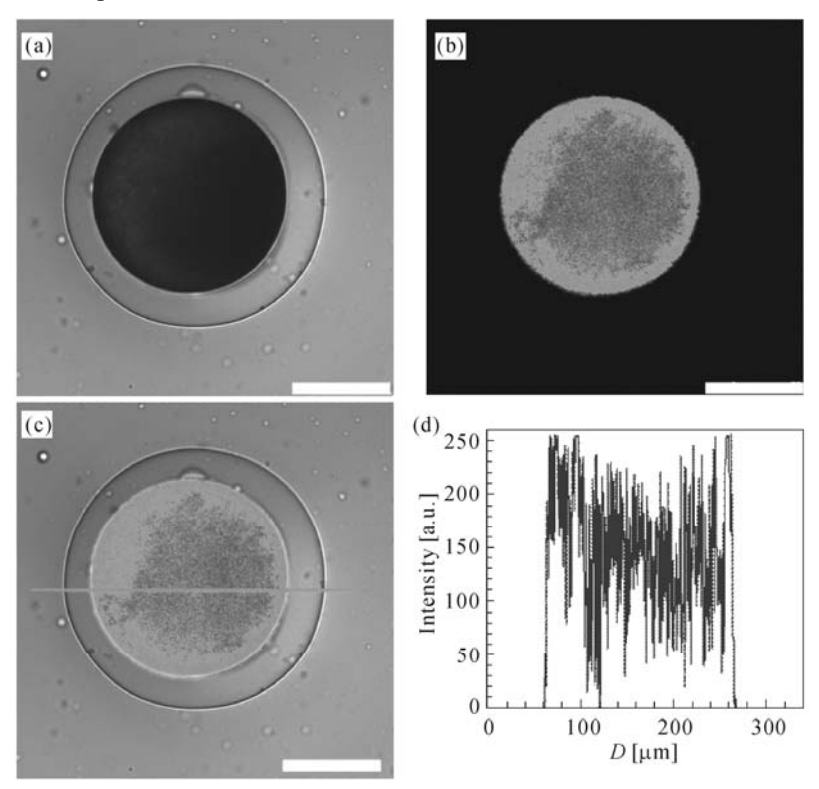


Fig.4.11. CLSM images of the prepared microcapsule at room temperature, in which (a) shows transmission channel image, (b) shows green channel image and (c) shows the overlay of green channel and transmission channel images. Scale bars are $100~\mu m$. (d) Fluorescence intensity profile corresponding to (c) (Reproduced with permission from Ref. [28]). Copyright (2010), The Royal Society of Chemistry

In a bright field under a microscope at room temperature (below the LCST), the PNIPAM hydrogel membrane is transparent while the inner primary emulsion is dark (**Fig.4.11a**). Actually, the thickness of the hydrogel membrane of the prepared microcapsule is not perfectly uniform along the circumference, as seen in **Fig.4.11a** This membrane thickness difference results from the density difference between the encapsulated W/O emulsion and the NIPAM monomer solution in the (W/O)/W/O emulsion. Although the density of both the inner W/O phase and the middle aqueous monomer phase has been adjusted carefully, a slight density difference does still exist, so the encapsulated W/O emulsion is not in the exact center of the (W/O)/W/O emulsion droplet. Consequently, the thickness of the polymerized hydrogel membrane is a little thicker on one side, but a little thinner

on the other side, of the microcapsule. The CLSM fluorescent images illustrate that no leakage of nanoparticles from the prepared hydrogel capsule is observed (**Figs.4.11b and 4.11c**). This result is also assured by the fluorescence intensity profile (**Fig.4.11d**). Inside the microcapsule the intensity is quite high (from 50 to 260), whereas the intensity outside is nearly zero. The innermost nanoparticle suspension is separated from the hydrogel membrane by the continuous oil phase of W/O emulsion inside the capsule, and the oil phase cannot permeate through the PNIPAM hydrogel membrane and then prevent the encapsulated nanoparticles from leaking.

4.4.1.2 Thermo-Responsive Burst Squirting for Nanoparticle Delivery

To observe the squirting of nanoparticles from the prepared microcapsules upon heating, a glass slide with a drop of microcapsule suspension is placed on a thermostatic stage under a microscope. When the temperature increases from 20 °C to 50 °C, the hydrogel membrane of the microcapsule shrinks rapidly. The inner oil phase cannot permeate through the shrinking hydrogel membrane, leading to deformation of the capsule. During the deformation in the thermo-triggered squirting process, the encapsulated W/O phase tends to breach the thinner side of the hydrogel membrane which is stretched by the incompressible inner oil phase. When the shrinkage reaches a high degree, the hydrogel membrane turns into an "8" shape, of which one head (the side with the thinner membrane) is full of the encapsulated W/O primary emulsion and the hydrogel membrane becomes extremely thin. When the inner pressure reaches a critical value, the hydrogel membrane ruptures and the contained oil phase, together with the encapsulated nanoparticles, are squirted out into the surrounding water (Fig.4.12a). [28] Fig.4.12b shows the snapshots of the thermo-triggered squirting process in a dark field. [28] Because the squirting direction is upward, the "8" deformation is not as obvious as that shown in Fig.4.12a. During the squirting process, the large bright area indicates the considerably wide distribution of the squirted substance.

Fig.4.13a is a CLSM image of typical distribution of nanoparticles after the squirting release. The fluorescent intensity in the central area is very low (from 50 to 100), while around the shrunken and ruptured capsule the fluorescent intensity is quite high (about 250) and graudually fades away at 200 μm from the center of the microcapsule (**Fig.4.13b**), which indicates that encapsulated nanoparticles are completely squirted out from the capsule. We find that capsules squirt out nanoparticles in different directions. Some capsules squirt nanoparticles sideways, for example the capsule shown in **Fig.4.13a**. In this case, the fluorescent trail of nanoparticles indicates the squirting direction (**Fig.4.13c**) and the fluorescent intensity in the squirting direction is as high as about 250, while that in the opposite direction is only about 130 (**Fig.4.13d**). We also observe an interesting phenomenon where the squirted nanoparticles are distributed like a vortex (**Figs.4.13e** and **4.13f**). From **Fig.4.13e**, we can see that at least two peaks of the fluorescent intensity reach about 250 on the left side of the microcapsule.

This may be caused by rotation of capsules during the squirting process. We presume the rotation in this case is caused by squirting in a tangental direction; however, the nanoparticles are usually squirted out in a radial direction in other cases.

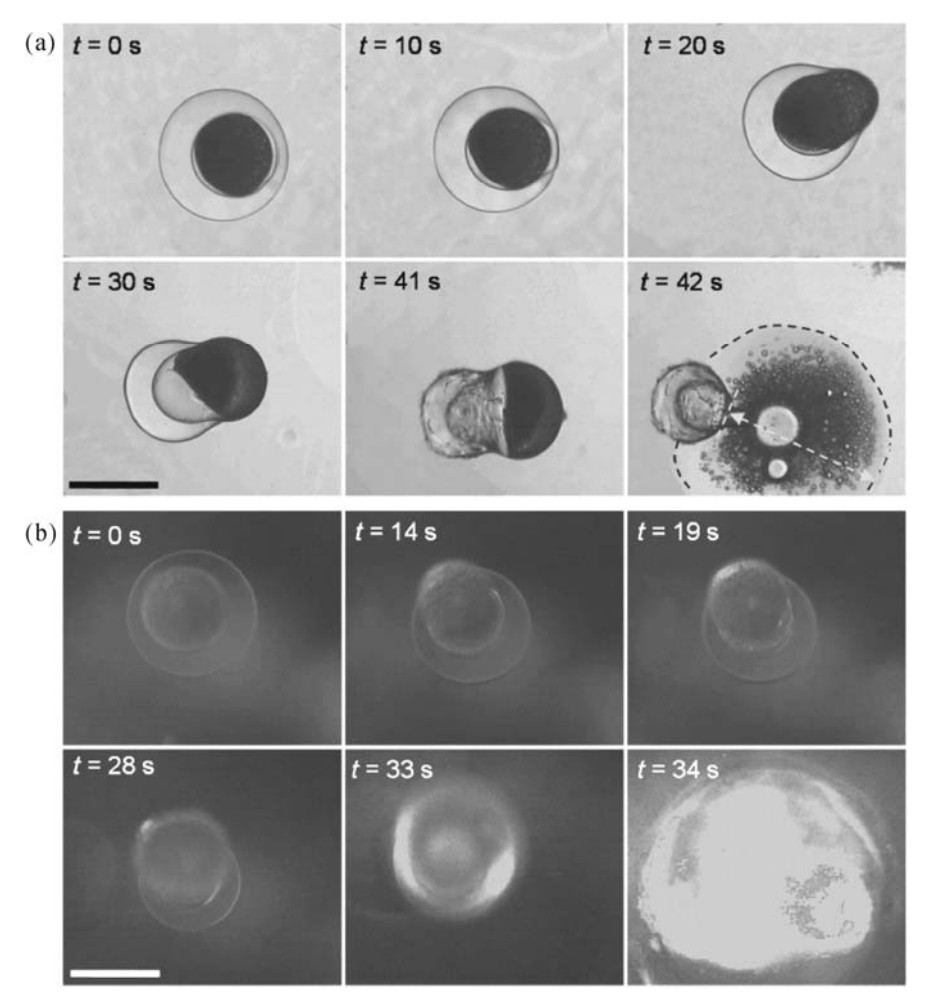


Fig.4.12. Bright-field (a) and dark-field (b) microscope snapshots of thermo-triggered squirting of nanoparticles from microcapsules by increasing environmental temperature from 20 to 50 $^{\circ}$ C. The dashed line in (a) indicates the propagating front of the squirted liquid containing nanoparticles, and the arrow shows the propagating distance of the squirted liquid containing nanoparticles. The scale bars are 200 μm (Reproduced with permission from Ref. [28]). Copyright (2010), The Royal Society of Chemistry



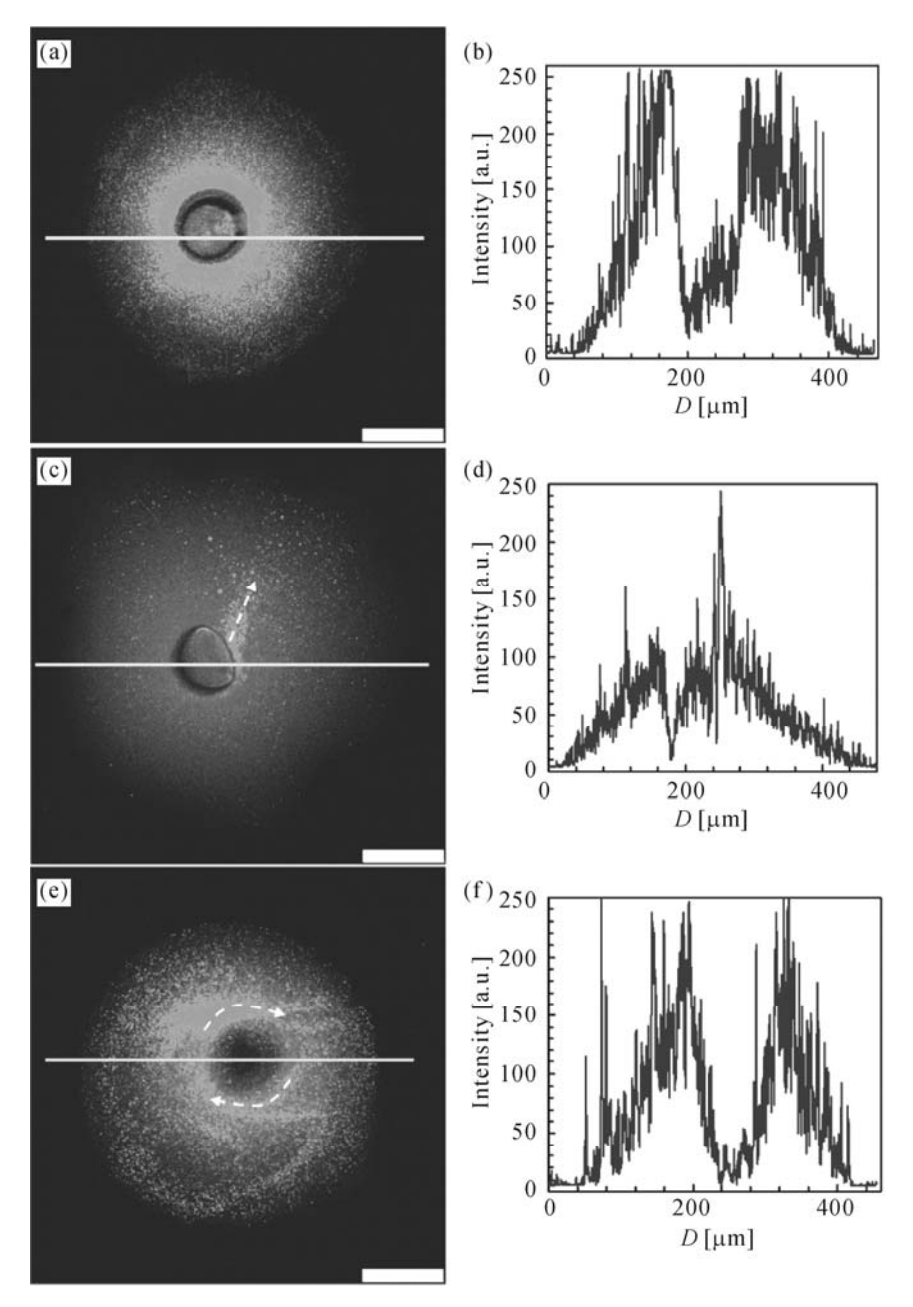


Fig.4.13. CLSM images (a, c, e) of diverse distributions of nanoparticles squirted from microcapsules triggered by local heating and their fluorescence intensity profiles (b, d, f), respectively. The white arrows indicate the squirting direction. Scale bars are 100 µm (Reproduced with permission from Ref. [28]). Copyright (2010), The Royal Society of Chemistry

4.4.2 Thermo-Responsive Trojan-Horse-Like Microcapsules

Recently, the author developed a novel scalable and controllable microfluidic technique, which can be used to fabricate highly monodisperse multiple emulsions with independent control of both the size and the number of inner droplets. [29] This technique is easily scalable to a higher order multiple emulsions, *e.g.*, monodisperse and controllable triple emulsions. The utility of the tight control afforded by this technique makes it an effective way to fabricate novel thermo-responsive Trojanhorse-like microcapsules with a crosslinked PNIPAM hydrogel membrane.

4.4.2.1 Fabrication Strategy and Microstructure Control

Fig.4.14 illustrates the schematic diagram of the capillary microfluidic device for generating controllable monodisperse triple emulsions. [29] As shown in Fig.4.15. [29] both the diameter and number of the individual drops, at every level, are precisely controllable, as illustrated by the series of drops, with the innermost varying in number from one to seven and the middle ones varying in number from one to three. To prepare the Trojan-horse-like microcapsules with a PNIPAM hydrogel membrane containing controllable aqueous droplets inside, W/O/W/O emulsion droplets are used as synthesis templates. [29] The outermost fluid is an oil phase containing surfactant, while the outer middle fluid (II) is an aqueous solution of the monomer NIPAM, crosslinker and initiator. The inner middle fluid (I) is an oil phase containing the reaction accelerator while the innermost fluid is another aqueous solution containing to-be-released chemicals. Once the triple emulsions are formed, the accelerator in the middle fluid (I) diffuses into the outer aqueous phase containing the monomer NIPAM and the initiator and catalyzes polymerization of NIPAM. Fig.4.16 shows the optical micrograph of a typical Trojan-horse-like microcapsule consisting of a membrane of thermo-responsive PNIPAM hydrogel which encapsulates an oil drop containing several water droplets.

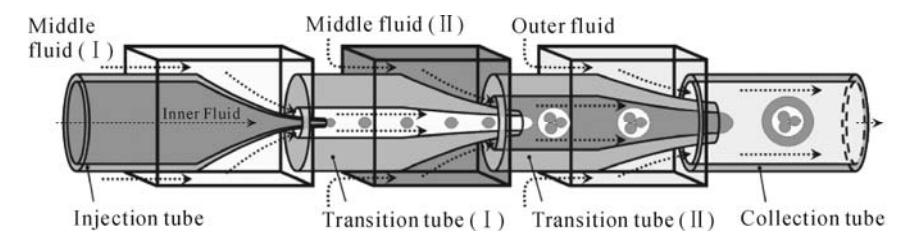


Fig.4.14. Schematic diagram of the capillary microfluidic device for generating triple emulsions (Reproduced with permission from Ref. [29]). Copyright (2007), Wiley-VCH Verlag GmbH & Co. KGaA

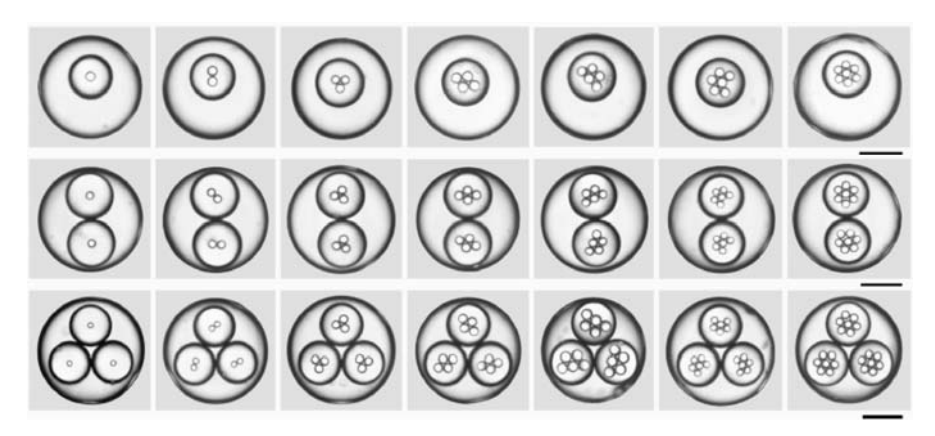


Fig.4.15. Optical micrographs of triple emulsions that contain a controlled number of inner and middle droplets. The scale bar is 200 μ m (Reproduced with permission from Ref. [29]). Copyright (2007), Wiley-VCH Verlag GmbH & Co. KGaA

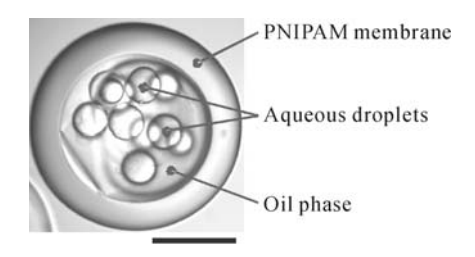


Fig.4.16. Optical micrograph of a typical Trojan-horse-like microcapsule consisting of a membrane of thermo-responsive PNIPAM hydrogel which encapsulates an oil drop containing several water droplets. The scale bar is 200 μm

4.4.2.2 Thermo-Responsive Controlled-Release Characteristics

Fig.4.17 shows the optical micrograph time-series with the forced expulsion of the oil and water droplets contained within the PNIPAM microcapsule when the temperature is rapidly increased from 25 to 50 °C. Upon heating from 25 to 50 °C, the thermo-responsive hydrogel rapidly shrinks by expelling water; however, because of the incompressibility of the inner oil, the hydrogel membrane breaks, providing spontaneous, pulsed release of the innermost water droplets into the continuous oil phase, as shown in **Figs.4.17b** ~ **4.17e**. This structure has Trojanhorse-like behavior, protecting the innermost water droplets in the hydrogel membrane until their temperature-induced release. This demonstrates the utility of this microfluidic technique to generate highly controlled capsules with multiple internal volumes that remain separate from each other; it also highlights the potential of this device to create highly engineered structures for controlled release of actives. Further refinements could adjust the thickness of the layers and the number of droplets, enabling fine control over diffusion of actives contained

within the innermost droplets. This would facilitate highly controlled release of the actives.

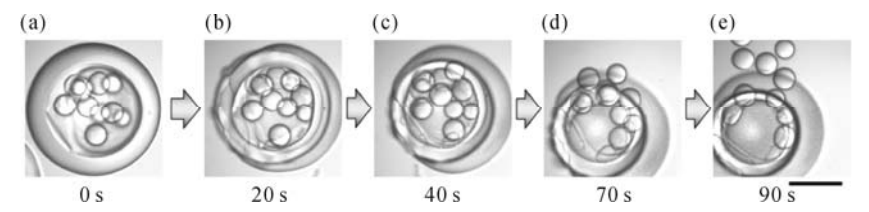


Fig.4.17. Optical micrograph time-series showing the forced expulsion of the oil and water droplets contained within the PNIPAM microcapsule when the temperature is rapidly increased from 25 to 50 $^{\circ}$ C. The scale bar is 200 μ m (Reproduced with permission from Ref. [29]). Copyright (2007), Wiley-VCH Verlag GmbH & Co. KGaA

4.5 Summary and Outlook

Smart microcapsules with thermo-responsive PNIPAM hydrogel membranes can be fabricated with either W/O single emulsions, O/W/O double emulsions, or W/O/W/O triple emulsions as synthesis templates, and have numerous potential applications in various fields. The LCST of PNIPAM-based thermo-responsive polymer can be precisely adjusted by copolymerizing with some hydrophilic or hydrophobic monomers. [30] So it is easy to design polymers with desired LCSTs for the microcapsule membranes to meet the environmental temperature requirements. As a result, controlled release can be achieved in various conditions. Such smart microcapsules with a PNIPAM hydrogel membrane can be easily converted into other stimuli-induced self-bursting ones by simply changing the thermo-responsive membranes into other stimuli-responsive ones, such as pH-induced, molecular-recognition-induced, glucose-induced, and so on. Besides the application in the field of targeted delivery and controlled release of drugs, such microcapsules can find myriad applications in various fields. For example, these microcapsules can be applied to site-specific and/or route-specific transport and release functional substances such as corrosion inhibitors, [31] self-healing agents^[31] and lubricants and other chemicals to certain sites, even to some hand-unreachable micro-spaces. Different reagents in a chemical reaction, which could react with each other once they meet, can also be targetedly transported by such microcapsules to a predefined spot where reaction stimuli-triggered burst-release. Moreover, developments in microfluidic technology provide the opportunity to prepare emulsions with tunable sizes, so microcapsules with different sizes and thicknesses can be obtained by further adjusting the microchannel dimensions of the microfluidic devices and the fluid flow rates.

References

- [1] Cheng C J, Chu L Y, Ren P W, Zhang J, Hu L. Preparation of monodisperse thermo-sensitive poly(*N*-isopropylacrylamide) hollow microcapsules. *Journal of Colloid and Interface Science*, **2007**, *313*: 383-388.
- [2] Cheng C J, Chu L Y, Xie R. Preparation of highly monodisperse W/O emulsions with hydrophobically modified SPG membranes. *Journal of Colloid and Interface Science*, **2006**, *300*: 375-382.
- [3] Chu L Y, Xie R, Zhu J H, Chen W M, Yamaguchi T, Nakao S. Study on SPG membrane emulsification processes for the preparation of monodispersed core-shell microcapsules. *Journal of Colloid and Interface Science*, **2003**, *265*: 187-196.
- [4] Liu L Y, Yang W T. Photoinitiated, inverse emulsion polymerization of acrylamide: Some mechanistic and kinetic aspects. *Journal of Polymer Science Part A–Polymer Chemistry*, **2004**, *42*: 846-852.
- [5] Ikkai F, Iwamoto S, Adachi E, Nakajima M. New method of producing mono-sized polymer gel particles using microchannel emulsification and UV irradiation. *Colloid & Polymer Science*, **2005**, *283*: 1149-1153.
- [6] Jung M, Hubert D H W, Bomans P H H, Frederik P M, Meuldijk J, van Herk A M, Fischer H, German A L. New vesicle-polymer hybrids: the parachute architecture. *Langmuir*, **1997**, *13*: 6877-6880.
- [7] Ikkai F, Adachi E. Novel method of producing polymer gels in aqueous solution using UV irradiation. *Macromolecular Rapid Communications*, **2004**, *25*: 1514-1517.
- [8] Yang W C, Xie R, Pang X Q, Ju X J, Chu L Y. Preparation and characterization of dual stimuli-responsive microcapsules with a superparamagnetic porous membrane and thermo-responsive gates. *Journal of Membrane Science*, **2008**, *321*: 324-330.
- [9] Kim G C, Li Y Y, Chu Y F, Cheng S X, Zhuo R X, Zhang X Z. Nanosized temperature-responsive Fe₃O₄-UA-*g*-P(UA-*co*-NIPAAm) magnetomicelles for controlled drug release. *European Polymer Journal*, **2008**, *44*: 2761-2767.
- [10] Soppimath K S, Liu L H, Seow W Y, Liu S Q, Powell R, Chan P, Yang Y Y. Multi-functional polymer core-shell nanoparticles self-assembled from pH-induced thermally responsive polymer for targeted anticancer drug delivery. *Advanced Functional Materials*, **2007**, *17*: 355-362.
- [11] Zhang L Y, Guo R, Yang M, Jiang X Q, Liu B R. Thermo and pH dual-responsive nanoparticles for anti-cancer drug delivery. *Advanced Materials*, **2007**, *19*: 2988-2992.
- [12] Shchukin D G, Gorin D A, Möhwald H. Ultrasonically induced opening of polyelectrolyte microcontainers. *Langmuir*, **2006**, *22*: 7400-7404.
- [13] Satarkar N S, Hilt J Z. Magnetic hydrogel nanocomposites for remote controlled pulsatile drug release. *Journal of Controlled Release*, **2008**, *130*: 246-251.

- [14] Hu S H, Tsai C H, Liao C F, Liu D M, Chen S Y. Controlled rupture of magnetic polyelectrolyte microcapsules for drug delivery. *Langmuir*, **2008**, 24: 11811-11818.
- [15] Wang W, Liu L, Ju X J, Zerrouki D, Xie R, Yang L, Chu L Y. A novel thermo-induced self-bursting microcapsule with magnetic-targeting property. *ChemPhysChem*, **2009**, *10*: 2405-2409.
- [16] Utada A S, Lorenceau E, Link D R, Kaplan P D, Stone H A, Weitz D A. Monodisperse double emulsions generated from a microcapillary device. *Science*, **2005**, *308*: 537-541.
- [17] Gu S C, Shiratori T, Konno M. Synthesis of monodisperse, magnetic latex particles with polystyrene core. *Colloid & Polymer Science*, **2003**, *281*: 1076-1081.
- [18] Sacanna S, Philipse A P. Preparation and properties of monodisperse latex spheres with controlled magnetic moment for field-induced colloidal crystallization and (dipolar) chain formation. *Langmuir*, **2006**, *22*: 10209-10216.
- [19] Allen T M, Cullis P R. Drug delivery systems: entering the mainstream. *Science*, **2004**, *303*: 1818-1822.
- [20] Giljohann D A, Seferos D S, Prigodich A E, Patel P C, Mirkin C A. Gene regulation with polyvalent siRNA-nanoparticle conjugates. *Journal of American Chemistry Society*, **2009**, *131*: 2072-2073.
- [21] Blummel J, Perschmann N, Aydin D, Drinjakovic J, Surrey T, Lopez-Garcia M, Kessler H, Spatz J P. Protein repellent properties of covalently attached PEG coatings on nanostructured SiO₂-based interfaces. *Biomaterials*, **2007**, 28: 4739-4747.
- [22] Mortera R, Vivero-Escoto J, Slowing I I, Garrone E, Onida B, Lin V S Y. Cell-induced intracellular controlled release of membrane impermeable cysteine from a mesoporous silica nanoparticle-based drug delivery system. *Chemical Communications*, **2009**, *22*: 3219-3221.
- [23] Vasir J K, Labhasetwar V. Quantification of the force of nanoparticle-cell membrane interactions and its influence on intracellular trafficking of nanoparticles. *Biomaterials*, **2008**, *29*: 4244-4252.
- [24] Discher B M, Won Y Y, Ege D S, Lee J C M, Bates F S, Discher D E, Hammer D A. Polymersomes: tough vesicles made from diblock copolymers. *Science*, **1999**, *284*: 1143-1146.
- [25] Hu S H, Liu D M, Tung W L, Liao C F, Chen S Y. Surfactant-free, self-assembled pva-iron oxide/silica core-shell nanocarriers for highly sensitive, magnetically controlled drug release and ultrahigh cancer cell uptake efficiency. *Advanced Functional Materials*, **2008**, *18*: 2946-2955.
- [26] Volodkin D V, Skirtach A G, Mohwald H. Near-IR remote release from assemblies of liposomes and nanoparticles. *Angewandte Chemie International Edition*, **2009**, *48*: 1807-1809.
- [27] Pardridge W M. shRNA and siRNA delivery to the brain. *Advanced Drug Delivery Reviews*, **2007**, *59*: 141-152.
- [28] Liu L, Wang W, Ju X J, Xie R, Chu L Y. Smart thermo-triggered squirting

- capsules for nanoparticle delivery. Soft Matter, 2010, 6: 3759-3763.
- [29] Chu L Y, Utada A S, Shah R K, Kim J W, Weitz D A. Controllable monodisperse multiple emulsions. *Angewandte Chemie International Edition*, **2007**, *46*: 8970-8974.
- [30] Xie R, Li Y, Chu L Y. Preparation of thermo-responsive gating membranes with controllable response temperature. *Journal of Membrane Science*, **2007**, 289: 76-85.
- [31] Lamaka S V, Shchukin D G, Andreeva D V, Zheludkevich M L, Möhwald H, Ferreira M G S. Sol-gel/polyelectrolyte active corrosion protection system. *Advanced Functional Materials*, **2008**, *18*: 3137-3147.
- [32] White S R, Sottos N R, Geubelle P H, Moore J S, Kessler M R, Sriram S R, Brown E N, Viswanathan S. Autonomic healing of polymer composites. *Nature*, **2001**, *409*: 794-797.

Thermo-Responsive Membranes for Chiral Resolution

In this chapter, the design, fabrication and performance of thermo-responsive membranes for chiral resolution with a high performance are introduced. The membrane is designed with both chiral selectivity based on molecular recognition of beta-cyclodextrin (β -CD) and thermo-sensitivity based on phase transition of PNIPAM. Linear PNIPAM chains are grafted onto porous Nylon6 membrane substrates by using the plasma-graft pore-filling polymerization method, acting as micro-environmental adjustors for β -CD molecules. β -CD moieties are introduced into the linear PNIPAM chains by the chemical grafting polymerization method, acting as chiral selectors. The phase transition of grafted PNIPAM chains affects the micro-environment of β -CD molecules and then the association between β -CD and guest molecules. The chiral selectivity of the prepared thermo-responsive membranes in chiral resolution operated at a temperature below the LCST of PNIPAM is higher than that of membranes with no thermo-sensitivity, while the decomplexation ratio of enantiomer-loaded thermo-responsive membranes in decomplexation operated at a temperature above the LCST is much higher than that of membranes with no thermo-sensitivity. By simply changing the operating temperature, high selective chiral resolution and efficient membrane regeneration can be achieved.

5.1 Introduction

Chiral recognition of molecules plays an important role in the biological processes. ^[1,2] Different enantiomers of a chiral drug usually exhibit different pharmacological activities, metabolic effects, metabolic rates and toxicities due to the high degree of stereoselectivity of enzymatic reactions and other biological processes. ^[3,4] Therefore, drugs have to be applied in an optically pure form to prevent unwanted

side effects or even toxicity. In the last two decades, enantioseparation technology has been developed rapidly in response to the demand for optically pure compounds in a wide variety of applications. [4] Membrane technology, because of its high efficiency, low energy usage, simplicity and continuous operability, has been considered as the most potential method for large-scale enantioseparation processes. [1,4-6] Consequently, much attention has been drawn to chiral membrane technology. It is well known that enantioselective solid membranes, which can fulfill the demand for industrial applications, [1,7] are more stable and stronger than liquid membranes.

Generally, enantioselective solid membranes can be classified into two categories, i.e., diffusion-selective membranes and adsorption-selective membranes. A diffusion-selective membrane is considered to be a membrane with no specific chiral selectors for the chiral interaction, but consists of a chiral polymer which can either be coated on a non-chiral support layer or can be self-supporting. [1,8-12] The main disadvantage of diffusion-selective membranes is the reverse relationship between selectivity and flux, which has hindered industrial-scale applications of diffusion-enantioselective membranes. Sorption-selective membranes mainly make use of a chiral selector embedded in a polymer matrix, and these selectors are known from analytical separation methods and form a one-to-one complex with enantiomers by means of specific molecular interaction. [1,13-17] Unlike diffusion-enantioselective membranes, an adsorption-enantioselective membrane can enhance the flux and selectivity simultaneously, which is the most promising approach for achieving high flux and selectivity as well as high efficiency and stability. This makes it applicable in industrial-scale chiral resolution processes. However, previous investigations focused mainly on the enhancement of flux and selectivity, no research was carried out on the improvement in regeneration of enantiomer-loaded membranes. It is a recognized fact that efficient regeneration of saturated membranes for re-use could greatly reduce the costs resulting from the consumption of raw materials and disposal of membranes.

Recently, the author's group reported on a novel thermo-responsive membrane for chiral resolution, which featured a simple and efficient process for membrane regeneration. The proposed membrane simultaneously exhibited chiral selectivity based on molecular recognition of beta-cyclodextrin (β -CD) and temperature sensitivity based on phase transition of poly(N-isopropylacrylamide) (PNIPAM). By simply changing the operating temperature, chiral resolution with high selectivity and efficient membrane regeneration was achieved.

5.2 Concept and Design of the Thermo-Responsive Membrane for Chiral Resolution

The concept of the thermo-responsive membrane for chiral resolution is schematically

illustrated in Fig.5.1. [18] The functional gates of the membrane are grafted thermoresponsive PNIPAM chains with appended β -CD moieties. β -CD molecules possess hydrophobic cavities and hydrophilic external surfaces. Through a series of weak intermolecular forces, such as hydrophobic, electrostatic and hydrogenbonding interactions, β -CD is a well-known host molecule capable of selectively associating with guest molecules having a similar size to its cavity, and is used widely as a chiral selector in enantioseparation membranes. [14,15,19] PNIPAM is a thermo-responsive polymer with an LCST around 32 °C. When the environmental temperature is below the LCST, PNIPAM is in a swollen and hydrophilic state in water; while it is in a shrunken and hydrophobic state when the environmental temperature is above the LCST. It has been reported that the phase transition of PNIPAM responding to temperature change could affect the association constant between β -CD and guest molecules in a PNIPAM-modified β -CD system. [20-24] When the temperature is above the LCST, the association constant of β -CD toward guest molecules is much smaller than that at a temperature below the LCST, due to the steric hindrance caused by the shrunken and hydrophobic PNIPAM chain. [20-24] Therefore, by using such a cooperation function between PNIPAM and β -CD, an interesting membrane process can be achieved for chiral resolution with the proposed membrane, as shown in Fig.5.1.

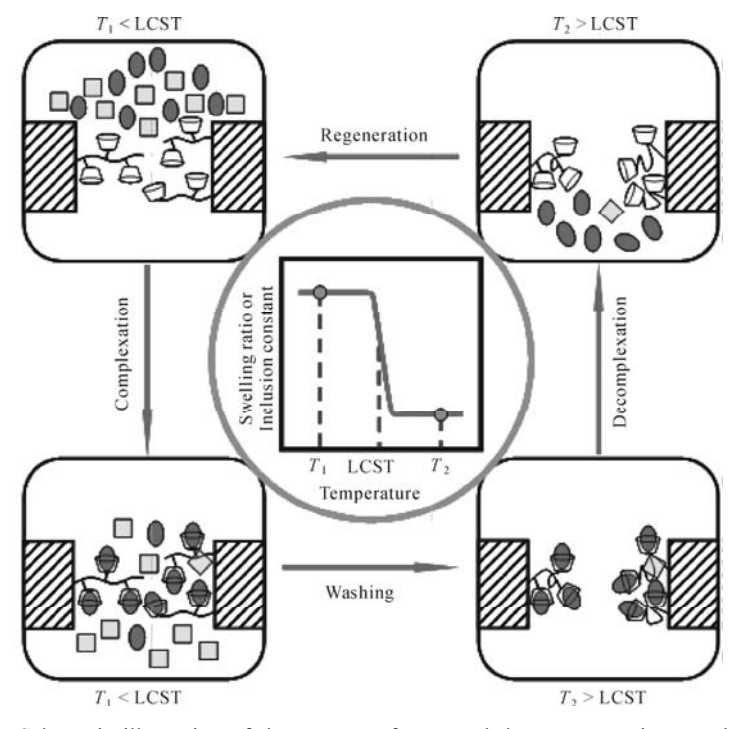


Fig.5.1. Schematic illustration of the concept of proposed thermo-responsive membrane for chiral resolution and the membrane process (Reproduced with permission from Ref. [18]). Copyright (2008), Wiley-VCH Verlag GmbH & Co. KGaA

In the designed membrane, β -CD molecules act as host molecules or chiral selectors and PNIPAM chains act as micro-environmental adjusters for the association constant of β -CD molecules toward guest molecules. The chiral resolution of enantiomers through the membrane is operated at a temperature below the LCST. Under this condition, the grafted PNIPAM chains are in a swollen and hydrophilic state and the association constant of β -CD toward recognized molecules is large; as a result, one of the two enantiomers is captured by β -CD molecules due to chiral recognition during the permeation of racemates, while the other is permeated. When the complexation between β -CD and captured molecules in the membrane reaches equilibrium, a wash process is carried out to remove the uncaptured or free molecules. Then, the operating temperature is increased to be higher than the LCST and the grafted PNIPAM chains turn into a shrunken and hydrophobic state. At the same time, the association constant between β -CD and captured molecules decreases significantly. As a result, decomplexation of captured enantiomers from β -CD molecules occurs, and thus the enantiomers are separated and the membrane is regenerated. Compared with currently existing affinity membrane processes, the proposed membrane process, especially the decomplexation process, is completely environmentally friendly and can be easily operated.

5.3 Preparation and Componential and Morphological Characterization of Membranes

In this section, the preparation and characterization of membranes will be introduced.

5.3.1 Preparation of Thermo-Responsive Chiral Membranes

The synthesis route of grafted functional polymeric gates in the developed membrane is shown in Fig.5.2. [18] First, poly(N-isopropylacrylamide-co-glycidyl methacrylate) (poly(NIPAM-co-GMA), PNG) linear chains were grafted onto porous Nylon6 membrane substrates by using plasma-graft pore-filling polymerization described in Section 2.2.1.1. Porous Nylon6 membranes with an average pore size of 0.22 μ m were used as porous membrane substrates. Then modified β -CD moieties (EDA- β -CD, CD) were appended onto the above-grafted copolymer chains by the chemical grafting polymerization method.

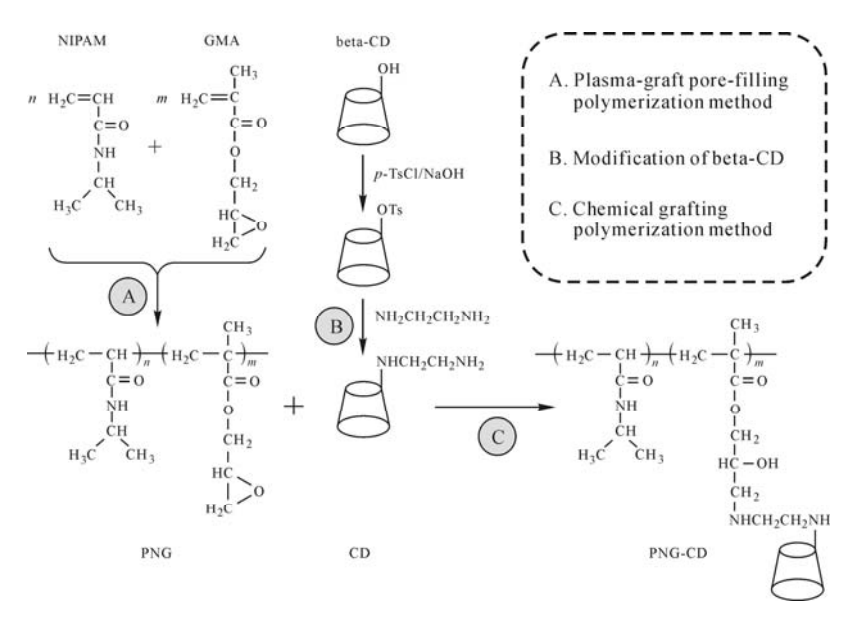


Fig.5.2. The synthesis route of grafted functional polymeric gates in the proposed membrane. A) Poly(NIPAM-co-GMA) (PNG) linear chains were grafted onto porous Nylon6 membrane substrates by using plasma-graft pore-filling polymerization, B) chemical modification of β-CD, and C) the modified β-CD molecules were appended onto above-grafted copolymer chains by chemical grafting polymerization (Reproduced with permission from Ref. [18]). Copyright (2008), Wiley-VCH Verlag GmbH & Co. KGaA

5.3.1.1 Preparation of Modified β -CD Moieties

To prepare the designed membranes, modified β -CD moieties (EDA- β -CD) should be synthesized first. Mono-6-OTs- β -CD was synthesized according to a published method. [25] Briefly, 100.0 g of β -CD was suspended in 833 ml of water and 33 ml of water containing 10.95 g of NaOH was added dropwise over 10 min. The suspension became homogeneous and slightly yellow before the addition was complete. 16.82 g of p-toluenesulfonyl chloride (p-TsCl) in 50 ml of acetonitrile was added dropwise over 75 min, causing an immediate white precipitate. After 2.5 h of vigorous stirring at 25 °C, a 1 mol·L⁻¹ HCl aqueous solution was added to modulate the pH value to 8 at the end of the reaction. Then the suspension was refrigerated overnight at 4 °C. The resulting white precipitate was recovered by suction filtration and then immersed in ethyl ether for 48 h to remove the residual p-TsCl. After washing twice with hot water and drying in vacuo at 70 °C overnight, 12.63 g of a pure white Mono-6-OTs-β-CD was obtained. ¹H NMR (300 MHz, DMSO): δ =7.75 (d, 2 H), δ =7.43 (d, 2 H), δ =5.58 (m, 14 H), δ =4.82 (s, 4 H), δ =4.76 (s, 3 H), δ =2.43 (s, 3 H) ppm. Synthesis of EDA- β -CD was carried out according to the method described in Ref. [26]. 5.0 g of Mono-6-OTs- β -CD was reacted with 30 ml of ethylenediamine (EDA) at 75 °C for 6 h. After evaporation of EDA, the reaction mixture was allowed to cool to room temperature, was poured into 250 ml of cold acetone and the precipitate was filtered. The precipitate was repeatedly dissolved in 80 ml of water/methanol (3:1, v/v) solution mixture and poured into 250 ml of acetone for the removal of unreacted EDA. After filtration, the precipitate was dried *in vacuo* at 50 °C for 3 d and 4.2 g of EDA- β -CD were obtained. IR (KBr): 3,381 cm⁻¹ (s, OH), 2,927 cm⁻¹ (w, CH₂), 1,030 cm⁻¹ (s, C-OH).

5.3.1.2 Preparation of Thermo-Responsive Chiral Membranes

Preparation of thermo-responsive chiral membranes included two steps, and the grafted polymeric chains on membranes were synthesized based on the chemical reaction route shown in **Fig.5.2**.^[18] Firstly, plasma-graft pore-filling polymerization was employed to graft linear poly(NIPAM-*co*-GMA) (PNG) chains onto Nylon6 membrane substrates according to the method described in **Section 2.2.1.1**. Briefly, the substrate was placed in a transparent glass tube, which was filled with argon gas and evacuated to a pressure of 10 Pa beforehand, and was then treated by plasma at 30 W for 60 s. After that, the membrane was dunked into the monomer solution and the grafting polymerization took place in a shaking constant-temperature bath at 60 °C for a predetermined time. The feed molar ratio of NIPAM and glycidyl methacrylate (GMA) in the monomer solution was 1:1 and the polymerization time varied from 2 to 24 h to obtain membranes with different grafting yields. The grafted membrane was rinsed in well-deionized water under vibration in a constant-temperature bath (30 °C) for 24 h to remove any non-reacted monomer and homopolymer and was then dried in an oven at 50 °C overnight.

EDA- β -CD was grafted onto the above-grafted PNG chains by chemical grafting polymerization. The reaction was conducted in 1,4-dioxane/water (1:1, v/v) solution mixture. Owing to the shield effect of macromolecular chains to epoxy groups and steric hindrance of β -CD, the grafting was performed in the presence of an excess amount of EDA- β -CD (2:1, β -CD/epoxy groups). According to the grafting yield of the first step, a fixed amount of EDA- β -CD was dissolved in the 1,4-dioxane/water solution mixture and then PNG grafted membranes were immersed in the solution. Consequently, the grafting polymerization took place in a shaking constant-temperature bath at 60 °C for 48 h. The grafted membrane was also rinsed in well-deionized water under vibration in a constant-temperature bath (30 °C) for 24 h, to remove any non-reacted monomer, and was then dried in an oven at 50 °C overnight.

5.3.1.3 Definition of Grafting Yields of Membranes

In the plasma-graft pore-filling polymerization, NIPAM and GMA were used as monomers and the grafted copolymer was PNG. The grafting yield (Y) of the membrane was defined as the weight increase of the membrane after grafting and

was calculated according to the following equation:[18]

$$Y_{\rm PNG} = \frac{W_1 - W_0}{A} \tag{5.1}$$

where Y_{PNG} stands for the grafting yield of PNG on the membrane substrate [mg·cm⁻²] A for the area of membrane [cm²] and W_1 and W_0 for the mass of the membrane after and before grafting, respectively [mg].

The relationship of grafting yields Y_{PNIPAM} , Y_{PGMA} and Y_{PNG} could be expressed as follows:

$$Y_{\text{PNIPAM}} + Y_{\text{PGMA}} = Y_{\text{PNG}} \tag{5.2}$$

$$\frac{Y_{\text{PNIPAM}}}{Y_{\text{PGMA}}} = \frac{M_{\text{NIPAM}} \times N_{\text{PNIPAM}}}{M_{\text{GMA}} \times N_{\text{PGMA}}}$$
(5.3)

where $Y_{\rm PNIPAM}$ and $Y_{\rm PGMA}$ stand for the grafting yields of PNIPAM and poly (glycidyl methacrylate) (PGMA) on the membrane substrates [mg·cm⁻²], $M_{\rm NIPAM}$ and $M_{\rm GMA}$ for the molecular weights of NIPAM and GMA [g/mol] and $N_{\rm PNIPAM}$ and $N_{\rm PGMA}$ for the mass of PNIPAM and PGMA in the grafted copolymer PNG [mol], respectively.

According to the results of X-ray photoelectron spectroscopy (XPS) spectra (Section 5.3.2), it was found that the molar ratio of PNIPAM and PGMA in PNG was approximately consistent with that of the feed molar ratio of 1:1, *i.e.*, N_{PNIPAM} were almost equal to N_{PGMA} . Thus Y_{PNIPAM} could be defined as follows:

$$Y_{\text{PNIPAM}} = \frac{Y_{\text{PNG}}}{1 + M_{\text{GMA}} / M_{\text{NIPAM}}} \tag{5.4}$$

In chemical grafting polymerization, the grafting yield of CD was also defined as the weight increase of the membrane after grafting of CD and was calculated by the following equation:^[18]

$$Y_{\rm CD} = \frac{W_2 - W_1}{A} \tag{5.5}$$

where $Y_{\rm CD}$ stands for the grafting yield of CD on the membrane substrate [mg·cm⁻²], A for the area of membrane [cm²] and W_2 and W_1 for the mass of the membrane after and before CD grafting [mg], respectively.

Because PNIPAM and CD are two functional components in the developed membranes, Y_{PNIPAM} and Y_{CD} are used to characterize the grafting yields of prepared membranes.

5.3.2 Componential and Morphological Characterization of Membranes

X-ray photoelectron spectroscope (XPS, XSAM800, KRATOS, U.K.) was employed to confirm the synthesis of membranes with grafted functional polymers by using a monochromatic Al K α X-ray source (1,486.6 eV photons). The core-level signals were obtained at the photoelectron take-off angle (α , with respect to the

sample surface) of 90°. In the analyses of high-resolution XPS spectra, a Gaussian peak shape was used and the analyses were performed with binding energies and the full-width-at-half-maxima (fwhm) of peaks kept constant at literature values but with the intensities varied. To study the temperature-dependent change in surface hydrophilicity of these membranes, a contact angle measurement system was employed to measure surface contact angles of ungrafted and grafted membranes at different temperatures. A pipette was used to deposit the same volume (3 µl) of water onto membranes. Scanning electron microscope (SEM, JSM-5900LV, JEOL, Japan) was employed to study the microscopic configuration of ungrafted and grafted membranes. Surface and cross-sectional structures of membranes were observed at an accelerating voltage of 20 kV by putting the membranes into liquid nitrogen for enough time, fracturing mechanically and sticking onto the sample holder.

Fig.5.3 shows SEM images of the surfaces and cross-sections of ungrafted Nylon6 membrane substrate and PNG-CD grafted Nylon6 membrane with $Y_{\rm PNIPAM}=131~{\rm mg\cdot cm^{-2}}/Y_{\rm CD}=62~{\rm mg\cdot cm^{-2}}.^{[18]}$ The ungrafted membrane substrate was constructed with a thin functional porous top layer and honeycombed pores were clearly seen in the ungrafted membrane (**Figs.5.3a** and **5.3b**). After grafting, both surface and cross-sectional micrographs show that the membrane pore size decreased. From the surface SEM images (**Figs.5.3a** and **5.3c**), it can be seen that the surface pores of the grafted membrane were smaller compared with those of the ungrafted membrane. From the cross-sectional SEM images (**Figs.5.3b** and **5.3d**), it can be obviously seen that the grafted polymers were formed inside the pores throughout the entire membrane thickness. It was consistent with the results in Chapter 2 with different substrates and different analysis methods. That means the functional polymer was grafted on both the outer surfaces of the membrane and the inner surfaces of the membrane pores.

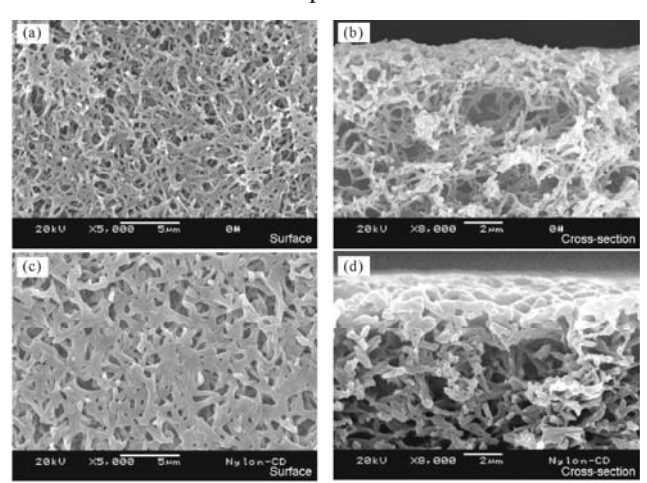


Fig.5.3. SEM photographs of surfaces and cross-sections of membranes. (a, b) Ungrafted Nylon6 membrane; (c, d) poly(NIPAM-co-GMA)-EDA-β-CD (PNG-CD) grafted Nylon6 membrane with Y_{PNIPAM} =131 mg·cm⁻²/ Y_{CD} =62 mg·cm⁻² (Reproduced with permission from Ref. [18]). Copyright (2008), Wiley-VCH Verlag GmbH & Co. KGaA

Fig.5.4 shows XPS spectra of ungrafted Nylon6 membrane, PNG grafted Nylon6 membrane with $Y_{PNIPAM}=130 \text{ mg}\cdot\text{cm}^{-2}/Y_{CD}=0 \text{ mg}\cdot\text{cm}^{-2}$ and PNG-CD grafted Nylon6 membrane with $Y_{PNIPAM}=131 \text{ mg}\cdot\text{cm}^{-2}/Y_{CD}=62 \text{ mg}\cdot\text{cm}^{-2}$. [18] There are only three peaks in the C1s spectrum of ungrafted Nylon6 membrane (Fig.5.4a), whose corresponding binding energies are 284.8 eV (C atom in C-C and C-H bond), 285.8 eV (C atom in C=N bond) and 287.8 eV (C atom in C=O bond) respectively. These are the characteristic peaks of Nylon6 membrane. The top peak in Fig.5.4a was the summation of the three ones below. Figs.5.4c and 5.4e show the spectra of PNG grafted Nylon6 membrane and PNG-CD grafted Nylon6 membrane. In both of the figures, a new peak at the binding energy of 288.3 eV, which stands for the C atom in the O=C-O bond of GMA (Figs. 5.4c and 5.4e), appears in addition to the above-mentioned three peaks in Fig.5.4a. The result indicated that PGMA had been successfully grafted on the surfaces of Nylon6 membranes. With respect to CD, according to the weight increase of the membrane in the step of CD grafting polymerization, it was confirmed that CD moieties had also been successfully introduced into the PNG chains, because the reactivity of epoxy groups toward primary amine groups is relatively high.^[27]

There is one peak in the O1s spectrum of the ungrafted Nylon6 membrane at the binding energy of 531.6 eV, which stands for the O atom in the C=O bond (Fig.5.4b). Compared with the spectrum of ungrafted membrane substrates, a new peak appears in the O1s spectra of the PNG grafted Nylon6 membrane and PNG-CD grafted Nylon6 membrane at the binding energy of 532.7 eV, which stands for the O atom in the C-O bond of the epoxy group in GMA (Figs.5.4d and 5.4f). The result also confirmed the existence of PGMA grafted on the membranes. The peak areas for the O atom in the C-O bond in Figs.5.4d and 5.4f are 3314.6 and 2419.3 respectively, the difference in which meant part of the epoxy groups were consumed by reaction with primary amine groups. The results confirmed that CD moieties had been successfully grafted on the PNG chains.

The evidence for the PNIPAM grafted on the membranes was also obtained. The temperature-dependent contact angle variations of ungrafted Nylon6 membrane, poly(GMA)-EDA- β -CD (PG-CD) grafted Nylon6 membrane with $Y_{\rm PNIPAM}$ =0 mg·cm⁻²/ $Y_{\rm CD}$ =36 mg·cm⁻², and PNG-CD grafted Nylon6 membrane with $Y_{\rm PNIPAM}$ =129 mg·cm⁻²/ $Y_{\rm CD}$ =24 mg·cm⁻² are shown in **Fig.5.5**. [18] The contact angle of the ungrafted Nylon6 membrane decreased somewhat from 34.0° to 32.1° when the environmental temperature increased from 25 to 45 °C because the liquid surface tension between liquid and air decreased with the temperature increase, which caused the decrease in the contact angle. [28,29] For the PG-CD grafted membrane, the contact angle variation was similar to that of the ungrafted membrane, and it changed from 62.7° to 60.5°. On the other hand, the contact angle of the PNG-CD grafted membrane showed a reverse change tendency. When the temperature changed from 25 °C to 45 °C, the contact angle increased greatly from 48.8° to 55.6°. This was due to the transition from hydrophilic state to hydrophobic state of the grafted PNIPAM chains on the membrane surface when the temperature was

increased above the LCST. As a result, the surface tension of the liquid was increased and thus the contact angle also became larger. In general, the liquid surface tension tended to decrease at a higher temperature. However, the effect was insignificant compared with the hydrophobic effect of the PNG-CD grafted membrane. As a result, the overall surface tension of water increased. The results indicated that PNIPAM has been successfully grafted onto the membrane.

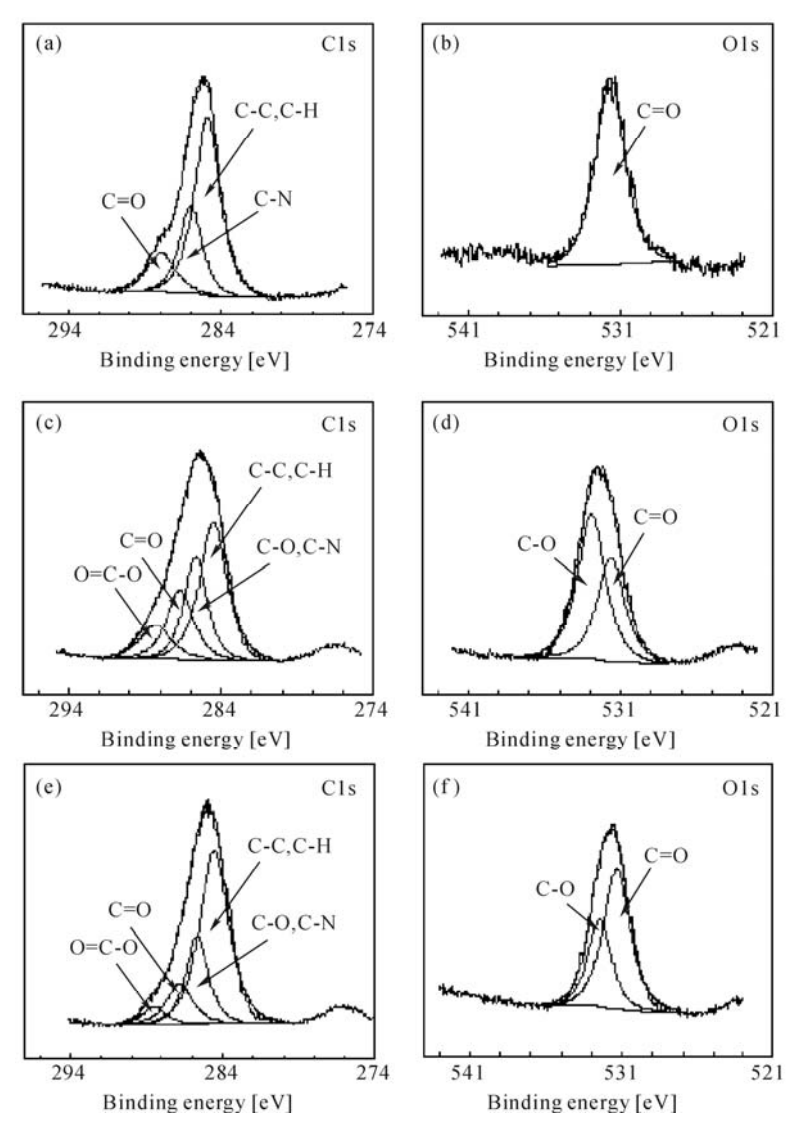


Fig.5.4. XPS spectra of membranes. (a, b) Ungrafted Nylon6 membrane; (c, d) PNG grafted Nylon6 membrane with $Y_{\text{PNIPAM}}=130 \text{ mg·cm}^2/Y_{\text{CD}}=0 \text{ mg·cm}^2$; (e, f) PNG-CD grafted Nylon6 membrane with $Y_{\text{PNIPAM}}=131 \text{ mg·cm}^2/Y_{\text{CD}}=62 \text{ mg·cm}^2$ (Reproduced with permission from Ref. [18]). Copyright (2008), Wiley-VCH Verlag GmbH & Co. KGaA

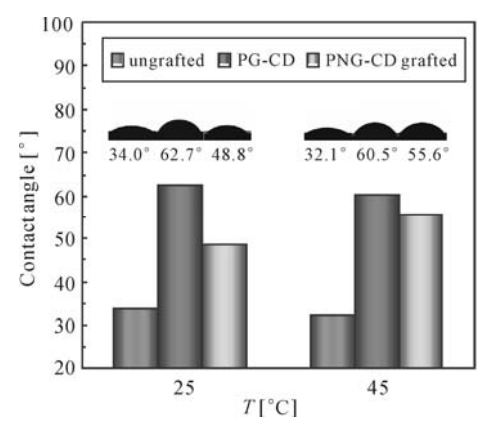


Fig.5.5. Temperature-dependent variations of contact angles of ungrafted Nylon6 membrane, poly(GMA)-EDA- β -CD (PG-CD) grafted Nylon6 membrane with Y_{PNIPAM} =0 mg·cm⁻²/ Y_{CD} = 36 mg·cm⁻² and PNG-CD grafted Nylon6 membrane with Y_{PNIPAM} =129 mg·cm⁻²/ Y_{CD} =24 mg·cm⁻² (Reproduced with permission from Ref. [18]). Copyright (2008), Wiley-VCH Verlag GmbH & Co. KGaA

5.4 Chiral Resolution Performance of Tryptophan Enantiomers with Thermo-Responsive Membranes

In this section, the chiral resolution performance of tryptophan enantiomers will be tested with above-prepared thermo-responsive membranes.

5.4.1 Permeation of D,L-Tryptophan through Grafted Thermo-Responsive Membranes

The permeation experiments of *D*,*L*-tryptophan were carried out using a standard side-by-side diffusion cell.^[18] The diffusion cell was located in a water bath to keep the temperature constant. Each tested membrane was kept in well-deionized water overnight before being loaded into the cell. After a check for leakage, well-deionized water and 4.9 mmol·L⁻¹ of a *D*,*L*-tryptophan solution treated by moist heat sterilization were added simultaneously to the receptor and donator cells, respectively, and stirred with a pair of magnetic stirrers. The solutions in receptor and donator cells were sampled at a fixed time interval and the concentration of *D*,*L*-tryptophan was determined by measuring UV absorbance. The wavelength of maximum absorbance determined for *D*,*L*-tryptophan was 278 nm. The relationship between concentration and absorbance was calibrated by taking spectra of known concentrations. The calibration curves showed a linear relation up to a total (*D*-tryptophan plus *L*-tryptophan) concentration.

The permeability of D,L-tryptophan through membranes (M) was calculated by the following equation

$$M = \frac{c \times V}{A_f} \tag{5.6}$$

where c stands for the concentration of D,L-tryptophan [g/ml], V for the volume of D,L-tryptophan solution [ml], A_f for the effective areas of membrane for chiral resolution [m²].

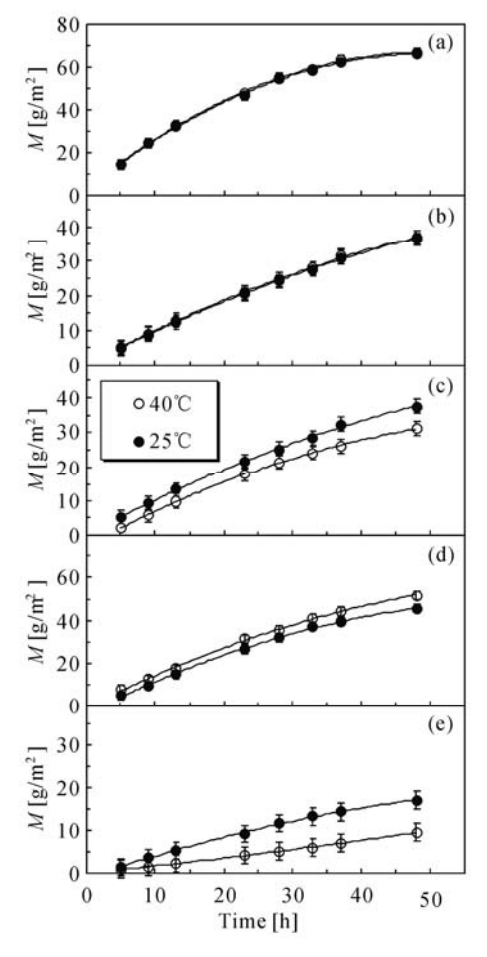


Fig.5.6. Effect of temperature on the permeability of D,L-tryptophan through different membranes. (a) Ungrafted Nylon6 membrane; (b) PG-CD grafted Nylon6 membrane with $Y_{PNIPAM}=0$ mg·cm²/ $Y_{CD}=23$ mg·cm²; (c, d, e) PNG-CD grafted Nylon6 membranes with $Y_{PNIPAM}=107$ mg·cm²/ $Y_{CD}=23$ mg·cm², $Y_{PNIPAM}=65$ mg·cm²/ $Y_{CD}=20$ mg·cm² and $Y_{PNIPAM}=134$ mg·cm²/ $Y_{CD}=25$ mg·cm², respectively (Reproduced with permission from Ref. [18]). Copyright (2008), Wiley-VCH Verlag GmbH & Co. KGaA

Fig.5.6 shows the effect of temperature on the total permeation of D,L-tryptophan through different membranes. For the ungrafted Nylon6 membrane, the permeability at 40 °C showed a small increase compared with that at 25 °C (**Fig.5.6a**), which was due to the increase in diffusion coefficient according to the Stokes-Einstein equation, denoted by [30]

$$D = \frac{k_B T}{6\pi\mu r_s} \tag{5.7}$$

where D is the diffusion coefficient, k_B is Boltzmann's constant, T is the absolute temperature, μ is the viscosity of solvent and r_S is the Stokes-Einstein radius of solute. The liquid viscosity decreases with an increase in temperature.

A series of PNG-CD grafted membranes with a wide range of grafting yields were prepared and comparison of the membrane performances was made. The permeability of $D_{,L}$ -tryptophan through the PG-CD grafted Nylon6 membrane with $Y_{\rm PNIPAM}=0~{\rm mg\cdot cm^{-2}}/Y_{\rm CD}=23~{\rm mg\cdot cm^{-2}}$ and PNG-CD grafted Nylon6 membrane with $Y_{\rm PNIPAM}=107~{\rm mg\cdot cm^{-2}}/Y_{\rm CD}=23~{\rm mg\cdot cm^{-2}}$ at 25 °C and 40 °C are shown in **Figs.5.6b** and **5.6c**. For the PG-CD grafted membrane, the effect of temperature on the permeability of $D_{,L}$ -tryptophan was the same as that on ungrafted membrane substrates, i.e. the grafted PG chains do not have thermo-responsive characteristics. However, for the PNG-CD grafted membrane, the effect of temperature on the permeability of $D_{,L}$ -tryptophan was quite different. The permeability of $D_{,L}$ -tryptophan at 40 °C was much lower than that at 25 °C, which was due to the transition from hydrophilic state to hydrophobic state of grafted PNIPAM chains in the membrane.

Figs.5.6c to 5.6e show the effect of the grafting yield of PNG-CD grafted membranes on the permeability of D,L-tryptophan. [18] It was demonstrated that the permeability of D,L-tryptophan decreased with the increase in the grafting yield. There was a dramatic difference between the permeability at 25 °C and 40 °C due to the conformational change of PNIPAM chains grafted in membrane pores. It was found that temperature had an opposite effect on the permeability of D,L-tryptophan across membranes with a low grafting yield of Y_{PNIPAM} = 65 mg·cm⁻²/ $Y_{\rm CD}$ =20 mg·cm⁻² (**Fig.5.6d**) and those with a high grafting yield of $Y_{\text{PNIPAM}} = 107 \text{ mg} \cdot \text{cm}^{-2} / Y_{\text{CD}} = 23 \text{ mg} \cdot \text{cm}^{-2}$ (Fig.5.6c). When the grafting yield of PNIPAM was lower, the diffusional coefficient of solute across the membrane was higher at temperatures above the LCST than that below the LCST, owing to the membrane pores being controlled "open" by the shrinking of grafted PNIPAM, which provided more space within the pores to allow the solute to diffuse through, above the LCST. On the other hand, when the grafting yield of PNIPAM was higher, the diffusional coefficient was lower at temperatures above the LCST than that below the LCST, owing to the significance of the hydrophobic state of the large amounts of grafted PNIPAM chains above the LCST. This blocked the paths of solute diffusion. In addition, because the solute tryptophan used in the experiments was water-soluble, its diffusion within the membranes occurred primarily within the water-filled regions in the spaces delineated by the grafted PNIPAM chains. Therefore, it was easier for the solute to find water-filled regions in membranes

with hydrophilic PNIPAM gates rather than in those with hydrophobic PNIPAM gates. When the grafting yield increased to $Y_{\rm PNIPAM}=134~{\rm mg\cdot cm^{-2}}/Y_{\rm CD}=25~{\rm mg\cdot cm^{-2}}$, the length and density of grafted chains were too long and large; as a result, the membrane pores were seriously choked by those tremendously grafted polymers. Therefore, the permeability of $D_{\star}L$ -tryptophan through the grafted membranes tended to decrease at both temperatures (**Fig.5.6e**). Therefore, to get satisfactory permeability, membranes with a grafting yield as high as $Y_{\rm PNIPAM}=134~{\rm mg\cdot cm^{-2}}/Y_{\rm CD}=25~{\rm mg\cdot cm^{-2}}$ (**Fig.5.6e**) or more were not suitable for subsequent enantioseparation studies. A proper grafting yield should be chosen for the membrane used in chiral resolution.

5.4.2 Effects of Grafting Yield and Temperature on Chiral Resolution of D,L-Tryptophan through Membranes

Quantitative analyses of tryptophan enantiomers were performed by an HPLC system (Waters, USA) including 515 pump, 2,487 dual λ absorbance detector and CBL Model 100 column oven. Data analyses were performed using an AllChrom Plus workstation (MultiLink, USA) with a Symmetry Shield RP18 column (3.9 mm×150 mm, 5 μ m), a constant temperature of 45 °C, a flow-rate of 1.0 ml/min, a 278 nm UV detector wavelength and a 20 μ l injection volume. The chiral ligand mobile phase consisted of a pre-mixed methanol/water (5:95, v/v) solution and the water contained 5 mmol·L⁻¹ of CuSO₄ and 6 mmol·L⁻¹ of *L*-phenylalanine (*L*-Phe). Prior to chromatographic analysis, the mobile phase mixture was degassed for 20 min. Chiral selectivity was calculated in terms of enantiomeric excess (e.e. %) of permeates which were determined from the peak areas of two enantiomers and could be calculated according to the following equation:

e.e. =
$$\frac{A_D - A_L}{A_D + A_L} \times 100\%$$
 (5.8)

where A_D and A_L stand for the peak areas of *D*-enantiomer and *L*-enantiomer, respectively.

Fig.5.7 shows the effect of grafting yields of PNG-CD grafted Nylon6 membranes on chiral selectivity. As shown in **Figs.5.7a** and **5.7b**, the e.e. value increased at both 25 °C and 40 °C with the increase in the grafting yield as time elapsed. Furthermore, for each resolution process, there was a peak of selectivity. As we know, the chiral selectivity is determined by the molecular recognition ability of CD to different enantiomers. Once recognition sites on membranes were saturated by guest molecules, the selectivity would gradually decrease. The peak was the critical point of saturation for recognition sites. Thus, if the loading of CD on a membrane increased with the increase in the grafting yield, chiral selectivity could be improved. **Fig.5.7c** shows the variation in the maximal e.e. value (e.e._{max}) of membranes with different grafting yields for chiral resolution at 25 °C and 40 °C.

The e.e._{max} values at 25 °C were always higher than those at 40 °C, and the change in e.e._{max} values with the grafting yield was in accordance with the rules discussed above. When the temperature was higher than the LCST of PNIPAM, the PNIPAM chains were in a shrunken state. Thus the steric hindrance caused by the shrinking of PNIPAM chains made the association constant between CD and tryptophan molecules decrease; as a result, the chiral selectivity decreased. By considering both permeability and selectivity, an optimum grafting yield was obtained as $Y_{\text{PNIPAM}}=107 \text{ mg} \cdot \text{cm}^{-2}/Y_{\text{CD}}=23 \text{ mg} \cdot \text{cm}^{-2}$ for subsequent investigations.

Fig.5.8 shows the effect of temperature on the chiral selectivity of the PNG-CD grafted Nylon6 membrane with $Y_{PNIPAM}=107 \text{ mg}\cdot\text{cm}^{-2}/Y_{CD}=23 \text{ mg}\cdot\text{cm}^{-2}$ and the PG-CD grafted Nylon6 membrane with $Y_{PNIPAM}=0$ mg·cm⁻²/ $Y_{CD}=23$ mg·cm⁻². [18] The e.e. values at 25 °C and 40 °C for both membranes were compared in Fig.5.8a. Both membranes had a chiral selectivity for D,L-tryptophan with a peak of e.e. value, which is defined as e.e.max. For the PG-CD grafted membrane, chiral selectivity at 40 °C was almost the same as that at 25 °C, which meant that the effect of temperature was very small on the chiral selectivity of the PG-CD grafted membrane. However, for the PNG-CD grafted membrane, the difference in chiral selectivity between 25 °C and 40 °C was remarkable. The selectivity of the PNG-CD grafted membrane was higher than that of the PG-CD grafted membrane at 25 °C but much lower at 40 °C. The reason for this phenomenon can be explained as follows. As shown in Fig.5.2, the copolymer of PNG chains was a diblock-structure of NIPAM and GMA, which caused the space between two CD molecules to be broad. The wide span facilitated molecular recognition between CD and tryptophan molecules, while for the PG-CD grafted membrane the recognition was incomplete due to the hindrance caused by the narrow span of CD molecules. That meant the utilization ratio of CD loaded on the PNG-CD grafted membrane was much higher than that on the PG-CD grafted membrane. Thus the chiral selectivity of the PNG-CD grafted membrane was higher than that of the PG-CD grafted membrane at 25 °C. Furthermore, as shown in Fig.5.5, the contact angle of the PNG-CD grafted membrane was lower than that of the PG-CD grafted membrane at 25 °C, which meant that the surface of the PNG-CD grafted membrane was more hydrophilic than that of the PG-CD grafted membrane. The association between CD and guest molecules might be improved in hydrophilic environments. Consequently, the selectivity of the PNG-CD grafted membrane was better than that of the PG-CD grafted membrane at 25 °C. However, the selectivity of the PNG-CD grafted membrane was much lower than that of the PG-CD grafted membrane at 40 °C. The reason is that at a temperature above the LCST, grafted PNIPAM chains were in a shrunken state in water and the steric hindrance around CD molecules from crowded neighboring grafted PNIPAM chains decreased the association constant between CD and enantiomers. Thus, at 40 °C, PNIPAM chains grafted on membranes played a negative role in the interaction between CD and guest molecules, and then the selectivity decreased significantly.

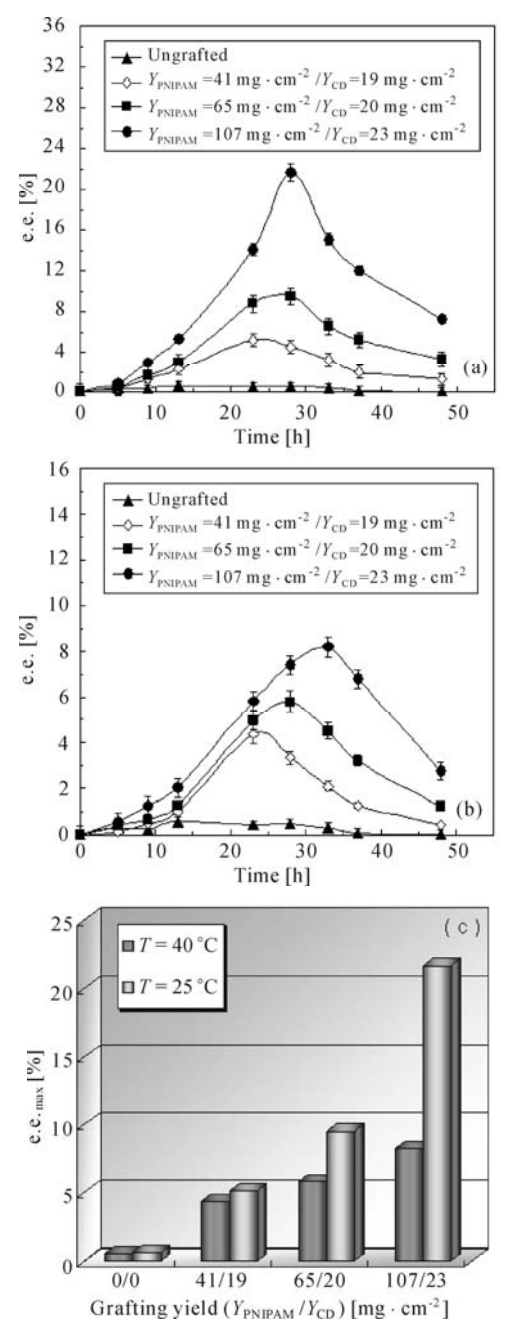


Fig.5.7. Effect of grafting yield of membranes on the enantiomeric excess (e.e.%) of *D,L*-tryptophan chiral resolution through membranes. (a) Operation at 25 °C; (b) Operation at 40 °C; (c) Variation of maximal e.e. value (e.e._{max}) (Reproduced with permission from Ref. [18]). Copyright (2008), Wiley-VCH Verlag GmbH & Co. KGaA

Fig.5.8b shows the effect of temperature on chiral selectivity clearly, in which the thermo-responsive coefficient $R_{\text{e.e.}(25/40)}$ is defined as follows:^[18]

$$R_{\text{e.e.}(25/40)} = \frac{\text{e.e.}_{25}}{\text{e.e.}_{40}}$$
 (5.9)

where e.e.₂₅ and e.e.₄₀ are e.e. values at environmental temperatures of 25 °C and 40 °C, respectively. If the e.e. values are the same at 25 °C and 40 °C, the thermoresponsive coefficient $R_{\text{e.e.}(25/40)}$ is 1.0. That means the membrane does not have any sensitivity to temperature in that case.

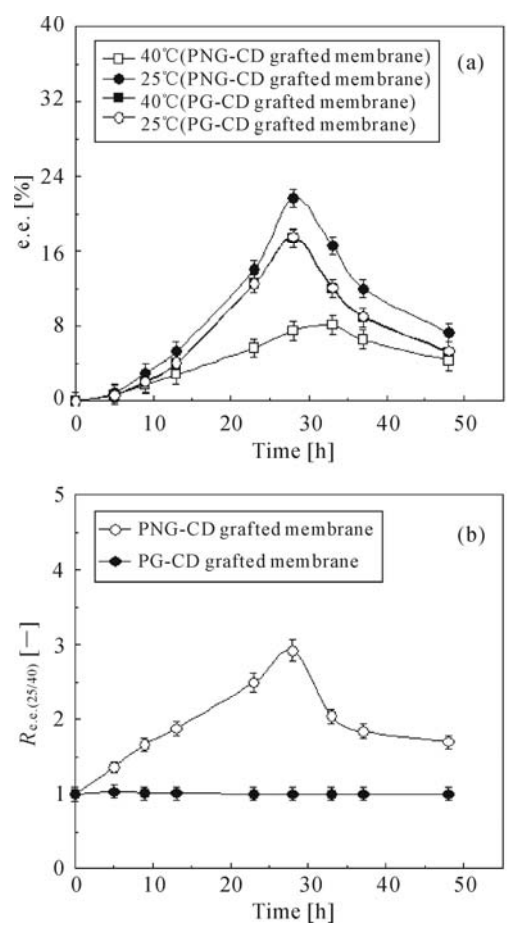


Fig.5.8. Effect of temperature on the enantiomeric excess (e.e.%) of D,L-tryptophan chiral resolution through membranes. The grafting yields of PNG-CD grafted Nylon6 membrane are $Y_{\rm PNIPAM}=107~{\rm mg\cdot cm^2}/Y_{\rm CD}=23~{\rm mg\cdot cm^2}$ and that of PG-CD grafted Nylon6 membrane are $Y_{\rm PNIPAM}=0~{\rm mg\cdot cm^2}/Y_{\rm CD}=23~{\rm mg\cdot cm^2}$. (a) Comparison of e.e. between 25 °C and 40 °C; (b) Comparison of the thermo-responsive coefficient $R_{\rm e.e.(25/40)}$ between membranes (Reproduced with permission from Ref. [18]). Copyright (2008), Wiley-VCH Verlag GmbH & Co. KGaA

As shown in **Fig.5.8b**, the $R_{\rm e.e.(25/40)}$ value of the PG-CD grafted membrane was always around 1.0 as time went by, which meant that the temperature had little effect on the chiral selectivity of the PG-CD grafted membrane. However, for the PNG-CD grafted membrane, when the time was less than 28 h, the thermoresponsive coefficient $R_{\rm e.e.(25/40)}$ increased over time, but it decreased when the time was more than 28 h. The results also indicated that the thermo-response of PNIPAM chains grafted on membranes affected the interaction between CD and guest molecules as mentioned above.

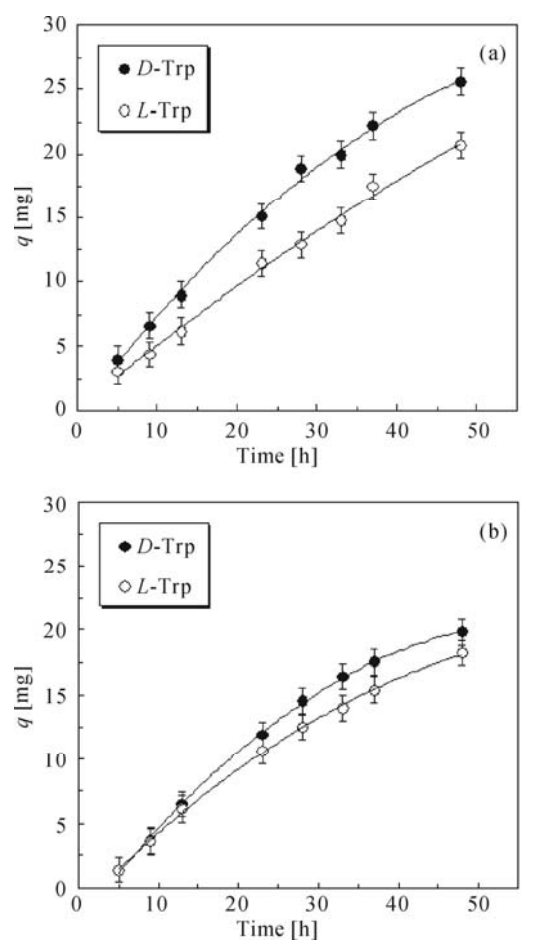


Fig. 5.9. Chiral resolution of D_{L} -tryptophan through PNG-CD grafted Nylon6 membrane with $Y_{\text{PNIPAM}}=107 \text{ mg} \cdot \text{cm}^{-2}/Y_{\text{CD}}=23 \text{ mg} \cdot \text{cm}^{-2}$. (a) At 25 °C; (b) At 40 °C (Reproduced with permission from Ref. [18]). Copyright (2008), Wiley-VCH Verlag GmbH & Co. KGaA

Fig.5.9 shows the chiral resolution performance of $D_{\star}L$ -tryptophan through a PNG-CD grafted Nylon6 membrane with $Y_{\rm PNIPAM}=107~{\rm mg\cdot cm^{-2}}/Y_{\rm CD}=23~{\rm mg\cdot cm^{-2}}$ at 25 °C and 40 °C. [18] For both two temperatures, the permeabilities of two optical

enantiomers were different. The concentration of D-tryptophan was more than that of L-tryptophan in the receptor cell, because the β -CD molecule has a higher association constant with L-tryptophan than with D-tryptophan in neutral environments. Thus, most of the tryptophan molecules absorbed in the membrane were L-tryptophan and the permeability of D-tryptophan was high. Another interesting result was also found in **Fig.5.9**. For the chiral resolution through a PNG-CD grafted membrane, the separation efficiency of two enantiomers at 25 °C was much better than that at 40 °C. The result demonstrated that separation efficiency was reduced with an increase in temperature, which accounted for the steric hindrance between host and guest molecules. The shrinking of PNIPAM chains at 40 °C hindered the association between CD and L-tryptophan molecules and then reduced the separation efficiency.

5.5 Decomplexation of Tryptophan Enantiomers from Thermo-Responsive Membranes

After the permeation experiments, membranes were immersed in a fixed amount of well-deionized water at 40 °C for the decomplexation of solutes absorbed during the permeation. The concentration of samples was also analyzed by UV absorbance measurement. The decomplexation ratio η was calculated by the following equation^[18]

$$\eta = \frac{q}{q_0}
\tag{5.10}$$

where q and q_0 stand for the amount of D,L-tryptophan desorbed from a membrane and that adsorbed in the membrane before decomplexation, respectively [mg].

Fig.5.10 shows the decomplexation of tryptophan enantiomers from membranes after chiral resolution. [18] The decomplexation performance of the PNG-CD grafted Nylon6 membrane with $Y_{PNIPAM}=107 \text{ mg}\cdot\text{cm}^{-2}/Y_{CD}=23 \text{ mg}\cdot\text{cm}^{-2}$ and the PG-CD grafted Nylon6 membrane with $Y_{PNIPAM} = 0$ mg·cm⁻²/ $Y_{CD} = 23$ mg·cm⁻² were compared. The decomplexation was operated at 40 °C, which was above the LCST of PNIPAM. From Fig.5.10a, it was found that the absolute amount of L-tryptophan and D-tryptophan released from the PNG-CD grafted membrane was much higher than that from the PG-CD grafted membrane. As shown in Fig.5.10b, the decomplexation ratio of the PNG-CD grafted membrane was much larger than that of the PG-CD grafted membrane. The above-mentioned interesting results confirmed the validity of the membrane design. With respect to the PNG-CD grafted membrane, when the environmental temperature was above the LCST, grafted PNIPAM chains on the membrane were in a shrunken state; as a result, the steric hindrance caused by shrinking and crowding of polymer chains made the association constant between β -CD and guest molecules decrease. Thus, the decomplexation ratio was high. However, in the case of the PG-CD grafted

membrane, the decomplexation ratio was much lower, only one third that of the PNG-CD grafted membrane. The above results demonstrated the promising regeneration capability of our thermo-responsive chiral membranes, which could be proposed for solving the choke-point problem of current enantioselective solid membranes.

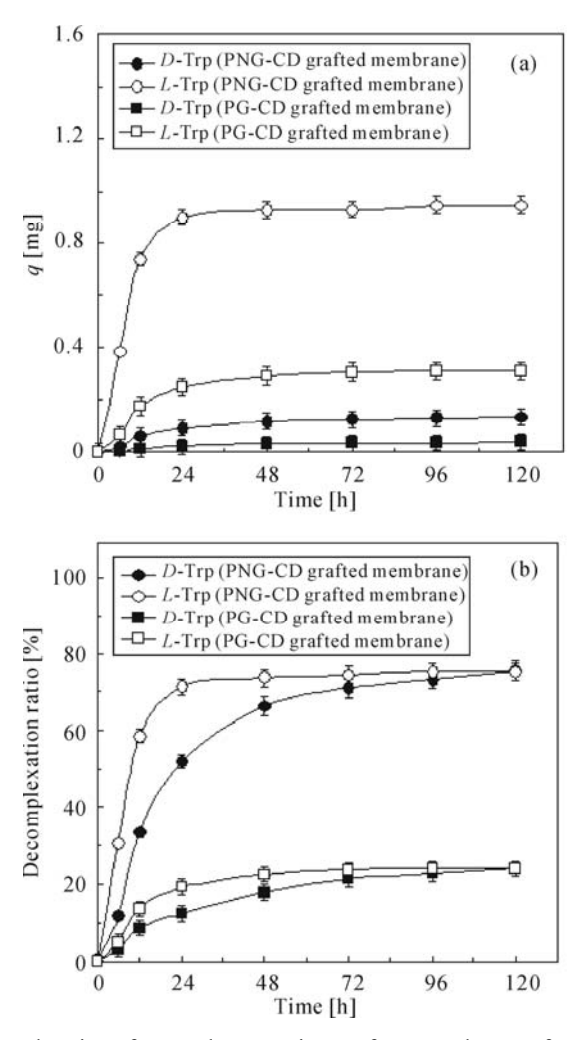


Fig.5.10. Decomplexation of tryptophan enantiomers from membranes after chiral resolution. The grafting yields of PNG-CD grafted Nylon6 membrane are $Y_{\text{PNIPAM}} = 107 \text{ mg} \cdot \text{cm}^{-2}/Y_{\text{CD}} = 23 \text{ mg} \cdot \text{cm}^{-2}$ and that of PG-CD grafted Nylon6 membrane are $Y_{\text{PNIPAM}} = 0 \text{ mg} \cdot \text{cm}^{-2}/Y_{\text{CD}} = 23 \text{ mg} \cdot \text{cm}^{-2}$. The operating temperature for decomplexation is 40 °C. (a) Time-dependent decomplexation of tryptophan enantiomers from membranes; (b) Variation in the decomplexation ratio (Reproduced with permission from Ref. [18]). Copyright (2008), Wiley-VCH Verlag GmbH & Co. KGaA

5.6 Summary

The thermo-responsive chiral membrane could simultaneously exhibit chiral selectivity based on molecular recognition of β -CD and thermo-sensitivity based on phase transition of PNIPAM. A proper grafting yield of the membrane must be designed to get satisfactory selectivity in chiral resolution. The phase transition of grafted polymers responding to temperature change affects the association between β -CD and tryptophan enantiomers. For the thermo-responsive chiral membranes, chiral selectivity in the chiral resolution operating at a temperature below the LCST of PNIPAM was larger than that of membranes with no thermo-sensitivity. In addition, the decomplexation ratio of the tryptophan-loaded PNG-CD grafted membrane at a temperature above the LCST was also much higher than that of membranes with no thermo-sensitivity. It means that by using the PNG-CD grafted thermo-responsive membrane, chiral resolution with a high selectivity and membrane regeneration with a high decomplexation ratio could be achieved by simply changing the operating temperature. To solve the difficult decomplexation problems of solid membranes for chiral resolution, the developed thermo-responsive membrane provides a new efficient way. This new technique shows promising potential in chiral resolution.

References

- [1] Xie R, Chu L Y, Deng J G. Membranes and membrane processes for chiral resolution. *Chemical Society Reviews*, **2008**, *37*: 1243-1263.
- [2] de Jong J J D, Lucas L N, Kellogg R M, van Esch J H, Feringa B L. Reversible optical transcription of supramolecular chirality into molecular chirality. *Science*, **2004**, *304*: 278-281.
- [3] Agranat I, Caner H. Intellectual property and chirality of drugs. *Drug Discovery Today*, **1999**, *4*: 313-321.
- [4] Maier N M, Franco P, Lindner W. Separation of enantiomers: needs, challenges, perspectives. *Journal of Chromatography A*, **2001**, *906*: 3-33.
- [5] Afonso C A M, Crespo J G. Recent advances in chiral resolution through membrane-based approaches. *Angewandte Chemie-International Edition*, **2004**, *43*: 5293-5295.
- [6] Van der Ent E M, Van't Riet K, Keurentjes J T F, Van der Padt A. Design criteria for dense permeation-selective membranes for enantiomer separations. *Journal of Membrane Science*, **2001**, *185*: 207-221.
- [7] Hadik P, Szabo L P, Nagy E. *D,L*-lactic acid and *D,L*-alanine enantioseparation by membrane process. *Desalination*, **2002**, *148*: 193-198.
- [8] Maruyama A, Adachi N, Takatsuki T, Torii M, Sanui K, Ogata N. Enantioselective permeation of α-amino acid isomers through poly(amino acid)-derived membranes. *Macromolecules*, **1990**, *23*: 2748-2752.

- [9] Aoki T, Ohshima M, Shinohara K I, Kaneko T, Oikawa E. Enantioselective permeation of racemates through a solid (+)-poly{2-[dimethyl(10-pinanyl) silyl] norbornadiene} membrane. *Polymer*, **1997**, *38*: 235-238.
- [10] Aoki T, Tomizawa S, Oikawa E. Enantioselective permeation through poly(gamma-[3-(pentamethyldisiloxanyl) propyl]-*L*-glutamate) membranes. *Journal of Membrane Science*, **1995**, *99*: 117-125.
- [11] Kim J H, Kim J H, Jegal J, Lee K H. Optical resolution of alpha-amino acids through enantioselective polymeric membranes based on polysaccharides. *Journal of Membrane Science*, **2003**, *213*: 273-283.
- [12] Randon J, Garnier F, Rocca J L, Maisterrena B. Optimization of the enantiomeric separation of tryptophan analogs by membrane processes. *Journal of Membrane Science*, **2000**, *175*: 111-117.
- [13] Ma J B, Chen L, He B L. The synthesis of crosslinked poly (vinyl alcohol) with L-proline pendant as the chiral stationary phase for resolution of amino acid enantiomers. *Journal of Applied Polymer Science*, **1996**, *61*: 2029-2034.
- [14] Krieg H M, Breytenbach J C, Keizer K. Chiral resolution by β -cyclodextrin polymer-impregnated ceramic membranes. *Journal of Membrane Science*, **2000**, *164*: 177-185.
- [15] Kusumocahyo S P, Sumaru K, Kanamori T, Iwatsubo T, Shinbo T. Synthesis and characterization of an ultrathin polyion complex membrane containing β -cyclodextrin for separation of organic isomers. *Journal of Membrane Science*, **2004**, *230*: 171-177.
- [16] Tone S, Masawaki T, Eguchi K. The optical resolution of amino acids by plasma polymerized terpene membranes. *Journal of Membrane Science*, **1996**, *118*: 31-40.
- [17] Yoshikawa M, Yonetani K. Molecularly imprinted polymeric membranes with oligopeptide tweezers for optical resolution. *Desalination*, **2002**, *149*: 287-292.
- [18] Yang M, Chu L Y, Wang H D, Xie R, Song H, Niu C H. A novel thermo-responsive membrane for chiral resolution. *Advanced Functional Materials*, **2008**, *18*: 652-663.
- [19] Krieg H M, Lotter J, Keizer K, Breytenbach J C. Enrichment of chlorthalidone enantiomers by an aqueous bulk liquid membrane containing β-cyclodextrin. *Journal of Membrane Science*, **2000**, *167*: 33-45.
- [20] Nozaki T, Maeda Y, Ito K, Kitano H. Cyclodextrins modified with polymer chains which are responsive to external stimuli. *Macromolecules*, **1995**, *28*: 522-524.
- [21] Nozaki T, Maeda Y, Kitano H. Cyclodextrin gels which have a temperature responsiveness. *Journal of Polymer Science Part A-Polymer Chemistry*, **1997**, *35*: 1535-1541.
- [22] Yanagioka M, Kurita H, Yamaguchi T, Nakao S. Development of a molecular recognition separation membrane using cyclodextrin complexation controlled by thermosensitive polymer chains. *Industrial & Engineering Chemistry Research*, **2003**, *42*: 380-385.
- [23] Ohashi H, Hiraoka Y, Yamaguchi T. An autonomous phase transition-

- complexation/decomplexation polymer system with a molecular recognition property. *Macromolecules*, **2006**, *39*: 2614-2620.
- [24] Wang H D, Chu L Y, Yu X Q, Xie R, Yang M, Xu D, Zhang J, Hu L. Thermosensitive affinity behavior of poly(N-isopropylacrylamide) hydrogels with β -cyclodextrin moieties. *Industrial & Engineering Chemistry Research*, **2007**, *46*: 1511-1518.
- [25] Petter R C, Salek J S, Sikorski C T, Kumaravel G, Lin F T. Cooperative binding by aggregated mono-6-(alkylamino)-β-cyclodextrins. *Journal of the American Chemical Society*, **1990**, *112*: 3860-3868.
- [26] Liu Y Y, Fan X D, Gao L. Synthesis and characterization of β -cyclodextrin based functional monomers and its copolymers with *N*-isopropylacrylamide. *Macromolecular Bioscience*, **2003**, *3*: 715-719.
- [27] Virtanen J, Baron C, Tenhu H. Grafting of poly(*N*-isopropylacrylamide) with poly(ethylene oxide) under various reaction conditions. *Macromolecules*, **2000**, *33*: 336-341.
- [28] Extrand C W, Kumagai Y. An experimental study of contact angle hysteresis. *Journal of Colloid and Interface Science*, **1997**, *191*: 378-383.
- [29] Henn A R. The surface tension of water calculated from a random network model. *Biophysical Chemistry*, **2003**, *105*: 533-543.
- [30] Chu L Y, Niitsuma T, Yamaguchi T, Nakao S. Thermo-responsive transport through porous membranes with grafted PNIPAM gates. *AIChE Journal*, **2003**, *49*: 896-909.
- [31] Tabushi I, Kuroda Y, Mizutani T. Artificial receptors for amino acids in water. Local environmental effect on polar recognition by 6A-amino-6B-carboxy-and 6B-amino-6A-carboxy-beta-cyclodextrins. *Journal of the American Chemical Society*, **1986**, *108*: 4514-4518.
- [32] Liu Y, Han B H, Li B, Zhang Y M, Zhao P, Chen Y T, Wada T, Inoue Y. Molecular recognition study on a supramolecular system. 14. synthesis of modified cyclodextrins and their inclusion complexation thermodynamics with *L*-tryptophan and some naphthalene derivatives. *Journal of Organic Chemistry*, **1998**, *63*: 1444-1454.

Thermo-Responsive Membranes for Affinity Separation

In this chapter, the design, fabrication and performance of thermo-responsive adsorption/desorption membranes for affinity separation are introduced. Firstly, the design of fabrication of thermo-responsive affinity membranes with nanostructured pores and grafted PNIPAM surface layer for hydrophobic adsorption are described. The membrane shows efficient "adsorbing at a temperature above the LCST-desorbing at a temperature below the LCST" performance for bovine serum albumin molecules. Then a temperature-dependent molecular-recognizable membrane with both grafted PNIPAM chains and immobilized β -CD moieties for affinity separation is introduced. Contrariwise to the first kind of membrane, this membrane demonstrates effective "adsorbing at a temperature below the LCST-desorbing at a temperature above the LCST" performance for guest molecules.

6.1 Introduction

As mentioned in Section 1.3.1, poly(N-isopropylacrylamide) (PNIPAM) is a popular thermo-responsive polymer. It shows a distinct and reversible phase transition at the lower critical solution temperature (LCST) around 32 °C. When the environmental temperature is lower than the LCST, the PNIPAM can bind plenty of water molecules on its amide groups through hydrogen-bonding interaction, and thus it is in a swollen and hydrophilic state; however, when the temperature is higher than the LCST, the PNIPAM is dehydrated because of the cleavage of the hydrogen-bonding, and thus it is in a shrunken and hydrophobic state. Furthermore, it has been reported that the phase transition of PNIPAM responding to temperature change could affect the association constant between β -CD and guest molecules in a PNIPAM-modified β -CD system (Chapter 5). Such

dramatic phase transition characteristics make PNIPAM extremely attractive for developing thermo-responsive smart membranes for affinity separation. In this chapter, two kinds of PNIPAM-based thermo-responsive membranes for affinity separation, which are thermo-responsive membranes with nano-structured pores and grafted PNIPAM surface layer for hydrophobic adsorption, [2] and thermo-responsive molecular-recognizable membranes for affinity separation, [3] will be introduced.

6.2 Thermo-Responsive Affinity Membrane with Nano-Structured Pores and Grafted PNIPAM Surface Layer for Hydrophobic Adsorption

Affinity membranes are membranes that can identify and separate specific molecules. In the fields of separation and purification of protein, enzyme, chiral substance, hydrophobic solutes and so on, affinity membranes have been widely studied. [4-7] It has been reported that thermo-responsive affinity membranes with PNIPAM functional surface layers can be used for hydrophobic adsorption and separation of hydrophobic solutes, [8] because the surfaces of PNIPAM-grafted membranes can change from a hydrophobic to hydrophobic state when the environmental temperature increases across the LCST of PNIPAM and *vice versa*.

It has been verified that the micro- and nano-structures on the surfaces of some natural plants such as lotus leaves contribute significantly to their surface superhydrophobicity. [9] Inspired by such natural phenomena, micro- and nano-structures have been applied to achieve artificial superhydrophobic surfaces. [9] For PNIPAM-modified functional surfaces, it has been found that micro- and/or nano-structured surfaces could enhance the thermo-responsive wettability change between hydrophobicity and hydrophilicity, [10-13] i.e., microand/or nano-structured surface architectures could make the PNIPAM-modified surfaces more hydrophilic at temperatures below the LCST but more hydrophobic above the LCST. For example, surface-initiated atom-transfer radical polymerization was used to fabricate thermo-responsive PNIPAM thin film on both flat and nano-structured silicon substrates, and the results showed that the water contact angle of the flat surface increased from 63° to 93° when the temperature changed from 25 °C to 40 °C, while the water contact angle value of the nano-structured surface was about 0° below 29 °C and about 150° above 40 °C. [10] Such results show a promising approach for improving the hydrophobic adsorption performance of PNIPAM-grafted thermo-responsive membranes. It means that if we introduce nano-structures onto the membrane surfaces and membrane pore surfaces before grafting the PNIPAM surface layer, the reversible hydrophobic-adsorption/ hydrophilic-desorption performance could be improved

by the enhanced switching of thermo-responsive hydrophilic/hydrophobic surface wettability and the nano- structured surface architectures.

Recently, the author's group developed a thermo-responsive affinity membrane with nano-structured pores and grafted a PNIPAM surface layer for hydrophobic adsorption. [2]

6.2.1 Design of Thermo-Responsive Affinity Membrane with Nano-Structured Pores and Grafted PNIPAM Surface Layer

The schematic illustration of the preparation and thermo-responsive surface property change of the thermo-responsive affinity membrane with nano-structured pores and grafted PNIPAM surface layer is shown in Fig.6.1. [2] Shirasu porous glass (SPG) membranes are used as the substrate membranes, SiO₂ nano-particles are deposited onto the SPG membranes to construct the nano-structured surfaces of membrane pores, and then PNIPAM brushes are grafted onto the nanostructured membrane pores. SPG membranes are obtained by phase separation of a primary CaO-Al₂O₃-B₂O₃-SiO₂ type glass, made of Shirasu (volcanic ash from the southern part of Kyushu Island, Japan), calcium carbonate and boric acid. [14] SPG membranes are a special kind of porous inorganic glass membrane, so SiO₂ nano-particles can be deposited on hydroxylated SPG membrane surfaces by chemical deposition. When the nano-particles are deposited on the SPG membranes, the smooth membrane surfaces turn to nano-structured concavoconvex rough surfaces. The proposed nano-structured membrane surface could bring three main advantages to the thermo-responsive hydrophobic-adsorption/ hydrophilic-desorption performance of Bovine serum albumin (BSA) molecules by using PNIPAM-grafted membranes. Firstly, the nano-structured membrane surface can enhance the surface hydrophilicity of the PNIPAM-grafted membrane at a temperature below the LCST by the capillary effect from the nano-concavespaces between adjacent SiO2 nano-particles as nano-capillaries. Secondly, the nano-structured membrane surface can provide more adsorption surface because of the increase in the total specific surface area. Thirdly, the nano-structured concavo-convex surface can provide a BSA molecule with two or three stereo sites for its adsorption on the membrane surface by hydrophobic interaction, which enhances the thermo-responsive hydrophobic-adsorption performance of PNIPAMgrafted membranes.

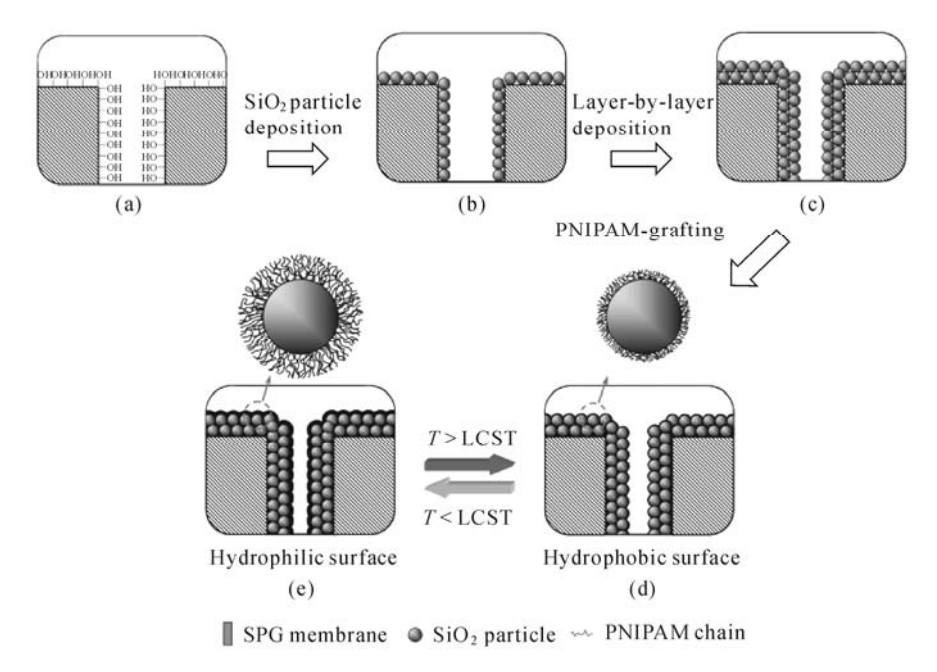


Fig.6.1. Schematic illustration of preparation of the thermo-responsive affinity membrane with nano-structured pores and grafted PNIPAM surface layer for hydrophobic adsorption. (a) Hydroxylated substrate SPG membrane; (b) Nano-structured SPG membrane by depositing SiO₂ particles once; (c) Nano-structured SPG membrane by depositing SiO₂ particles twice; (d) PNIPAM-grafted nano-structured SPG membrane with hydrophobic surface at temperature above the LCST; (e) PNIPAM-grafted nano-structured SPG membrane with hydrophilic surface at temperature below the LCST (Reproduced with permission from Ref. [2]). Copyright (2010), Elsevier

6.2.2 Preparation and Characterization of Thermo-Responsive Membrane with Nano-Structured Pores and Grafted PNIPAM Surface Layer

In this section, the preparation and characterization of thermo-responsive membrane with nano-structured pores and grafted PNIPAM surface layer will be introduced.

6.2.2.1 Preparation of PNIPAM-Grafted Nano-Structured SPG Membranes

The designed PNIPAM-grafted nano-structured SPG membranes were fabricated in a three-step process.^[2] In the first step, hydroxyl groups were generated on the pore surfaces of SPG membranes by treating the SPG substrate membranes with a slightly boiled piranha solution at 90 °C for 90 min (**Fig.6.1a**). In order to fill the

piranha solution in the membrane pores, the SPG membranes were immersed into piranha solution with ultrasonic treatment. The piranha solution was a mixture of 98 wt% H_2SO_4 and 30 vol% H_2O_2 (v:v = 7:3). The treated membranes were rinsed with abundant water and the water was blown away with nitrogen gas, then the membranes were dried in a vacuum oven at 50 °C for 12 h.

In the second step, the SPG membranes with nano-structured pores were fabricated by depositing SiO₂ nano-particles onto the membrane pore surface (Fig.6.1b). In order to fill the nano-particle solution in the membrane pores, the SPG membranes were immersed in SiO₂ nano-particle solution with ultrasonic treatment. The SiO₂ nano-particle solution was prepared by the above-mentioned Stober method. [16] The recipe and procedure for preparing the SiO₂ nano-particle solution were briefly as follows: 3.5 ml of deionized water, 46.5 ml of ethanol and 1 ml of ammonia (25 wt%) were mixed well first, and afterwards 3 ml of tetraethyl *ortho*silicate (TEOS, Si(OC₂H₅)₄, SiO₂ content \geq 28%) was added with agitation. Then the reaction mixture was stirred at 25 °C for 48 h. After ultrasonic treatment, the SPG substrate membranes were removed from the SiO₂ nano-particle solution and calcined in an oven at 210 °C for 2 h, then rinsed with an abundant amount of water and the water was blown away with nitrogen gas, and finally the membranes were dried in a vacuum oven at 50 °C for 12 h. As a result, SiO₂ nano-particles were deposited onto the pore surfaces of the SPG membranes. Nano-structured SPG membranes with uniform and compact SiO₂ nano-particles deposited on the pore surfaces could be obtained by repeating the nano-particle deposition process (Fig.6.1c). [15] The nano-particle deposition process was operated three times.

In the third step, plasma-graft pore-filling polymerization was employed to graft the linear PNIPAM chains onto nano-structured SPG membrane pores according to the method described in Chapter 2. Briefly, the nano-structured SPG membrane was placed in a transparent glass tube, which was filled with argon gas, evacuated to a pressure of 10 Pa beforehand and then treated by plasma at 50 W for 60 s. After that, the membrane was dunked into the monomer solution and the grafting polymerization took place in a shaking constant-temperature bath at 40 °C for a predetermined time. The feed weight ratio of NIPAM and deionized water was 1:100, and the polymerization time was 6 h to obtain membranes with a thin PNIPAM film. The grafted membrane was rinsed in well-deionized water under vibration in a constant-temperature bath (30 °C) for 24 h to remove any unreacted monomer and homopolymer and then was dried in a vacuum oven at 50 °C overnight. The PNIPAM-grafted nano-structured SPG membrane could then exhibit a thermo-responsive surface property (Figs. 6.1d and 6.1e). The grafting yield (Y_{PNIPAM}) of PNIPAM onto the membrane, which is defined as the weight increase percentage of the membrane after grafting, was measured by weighing the ungrafted and grafted membranes.

6.2.2.2 Characterization of Membranes

The microscopic configurations of the substrate and PNIPAM-grafted nano-structured SPG membranes were investigated by SEM (JSM-5900LV, JEOL, Japan). To observe the inner surfaces of membranes, the substrate and PNIPAM-grafted nano-structured SPG membranes were fractured mechanically before sticking to the sample holder. The mean pore sizes and the total pore surface area of the membranes before and after modification were measured by the mercury intrusion method (AutoPore IV 9500, Micromeritics Instrument, USA). XPS (XSAM800, KRATOS, UK) was employed to study the chemical composition of the membrane surfaces before and after grafting PNIPAM.

At temperatures below and above the LCST of PNIPAM respectively, the surface wettability of the prepared thermo-responsive affinity membrane with nano-structured pores and grafted PNIPAM surface layer was investigated by measuring the water contact angle on the membrane surface with a contact angle instrument (DSA100, Krüss, Germany). Before the test, the examined membrane was pre-wetted without any obvious water on the surface and then fixed on the sample holder, which was heated up to a predetermined temperature. After the temperature of the membrane equilibrated at the predetermined temperature, a small drop of water (3 μ l) was dripped onto the surface of the membrane. Simultaneously, the whole process was recorded by high-speed video camera. The contact angle value of the examined membrane in the paper was the arithmetic average value of five repetitive tests on the same membrane. The temperatures were selected as 20 °C and 40 °C respectively, which were lower and higher than the LCST of PNIPAM (around 32 °C).

Fig.6.2 shows SEM images of inner surfaces of the substrate and PNIPAM-grafted nano-structured SPG membranes. [2] For the substrate SPG membrane, (**Figs.6.2a** and **6.2b**), the pore surface is relatively smooth. On the other hand, for the PNIPAM-grafted nano-structured SPG membrane, (**Figs.6.2c** and **6.2d**), SiO_2 nano-particles with an average diameter of 125 nm are obviously observed on the membrane pore surfaces. For the modification of SPG membranes with a pore size of 1.8 μm, it is improper to deposit the SiO_2 nano-particles too many times, because too many nano-particles might cause clogging of the membrane pores. So the nano-particle deposition is operated three times, which is optimized from certain primary experimental results. It is clearly seen that the pores of the PNIPAM-grafted nano-structured SPG membrane are not clogged by the deposited SiO_2 nano-particles and grafted PNIPAM polymers, and the stereo-structures of membrane pores are almost unchanged after depositing the SiO_2 nano-particles are found to be uniformly and compactly covered on the membrane pore surface.

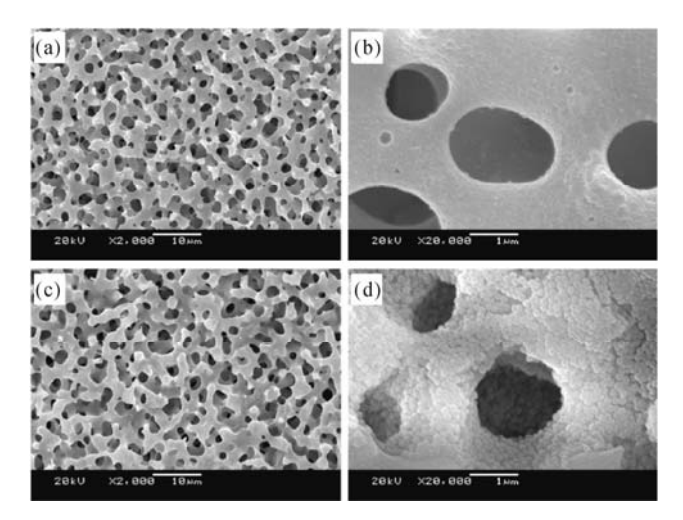


Fig.6.2. SEM images of inner surfaces of substrate SPG membrane (a, b) and PNIPAM-grafted nano-structured SPG membrane ($Y_{\text{PNIPAM}} = 0.1 \text{ wt}\%$) (c, d). The mean pore size of substrate SPG membrane is 1.8 µm. The average diameter of SiO₂ nano-particles is 125 nm (Reproduced with permission from Ref. [2]). Copyright (2010), Elsevier

The mercury intrusion measurement results show that the calculated mean pore size of the substrate SPG membrane and that of the PNIPAM-grafted nano-structured SPG membrane are 1.57 µm and 1.56 µm respectively, and the specific surface areas are 5.668 m²·g⁻¹ and 6.814 m²·g⁻¹, respectively.^[2] It is verified again that the mean pore size of the substrate SPG membrane and that of the PNIPAM-grafted nano-structured SPG membrane is almost the same. On the other hand, the total surface area of the PNIPAM-grafted nano-structured SPG membrane increases by 36% compared with that of the substrate SPG membrane, which indicates that the nano-structured SPG membrane could provide more adsorption surface area for the hydrophobic adsorption than the substrate membrane.

The XPS spectra of nano-structured SPG membranes before and after grafting PNIPAM ($Y_{\text{PNIPAM}} = 0.1 \text{ wt\%}$) are shown in Fig.6.3. [2] For the C1s spectra of the ungrafted nano-structured SPG membrane (Fig.6.3a), there is only one peak with binding energy of 284.715 eV (C atom in C–H bond). On the other hand, for the C1s spectra of the PNIPAM-grafted nano-structured SPG membrane (Fig.6.3b), two new peaks appear with binding energies of 286.860 eV (C atom in C–N bond) and 288.370 eV (C atom in C=O bond), respectively. Similarly, there is only one peak in the O1s spectra of the ungrafted nano-structured SPG membrane (Fig.6.3c) with binding energy of 532.619 eV (O atom in Si–O bond), while a new peak with binding energy of 531.538 eV (O atom in C=O bond) appears in O1s spectra of the PNIPAM-grafted nano-structured SPG membrane (Fig.6.3d). For the N1s spectra, no peak appears for the ungrafted membrane (Fig.6.3e) while a new peak appears with a binding energy of 399.626 eV (N atom in C–N bond) for the PNIPAM-grafted nano-structured SPG membrane (Fig.6.3f). Compared with those of the ungrafted membrane, the components of the C and N elements of the

PNIPAM-grafted membrane increase from 11.79% to 58.49% and from 0.00% to 6.29% respectively, while the component of the O element decreases from 47.08% to 20.43%. From the above data, it is verified that PNIPAM has been successfully grafted onto the nano-structured SPG membrane surface.

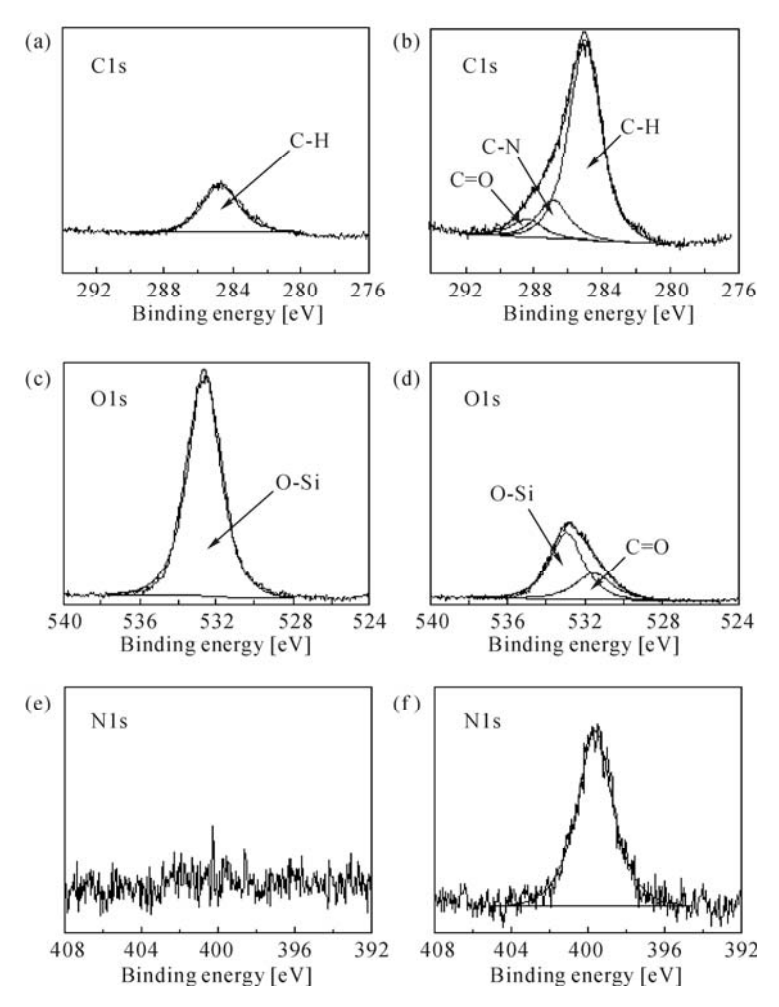


Fig.6.3. XPS spectra of ungrafted nano-structured SPG membrane (a, c, e) and PNIPAM-grafted nano-structured SPG membrane with $Y_{PNIPAM} = 0.1$ wt% (b, d, f) (Reproduced with permission from Ref. [2]). Copyright (2010), Elsevier

Fig.6.4 shows the snapshots of dynamic contacting processes of water droplets onto the surfaces of substrate SPG membrane at 20 °C, nano-structured SPG membrane at 20 °C and PNIPAM-grafted nano-structured SPG membranes at 20 and 40 °C, respectively.^[2] All the water contact angles of the substrate SPG membrane, ungrafted nano-structured SPG membrane and PNIPAM-grafted nano-structured membrane at 20 °C become 0° finally, although the time periods for the water droplet spreading

and/or disappearing processes are different. Because the substrate SPG membrane, ungrafted nano-structured SPG membrane and PNIPAM-grafted nano-structured membrane at 20 °C are hydrophilic and porous, the water droplets spread fast on the membrane surfaces and finally are wicked into the membrane pores. Compared with the substrate SPG membrane (**Fig.6.4a**), the nano-structured architecture of the nano-structured SPG membrane (**Fig.6.4b**) promotes the water droplet spreading and disappearing process. The water contact angle of the substrate SPG membrane becomes 0° at 2 s, while that of the nano-structured SPG membrane becomes 0° in a time period as short as 24 ms. For the PNIPAM-grafted nano-structured membrane at 20 °C (**Fig.6.4c**), although the nano-particle effect is still working, the grafted PNIPAM chains are swollen in the membrane pores; as a result the time period for the water droplet being totally wicked into the membrane pores is relatively longer (being 8 s). However, for the PNIPAM-grafted nano-structured membrane at 40 °C (**Fig.6.4d**), although the membrane is also porous, the water contact angle on the membrane surface does not change with time and constantly keeps to 130°.

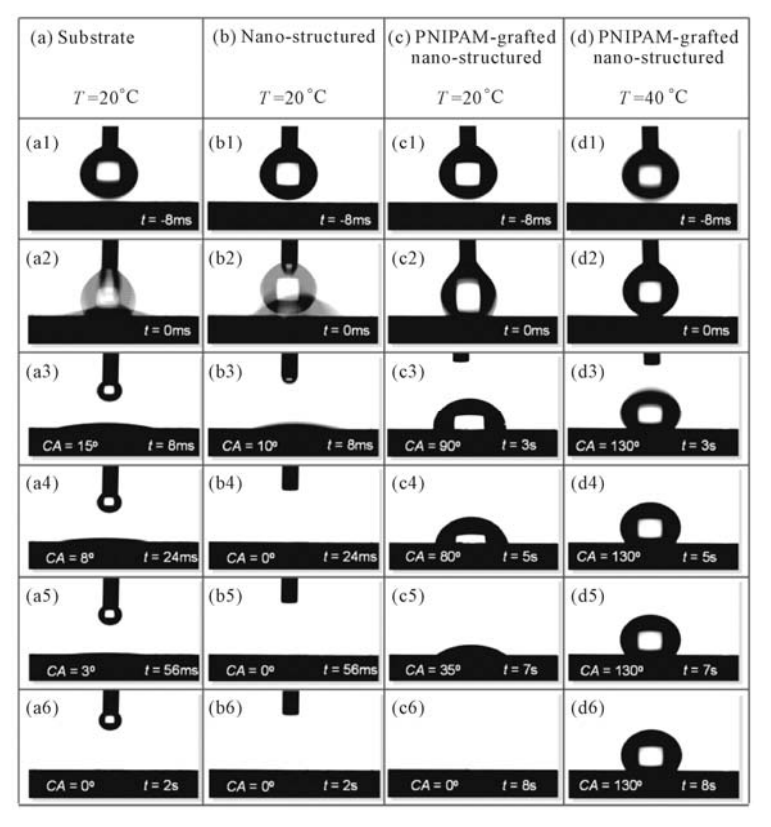


Fig.6.4. Snapshots of dynamic contacting processes of water droplets (3 μl each) onto different membrane surfaces. (a) Substrate SPG membrane; (b) Nano-structured SPG membrane; (c, d) PNIPAM-grafted nano-structured SPG membranes at 20 °C and 40 °C, respectively. "*CA*" means contact angle (Reproduced with permission from Ref. [2]). Copyright (2010), Elsevier

Under steady states, for the surface of the PNIPAM-grafted nano-structured SPG membrane, the water contact angles are about 0° at 20 °C (below the LCST) and about 130° at 40 °C (above the LCST). It is well known that thermo-responsive PNIPAM polymer chains are in a swollen and hydrophilic state at temperatures lower than the LCST, while they become shrunken and hydrophobic at temperatures higher than the LCST. It has been reported that nano-structures on the hydrophilic surface will enhance the surface hydrophilicity by the capillary effect from nano-capillaries. On the surface of the as-prepared PNIPAM-grafted nano-structured SPG membrane, the nano-concave-spaces between adjacent SiO₂ nanoparticles might act as nano-capillaries. Therefore, the prepared PNIPAM-grafted nano-structured SPG membrane exhibits very hydrophilic surface wettability (contact angle = 0°) at 20 °C. On the other hand, at 40 °C the nano-structures will enhance the hydrophobicity of the membrane surfaces because of the existence of nanoparticles on the surfaces^[9] and the water contact angle is as high as 130°.

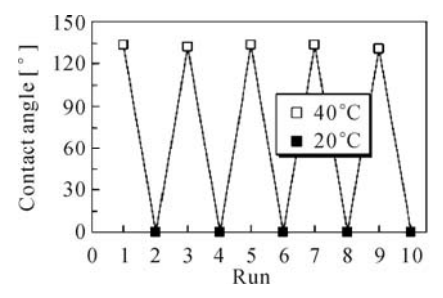


Fig.6.5. Reversibly temperature-responsive change of water contact angle data of PNIPAM-grafted nano-structured SPG membrane surfaces. The water contact angle data are the average values of both the inside and outside surfaces of the membrane. The volume of the water droplet for measuring the contact angle is 3 μ l (Reproduced with permission from Ref. [2]). Copyright (2010), Elsevier

The thermo-responsive surface wettability change of the PNIPAM-grafted nano-structured SPG membrane is highly reversible and repeatable. **Fig.6.5** shows the thermo-responsive water contact angle changes of the PNIPAM-grafted nano-structured SPG membrane surface by repeatedly changing the temperature between 20 and 40 °C. Within 10 runs, the average water contact angle on the membrane surface at 20 °C is always about 0° and that at 40 °C is always about 130°. That is to say, the as-prepared PNIPAM-grafted nano-structured SPG membrane can be used repeatedly.

6.2.3 Thermo-Responsive Adsorption/Desorption Characteristics

The thermo-responsive hydrophobic adsorption performance of the PNIPAM-grafted nano-structured SPG membrane was studied by carrying out dynamic adsorption experiments using BSA as solute. [19,20] In the adsorption experiments,

the environmental temperatures were changed across the LCST of PNIPAM (20 °C and 40 °C respectively). The adsorption experiment started immediately after immersing the examined membrane into 15 ml of BSA aqueous solution (BSA concentration 1.0 mg·ml⁻¹), which was constantly at 40 °C (above the LCST) and well stirred. At fixed time intervals, a small amount of solution was taken out and its absorbance was analyzed by UV-visible spectrophotometer at a wavelength of 280 nm. After the membrane reached the adsorption equilibrium at 40 °C, the temperature of the BSA solution was promptly changed to 20 °C (below the LCST). After the membrane reached the adsorption equilibrium at 20 °C, the temperature changed again for another thermo-responsive adsorption run. From the adsorption of BSA on the membrane with the environmental temperature changing from 40 °C \rightarrow 20 °C \rightarrow 40 °C \rightarrow 20 °C, the thermo-responsive hydrophobic adsorption performance of the prepared membrane could be obtained.

The thermo-responsive hydrophobic-adsorption/hydrophilic-desorption performance of PNIPAM-grafted nano-structured SPG membranes is studied by investigating the dynamic adsorption behavior of BSA on the membrane, with temperatures changing across the LCST. The amount of BSA adsorbed on the membrane surface (Q_m , mg·m⁻²) is calculated by the following equation:

$$Q_m = \frac{(C_0 - C_t) \cdot V}{A_m} \tag{6.1}$$

where C_0 is the initial concentration of BSA aqueous solution at the beginning of the dynamic adsorption experiment $(t = 0) \text{ [mg·ml}^{-1}]$, C_t is the BSA concentration in solution at different time intervals $(t = t) \text{ [mg·ml}^{-1}]$, V is the volume of BSA solution [ml] and A_m is the membrane surface area [m²]. Both C_0 and C_t could be measured by UV-visible spectrophotometer and the membrane surface area is measured by the mercury intrusion method.

The experimental results of temperature-dependent dynamic adsorption and desorption of model protein BSA on the substrate SPG membrane, the nano-structured SPG membrane and the PNIPAM-grafted nano-structured SPG membrane $(Y_{\text{PNIPAM}} = 0.1\%)$, are shown in **Fig.6.6**. The substrate SPG membrane almost does not adsorb BSA molecules, whether the environmental temperature is 20 °C or 40 °C. Because the BSA molecules are macromolecules with a molecular weight of 68 kDa and a molecular dimension of 4×4×14 nm, [21] the smooth pore surface of the SPG substrate membrane has difficulty trapping the protein macromolecule (Fig.6.7a). As for the ungrafted nano-structured membrane, the Q_m value increases to about 0.5 mg·m⁻² within 3 h at the beginning and then stays the same no matter how much the environmental temperature changes. Compared with the substrate SPG membrane, BSA molecules are easier to be adsorbed on the nano-structured SPG membrane, because the nano-structured concavo-convex surface can provide a BSA molecule with two or three stereo sites for its adsorption on the membrane surface and also can provide a larger total specific surface area for adsorption (Fig.6.7b). [2] However, it is obvious from Fig.6.6 that there is no thermo-response for the adsorption of BSA on the ungrafted nanostructured SPG membrane.

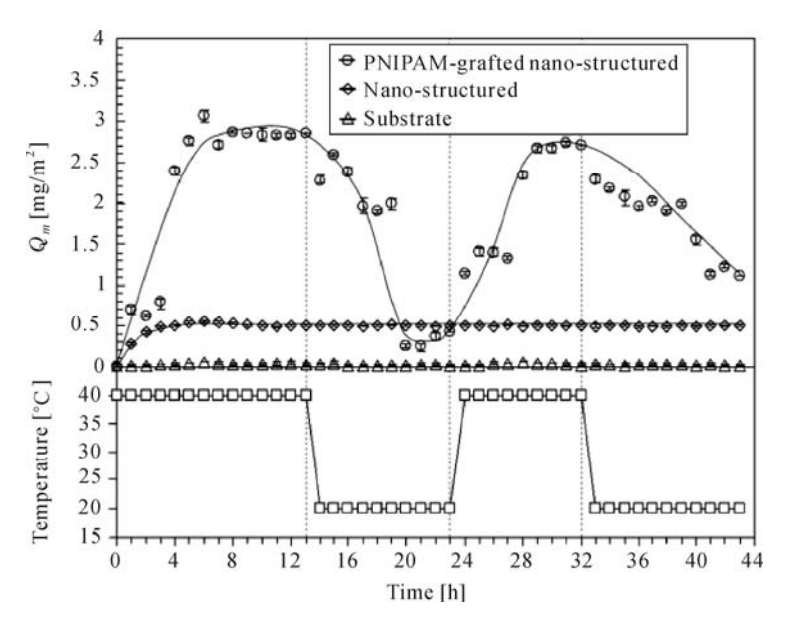


Fig.6.6. Temperature-dependent dynamic adsorption and desorption of BSA on the substrate SPG membrane, the nano-structured SPG membrane and the PNIPAM-grafted nano-structured SPG membrane (Reproduced with permission from Ref. [2]). Copyright (2010), Elsevier

For the PNIPAM-grafted nano-structured SPG membrane, the equilibrium $Q_{\rm m}$ value at 40 °C is about 2.95 mg·m⁻², which is much larger than that of the ungrafted nano-structured SPG membrane (0.5 mg·m⁻²). It is attributed to the hydrophobic PNIPAM-grafted surface of the PNIPAM-grafted nano-structured SPG membrane at a temperature higher than the LCST, because BSA adsorption mainly results from the hydrophobic interaction. More importantly, the PNIPAM-grafted nanostructured SPG membrane exhibits excellent thermo-responsive hydrophobicadsorption/hydrophilic-desorption characteristics toward BSA. At 40 °C, the $Q_{\rm m}$ value of the PNIPAM-grafted nano-structured SPG membrane increases sharply to about 2.95 mg·m⁻² within the first 6 h, and stays almost the same over the next 7 h. With a decrease in the environmental temperature to 20 °C, the $Q_{\rm m}$ value goes down rapidly to about 0.25 mg·m⁻² within 6 h, and then stays almost the same over the next 4 h. When the environmental temperature is heated back to 40 °C, the $Q_{\rm m}$ value goes up to about 2.95 mg·m⁻² again. When the temperature is decreased to 20 °C once more, the $Q_{\rm m}$ value also decreases again. The desorption performance of BSA molecules becomes a little worse in the second run, mainly because the membrane has been fouled by BSA molecules in the first run. Not all the BSA molecules adsorbed on the membrane in the first run can desorb in the next run.

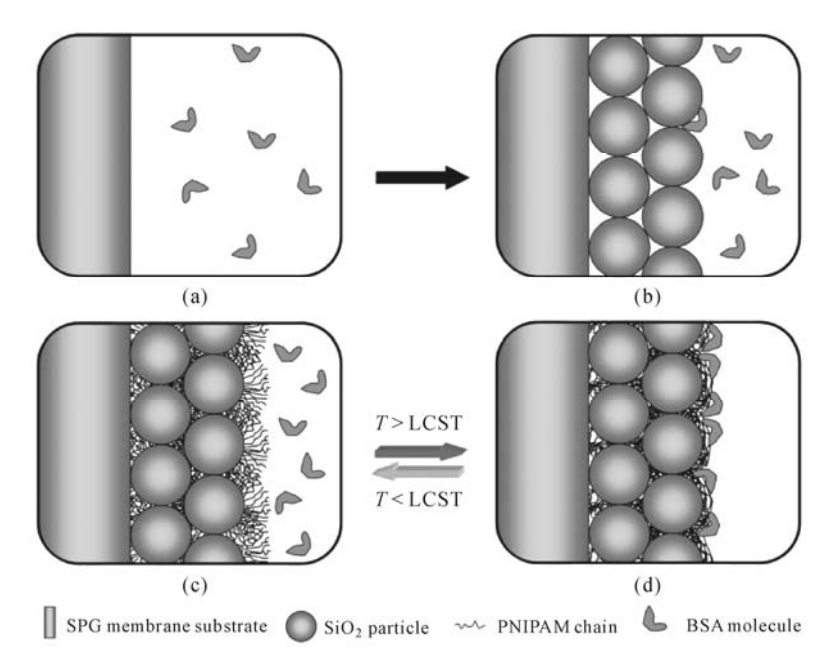


Fig.6.7. Schematic illustration of the adsorption of BSA molecules onto membranes with different surfaces. (a) Substrate SPG membrane; (b) Nano-structured SPG membrane; (c) PNIPAM-grafted nano-structured SPG membrane at temperature below the LCST; (d) PNIPAM-grafted nano-structured SPG membrane at temperature above the LCST (Reproduced with permission from Ref. [2]). Copyright (2010), Elsevier

It takes time for the adsorption and desorption to reach equilibrium, which is due to the following two main reasons. On the one hand, BSA molecules are macromolecules with a molecular weight of 68 kDa and a molecular dimension of 4×4×14 nm. [21] Such a large dimension prevents the BSA molecules from moving/adsorbing/desorbing fast. It has been reported that the time it takes to reach the adsorption/desorption equilibrium of BSA molecules on nonporous materials is usually in the range of 1 to 10 h, and the maximum is 16 h. [22,23] On the other hand, the SPG membrane is a kind of homogeneous porous membrane, i.e. the pores are of almost the same dimensions and are interconnected throughout the whole membrane thickness.^[24] The nano-structured and PNIPAM-grafted surface layer has been introduced on the pore surfaces throughout the whole thickness of the SPG membrane. That means the adsorption sites for BSA molecules are distributed throughout the whole thickness of the membrane. It takes time for the BSA molecules with large dimensions to diffuse through the zigzag pores and adsorb to and/or desorb from those adsorption sites that are far away from the membrane surface.

In a word, the as-prepared PNIPAM-grafted nano-structured SPG membrane exhibits satisfactory "adsorption at a temperature above the LCST – desorption at a temperature below the LCST" performance for BSA molecules, which is a simple and efficient mode for the adsorption/desorption of hydrophobic solutes. At

a temperature higher than the LCST (40 °C in this study), the grafted PNIPAM polymer chains on the nano-structured SPG membrane are in a shrunken and hydrophobic state; as a result, the BSA molecules with hydrophobic groups are easily adsorbed on the membrane pore surface by the hydrophobic interaction (Fig.6.7d). ^[2] On the other hand, at a temperature lower than the LCST (20 °C in this study), the grafted PNIPAM polymer chains on the nano-structured SPG membrane become swollen and are in a hydrophilic state, and the nano-structured membrane pore surfaces could enhance the surface hydrophilicity as mentioned above. Therefore, the adsorbed BSA molecules on the membrane surface desorb from the very hydrophilic membrane pore surface due to the absence of hydrophobic sites on the membrane surface (Fig.6.7c). ^[2]

For the PNIPAM-grafted nano-structured SPG membrane with a grafting yield of $Y_{\text{PNIPAM}} = 0.1\%$, the difference between the maximum Q_m value at 40 °C and the minimum Q_m value at 20 °C is about 2.7 mg·m⁻². That means more than 90% of BSA proteins adsorbed on the as-prepared membrane at 40 °C can be desorbed just by cooling the environmental temperature down to 20 °C, which means a convenient and efficient approach for the adsorption/desorption of BSA proteins.

6.3 Temperature-Dependent Molecular-Recognizable Membranes for Affinity Separation

For those thermo-responsive and molecular-recognizable gating membranes prepared with grafted PNIPAM chains and immobilized β -cyclodextrin (β -CD), it has been reported that the binding constants of β -CDs with guest molecules are influenced dramatically by grafted PNIPAM chains with changing environmental temperature across the LCST. [25] Recently, a novel temperature-dependent molecular-recognizable membrane, P(NIPAM-co-GMA/CD)-g-PET, was developed in the author's group by a combination of plasma-induced pore-filling grafting polymerization and chemical reaction. [3] During the dynamic adsorption experiments, the guest molecules, 8-anilino-1-naphthalenesulfonic acid ammonium salt (ANS) molecules, are adsorbed onto the P(NIPAM-co-GMA/CD)-g-PET membrane at a lower temperature (i.e., 25 °C) and desorbed from the P(NIPAM-co-GMA/CD)-g-PET membrane at a higher temperature (i.e., 40 °C) with good repeatability. [3]

6.3.1 Design and Preparation of Thermo-Responsive Molecular-Recognizable Membranes for Affinity Separation

The thermo-responsive molecular-recognizable membrane for affinity separation is designed on the basis of cooperation between PNIPAM and β -CD. The preparation route of the membranes is described briefly as follows.^[3] Firstly, a

primary amino group is introduced into one of seven primary hydroxyl groups of β -CD in two steps, according to the method described in Chapter 5. Next, two monomers, NIPAM and glycidyl methacrylate (GMA containing both a vinyl group and an epoxy group), are simultaneously grafted on the porous substrate membranes by plasma-induced pore-filling grafting polymerization. Polyethylene terephthalate (PET) track-etched membranes with average pore size of 200 nm, thickness of 10 μ m and porosity of 9.42%, are chosen as porous substrates because of their straight trans-membrane pores with narrow size distribution. Finally, the primary-amino-containing β -CDs react with the P(NIPAM-co-GMA) polymer grafted on the membranes though epoxy groups.

The temperature-dependent molecular-recognizable P(NIPAM-co-GMA/CD)g-PET membranes are fabricated in two steps as schematically illustrated in Fig.6.8.^[3] In the first step (left side in Fig.6.8), two monomers, NIPAM and GMA, are simultaneously grafted on the PET membranes via plasma-induced pore-filling grafting polymerization as described in Section 2.2.1.1. The concentrations of NIPAM and GMA in comonomer solution are 3 wt% and 2.25 vol%, respectively. The treatment time, power, polymerization temperature and polymerization time are 90 s, 15 W, 60 °C and $8 \sim 48$ h, respectively. In order to remove unreacted monomer and homopolymer, the resultant grafted P(NIPAM- co-GMA)-g-PET membrane is rinsed with well deionized water for 24 h under vibration at 30 °C. The washed membrane is dried in an oven at 50 °C overnight. With the same method and conditions as that in the preparation of P(NIPAM- co-GMA)-g-PET membranes, PGMA-g-PET membranes are prepared in the absence of NIPAM. The amount of copolymer chains grafted on the membranes is estimated by the grafting yield, which is the percentage of the increased weight of the grafted membrane in comparison with that of the substrate membrane.

In the second step, EDA-CDs are appended onto P(NIPAM-co-GMA) polymer chains grafted on PET membranes by virtue of high reactivity between primary amino groups and epoxy groups. P(NIPAM-co-GMA)-g-PET membranes are immersed into an EDA-CD aqueous solution and the chemical reaction is carried out at 50 °C for 48 h under vibration. The molar ratio of EDA-CD to the epoxy group of grafted membranes is about 18:1. The resultant P(NIPAM-co-GMA/CD)-g-PET membranes are washed with plenty of deionized water to remove unreacted EDA-CD and dried in an oven at 50 °C. As reference, PGMA-g-PET membranes immobilized EDA-CD (PGMA/CD-g-PET) are also fabricated by the abovementioned method. The content of EDA-CD immobilized on the grafted membranes after reacting with EDA-CD is determined by Eq.(6.2):^[3]

$$q = \frac{W_{\rm gc} - W_{\rm g}}{A_{\rm m}} \tag{6.2}$$

where q is the amount of immobilized EDA-CD per unit membrane area ($\mu g \cdot cm^{-2}$). W_g is the weight of the grafted membrane and W_{gc} represents the weight of the grafted membrane after immobilization of EDA-CD. A_m is the grafted membrane area (cm^2).

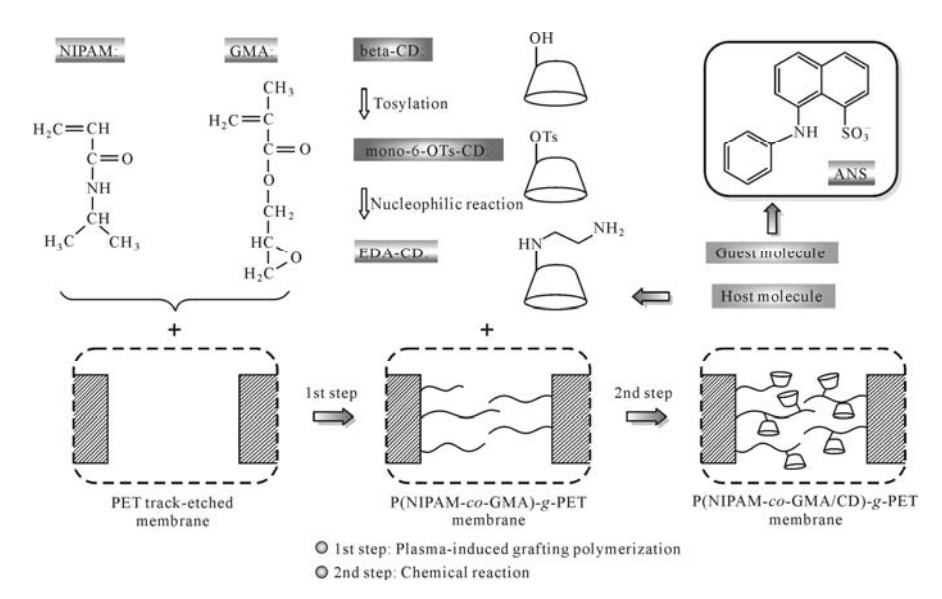


Fig.6.8. Schematic illustration of fabrication route of P(NIPAM-*co*-GMA/CD)-*g*-PET membranes (Reproduced with permission from Ref. [3]). Copyright (2009), Elsevier

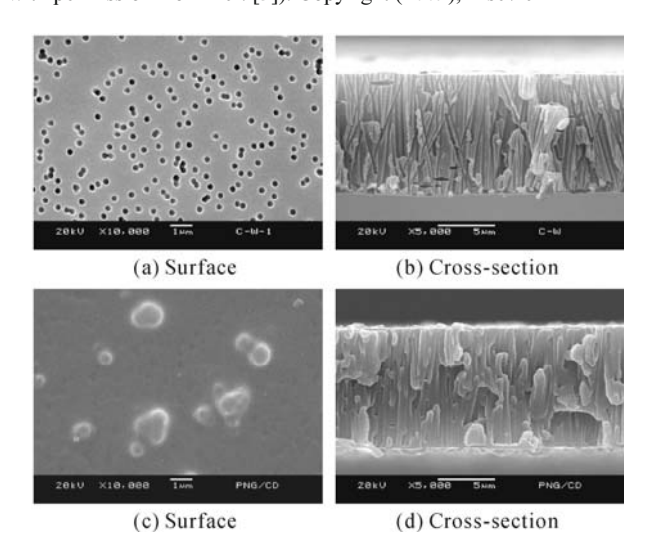


Fig.6.9. SEM images of surfaces and cross-sections of ungrafted and grafted PET membranes. (a, b) Ungrafted; (c, d) P(NIPAM-co-GMA/CD)-g-PET (Y = 10.84%, q = 12.9 μg ·cm⁻²) (Reproduced with permission from Ref. [3]). Copyright (2009), Elsevier

6.3.2 Morphological Characterization of Membranes

To probe microscopic morphology and the microstructure of grafted membranes,

the surface and cross-section of grafted membranes as well as those of the ungrafted membranes are investigated by SEM (Fig.6.9).[3] From the surface and cross-sectional SEM photographs of ungrafted membranes (Figs.6.9a and 6.9b), it is clear that the ungrafted membrane has cylindrical and vertical transmembrane pores with diameters of approximate 0.2 μ m. After grafting PGMA (Y = 10.84%) and immobilizing EDA-CD ($q = 14.5 \, \mu \text{g·cm}^{-2}$), all the pores of the P(NIPAMco-GMA/CD)-g-PET membrane are filled uniformly and completely (Figs.6.9c and 6.9d). Clearly, this is attributable to the uniform polymer layer grafted on the outer surface and pore surface of the membrane. Compared with that of the ungrafted membrane, the thickness of the P(NIPAM-co-GMA/CD)-g-PET membrane increases slightly by tens of nanometers.

6.3.3 Thermo-Responsive Adsorption/Desorption Characteristics

The thermo-responsive adsorption/desorption characteristics of P(NIPAM-co-GMA/CD)-g-PET membranes are studied by absorption experiments using 8-anilino-1-naphthalenesulfonic acid ammonium salt (ANS) as guest molecules. [3] The adsorption experiment is carried out as soon as the examined membrane is immersed into 100 ml of ANS aqueous solution (0.1 mmol·L⁻¹) which is constant at 25 °C in advance and well-mixed. At fixed time intervals, a small amount of solution is taken out and its absorbance is analyzed by a UV-visible spectrophotometer at a wavelength of 350 nm. After the membrane reaches the adsorption equilibrium, the temperature of ANS solution is promptly changed to a higher temperature of 40 °C. Similarly, the absorbance of ANS solution is analyzed by UV-vis at time intervals until equilibrium. Such low/high-temperature variations are repeated once or twice, namely 25 °C \rightarrow 40 °C or 25 °C \rightarrow 40 °C \rightarrow 25 °C \rightarrow 40 °C, in order to observe the dynamic temperature-dependent molecular-recognizable phenomena. The investigated temperatures in these adsorption experiments are chosen as 25 °C and 40 °C, which are lower and higher than the LCST of P(NIPAM-co-GMA) chains grafted on the membrane, respectively. Throughout the adsorption experiments, the ANS solution is sufficiently stirred to obtain uniform concentration.

The amount of ANS adsorbed on the membrane is estimated by the ANS amount per unit membrane area ($Q_{\rm m}$, $\mu g \cdot cm^{-2}$) and can be calculated by Eq.(6.3):^[3] $Q_{\rm m} = \pm \frac{(C_0 - C_{\rm s}) \times V_{\rm s} \times M}{A_{\rm m}} \times 10^6$ (6.3)

$$Q_{\rm m} = \pm \frac{(C_0 - C_{\rm s}) \times V_{\rm s} \times M}{A_{\rm m}} \times 10^6$$
 (6.3)

where C_0 is the initial concentration of ANS aqueous solution at the beginning of each temperature variation sequence. C_s is the ANS concentration in solution at different time intervals. Both C_0 and C_s can be calculated from the equation for the calibration curve. The plus sign and minus sign in Eq.(6.3) are used to calculate $Q_{\rm m}$ in low-temperature (adsorption) and high-temperature (desorption) variation, respectively. $V_{\rm s}$, M and $A_{\rm m}$ represent the volume of ANS solution (i.e., 100 ml),

molecular weight of ANS (i.e., 316.37 g/mol) and membrane area (cm²), respectively.

The results of dynamic adsorption experiments on the P(NIPAM-co-GMA/CD)g-PET membrane (Y=5.95%, q=10.5 µg·cm⁻²) toward the model guest molecule ANS in two low/high-temperature variation sequences are shown in Fig.6.10.[3] At 25 °C, as for the P(NIPAM-co-GMA/CD)-g-PET membrane, the ANS amount adsorbed on per unit membrane area (Q_m) increases sharply during the first 50 min, climbs slowly to 2.1 µg·cm⁻² in the next 70 min and then remains the same. With the temperature heated up to 40 °C, the $Q_{\rm m}$ goes down rapidly from 2.1 µg·cm⁻² to 0.8 μg·cm⁻² within 50 min and then remains unchanged. The same phenomenon is observed during the subsequent absorption experiment in the next low/hightemperature variation sequence. When the temperature is cooled down to 25 °C again, the $Q_{\rm m}$ goes up until the P(NIPAM-co-GMA/CD)-g-PET membrane reaches adsorption equilibrium, and goes down again till equilibrium at 40 °C. This phenomenon of adsorption at low temperature and desorption at high temperature of the P(NIPAM-co-GMA/CD)-g-PET membrane agrees with the static adsorption results. [25] At a temperature lower than the LCST, the P(NIPAM-co-GMA) polymer chains grafted on the membrane swell and there is small steric hindrance near the CD cavities, which leads to the ANS molecules easily being included in the CD cavity. ANS molecules can be partially captured in the CD cavities with the naphthalene group enclosed inside the cavities, while the benzene group remains outside. [25] The swollen polymer chains around ANS molecules can provide enough space so that the binding constant of the complex of the CD cavity and ANS molecule is comparatively high at a temperature below the LCST. Whereas at a temperature above the LCST, the P(NIPAM-co-GMA) polymer chains shrink and agglomerate, and it is so crowded around the CD cavities that the steric hindrance increases and the complex becomes unstable, leading to a small binding constant. This phenomenon verifies that the P(NIPAM-co-GMA/CD)g-PET membrane is provided with thermo-responsive adsorption/desorption properties, which could be applied to temperature-controlled affinity separation.

The equilibrium adsorption amount of ANS on per unit membrane area $Q_{\rm m}'$ is defined as the $Q_{\rm m}$ value at adsorption or desorption equilibrium. The $Q_{\rm m}'$ values at different temperatures are plotted in **Fig.6.10b**. [3] As for P(NIPAM-co-GMA/CD)-g-PET membrane (Y=5.95%, q=10.5 μg ·cm⁻²), the difference of $Q_{\rm m}'$ between 25 °C and 40 °C is approximately 1.2 μg ·cm⁻². The difference value shows good repeatability in two low/high-temperature variations.

To further verify the mechanism of thermo-responsive adsorption/desorption characteristics, the adsorption ability of ungrafted, P(NIPAM-co-GMA)-g-PET (Y=6.21%) and PGMA/CD-g-PET (Y=5.33%, q=11.4 μg ·cm⁻²) membranes are studied by ANS adsorption experiment, too.^[3] As for the three membranes, the changes of Q_m values over time in one low/high-temperature variation are shown in **Fig.6.11** and they have a similar tendency.^[3] At 25 °C, the Q_m values increase at the beginning of adsorption experiments and then stay the same, even at 40 °C. The results clarify the ungrafted membrane, grafted membrane lack of EDA-CDs

(P(NIPAM-co-GMA)-g-PET) and the grafted membrane in the absence of PNIPAM (PGMA/CD-g-PET) has no thermo-responsive adsorption/desorption characteristics. The $Q_{\rm m}'$ values of the PGMA/CD membrane immobilized EDA-CDs are much higher (3.5 $\mu {\rm g \cdot cm}^{-2}$) than those of membranes without EDA-CDs (*i.e.*, ungrafted PET and P(NIPAM-co-GMA)-g-PET, about 0.5 $\mu {\rm g \cdot cm}^{-2}$). The adsorption of ANS molecules onto the P(NIPAM-co-GMA/CD)-g-PET membrane could be mainly attributable to stronger recognition capability of EDA-CDs toward ANS, while the adsorption of the substrate and P(NIPAM-co-GMA)-g-PET membrane toward ANS is relatively weak. At the same time, P(NIPAM-co-GMA) grafted polymer chains have no effects on ANS adsorption since the $Q_{\rm m}'$ values of the ungrafted and P(NIPAM-co-GMA)-g-PET membranes are almost the same.

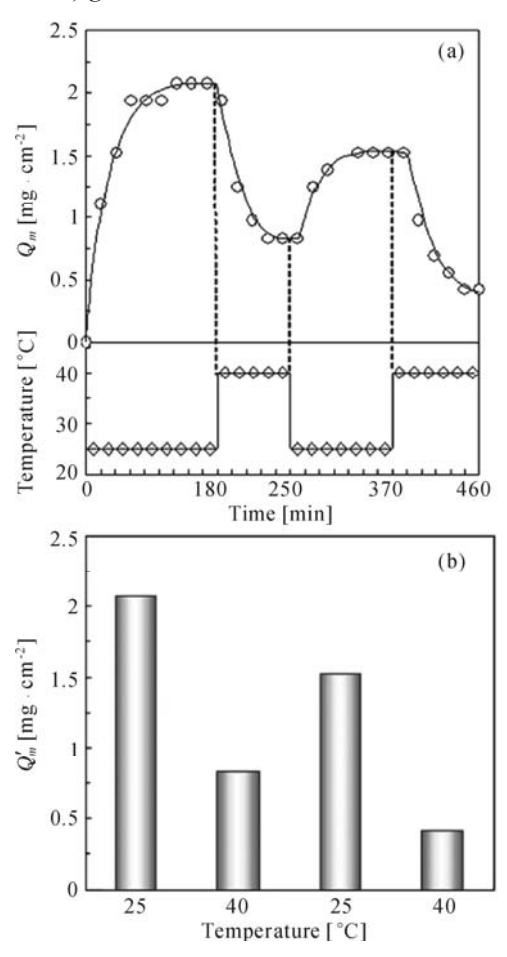


Fig.6.10. Temperature-responsive adsorption/desorption of ANS on P(NIPAM-co-GMA/CD)-g-PET membrane (Y = 5.95%, $q = 10.5 \ \mu g \cdot cm^{-2}$) (Reproduced with permission from Ref. [3]). Copyright (2009), Elsevier

164

As pointed out above, there are no thermo-responsive adsorption/desorption characteristics either for the membrane without EDA-CDs (P(NIPAM-co-GMA)g-PET) or in the absence of PNIPAM chains (PGMA/CD-g-PET). That is to say, the thermo-responsive adsorption/desorption characteristics of the P(NIPAM-co-GMA/CD)-g-PET membrane are attributable to the effect of swelling and shrinking of P(NIPAM-co-GMA) chains on the binding ability of EDA-CD toward ANS at a temperature below and above the LCST. At temperatures below the LCST, the swollen P(NIPAM-co-GMA) grafted chains provide enough space for stable complexation of EDA-CD and ANS, and many ANS molecules are adsorbed on the P(NIPAM-co-GMA/CD)-g-PET membrane. Meanwhile, at temperatures above the LCST, the shrunken polymer chains make the complexation unstable and the adsorbed ANS molecules are desorbed from the membrane. The cooperation of the "swollen-shrunken" configuration change of P(NIPAM-co-GMA) grafted chains around the LCST and the stronger recognition of CD toward ANS endow the P(NIPAM-co-GMA/CD)-g-PET membrane with remarkable thermo-responsive adsorption/desorption characteristics.

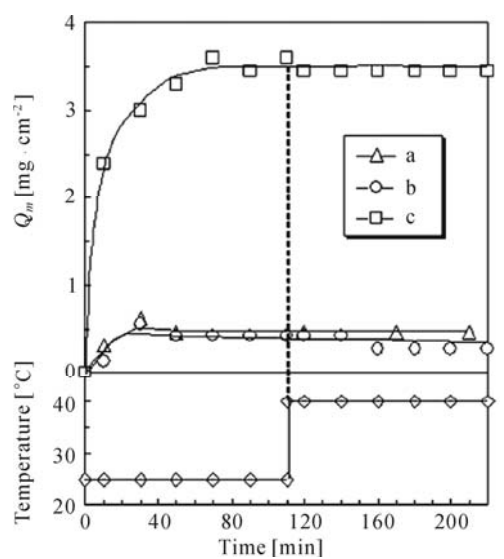


Fig.6.11. Adsorption of ANS on ungrafted and grafted PET membranes. (a) Ungrafted; (b) P(NIPAM-*co*-GMA)-*g*-PET (*Y*=6.21%); (c) PGMA/CD-*g*-PET (*Y*=5.33%, *q*=11.4 μg·cm⁻²) (Reproduced with permission from Ref. [3]). Copyright (2009), Elsevier

The EDA-CD content also affects the thermo-responsive adsorption/desorption characteristics of P(NIPAM-*co*-GMA/CD)-*g*-PET membranes.^[3] The dynamic adsorption experiment on the P(NIPAM-*co*-GMA/CD)-*g*-PET membrane with higher grafting yield and lower EDA-CD content (*i.e.*, *Y*=11.79%, *q*=4 μg·cm⁻²) than that of the P(NIPAM-*co*-GMA/CD)-*g*-PET membrane shown in **Fig.6.10** is carried out (**Fig.6.12a**). During three low/high-temperature variations, ANS molecules are adsorbed onto the P(NIPAM-*co*-GMA/CD)-*g*-PET membrane at

25 °C and desorbed from the membrane at 40 °C, while the ungrafted membrane remains unchanged either at 25 °C or at 40 °C after reaching adsorption equilibrium (**Fig.6.12**). The $Q_{\rm m}'$ values show good repeatability, as illustrated in **Fig.6.12b**. The difference in $Q_{\rm m}'$ values of the P(NIPAM-co-GMA/CD)-g-PET membrane with q=4 μg ·cm⁻² at between 25 °C and 40 °C is around 0.7 μg ·cm⁻², which is much smaller than that of the P(NIPAM-co-GMA/CD)-g-PET membrane with EDA-CD content of 10.5 μg ·cm⁻² (about 1.2 μg ·cm⁻²). As EDA-CD content increases, the difference in the ANS adsorption amount of the P(NIPAM-co-GMA/CD)-g-PET membrane between 25 °C and 40 °C becomes larger.

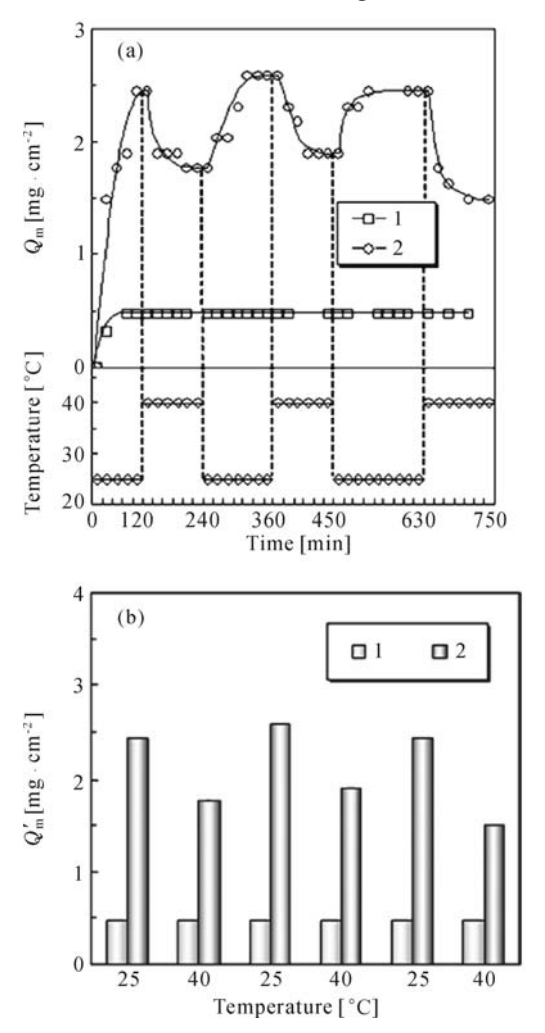


Fig.6.12. Temperature-responsive adsorption/desorption of ANS on ungrafted and grafted PET membranes. a) ungrafted and b) P(NIPAM-co-GMA/CD)-g-PET (Y=11.79%, q=4 μg ·cm⁻²) (Reproduced with permission from Ref. [3]). Copyright (2009), Elsevier

6.4 Summary

Thermo-responsive adsorption/desorption membranes for affinity separation are introduced in this chapter. The thermo-responsive adsorption/desorption characteristics of membranes can be achieved by grafting the PNIPAM surface layer or by jointly grafting PNIPAM chains and immobilizing β -CD moieties, from which both "adsorption at a temperature above the LCST" performance and the contrariwise "adsorption at a temperature below the LCST" performance and the contrariwise "adsorption at a temperature below the LCST" performance result. Such thermo-responsive adsorption/desorption membranes for affinity separation are easy to operate, because only a change in the environmental temperature across the LCST is necessary to accomplish the separation process.

References

- [1] Schild H G. Poly(*N*-isopropylacrylamide): experiment, theory and application. *Progress in Polymer Science*, **1992**, *17*: 163-249.
- [2] Meng T, Xie R, Chen Y C, Cheng C J, Li P F, Ju X J, Chu L Y. A thermo-responsive affinity membrane with nano-structured pores and grafted poly(*N*-isopropylacrylamide) surface layer for hydrophobic adsorption. *Journal of Membrane Science*, **2010**, *349*: 258-267.
- [3] Xie R, Zhang S B, Wang H D, Yang M, Li P F, Zhu X L, Chu L Y. Temperature-dependent molecular-recognizable membranes based on poly (*N*-isopropylacrylamide) and β-cyclodextrin. *Journal of Membrane Science*, **2009**, *326*: 618-626.
- [4] Roper D K, Lightfoot E N. Separation of biomolecules using adsorptive membranes. *Journal of Chromatography A*, **1995**, 702: 3-26.
- [5] Charcosset D. Purification of proteins by membrane chromatography. *Journal of Chemical Technology and Biotechnology*, **1998**, 71: 95-110.
- [6] Guo W, Ruckenstein E. Separation and purification of horseradish peroxidase by membrane affinity chromatography. *Journal of Membrane Science*, **2003**, *211*: 101-111.
- [7] Zeng X, Ruckenstein E. Membrane chromatography: preparation and applications to protein separation. *Biotechnology Progress*, **1999**, *15*: 1003-1019.
- [8] Choi Y J, Yamaguchi T, Nakao S. A novel separation system using porous thermosensitive membranes. *Industrial & Engineering Chemistry Research*, **2000**, *39*: 2491-2495.
- [9] Feng L, Li S, Li Y, Li H, Zhang L, Zhai J, Song Y, Liu B, Jiang L, Zhu D. Super-hydrophobic surfaces: from natural to artificial. *Advanced Materials*, **2002**, *14*: 1857-1860.
- [10] Sun T, Wang G, Feng L, Liu B, Ma Y, Jiang L, Zhu D. Reversible switching between superhydrophilicity and superhydrophobicity. *Angewandte Chemie*

- International Edition, 2004, 43: 357-360.
- [11] Xia F, Feng L, Wang S, Sun T, Song W, Jiang W, Jiang L. Dual-responsive surfaces that switch between superhydrophilicity and superhydrophobicity. *Advanced Materials*, **2006**, *18*: 432-436.
- [12] Xia F, Ge H, Hou Y, Sun T, Chen L, Zhang G, Jiang L. Multiresponsive surfaces change between superhydrophilicity and superhydrophobicity. *Advanced Materials*, **2007**, *19*: 2520-2524.
- [13] Song W, Xia F, Bai Y, Liu F, Sun T, Jiang L. Controllable water permeation on a poly(*N*-isopropylacrylamide)-modified nanostructured copper mesh film. *Langmuir*, **2007**, *23*: 327-331.
- [14] Vladisavljevica G T, Shimizu M, Nakashima T. Permeability of hydrophilic and hydrophobic Shirasu-porous-glass (SPG) membranes to pure liquids and its microstructure. *Journal of Membrane Science*, **2005**, *250*: 69-77.
- [15] Zhang L, Li Y, Sun J, Shen J. Layer-by-layer fabrication of broad-band superhydrophobic antireflection coatings in near-infrared region. *Journal of Colloid and Interface Science*, **2008**, *319*: 302-308.
- [16] Stober W, Fink A, Bohn E. Controlled growth of monodisperse silica spheres in the micron size range. *Journal of Colloid and Interface Science*, **1968**, *26*: 62-69.
- [17] Wang R, Hashimoto K, Fujishima A, Chikuni M, Kojima E, Kitamura A, Shimohigoshi M, Watanabe T. Light-induced amphiphilic surfaces. *Nature*, **1997**, *388*: 431-432.
- [18] Ivanov D, Petrova H. Capillary effects. *Physics Education*, **2000**, *35*: 262-266.
- [19] Shamim N, Hong L, Hidajat K, Uddin M S. Thermosensitive-polymer-coated magnetic nanoparticles: Adsorption and desorption of Bovine Serum Albumin. *Journal of Colloid and Interface Science*, **2006**, *304*: 1-8.
- [20] Kapur V, Charkoudian J, Anderson J L. Transport of proteins through gel-filled porous membranes. *Journal of Membrane Science*, **1997**, *131*: 143-153.
- [21] Peters T J. *All about Albumin: Biochemistry, Genetics, and Medical Applications*. Academic Press, San Diego, CA, **1996**.
- [22] Rezwan K, Meier L P, Rezwan M, Voros J, Textor M, Gauckler L J. Bovine serum albumin adsorption onto colloidal Al₂O₃ particles: a new model based on zeta potential and UV-Vis measurements. *Langmuir*, **2004**, *20*: 10055-10061.
- [23] Alkan M, Demirbas O, Dogan M, Arslan O. Surface properties of bovine serum albumin–adsorbed oxides: adsorption, adsorption kinetics and electrokinetic properties. *Microporous and Mesoporous Materials*, **2006**, *96*: 331-340.
- [24] Cheng C J, Chu L Y, Ren P W, Zhang J, Hu L. Preparation of monodisperse thermo-sensitive poly(*N*-isopropylacrylamide) hollow microcapsules. *Journal of Colloid and Interface Science*, **2007**, *313*: 383-388.
- [25] Yanagioka M, Kurita H, Yamaguchi T, Nakao S. Development of a molecular recognition separation membrane using cyclodextrin complexation controlled by thermosensitive polymer chains. *Industrial & Engineering Chemistry Research*, **2003**, *42*: 380-385.

pH-Responsive Gating Membrane Systems with Pumping Effects

In this chapter, the design, fabrication and performance of a composite pH-responsive membrane system for improved controlled-release, which is composed of a porous membrane with linear-grafted positively pH-responsive polymeric gates acting as functional valves, and a crosslinked negatively pH-responsive hydrogel inside the reservoir working as a functional pumping element, are introduced. The composite membrane system is featured with a large responsive release rate that goes effectively beyond the limit of concentration-driven diffusion due to the pumping effects of the negatively responsive hydrogel inside the reservoir. The system provides a new mode for pH-responsive smart controlled-release systems, which is highly attractive for drug delivery systems, chemical carriers, and sensors and so on.

7.1 Introduction

The target of a controlled drug delivery system is for improved drug treatment (outcome) through rate-and time-programmed and site-specific drug delivery. ^[1,2] Environmental stimuli-responsive controlled-release delivery systems have been developed specifically for this purpose and have attracted great interest in recent years. ^[3,4] These environmental stimuli-responsive delivery systems can release specified chemicals or drugs at a particular site where an environmental condition, such as pH, temperature or other information, is different from that at other sites.

It has been well-known that the interstitial fluids of a number of tumors or inflamed sites in humans and animals have an ambient pH that is considerably lower than that of normal tissues, [5,6] and the pH values are different from place to place in the gastrointestinal tract. [7] Consequently, pH-responsive controlled-release delivery systems enable drugs to be targeted at specific areas of the body such as tumors, sites of inflammation and inflection, or the colonic region. [5,8-10] Therefore, the development of pH-responsive controlled-release delivery systems

is of both scientific and technological interest.

For the environmental stimuli-responsive controlled-release systems, it is very important to manipulate them to respond as quickly as possible upon receiving environmental signals, because a fast response is the key for their successful applications. Up to now, most environmental stimuli-responsive controlled-release systems were fabricated by stimuli-responsive polymeric hydrogels. To increase the response dynamics of stimuli-responsive polymeric hydrogels, several strategies have been explored, such as improving the internal architecture or structure of the hydrogels, [11-13] developing microgels or hydrogel particles with micro-or nano-dimensions, [14-17] and introducing linear-grafted hydrogel chainconfigurations with freely mobile ends. [18] However, most of the investigations were concentrated mainly on the improvement of the response time of phase transitions of the hydrogels themselves, but not nearly enough on the improvement of the stimuli-responsive release rate. It is equally important that the delivery systems release drugs as quickly as possible upon meeting environmental stimuli. For example, although the response time or the responsive conformational change of linear-grafted hydrogel gates of gating membrane systems to environmental stimuli is much faster than that of crosslinked hydrogel membrane systems, because of the chain-configurations with freely mobile ends, [18] the maximum release rate of drugs from the gating membrane systems is still limited by the concentration-driven diffusion. The limitation of the release rate restrains the development of fast-response rate-programmed drug delivery systems.

Recently, the author's group developed a composite pH-responsive membrane system for improved controlled-release, which is coupled with a positively pH-responsive linear-grafted gating membrane and a negatively pH-responsive crosslinked hydrogel inside the reservoir. The composite system is featured with a fast response because of the linear-grafted gates and, more importantly, with a large responsive release rate that goes effectively beyond the limit of concentration-driven diffusion due to the pumping effects of the negatively responsive hydrogel. ^[19] In this chapter, the design, fabrication and performance of the composite pH-responsive membrane system will be introduced.

7.2 Design of the Composite pH-Responsive Gating Membrane System with Pumping Effects

The concept of the developed pH-responsive gating membrane system with pumping effects is schematically illustrated in **Fig.7.1**.^[19] The system is composed of a gating membrane with linear-grafted poly(methacrylic acid) (PMAA) gates and a crosslinked poly(*N*,*N*-dimethylaminoethyl methacrylate) (PDM) hydrogel inside the reservoir. The phase transition characteristics of PMAA and PDM have been verified to be opposite.^[20] PMAA hydrogels are featured with a positively pH-responsive volume phase transition characteristic, *i.e.*, the hydrogel swelling is induced by an increase in the environmental pH. On the contrary, PDM hydrogels

show a negatively pH-responsive volume phase transition characteristic, i.e., the hydrogel swelling is induced by a decrease in the environmental pH. The lineargrafted positively pH-responsive PMAA polymers in the membrane pores act as pH-sensitive "gates" and the crosslinked negatively pH-responsive PDM hydrogel in the reservoir acts as a pH-sensitive "pumping element". The effective dissociation constant (pK) of PMAA (p K_{PMAA}) has been reported to be 4.65~5.35. [21-23] Although the pK value of the DM monomer is around 8.00, [22-24] the pK value of crosslinked PDM networks (p K_{PDM}) has been found to be much lower (about 4.5~5.5). [24-26] The swelling/deswelling behavior of both PMAA polymer and crosslinked PDM networks has been verified to be consistent with their pK values. [20,21,24-26] When the environmental pH is higher than the value of $max(pK_{PMAA}, pK_{PDM})$, the inner PDM hydrogel shrinks. At the same time, the grafted PMAA swells and then closes the membrane pores and as a result the release rate is slow. On the other hand, when the ambient pH is decreased to be lower than the value of $min(pK_{PMAA})$, pK_{PDM}), the grafted PMAA shrinks and consequently the membrane pores open. At the same time, the PDM hydrogel swells and then accelerates the release rate. Therefore, the maximum release rate of drugs from the proposed systems responding to environmental pH changes can be effectively improved, because the limitation of the release rate that is restricted by the concentration-driven diffusion can be broken, due to the pumping effects of the negatively pH-responsive hydrogel inside the reservoir.

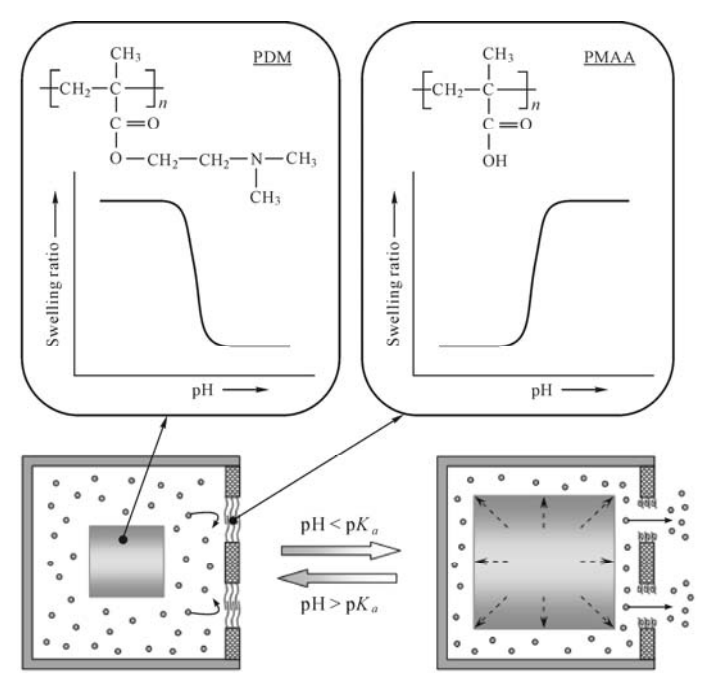


Fig.7.1. Schematic representation of the proposed pH-responsive controlled-release system with functional gating and pumping effects (Reproduced with permission from Ref. [19]). Copyright (2006), Wiley-VCH Verlag GmbH & Co. KGaA

7.3 Preparation and Characterization of the Composite pH- Responsive Membrane System

In this section, the preparation and characterization of the above-designed composite pH-responsive membrane system will be introduced.

7.3.1 Preparation and Characterization of pH-Responsive PMAA- g-PVDF Gating Membranes

First of all, let's start from the preparation and characterization of pH-responsive PMAA-g-PVDF gating membranes.

7.3.1.1 Preparation of Membranes

Porous PVDF membranes with a mean pore diameter of 220 nm and a thickness of 90 μm, supplied by Xidoumen Membrane Co. Ltd, China, were used as the substrates. Plasma-graft pore-filling polymerization was employed to graft PMAA chains in the pores of the porous PVDF membrane substrates according to the method described in **Section 2.2.1.1**. The argon plasma treatment power was from 30 to 50 W, and the plasma treatment time was 60 s. The graft polymerization was carried out under vibration in a constant-temperature bath (30 °C) for a fixed period. The MAA monomer concentration was from 3.0 to 10.0 vol.%, and the polymerization time was from 3 to 10 h. After the reaction, the PMAA-grafted membranes were repeatedly washed in water and then dried *in vacuo* at 50 °C. The grafting yield of the membrane was defined as the mass increase in the membrane after the grafting, which is given by

$$Y = \frac{W_{\rm g} - W_{\rm o}}{W_{\rm o}} \times 100\% \tag{7.1}$$

where Y stands for the grafting yield of PMAA onto the membrane substrate [%] and $W_{\rm g}$ and $W_{\rm 0}$ stand for the mass of the membrane after and before grafting respectively [g].

7.3.1.2 Morphological and Compositional Characterization of Membranes

In order to observe the microstructure of the membranes before and after grafting PMAA, a scanning electron microscope (SEM, JSM-5900LV, Japan) was used. The cross-sectional structures of the membranes were observed at an accelerating voltage of 20 kV by putting the membranes into liquid nitrogen, fracturing mechanically and then gilding the membranes. To confirm the fabrication of

membranes with grafted PMAA gates, the PVDF substrate and the PMAA-g-PVDF membrane were analyzed by X-ray photoelectron spectroscopy (XPS, XSAM800, Kratos, Britain) using a monochromatized Al K α X-ray source (1486.6 eV photons).

Fig.7.2 shows SEM micrographs of the cross-sections of virgin PVDF substrate membrane and PMAA-*g*-PVDF membrane.^[19] It can be seen from the cross-sections of the virgin (**Fig.7.2a**) and PMAA-grafted (**Fig.7.2b**, *Y*=8.58%) membranes that the microstructures were different. After grafting PMAA onto the inner pore surfaces of the porous PVDF membrane substrate by plasma-graft pore-filling polymerization, a significant grafted PMAA layer was homogeneously formed across the cross-section of the membrane. The microstructural change in the membrane indicated that PMAA had been successfully grafted onto the porous membrane substrate.

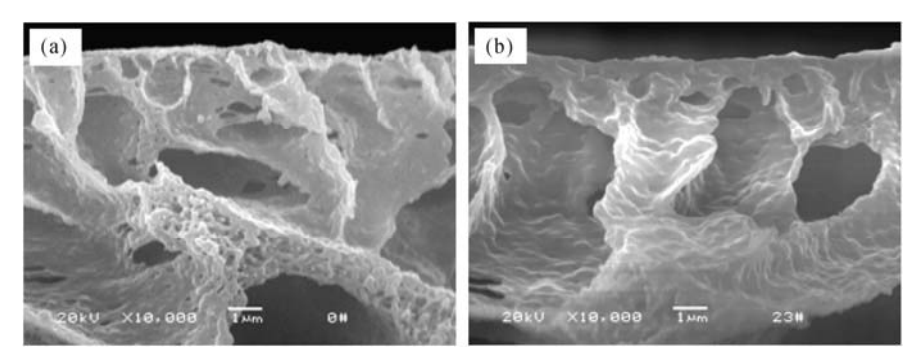


Fig.7.2. SEM images of the cross-sections of (a) virgin PVDF substrate membrane; (b) PMAA*g*-PVDF membrane (Y=8.58%). Scale bar 1 μ m (Reproduced with permission from Ref. [19]). Copyright (2006), Wiley-VCH Verlag GmbH & Co. KGaA

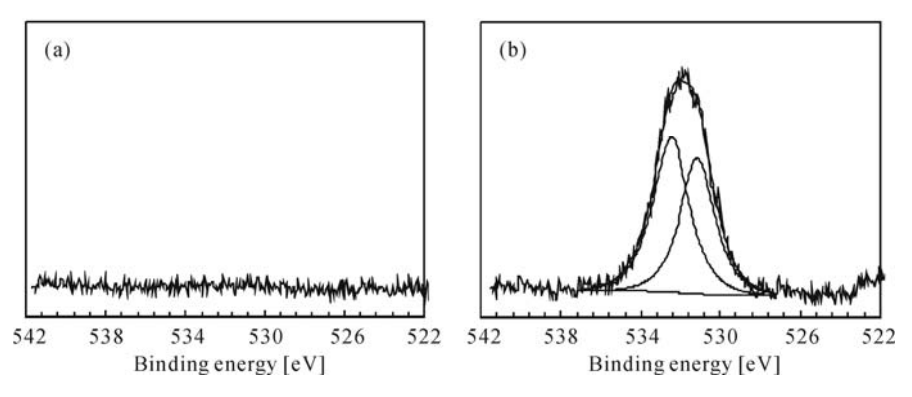


Fig.7.3. XPS O_{1s} core-level spectra of a) virgin PVDF substrate membrane and b) PMAA*g*-PVDF membrane (*Y*=5.80%) (Reproduced with permission from Ref. [19]). Copyright (2006), Wiley-VCH Verlag GmbH & Co. KGaA

Fig.7.3 shows the XPS O_{1s} core-level spectra of the virgin PVDF substrate

membrane and the PMAA-g-PVDF membrane with Y=5.80%. ^[19] There is no peak in the O_{1s} core-level spectrum of the PVDF substrate membrane (**Fig.7.3a**), *i.e.*, there is no oxygen (O) element in the composition of the substrate membrane, while the O_{1s} core-level spectrum of the PMAA-g-PVDF membrane can be curve-fitted with two peak components, having BEs of 531.1 eV for the C=O species and 532.5 eV for the O—H species. The new peak components are assigned to the COOH species of the grafted PMAA polymers in the membrane. These experimental observations confirm the PMAA grafting in the fabrication of the PMAA-g-PVDF gating membranes.

7.3.1.3 pH-Responsive Change in the Effective Pore Size of PMAA-g-PVDF membranes

The pH-responsive changes in the pore size of PMAA-g-PVDF membranes were estimated by filtration experiments on various aqueous pH buffer solutions with a constant ionic strength of 0.1 mol·L⁻¹. The ionic strength was adjusted by adding a certain amount of NaCl. The hydraulic permeability experiments or filtration experiments of virgin PVDF substrate and PMAA-g-PVDF membranes were carried out under a constant trans-membrane pressure of 90 kPa. The diameter of the effective membrane area for filtration was 60 mm. The temperatures of the membrane system and the pH buffer solutions were controlled at 37 °C by a thermostatic unit. The feed solutions were buffered from pH=2 to pH=7. The hydraulic permeability through the virgin PVDF substrate and PMAA-g-PVDF membranes under different pH conditions was studied by measuring the water flux. To minimize the contributions from random error, the flux measurements were carried out three to five times and the arithmetically averaged values were taken as the results under each condition. The pH-responsive change in the pore size of PMAA-g-PVDF membranes could then be calculated according to Hagen-Poiseuille's law. [27,28] The ratio of the effective pore diameter of the PMAA-g-PVDF membrane at pH=x (x was in the range from 2 to 7) to that at pH=7, which was defined as the pH-responsive gating factor of the membrane pore size, could be evaluated using the measured water fluxes with the following equation, derived from Hagen-Poiseuille's law:[19]

$$R_{d,pHx/pH7} = \frac{d_{pH=x}}{d_{pH=7}} = \left(\frac{J_{pH=x}}{J_{pH=7}}\right)^{\frac{1}{4}}$$
 (7.2)

where $R_{d,pHx/pH7}$ stands for the pH-responsive gating factor of the membrane pore size [-], $d_{pH=x}$ and $d_{pH=7}$ are the effective pore diameters of the PMAA-grafted membranes at pH=x and pH=x, respectively [cm], $J_{pH=x}$ and $J_{pH=7}$ are the measured water fluxes at pH=x and pH=x, respectively [ml·cm⁻²·s⁻¹].

Fig.7.4 shows the pH-responsive change of the effective pore size of a PMAA-g-PVDF membrane with Y=5.98%, [19] which was calculated using Hagen-

Poiseuille's law.^[27,28] As expected, the effective pore size of the PMAA-grafted membrane changed dramatically at pH values around the pK_{PMAA} as a result of the conformational change of the grafted PMAA chains. When the ambient pH value was less than pH=3 or larger than pH=6, the effective pore size remained nearly unchanged. It was due to the fact that the conformation of the grafted PMAA chains presented a steady state at these pH ranges.

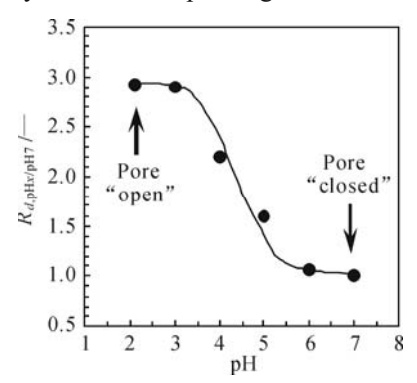


Fig.7.4. pH-responsive change of the effective pore size of PMAA-*g*-PVDF membrane (*Y* = 5.98%) (Reproduced with permission from Ref. [19]). Copyright (2006), Wiley-VCH Verlag GmbH & Co. KGaA

7.3.2 Preparation and Characterization of Crosslinked pH-Responsive PDM Hydrogels

Secondly, crosslinked pH-responsive PDM hydrogels are prepared and characterized for the designed pH-responsive system.

7.3.2.1 Preparation of Crosslinked pH-Responsive PDM Hydrogels

The crosslinked PDM hydrogels were synthesized by free-radical crosslinking polymerization. Monomer (N,N-dimethylaminoethyl methacrylate) ([DM] = 1.4 or 1.8 mol·L⁻¹), cross-linker N,N'-methylene-bisacrylamide ([MBA] = 40.0, 37.5 or 30.0 mmol·L⁻¹), initiator potassium persulfate ([KPS] = 3.0 g/L) were dissolved in a certain amount of deionized water at room temperature and nitrogen gas was bubbled into the solution for 5 min to remove dissolved oxygen in the system. Next, the solution was immediately transferred into small glass tubes with inner diameters of 6 mm, the small glass tubes were sealed immediately and then immersed in a constant-temperature water bath. The temperature of the water bath was kept at a constant 60 °C using a thermostatic unit. The polymerization was carried out for 24 h. After the gelation was completed, the prepared cylindrical

hydrogels were pushed out from the glass tubes and immersed and washed in an excess of deionized water. The water was replaced every 12 h to remove the residual unreacted components and the washing continued at least for one week, followed either by freeze-drying or by vacuum-drying at 40 °C.

7.3.2.2 Morphological Characterization of Hydrogels

In order to observe the microstructure of the freeze-dried and vacuum-dried PDM hydrogels, SEM was also used. The cross-sectional structures of the hydrogels were observed at an accelerating voltage of 20 kV by putting the hydrogels into liquid nitrogen, then fracturing mechanically and gilding the hydrogels.

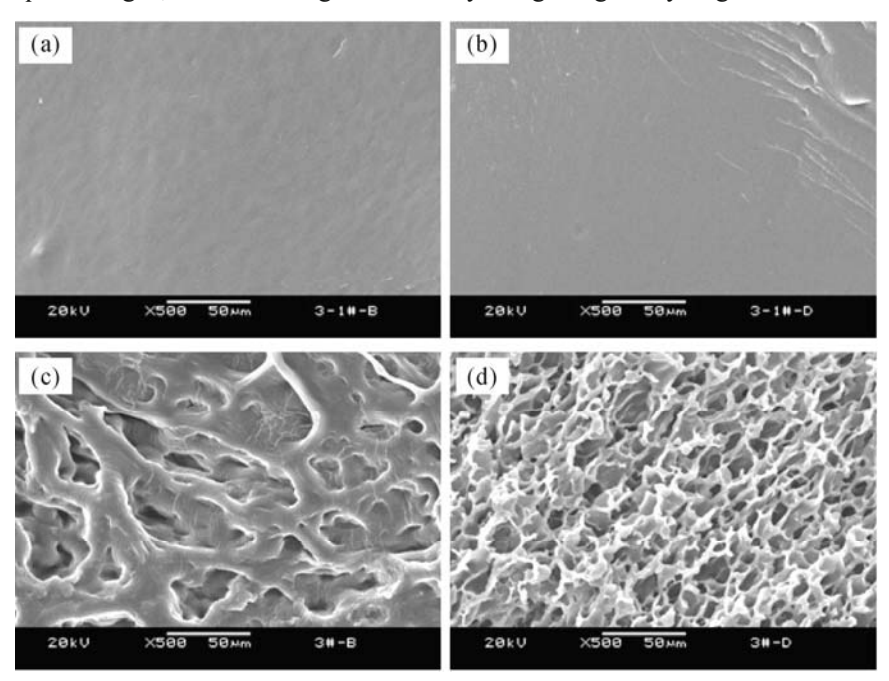


Fig.7.5. SEM images of (a, b) vacuum-dried PDM hydrogel; (c, d) freeze-dried PDM hydrogel prepared with [DM]=1.8 mol·L⁻¹ and [MBA]=40.0 mmol·L⁻¹; (a, c) Surfaces; (b, d) Cross-sections. Scale bar =50 μ m (Reproduced with permission from Ref. [19]). Copyright (2006), Wiley-VCH Verlag GmbH & Co. KGaA

Fig.7.5 shows SEM images of the surfaces and cross-sections of vacuum-dried and freeze-dried PDM hydrogels prepared with [DM]=1.8 mol·L⁻¹ and [MBA]= 40.0 mmol·L⁻¹. The surface of the vacuum-dried hydrogel was smooth (**Fig.7.5a**), whereas that of the freeze-dried hydrogel was very uneven (**Fig.7.5c**). The cross- sectional view of the vacuum-dried hydrogel exhibited a dense internal microstructure (**Fig.7.5b**); on the other hand, the freeze-dried hydrogel showed a

honeycombed porous microstructure inside (**Fig.7.5d**). Thermo-responsive hydrogels with macroporous structures have been reported to be featured with rapid swelling/deswelling properties, *i.e.*, it has been verified that large pore sizes and porosities of hydrogels can lead to a more rapid response to environmental stimuli.^[29] Therefore, due to the porous microstructure, the response rate of the freeze-dried PDM hydrogels to environmental pH change was expected to be more rapid than that of the vacuum-dried hydrogels.

7.3.2.3 pH-Responsive Swelling/Deswelling Characteristics of PDM Hydrogels

To determine the pH-responsive swelling/deswelling properties of crosslinked PDM hydrogels, pre-weighed freeze-dried or vacuum-dried hydrogel samples were immersed in buffer solutions with different pH values. The buffer solutions were kept at a constant 37 °C by a thermostatic unit and the ionic strengths of buffer solutions with different pH values were all adjusted to 0.1 mol·L^{-1} by adding certain amounts of NaCl. After a fixed period of time (for measuring the swelling kinetics) or when the equilibrium state of swelling/deswelling had been reached (for measuring the equilibrium swelling/deswelling characteristics), the hydrogel samples were taken out from the buffer solutions, the excess solutions on their surfaces were wiped off and then they were immediately weighed. The measurements were carried out three times and the data were in good agreement within a standard deviation of 2%. The swelling ratio of the hydrogel was defined as W_s/W_d , where W_s and W_d showed the weight of the hydrogel swollen in buffer solution at a certain pH and the weight in a dry state, respectively.

To determine the pH-responsive dynamic volume-change rate of PDM hydrogels, the pH value of the ambient buffer solution was designed to change from pH=7 to pH=2. The dynamic volume-change rate was measured by transferring a PDM hydrogel sample, which had been swollen in the buffer solution with pH=7 at 37 °C for such a long time that the equilibrium state of swelling/deswelling had been reached, into another buffer solution with pH=2 at the same temperature. At pre-determined time intervals, the swollen hydrogels were weighed and the swelling ratios were calculated as described above.

Fig.7.6 shows the swelling kinetics of vacuum-dried and freeze-dried PDM hydrogels in buffer solutions with pH=2 and pH=7. [19] Just as expected, the swelling rate of freeze-dried hydrogel in the buffer solution with pH=2 was significantly faster than that of vacuum-dried hydrogel at the same pH. On the other hand, when the solution was buffered with pH=7, the swelling rate of freeze-dried hydrogel was just slightly faster than that of vacuum-dried hydrogel. The experimental results verified that freeze-dried hydrogels were preferred in obtaining a rapid response rate for the hydrogels. Consequently, freeze-dried PDM samples were used in the subsequent experiments.

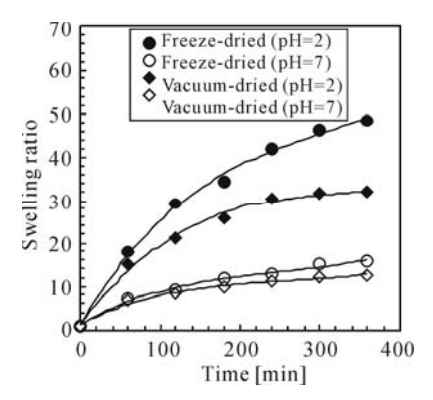


Fig.7.6. Swelling kinetics of vacuum-dried and freeze-dried PDM hydrogels in buffer solutions with pH=2 and pH=7. The PDM hydrogels were prepared with [DM]=1.8 $mol\cdot L^{-1}$ and [MBA]=40.0 $mmol\cdot L^{-1}$ (Reproduced with permission from Ref. [19]). Copyright (2006), Wiley-VCH Verlag GmbH & Co. KGaA

Fig.7.7 shows the pH-responsive equilibrium volume-change of freeze-dried PDM hydrogel prepared with [DM]=1.4 mol·L⁻¹ and [MBA]=37.5 mmol·L⁻¹. [19] When the environmental pH changed across the p $K_{\rm PDM}$, the volume of the crosslinked PDM hydrogel changed dramatically. When the ambient pH was lower than the p $K_{\rm PDM}$, the amine groups protonated and the produced electrostatic repulsion initiated a swelling of the crosslinked PDM polymer networks. When the ambient pH was higher than the p $K_{\rm PDM}$, the PDM polymer networks deswelled, due to the deprotonation of the amine groups, and the swelling ratio of hydrogels at that moment decreased abruptly. The significant volume phase-transition was satisfactory, as required for developing the proposed composite system illustrated in **Fig.7.1**.

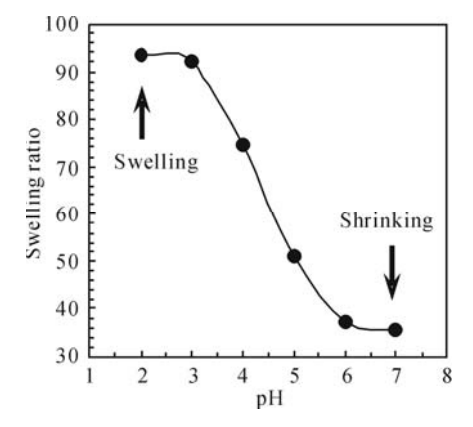


Fig.7.7. pH-responsive equilibrium volume-change of freeze-dried PDM hydrogel prepared with [DM]=1.4 mol·L⁻¹ and [MBA]=37.5 mmol·L⁻¹ (Reproduced with permission from Ref. [19]). Copyright (2006), Wiley-VCH Verlag GmbH & Co. KGaA

Fig.7.8 shows the pH-responsive dynamic volume-change property of freezedried PDM hydrogel when the pH value of the ambient buffer solution changed from pH=7 to pH=2. [19] It can be seen that the freeze-dried PDM hydrogel swelled quickly when the environmental pH value changed from pH=7 to pH=2. The swelling ratio increased from 57.8 to 73.4 within 6 min, and to 90.1 within 24 min. The fast response rate of the PDM hydrogels was also satisfactory for the proposed composite system.

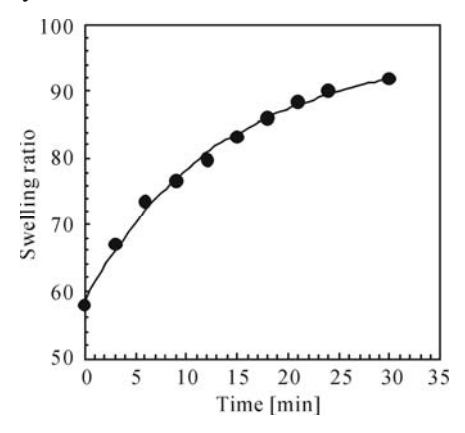


Fig.7.8. pH-responsive dynamic volume-change behavior of freeze-dried PDM hydrogel when the pH value of the ambient buffer solution changed from pH=7 to pH=2. The PDM hydrogel was prepared with [DM]=1.4 mol·L⁻¹ and [MBA]=30.0 mmol·L⁻¹ (Reproduced with permission from Ref. [19]). Copyright (2006), Wiley-VCH Verlag GmbH & Co. KGaA

7.4 pH-Responsive Controlled-Release Characteristics of the Composite Membrane System with Pumping Effects

The release rate of the solute (VB₁₂) from the prepared system was measured by determining the increase in the solute concentration of the surrounding medium over time, after immersing the prepared system (as the donor cell) into the pure buffer solution (without solutes at first) inside a receptor cell. ^[19] The PMAA-*g*-PVDF gating membrane and the crosslinked PDM hydrogels were coupled in the prepared system. Before being put into the reservoir of the prepared system, the crosslinked PDM hydrogels were cut into segments of the same length at 25 °C and then were immersed in 0.2 mmol·L⁻¹ VB₁₂ buffer solutions with pH=7 at room temperature for at least 72 h. The VB₁₂ buffer solutions were refreshed periodically to ensure the VB₁₂ concentration inside the hydrogels could be 0.2 mmol·L⁻¹. The spare space inside the reservoir of the prepared system was filled with 0.2 mmol·L⁻¹ VB₁₂ buffer solutions with pH=7. Each test membrane was soaked first in 50 vol% aqueous solution of alcohol to wet the membrane and then was immersed in the 0.2 mmol·L⁻¹ VB₁₂ buffer solution with pH=7 for 24 h before starting the release experiments. Before starting the release experiments, both the fully assembled

system and the receptor cell with 100 ml of buffer solution with pH=7 were kept at a constant 37 °C using a thermostatic unit. The prepared composite system was then immersed in the buffer solution with pH=7 inside the receptor cell and the buffer solution was stirred with a magnetic stirrer. The temperature of the whole release system was always maintained at 37 °C during the experiments. To investigate the pH-responsive controlled-release characteristics of solute VB₁₂ from the proposed system, the pH values of the solutions in both donor and receptor compartments were both changed from pH=7 to pH=2 at the same time after a period of release, by refreshing the solutions with those buffered at pH=2. The ionic strengths of both pure buffer solutions and VB₁₂ buffer solutions were adjusted to 0.1 mol·L⁻¹. The VB₁₂ concentration was determined using a UV-visible recording spectrophotometer at a wavelength of 361 nm. To quantitively describe the pH-responsive controlled-release characteristic, a parameter called the controlled factor (*CF*) was defined as^[19]

$$CF = \frac{v_{\text{pH}=2}}{v_{\text{pH}=7}} \tag{7.3}$$

where $v_{pH=2}$ and $v_{pH=7}$ stand for the release rates of VB₁₂ at pH=2 and pH=7 respectively, [mol·m⁻²·s⁻¹].

Fig.7.9 shows the pH-responsive controlled-release characteristics of VB₁₂ from different systems,^[19] in which **Fig.7.9a** shows the release results from a system without pH-responsive gates in the membrane and no PDM hydrogels inside the reservoir either. **Fig.7.9b** shows the release results from a system with grafted PMAA gates in the membrane but no PDM hydrogel inside the reservoir. **Fig.7.9c** shows the results from a system with only PDM hydrogel inside the reservoir but without pH-responsive gates in the membrane and **Fig.7.9d** shows the release results from the proposed composite system with both crosslinked PDM hydrogel inside the reservoir and grafted PMAA gates in the membrane.

For the system with a virgin PVDF membrane and no PDM hydrogels inside the reservoir (**Fig.7.9a**), the controlled factor (*CF*) for the VB₁₂ release was 1.00 when the environmental pH was changed from pH=7 to pH=2. In other words, there was no change in the release rate of VB₁₂ at all when the ambient pH changed from pH=7 (higher than the value of $\max(pK_{PMAA}, pK_{PDM})$) to pH=2 (lower than the value of $\min(pK_{PMAA}, pK_{PDM})$). That means the VB₁₂ release from this system did not show any pH-responsive characteristic.

For the system with the PMAA-g-PVDF membrane (Y=15.65%) but no PDM hydrogel inside the reservoir (**Fig.7.9b**), the controlled factor for the VB $_{12}$ release was increased to 1.86 when the environmental pH was changed from pH=7 to pH=2. When the environmental pH changed from pH=7 (higher than the value of max(p K_{PMAA} , p K_{PDM})) to pH=2 (lower than the value of min(p K_{PMAA} , p K_{PDM})), the pores of the PMAA-g-PVDF membrane changed from a "closed" situation into an "open" situation due to the conformational change of grafted PMAA chains in the membrane pores. Therefore, the diffusion channels for the VB $_{12}$ solutes became wider; as a result the release rate of VB $_{12}$ became faster. The results verified that the grafted PMAA chains in the PVDF membrane pores acted successfully as pH-responsive functional valves for the VB $_{12}$ release.

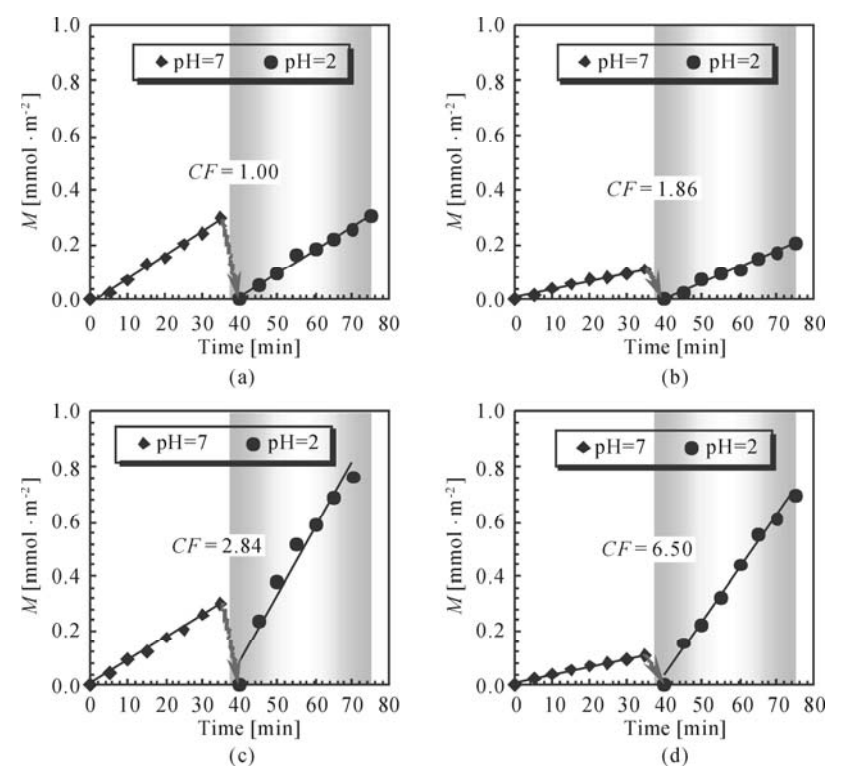


Fig.7.9. pH-responsive controlled-release characteristics of VB₁₂ from different systems. a) With virgin PVDF substrate membrane and without PDM hydrogel inside the reservoir; b) with PMAA-g-PVDF gating membrane (Y = 15.65%) but without PDM hydrogel inside the reservoir; c) with virgin PVDF substrate membrane but with freeze-dried PDM hydrogel ([DM]=1.4 mol·L⁻¹ and [MBA]=30.0 mmol·L⁻¹) inside the reservoir and d) with PMAA-g- PVDF gating membrane (Y = 15.65%) and with freeze-dried PDM hydrogel ([DM]=1.4 mol·L⁻¹ and [MBA]=30.0 mmol·L⁻¹) inside the reservoir (Reproduced with permission from Ref. [19]). Copyright (2006), Wiley-VCH Verlag GmbH & Co. KGaA

For the system with a virgin PVDF membrane and crosslinked PDM hydrogel inside the reservoir (**Fig.7.9c**), the controlled factor for the VB₁₂ release was 2.84 when the environmental pH was changed from pH=7 to pH=2. The pumping effects of the crosslinked PDM hydrogel on the release rate were significant. When the ambient pH was higher than the value of $\max(pK_{PMAA}, pK_{PDM})$, the crosslinked PDM hydrogel was in a shrinking state; when the pH was decreased to be lower than the value of $\min(pK_{PMAA}, pK_{PDM})$, the crosslinked PDM hydrogel started to swell and acted as a micro-pumping element for the VB₁₂ release from the system. The results verified the pH-responsive pumping function for the release of solutes by the inner crosslinked PDM hydrogel.

For the proposed composite system with both crosslinked PDM hydrogel inside the reservoir and grafted PMAA gates in the membrane (**Fig.7.9d**), the controlled factor for the VB₁₂ release was increased, so as to be as large as 6.50.

Due to the dual function of the grafted PMAA gates in the porous membrane and the crosslinked PDM hydrogel in the reservoir, the controlled factor was higher than both of the systems with the pH-responsive gating membrane only (Fig.7.9b) and with the crosslinked PDM hydrogel only (Fig.7.9c). Compared to that of the single PMAA-grafted membrane system shown in Fig.7.9b, the controlled factor of the proposed system was improved 3.5 times. That means that with the cooperative action of the membrane "gating" function and the crosslinked hydrogel "pumping" effect, the proposed composite system exhibited a much better performance of pH-responsive controlled-release than those currently existing gating membrane systems, and the limitation of the release rate that was restricted by the concentration-driven diffusion has been effectively broken by the pumping effects of the negatively responsive hydrogel.

The proposed system could also be easily applied to micro-scale systems by fabricating negatively responsive microgels or hydrogel nano-particles inside the hollow microcapsules with porous membranes and functional gates.[18,30] In such a microcapsule system, the inner PDM hydrogel would respond to the pH variation of the environment (externally to the outer PMAA-grafted microcapsule membrane), so quickly as to be effective in the delivery of the active substance: when the system goes from an environment with higher pH toward an environment with lower pH, the grafted PMAA shrinks, the membrane pores open, the external solution diffuses inside the microcapsule, the pH inside the system lowers and then the PDM hydrogel responds by swelling and pumping the drug solutes externally to the system, through the pores of the microcapsule membrane.

7.5 Summary

In summary, the developed composite pH-responsive system, which is composed of a porous membrane with linear-grafted PMAA gates acting as functional valves and a crosslinked PDM hydrogel inside the reservoir working as a functional pumping element, demonstrates an improved controlled-release performance. Because of the cooperative action of the PMAA-g-PVDF gating membrane and the crosslinked PDM hydrogel, the composite system exhibits a large responsive release rate that goes effectively beyond the limit of concentration-driven diffusion, which provides a new mode for pH-responsive smart or intelligent controlled-release systems. This new mode could be easily applied to micro-scale systems by introducing negatively responsive microgels or hydrogel nano-particles into the inner space of porous microcapsules with functional gates.

References

[1] Breimer D D. Future challenges for drug delivery. Journal of Controlled

- Release, 1999, 62: 3-6.
- [2] Allen T M, Cullis P R. Drug delivery systems: entering the mainstream. *Science*, **2004**, *303*: 1818-1822.
- [3] Zhu Y, Shi J, Shen W, Dong X, Feng J, Ruan M, Li Y. Stimuli-responsive controlled drug release from a hollow mesoporous silica sphere/polyelectrolyte multilayer core-shell structure. *Angewandte Chemie International Edition*, **2005**, *44*: 5083-5087.
- [4] Giri S, Trewyn B G, Stellmaker M P, Lin V S Y. Stimuli-responsive controlled-release delivery system based on mesoporous silica nanorods capped with magnetic nanoparticles. *Angewandte Chemie International Edition*, **2005**, *44*: 5038-5044.
- [5] Yatvin M B, Kreutz W, Horwitz B A, Shinitzky M. pH-sensitive liposomes: possible clinical implications. *Science*, **1980**, *210*: 1253-1255.
- [6] Helmlinger G, Yuan F, Dellian M, Jain R K. Interstitial pH and pO₂ gradients in solid tumors *in vivo*: high-resolution measurements reveal a lack of correlation. *Nature Medicine*, **1997**, *3*: 177-182.
- [7] Evans D F, Pye G, Bramley R, Clark A G, Dyson T J, Hardcastle J D. Measurement of gastrointestinal pH profiles in normal ambulant human subjects. *Gut*, **1988**, *29*: 1035-1041.
- [8] Na K, Lee E S, Bae Y H. Adriamycin loaded pullulan acetate/sulfonamide conjugate nanoparticles responding to tumor pH: pH-dependent cell interaction, internalization and cytotoxicity in vitro. *Journal of Controlled Release*, **2003**, 87: 3-13.
- [9] Rodriguez M, Vila-Jato J L, Torres D. Design of a new multiparticulate system for potential site-specific and controlled drug delivery to the colonic region. *Journal of Controlled Release*, **1998**, *55*: 67-77.
- [10] Hu Z, Kimura G, Ito Y, Mawatari S, Shimokawa T, Yoshikawa H, Yoshikawa Y, Takada K. Technology to obtain sustained release characteristics of drugs after delivered to the colon. *Journal of Drug Targeting*, **1999**, *6*: 439-448.
- [11] Yoshida R, Uchida K, Kaneko Y, Sakai K, Kikuchi A, Sakurai Y, Okano T. Comb-type grafted hydrogels with rapid deswelling response to temperature changes. *Nature*, **1995**, *374*: 240-242.
- [12] Wu X S, Hoffman A S, Yager P J. Synthesis and characterization of thermally reversible macroporous poly(*N*-isopropylacrylamide) hydrogels. *Journal of Polymer Science Part A*: *Polymer Chemistry*, **1992**, *30*, 2121-2129.
- [13] Kwon I C, Bae Y H, Kim S W. Electrically credible polymer gel for controlled release of drugs. *Nature*, **1991**, *354*: 291-293.
- [14] Pelton R. Temperature-sensitive aqueous microgels. *Advances in Colloid and Interface Science*, **2000**, *85*: 1-33.
- [15] Gan D, Lyon L A. Interfacial nonradiative energy transfer in responsive core-shell hydrogel nanoparticles. *Journal of American Chemical Society*, **2001**, *123*: 8203-8209.
- [16] Xiao X C, Chu L Y, Chen W M, Wang S, Li Y. Positively thermo-sensitive monodisperse core-shell microspheres. *Advanced Functional Materials*, **2003**, *13*: 847-852.

- [17] Xiao X C, Chu L Y, Chen W M, Wang S, Xie R. Preparation of submicronsized monodispersed thermoresponsive core-shell hydrogel microspheres. *Langmuir*, **2004**, *20*: 5247-5253.
- [18] Chu L Y, Park S H, Yamaguchi T, Nakao S. Preparation of small-sized monodispersed thermo-responsive core-shell microcapsules. *Langmuir*, **2002**, *18*: 1856-1864.
- [19] Qu J B, Chu L Y, Yang M, Xie R, Hu L, Chen W M. A pH-responsive gating membrane system with pumping effects for improved controlled-release. *Advanced Functional Materials*, **2006**, *16*: 1865-1872.
- [20] Park K, Park H. *Polymeric Materials Encyclopedia*, *Vol. 10* (Editor-in-Chief: Salamone J C), CRC Press, Florida, **1996**.
- [21] Diez-Pena E, Quijada-Garrido I, Frutos P, Barrales-Rienda J M. Analysis of the swelling dynamics of crosslinked P(*N*-iPAAm-*co*-MAA) copolymers, the corresponding homopolymers and their interpenetrating networks. Kinetics of water penetration into the gel above the pKa of MAA comonomeric units. *Polymer International*, **2003**, *52*: 956-965.
- [22] Merle Y. Synthetic polyampholytes. 5. Influence of nearest-neighbor interactions on potentiometric curves. *Journal of Physical Chemistry*, **1987**, *91*: 3092-3098.
- [23] Lowe A B, McCormick C L. Synthesis and solution properties of zwitterionic polymers. *Chemical Reviews*, **2002**, *102*: 4177-4190.
- [24] Hadjiyannakou S C, Yamasaki E N, Patrickios C S. Randomly cross-linked homopolymer networks: synthesis by group transfer polymerization in solution and characterization of the aqueous degree of swelling. *Polymer*, **2001**, *42*: 9205-9209.
- [25] Simmons M R, Yamasaki E N, Patrickios C S. Cationic amphiphilic model networks: synthesis by group transfer polymerization and characterization of the degree of swelling. *Macromolecules*, **2000**, *33*: 3176-3179.
- [26] Sen M, Sari M. Radiation synthesis and characterization of poly(*N*,*N*-dimethylaminoethyl methacrylate-*co-N*-vinyl 2-pyrrolidone) hydrogels. *European Polymer Journal*, **2005**, *41*: 1304-1314.
- [27] Li Y, Chu L Y, Zhu J H, Wang H D, Xia S L, Chen W M. Thermo-responsive gating characteristics of poly(*N*-isopropylacrylamide)-grafted porous polyvinylidene fluoride membranes. *Industrial & Engineering Chemistry Research*, **2004**, *43*: 2643-2649.
- [28] Xie R, Chu L Y, Chen W M, Xiao W, Wang H D, Qu J B. Characterization of microstructure of poly(*N*-isopropylacrylamide)-grafted polycarbonate tracketched membranes prepared by plasma-graft pore-filling polymerization. *Journal of Membrane Science*, **2005**, *258*: 157-166.
- [29] Yan Q, Hoffman A S. Synthesis of macroporous hydrogels with rapid swelling and deswelling properties for delivery of macromolecules. *Polymer*, **1995**, *36*: 887-889.
- [30] Chu L Y, Park S H, Yamaguchi T, Nakao S. Preparation of thermo-responsive core-shell microcapsules with a porous membrane and poly(*N*-isopropylacrylamide) gates. *Journal of Membrane Science*, **2001**, *192*: 27-39.

Smart Microcapsules with pH-Responsive Hydrogel Membranes

In this chapter, the design, fabrication and performance of smart microcapsules with pH-responsive chitosan hydrogel membranes are introduced. The pH-responsive microcapsules with crosslinked chitosan membranes are fabricated with a microfluidic approach using monodisperse O/W/O emulsions as templates to form a crosslinked chitosan membrane at the inner O/W interface via interfacial crosslinking reaction between chitosan and terephthalaldehyde. The chitosan microcapsule membranes show acid-induced pH-responsive swelling and decomposing behavior. Such monodisperse polysaccharide microcapsules with pH-responsive chitosan hydrogel membranes could serve as promising candidates for pH-responsive drug delivery systems.

8.1 Introduction

As mentioned in Chapter 7, pH-responsive controlled-release delivery systems enable drugs to be targeted at specific areas of the body, such as tumors, sites of inflammation and inflection, or the colonic region, and the development of pH-responsive controlled-release delivery systems is of both scientific and technological interest. Chitosan is a copolymer of *D*-glucosamine and *N*-acetylglucosamine and it is derived from the natural polymer chitin. Due to its excellent biological activity, [1,2] good biocompatibility and biodegradability, [3,4] and ability to form hydrogels, [5,6] chitosan is a highly versatile cationic polysaccharide. Chitosan hydrogels exhibit pH-responsive volume phase change and have been extensively used in developing pH-responsive systems. [7,8] Recently, the author's group developed a simple microfluidic approach to prepare monodisperse chitosan microcapsules with a uniform membrane. [9] In this chapter, the design, microfluidic preparation and pH-responsive behavior of chitosan microcapsule membranes will be introduced.

8.2 Design and Fabrication Strategy of Smart Microcapsules with pH-Responsive Chitosan Hydrogel Membranes

Crosslinked chitosan hydrogels can be prepared with terephthalaldehyde as crosslinker (**Fig.8.1**). The microfluidic technique provides a facile approach to produce monodisperse double emulsions which could be utilized as templates to prepare hollow microcapsules. Our strategy for chitosan microcapsule membrane preparation is to fabricate monodisperse oil-in-water-in-oil (O/W/O) double emulsions by the microfluidic technique first (**Fig.8.2**), and then fabricate chitosan microcapsule membranes via interfacial crosslinking reaction with the O/W/O emulsions as templates (**Fig.8.3**). In the O/W/O double emulsions, the inner oil phase contains the oil-soluble terephthalaldehyde which acts as crosslinker in the subsequent interfacial crosslinking reaction. Due to the formation of a Schiff base, the interfacial crosslinking reaction of chitosan with terephthalaldehyde occurs at the inner O/W interface of the O/W/O emulsions (**Figs.8.1** and **8.3**). After the interfacial crosslinking reaction, microcapsules with chitosan hydrogel membranes are obtained.

Microcapsules with crosslinked chitosan hydrogel membranes could exhibit pH-responsive properties. In an acidic medium, due to the acidic hydrolysis of the Schiff base formed by the crosslinking reaction of chitosan and terephthalaldehyde, the microcapsule membrane could be decomposed and dissolved (**Fig.8.4**). Such a pH-responsive behavior makes it promising for the microcapsules with crosslinked chitosan hydrogel membranes to find potential applications in the field of stimuli-responsive drug delivery where rapid pH-responsive release of encapsulated substance is required.

Fig.8.1. Preparation of crosslinked chitosan hydrogel with terephthalaldehyde as crosslinker

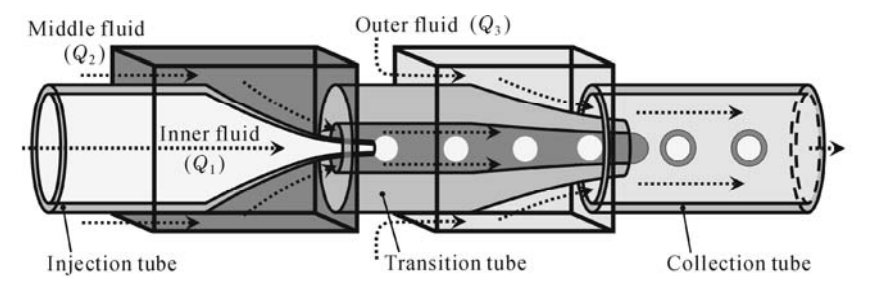


Fig.8.2. Schematic diagram of capillary microfluidic device and the formation of monodisperse O/W/O double emulsions

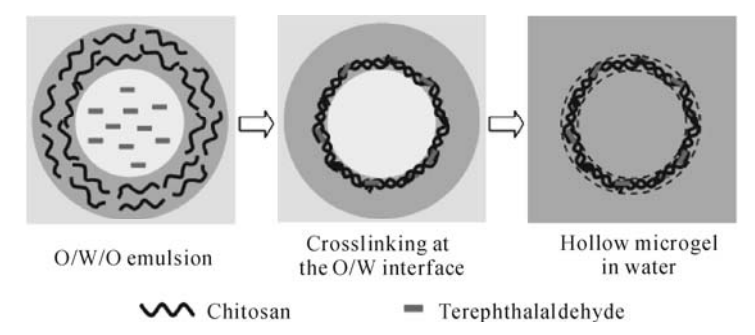


Fig.8.3. Schematic illustration of fabrication of microcapsule with crosslinked chitosan hydrogel membrane with O/W/O double emulsion as template

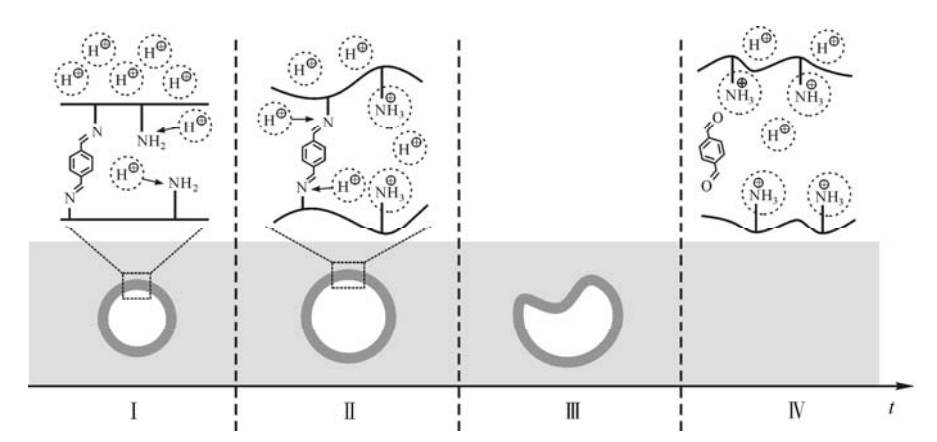


Fig.8.4. Schematic illustration of pH-responsive behavior of crosslinked chitosan microcapsules in acidic medium. The whole process can be divided into four stages: (I) initial status; (II) swelling stage; (III) collapsing stage; (IV) decomposing and dissolving stage

8.3 Preparation of Microcapsules with Crosslinked Chitosan Hydrogel Membranes

In this section, the preparation of microcapsules with crosslinked chitosan hydrogel membranes will be introduced.

8.3.1 Microfluidic Device

The microfluidic device was fabricated by assembling glass capillary tubes on glass slides. The outer diameters of all the cylindrical capillary tubes were the same at 1.0 mm. The square capillary tubes had an inner dimension of 1.0 mm. The inner diameters of the injection tube, the transition tube and the collection tube were 580, 250 and 580 µm, respectively. A micropuller (Narishige, Japan) was used to taper the end of the cylindrical capillaries and the orifice dimensions of tapered ends were adjusted by a microforge (Narishige, Japan). The inner diameters of the tapered end of the injection and transition tubes were 60 and 220 µm, respectively. All cylindrical capillary tubes were coaxially aligned within the larger square capillary tubes by matching the outer diameters of the cylindrical tubes to the inner dimensions of the square ones (Fig.8.2).

8.3.2 Preparation of Microcapsules with Crosslinked Chitosan Hydrogel Membranes

2.0 wt% water-soluble chitosan (M_w =5,000, degree of deacetylation 85%) and 2.0 wt% hydroxyethylcellulose ($M_{\rm w}$ =500,000, degree of molar substitution 2.0) were dissolved in water and the pH of the solution was adjusted to 6.7 by adding 1.0 mol·L⁻¹ NaOH dropwise, which was used as the water phase after addition of Pluronic F-127 to a final concentration of 0.5 wt%. A mixture of soybean oil and benzyl benzoate (1:2, v/v) containing 2.0 wt% terephthalaldehyde was used as the inner oil phase. The outer oil phase was soybean oil containing 8.0 wt% polyglycerol polyricinoleate (PGPR, Danisco). To prepare the O/W/O double emulsions, inner oil phase, middle water phase and outer oil phase solutions were separately pumped into the injection tube, the transition tube and the collection tube through polyethylene tubing attached to disposable syringes. The fluid flow was driven by syringe pumps. Based on the coaxial co-flow geometry, monodisperse O/W single emulsions were generated in the transition tube and monodisperse O/W/O double emulsions were generated in the collection tube (Fig.8.2). The flow rates of the inner, middle and outer fluids were $Q_1 = 400 \text{ } \mu \text{l·h}^{-1}$, $Q_2 = 600 \text{ } \mu \text{l·h}^{-1}$ and $Q_3 = 5,500 \, \mu l \cdot h^{-1}$, respectively. The obtained O/W/O double emulsions were collected in a container, and the microcapsules were prepared through the interfacial

crosslinking reaction between chitosan and terephthalaldehyde at the inner O/W interface. The microfluidic production of double emulsions and subsequent interfacial crosslinking reaction were all performed at 20 °C. The resultant microcapsules were washed, using a mixture of ethyl acetate and isopropanol to remove the inner and outer oil solutions, and finally dispersed into water.

8.4 Morphological Characterization of Chitosan Microcapsules

The morphology and size of the emulsions and microcapsules dispersed in water were characterized using an optical microscope (BX 61, Olympus, Japan). The size and size distribution of samples were determined by using automatic analytic software on the basis of optical micrographs. The average outer diameter of each sample was calculated from the measured results of more than 200 particles. The morphology of the microcapsules in a dried state was observed using scanning electron microscope (SEM, JSM-5900LV, JEOL, Japan). The sample of microcapsules was dried in the air prior to SEM observation.

The optical micrographs of the double emulsions and washed microcapsules in water are shown in **Figs.8.5a** and **8.5b**. It is obvious that both the emulsions and microcapsules are spherical and uniform-sized and the microcapsules exhibit a hollow structure with uniform size. The average outer diameters of the emulsions and microcapsules are about 335 μ m and 254 μ m, respectively. The thickness of the microcapsule membrane is about 20 μ m. The SEM image clearly shows the hollow structure of the microcapsule and the inner surface is slightly smoother than the outer surface (**Fig.8.5c**), which reflects the fact that the interfacial crosslinking reaction proceeds via the diffusion of terephthalaldehyde from the oil to the water phase. The coefficient of variation (CV), which is defined as the ratio of the standard deviation of the size distribution to its arithmetic mean, is usually used to characterize the size monodispersity of particles. As shown in **Fig.8.5d**, both the double emulsions and microcapsules have very narrow size distributions with the CV values below 2.5%.

It is notable that the outer diameter of the microcapsules is much smaller than that of double emulsions, while the inner diameters remain the same, which can be explained according to the microcapsule formation mechanism. At room temperature, the monodisperse double emulsions are quite stable and act as the templates for the interfacial crosslinking reaction. As terephthalaldehyde diffuses from the inner oil phase to the interface of oil/aqueous solutions and reacts with chitosan, a thin polysaccharide membrane forms at the interface between the internal oil droplet and middle water phase. Finally, microcapsules of uniform size are obtained with inner oil cores of the same size as those of double emulsions. Because the crosslinking of chitosan happens near the inner oil core, the outer diameter of the resultant microcapsule is slightly smaller than that of the double emulsion template (Fig.8.3).

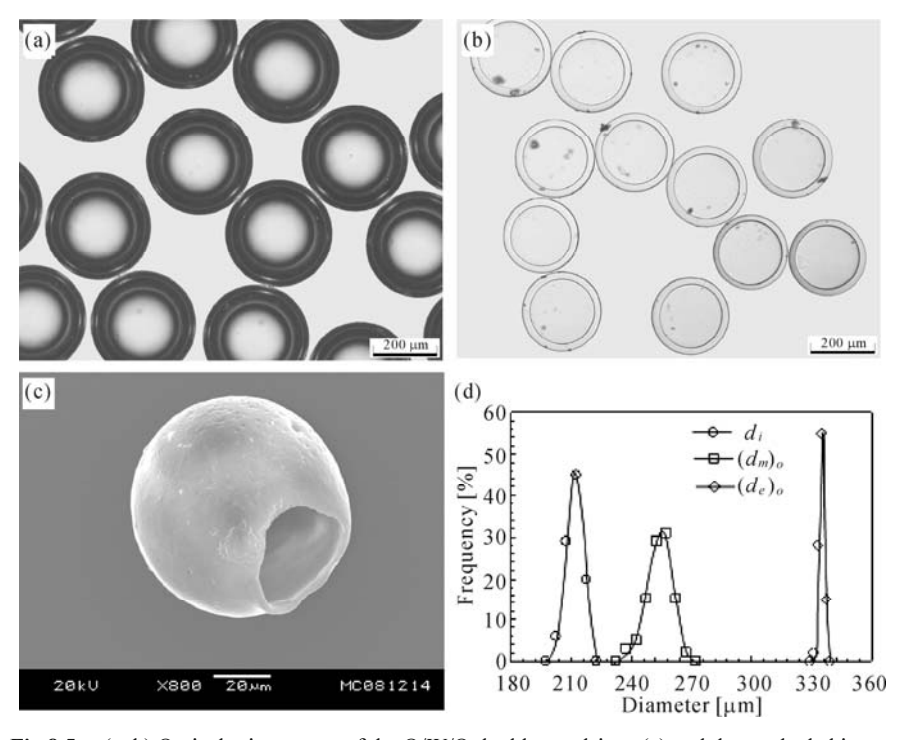


Fig. 8.5. (a, b) Optical micrograms of the O/W/O double emulsions (a) and the washed chitosan microcapsules dispersed in water (b). Both scale bars are 200 μ m. (c) SEM image of an air-dried chitosan microcapsule. (d) Size distributions of inner diameter d_i and outer diameter $(d_e)_o$ of the double emulsions and outer diameter $(d_m)_o$ of resultant microcapsules dispersed in water

8.5 pH-Responsive Property of Microcapsules with Chitosan Hydrogel Membranes

The pH-sensitivity of the microcapsules was studied in 0.01 mol·L⁻¹ phosphate buffer solutions (pH 7.1~2.9) and diluted HCl solution (pH 1.5). Ionic strengths of all buffer solutions were adjusted to 0.1M by adding sodium chloride. The pH values of the buffer solutions were directly measured at 37 °C using a pH meter (Sevenmulti Neutral Meter, Mettler-Toledo, Switzerland), calibrated at 4.01, 7.00 and 9.21. The experiments were performed in a home-made transparent glass container. Prior to tests, 0.5 ml aqueous suspension of microcapsule samples that had been equilibrated in deionized water were transferred into the container. To change the ambient pH in the microcapsule suspension, excess buffer solution with a certain pH was added into the container rapidly. The pH-dependent changes in size and morphology of the microcapsules were monitored by an optical microscope equipped with a thermostatic stage system (TS 62, Instec, USA) and a CCD camera. All experiments on pH-responsive behavior were performed at 37 °C.

In a neutral medium (pH 7.1), the optical micrograms of microcapsules were taken at regular time intervals and the size change of the microcapsules was analyzed. Meanwhile, a fresh buffer solution was supplemented regularly during the experiment to guarantee constant ionic concentration. In an acidic medium (pH 4.7~1.5), the pH-responsive behavior of the crosslinked chitosan microcapsules were continuously recorded using a CCD camera mounted on the optical microscope.

In the case of pH 7.1 (**Figs.8.6** and **8.7**), the microcapsules show continuous shrinkage during the initial period of 48 h and afterwards the size of the microcapsules hardly changes. The integrity and monodispersity of microcapsules are maintained throughout the process. Finally, the average outer diameter of the microcapsules is 201 μ m and the thickness of the capsule membrane decreases by 23% (**Fig.8.7**).

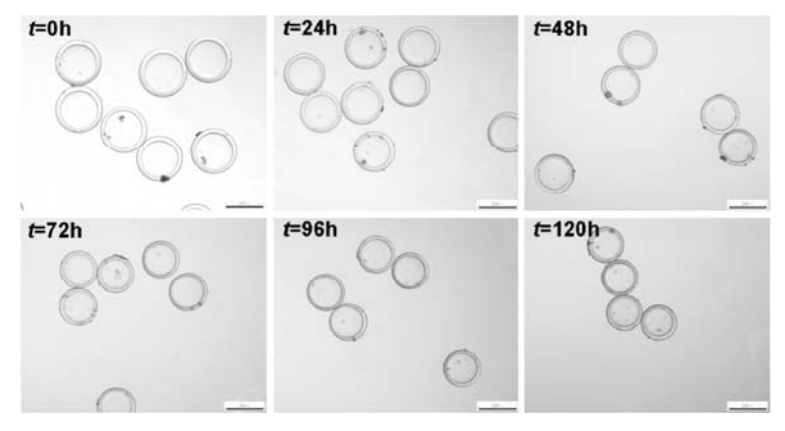


Fig.8.6. Optical micrograms of microcapsules in phosphate buffer solution (pH=7.1, ionic strength 0.1 mol·L⁻¹) at 37 °C at different time intervals. The microcapsules are initially dispersed in deionized water. Scale bar is 200 μm

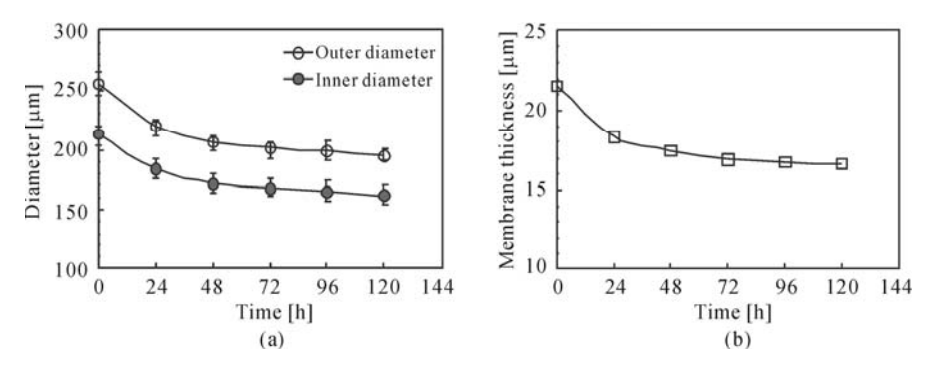


Fig.8.7. Time-dependent size-change of the outer/inner diameters (a) and membrane thickness (b) of microcapsules in phosphate buffer solution (pH=7.1, ionic strength 0.1 mol·L⁻¹) at 37 °C

Fig.8.8 shows the pH-responsive behavior of chitosan microcapsules as their surrounding environment is changed from deionized water to a phosphate buffer

with pH 4.7. During the initial 12 min, the microcapsules swell slowly and maintain a good sphericity and integral capsule membrane. The chitosan membrane of the microcapsule begins to collapse at around 14 min and finally decomposes in the medium. The whole process lasts about 22 min.

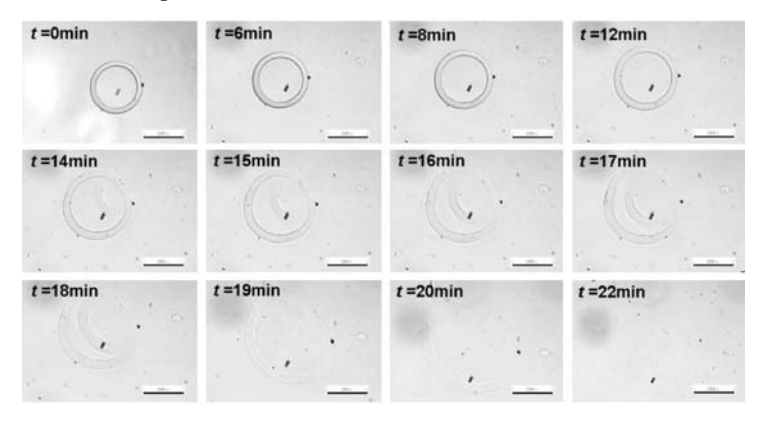


Fig.8.8. Optical microscope snapshots of the swelling, collapsing and decomposing behavior of microcapsules after being immersed in phosphate buffer solution (pH=4.7, ionic strength $0.1 \text{ mol} \cdot \text{L}^{-1}$) at 37 °C. The microcapsules are initially dispersed in deionized water. Scale bar is 200 μm

Fig.8.9 displays the pH-responsive behavior of microcapsules as their surrounding environment is changed from deionized water to a phosphate buffer with pH 3.9. Microcapsules swell slowly and begin to collapse at 180 s. The degree of collapse of the capsule membrane gradually increases as it accompanies the microcapsule swelling. At 270 s, microcapsules cannot maintain their integrity and the capsule membranes start to disappear partially and finally dissolve in the acidic medium with the decomposition of the microcapsules.

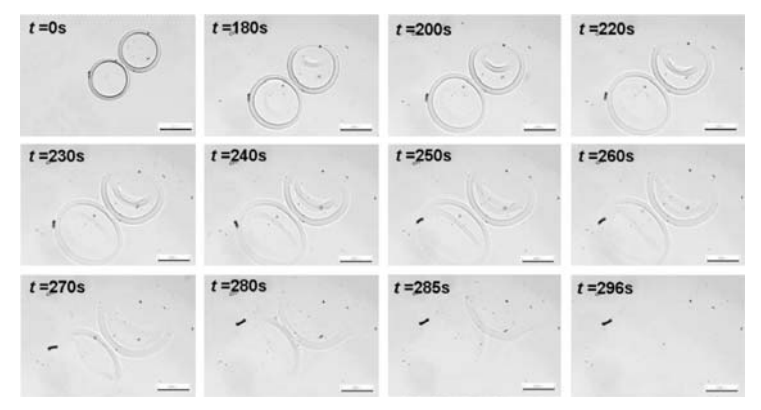


Fig.8.9. Optical microscope snapshots of the swelling, collapsing and decomposing behavior of microcapsules after being immersed in phosphate buffer solution (pH=3.9, ionic strength $0.1 \text{ mol} \cdot \text{L}^{-1}$) at 37 °C. The microcapsules are initially dispersed in deionized water. Scale bar is 200 μm

When the surrounding environment of the microcapsules is changed from deionized water to a phosphate buffer with pH 2.9, the microcapsules exhibit pH-responsive behavior similar to that in the buffer solution with pH 4.7 and pH 3.9, except in a faster fashion (**Fig.8.10**). The corresponding collapse and decomposition of microcapsules are delayed, starting at 13 s and 45 s respectively, and it takes about 60 s for the microcapsules to thoroughly dissolve in the solution. **Fig.8.11** shows the volume phase change of microcapsules in diluted HCl solution (pH 1.5). Microcapsules swell rapidly, immediately after the addition of HCl solution. Accompanying the rapid swell, microcapsules start to collapse at 11 s, decompose at 29 s, and finally dissolve completely within 40 s.

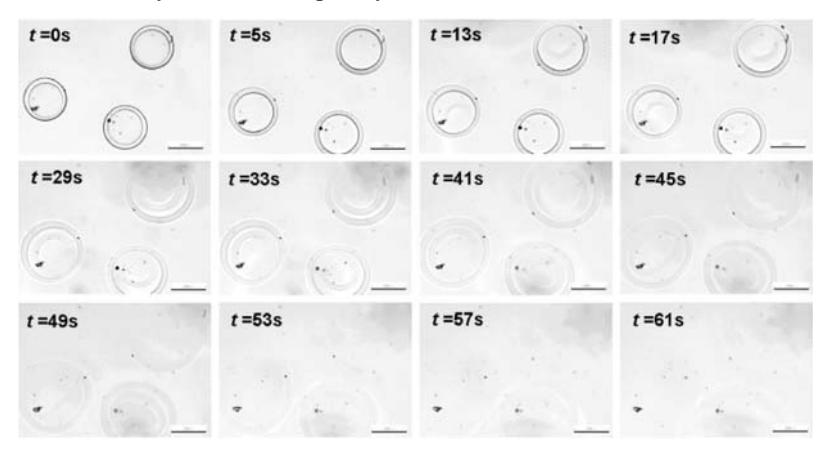


Fig.8.10. Optical microscope snapshots of the swelling, collapsing and decomposing behavior of microcapsules after being immersed in phosphate buffer solution (pH=2.9, ionic strength $0.1 \text{ mol} \cdot \text{L}^{-1}$) at 37 °C. The microcapsules are initially dispersed in deionized water. Scale bar is 200 μm

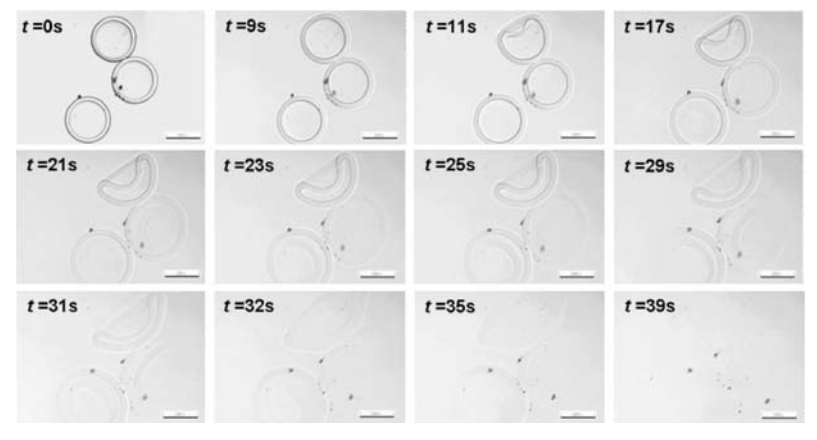


Fig.8.11. Optical microscope snapshots of the swelling, collapsing and decomposing behavior of microcapsules after being immersed in diluted HCl solution (pH=1.5, ionic strength 0.1 mol·L⁻¹) at 37 °C. The microcapsules are initially dispersed in deionized water. Scale bar is 200 μm

The results described above indicate a general trend in the pH-responsive behavior of microcapsules in an acidic medium with pH in the range of 4.7~1.5 as follows: all the microcapsules swell first, and then gradually collapse and decompose (as illustrated in Fig.8.4). The lower the pH value is, the faster the pH-responsive rate. In an acidic medium with pH in the range of 4.7~1.5, the free amino groups on chitosan are protonated firstly. As a result, the electrostatic repulsion among the positively charged polymer chains and the increased hydrophilicity make the microcapsules swell. The microcapsule membrane decomposes and finally dissolves, due to the acidic hydrolysis of the Schiff base formed by the crosslinking reaction of chitosan and terephthalaldehyde.

The pH-responsive behavior of the microcapsules with crosslinked chitosan membranes could be summarized as follows. On the one hand, in a neutral medium with pH 7.1, the chitosan microcapsule membranes exhibit slight shrinkage while maintaining their good spherical shape and structural integrity. On the other hand, in an acidic medium with pH ranging from 4.7 to 1.5, the chitosan microcapsule membranes show pH-responsive volume swelling behavior at the beginning and finally decomposition due to the acidic hydrolysis of the Schiff base.

8.6 Summary

In summary, pH-responsive microcapsules with crosslinked chitosan membranes are fabricated with a microfluidic approach. During the microcapsule preparation process, monodisperse O/W/O emulsion templates are generated in the microfluidic device first, and then microcapsules with a crosslinked chitosan membrane are formed at the inner O/W interface via interfacial crosslinking reaction between chitosan and terephthalaldehyde. When the surrounding medium is neutral with pH 7.1, the chitosan microcapsule membranes maintain a good spherical shape and structural integrity. On the other hand, in an acidic medium with pH ranging from 4.7 to 1.5, the chitosan microcapsules show firstly a pH-responsive volume swelling behavior, and finally decompose due to the acidic hydrolysis of the Schiff base in the chitosan microcapsule membrane. Due to such pH-responsive properties, the chitosan microcapsule membranes are promising candidates for smart drug delivery in response to external pH change.

References

- Rabea E I, Badawy M E T, Stevens C V, Smagghe G, Steurbaut W. Chitosan [1] as antimicrobial agent: applications and mode of action. Biomacromolecules, **2003**, *4*: 1457-1465.
- Sogias I A, Williams A C, Khutoryanskiy V V. Why is chitosan mucoadhesive? [2]

- Biomacromolecules, 2008, 9: 1837-1842.
- [3] Hirano S, Tsuchida H, Nagao N. *N*-acetylation in chitosan and the rate of its enzymic hydrolysis. *Biomaterials*, **1989**, *10*: 574-576.
- [4] Mi F L, Tan Y C, Liang H F, Sung H W. *In vivo* biocompatibility and degradability of a novel injectable chitosan-based implant. *Biomaterials*, **2002**, *23*: 181-191.
- [5] Chenite A, Chaput C, Wang D, Combes C, Buschmann M D, Hoemann C D, et al. Novel injectable neutral solutions of chitosan form biodegradable gels in situ. *Biomaterials*, **2000**, *21*: 2155-2161.
- [6] Francis Suh J K, Matthew H W T. Application of chitosan-based polysaccharide biomaterials in cartilage tissue engineering: a review. *Biomaterials*, **2000**, *21*: 2589-2598.
- [7] Park S B, You J O, Park H Y, Haam S J, Kim W S. A novel pH-sensitive membrane from chitosan-TEOS IPN: preparation and its drug permeation characteristics. *Biomaterials*, **2001**, *22*: 323-330.
- [8] Wu J, Su Z H, Ma G H. A thermo-and pH-sensitive hydrogel composed of quaternized chitosan/glycerophosphate. *International Journal of Pharmaceutics*, **2006**, *315*: 1-11.
- [9] Yang J P. Study on preparation and properties of drug carriers based on natural polysaccharides. M.S. Thesis, Sichuan University, **2009**. (in Chinese)
- [10] Utada A S, Lorenceau E, Link D R, Kaplan P D, Stone H A, Weitz D A. Monodisperse double emulsions generated from a microcapillary device. *Science*, **2005**, *308*: 537-541.
- [11] Utada A S, Chu L Y, Fernandez-Nieves A, Link D R, Holtze C, Weitz D A. Dripping, jetting, drops and wetting: the magic of microfluidics. *MRS Bulletin*, **2007**, *32*: 702-708.
- [12] Chu L Y, Utada A S, Shah R K, Kim J W, Weitz D A. Controllable monodisperse multiple emulsions. *Angewandte Chemie International Edition*, **2007**, *46*: 8970-8974.
- [13] Wang W, Liu L, Ju X J, Zerrouki D, Xie R, Yang L, Chu L Y. A novel thermo-induced self-bursting microcapsule with magnetic-targeting property. *ChemPhysChem*, **2009**, *10*: 2405-2409.
- [14] Liu L, Yang J P, Ju X J, Xie R, Yang L, Liang B, Chu L Y. Microfluidic preparation of monodisperse ethyl cellulose hollow microcapsules with non-toxic solvent. *Journal of Colloid and Interface Science*, **2009**, *336*: 100-106.
- [15] Zhang H, Ju X J, Xie R, Cheng C J, Ren P W, Chu L Y. A microfluidic approach to fabricate monodisperse hollow or porous poly(HEMA-MMA) microspheres using single emulsions as templates. *Journal of Colloid and Interface Science*, **2009**, *336*: 235-243.
- [16] Ren P W, Ju X J, Xie R, Chu L Y. Monodisperse alginate microcapsules with oil core generated from a microfluidic device. *Journal of Colloid and Interface Science*, **2010**, *343*: 392-395.

Glucose-Responsive Gating Membranes

In this chapter, the design, fabrication and performance of glucose-responsive gating membranes with grafted poly(acrylic acid) (PAAC) gates and covalently bound glucose oxidase (GOD) enzymes, including both flat membranes and microcapsule membranes, are introduced. The linear grafted PAAC chains in the membrane pores act as the pH-responsive gates or actuators, and the immobilized GOD acts as the glucose sensor and catalyzer because it is sensitive to glucose and catalyzes the glucose conversion to gluconic acid. The pore size and permeability control of the glucose-responsive gating membranes will be described systematically. The glucose-responsivity of the solute diffusional permeability through the prepared flat membranes is heavily dependent on the PAAC grafting yield, because the pH-responsive change of pore size governed the glucose-responsive diffusional permeability. It is very important to design a proper grafting yield to obtain an ideal gating response. The prepared PAAC-grafted and GOD-immobilized microcapsule membranes demonstrate reversible glucose-responsive release characteristics.

9.1 Introduction

The development of a glucose-responsive insulin-releasing system for diabetes therapy is a long-standing challenge for biomedical engineers. [1,2] Although diabetes mellitus is a major cause of death in industrialized countries, periodical parenteral injections of insulin are currently the standard treatment for insulin-dependent diabetic patients. However, poor control of the blood glucose level and poor patient compliance are associated with this method. [3] Therefore, there is a need for self-regulated delivery systems having the capability of adapting the insulin release rate in response to changes in glucose concentration in order to keep the blood glucose levels within the normal range. [2,4]

Several kinds of glucose-responsive insulin delivery systems have been devised. [2-19] However, none of these systems could fully mimic the physiology of insulin secretion as yet. [4] Therefore, better ways of glucose-responsive self-regulated administration of insulin delivery are still being sought. For glucose-responsive

self-regulated insulin release systems, stability and responsivity of the system are very important and essential, because only a stable system can ensure safety during therapy and only a fast response can ensure exact self-regulated insulin-release during changes in glucose concentration. To meet both stability and responsivity, glucose-responsive gating membranes with porous substrates and linear-grafted functional polymeric gates are competent. The porous membrane substrates can provide mechanical strength and dimensional stability. As the linear grafted polymeric chains have freely mobile ends, which are different from the typical crosslinked network structure of the hydrogels that gives rise to relatively immobile chain ends, the responsiveness of the prepared membranes to the environmental stimuli could therefore be faster than that of their corresponding homogeneous analogs, owing to the more rapid conformational changes of the functional polymers.

Recently, the author's group fabricated glucose-responsive gating membranes with grafted poly(acrylic acid) (PAAC) gates and covalently bound glucose oxidase (GOD) by grafting PAAC onto porous polyvinylidene fluoride (PVDF) membrane substrates with a plasma-graft pore-filling polymerization method, as described in Section 2.2.1.1, and immobilizing GOD onto the grafted membranes by a carbodiimide method. ^[20] Investigations were carried out on the morphological examination of the grafting, on the control of the pH-responsive pore size of the membrane and pH-and glucose-responsive permeability through the membrane by the PAAC grafting yield, and on the glucose-responsive insulin diffusion coefficient. ^[20] On the basis of the experimental investigation of flat membranes, the author's group also developed a glucose-responsive microcapsule with a porous membrane and with linear-grafted PAAC chains and covalently bound GOD enzymes in the membrane pores acting as functional gates. ^[21] In this chapter, the design, fabrication and performance of glucose-responsive flat and microcapsule membranes will be introduced.

9.2 Glucose-Responsive Flat Gating Membranes

In this section, glucose-responsive flat gating membranes will be introduced.

9.2.1 Fabrication of Glucose-Responsive Flat Gating Membranes

The preparation process route and the principle of glucose-responsive control of the permeation through the gating membrane are schematically illustrated in **Fig.9.1**.^[20]

9.2.1.1 Grafting Poly(Acrylic Acid) Gates by Plasma-Graft Pore-Filling Polymerization

Porous PVDF membranes with an average pore size of 0.22 µm and a thickness of

62.5 µm were used as the porous membrane substrates. Plasma-graft pore-filling polymerization was employed to graft the linear PAAC chains into the pores of the PVDF membrane substrate according to the method described in Section 2.2.1.1. [20] Briefly, the PVDF membrane substrate was placed in a transparent glass tube, which was then filled with argon gas. The tube was then evacuated to a pressure of 10 Pa, and the membrane substrate was subjected to a radio-frequency plasma operating at 13.56 MHz, delivering 30 W for 60 s. Then, under inert atmosphere conditions, the PVDF membrane substrate was immersed into the AAC monomer solution and the graft polymerization was carried out under vibration in a constant-temperature bath (30 °C) for a fixed period. In the experiments, the AAC concentrations in the monomer solutions were from 3 wt% to 7 wt% and the grafting time was from 60 min to 300 min. The PAAC-grafted membranes were washed three times with deionized water under vibration in a constant-temperature bath (30 °C) for 24 h to remove any non-reacted monomer and homopolymer. They were then dried in a vacuum oven at 50 °C. The grafting yield of PAAC onto the PVDF membrane (Y, %) was defined as the weight increase in the membrane after the grafting.

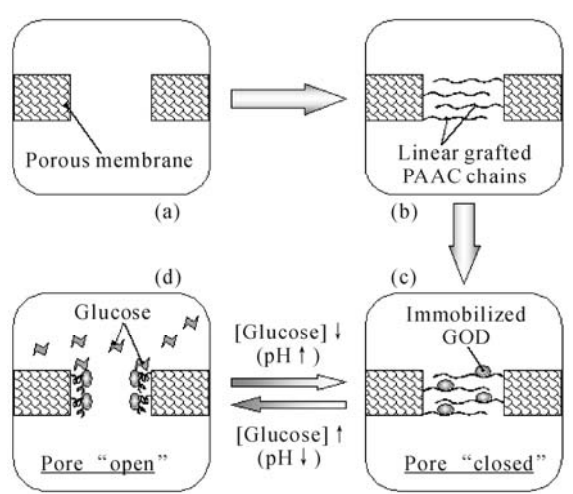


Fig.9.1. Schematic illustration of the preparation process route and the principle of glucose-responsive control of the permeation through the gating membrane: (a) porous membrane substrate; (b) pH-responsive gating membrane with poly(acrylic acid) (PAAC) gates prepared using a plasma-graft pore-filling polymerization to graft linear PAAC chains into the pores of the membrane substrate; (c) glucose-responsive gating membrane prepared by immobilizing glucose oxidase (GOD) onto the PAAC-grafted membrane. At neutral pH in the absence of glucose, the carboxyl groups of the grafted PAAC chains are dissociated and negatively charged, therefore the membrane gates "closed" because the repulsion between negative charges make the PAAC chains extended; (d) when glucose concentration increased, GOD catalyzes the oxidation of glucose into gluconic acid, thereby lowering the local pH in the microenvironment, protonating the carboxylate groups of the grafted PAAC chains. Therefore, the gates "open" because of the reduced electrostatic repulsion between the grafted PAAC chains in the pores (Reproduced with permission from Ref. [20]). Copyright (2004), Elsevier

9.2.1.2 Preparation of Glucose-Responsive Membranes by Immobilizing Glucose Oxidase

Immobilization of glucose oxidase (GOD) was carried out by the carbodiimide method that was described by Ito *et al.*^[12] The PAAC-grafted PVDF membrane was immersed in a 10 wt% aqueous solution of 1-(3-dimethyl-aminopropyl)-3-ethylcarbodiimide hydrochloride, which is a water-soluble carbodiimide (WSC), for 1 h at 4 °C. This WSC solution was buffered at pH 4.75 with 0.1 mol·L⁻¹ 2-(*N*-morpholino)ethanesulfonic acid (MES). After being activated, the membrane was rapidly washed three times with the MES buffer solution to remove unreacted carbodiimide molecules. Then, the activated membrane was immediately immersed in a 1 wt% aqueous solution of GOD (127 U/mg), buffered at pH 4.75 with 0.1 mol·L⁻¹ MES, for 24 h at 4 °C. After the immobilization of GOD onto the PAAC- grafted PVDF membrane, the membrane was washed repeatedly with deionized water to remove any non-covalently bound GOD enzymes, until no further release of free GOD into the washings was detectable by UV measurement.^[20]

9.2.2 Characterization of Glucose-Responsive Flat Gating Membranes

Fourier transform infrared (FT-IR) spectra of the ungrafted and the PAAC-grafted membranes were measured on a spectrophotometer to ascertain the grafted PAAC formation. FT-IR spectra of ungrafted and PAAC-grafted PVDF membranes are illustrated in **Fig.9.2**.^[20] After grafting PAAC onto the PVDF porous substrate, the peak at 1,715 cm⁻¹ (which is the characteristic peak of PAAC) was enhanced, and two other characteristic peaks of PAAC at 1,453 cm⁻¹ and 800 cm⁻¹ appeared as new in the spectrum compared with that of the ungrafted membrane. The comparison result confirmed that PAAC was grafted on the membrane substrate by plasma-graft pore-filling polymerization.

9.2.3 pH-Responsive Control of the Pore Size of PAAC-Grafted Membranes

The pH-responsive changes in the pore size of membranes with different grafting yields of PAAC were estimated by filtration experiments on aqueous solutions. [20] The hydraulic permeability experiments or filtration experiments of membranes were carried out with trans-membrane pressure being 90 kPa. The diameter of the effective membrane area for filtration was 60 mm. The temperature of the feed solutions, buffered at pH 4 and pH 7 respectively, was controlled at 30 °C using a thermostatic unit. The hydraulic permeability through the ungrafted and the

PAAC-grafted membranes under different pH conditions was investigated by measuring the water flux. To minimize the experimental errors, the flux measurements were carried out three to five times and the arithmetically averaged values were taken as the results under each condition. The pH-responsive change in the pore size of PAAC-g-PVDF membranes could then be calculated according to Hagen-Poiseuille equation. [20]

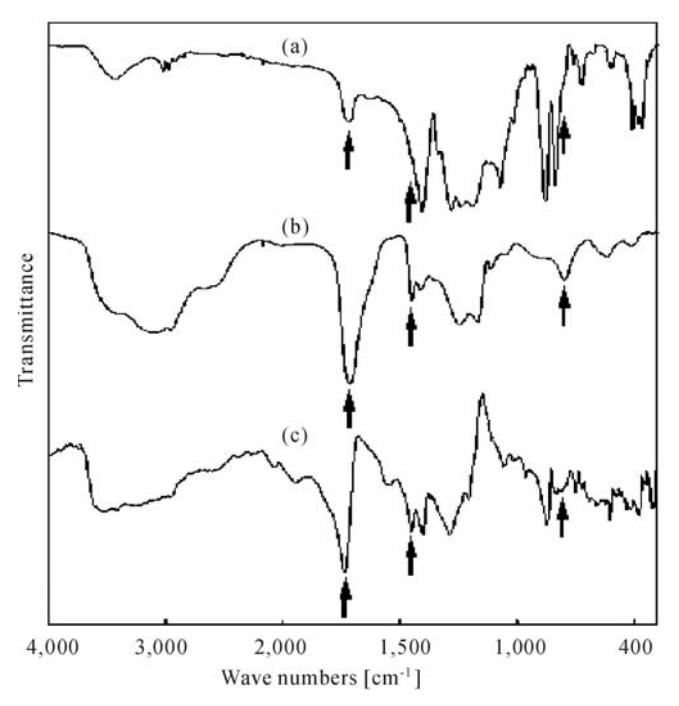


Fig.9.2. FT-IR spectra of (a) ungrafted PVDF membranes; (b) PAAC; (c) PAAC-*g*-PVDF membranes (Reproduced with permission from Ref. [20]). Copyright (2004), Elsevier

Fig.9.3 shows the effect of the PAAC grafting yield on the hydraulic permeability of PAAC-grafted membranes under different pH conditions. [20] The experimental results showed that, for the PAAC-grafted membranes, the water flux at pH=4 was always larger than that at pH=7. At neutral pH, the carboxyl groups of the grafted PAAC chains were dissociated and negatively charged. Therefore, the membrane gates "closed" because the repulsion between negative charges made the PAAC chains extended. As a result, the hydraulic permeability was low. On the other hand, at a pH that was lower than the p K_a of PAAC (about pH 4.58), the carboxylate groups of the grafted PAAC chains were protonated. Therefore, the gates "opened" because of the reduced electrostatic repulsion between the grafted PAAC chains in the pores. As a result, the water flux was large. The grafted PAAC chains in the membrane pores acted as intelligent pH-responsive gates.

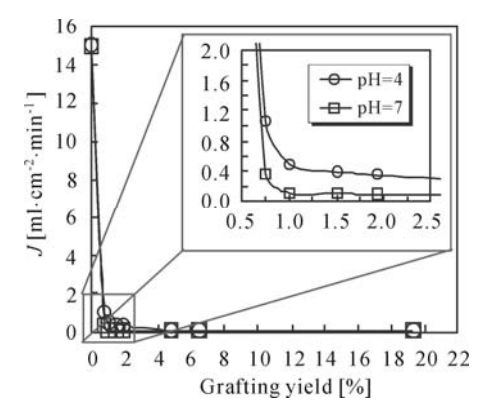


Fig.9.3. Effect of PAAC grafting yield on the pH-controlled water flux (Reproduced with permission from Ref. [20]). Copyright (2004), Elsevier

With an increase in the PAAC grafting yield, the water flux decreased at both pH=4 and pH=7. In the case that too much PAAC was grafted into the pores (*e.g.*, when the grafting yield was larger than 4.5%), the membrane pores could be opened only a little, even when the grafted PAAC chains are in a shrunken state at pH 4. Consequently, the water flux through the membrane became very small with a large grafting yield of PAAC.

The pH-responsive change in the pore size of PAAC-*g*-PVDF membranes can be estimated using the Hagen-Poiseuille equation. According to the Hagen-Poiseuille equation, the water flux of a skinless porous membrane can be expressed as^[20]

$$J = \frac{n\pi d^4 P}{128\eta l} \tag{9.1}$$

where J stands for the water flux [m³·m⁻²·s⁻¹], n for the number of pores per unit area [m⁻²], d for the pore diameter [m], P for the trans-membrane pressure [Pa], η for the viscosity of flowing liquid [Pa·s] and l for the membrane thickness [m].

In a plasma-graft pore-filling membrane, the grafted polymer forms a skin layer on the inner surface of the membrane pore, as described in Section 2.2.1.2. As indicated in Eq.(9.1), the water flux is governed by the fourth power of the pore diameter. Thus, the conformational change in the PAAC chains grafted on the inner surface of the membrane pore, *i.e.* coil-globule, affects the water flux greatly. As known from Eq.(9.1), the ratio of the effective pore diameter of the PAAC-grafted membrane to that of the ungrafted membrane can be evaluated using the measured water fluxes of water with the following formula^[20]

$$R_{\rm d} = \frac{d_{\rm g}}{d_{\rm o}} = \left(\frac{J_{\rm g}}{J_{\rm o}}\right)^{\frac{1}{4}} \tag{9.2}$$

where $R_{\rm d}$ is the ratio of the effective pore diameter of the PAAC-grafted membrane to that of the ungrafted membrane; $d_{\rm g}$ and $d_{\rm o}$ are respectively the effective pore diameters of the PAAC-grafted and ungrafted membranes [m] and $J_{\rm g}$ and $J_{\rm o}$ are the measured water fluxes through PAAC-grafted and ungrafted

membranes respectively [m³·m⁻²·s⁻¹].

Similarly, the ratio of the effective pore diameter of the PAAC-grafted membrane at pH=4 to that at pH=7, which is defined as the pH-responsive gating factor of the membrane pore size, can be calculated using the measured water fluxes and viscosities of water under different pH conditions with the following equation^[20]

$$N_{\text{pH}=4/\text{pH}=7} = \frac{d_{\text{g,pH}=4}}{d_{\text{g,pH}=7}} = \left(\frac{J_{\text{pH}=4}\eta_{\text{pH}=4}}{J_{\text{pH}=7}\eta_{\text{pH}=7}}\right)^{\frac{1}{4}}$$
(9.3)

where $N_{\rm pH=4/pH=7}$ is the pH-responsive gating factor of the membrane pore size; $d_{\rm g,pH=4}$ and $d_{\rm g,pH=7}$ are the effective pore diameters of the PAAC-grafted membranes at pH=4 and pH=7 respectively [m], $J_{\rm pH=4}$ and $J_{\rm pH=7}$ are respectively the measured water fluxes through PAAC-grafted membranes at the environmental pH=4 and pH=7 [m³·m⁻²·s⁻¹] and $\eta_{\rm pH=4}$ and $\eta_{\rm pH=7}$ are the viscosity coefficients of flowing liquid at pH=4 and pH=7 respectively [Pa·s].

The effect of the PAAC grafting yield on the ratio of the effective pore diameter of the PAAC-grafted membrane to that of the ungrafted membrane is shown in **Fig.9.4**.^[20] In a certain lower range of the PAAC grafting yield (*e.g.*, < 2%), the effective pore size of the PAAC-grafted membrane decreased rapidly with an increase in the grafting yield at both pH=4 and pH=7. When the grafting yield increased further, the effective pore diameter of the membrane did not decrease so remarkably any more. As expected, the effective pore size of the PAAC-grafted membrane at pH=4 was always larger than that at pH=7 no matter how large the grafting yield was.

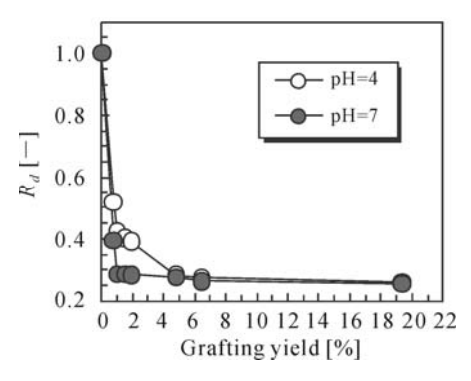


Fig.9.4. Effect of the grafting yield on the pore size of PAAC-grafted membranes under different pH conditions (Reproduced with permission from Ref. [20]). Copyright (2004), Elsevier

The architectures and relatively physicochemical properties of the grafted PAAC chains, such as the length and density of the PAAC chains and the pH-response time of these chains, will change with the variation in the grafting yield. Consequently, the pH-responsive gating characteristics of PAAC grafted membranes with different grafting yields will be different from each other.

Fig.9.5 shows the effect of the grafting yield on the pH-responsive gating

factor of the membrane pore size and the schematic illustration of pH-responsive control of the pore size. [20] For the membrane substrate, the pore size did not change with a variation in the environmental pH. For the PAAC-grafted membranes, the pH-responsive gating factor of the membrane pore size was heavily affected by the grafting yield. When the grafting yield was less than 1.01%, the pH-responsive gating factor of the membrane pore size increased with an increase in the grafting yield. However, when the grafting yield is larger than 4.78%, the pH-responsive gating factor of the membrane pore size tended to 1.0. It can be seen that, only when the grafting yield was less than 4.78%, did the grafted PAAC chains in the membrane pores act as effective pH-responsive gates or adjusting valves. Whereas, when the grafting yield was larger than 4.78%, the length and/or density of the grafted PAAC chains in the membrane pores were too long and/or too large, resulting in the chains losing the function of effective pH-responsive gates or adjusting valves.

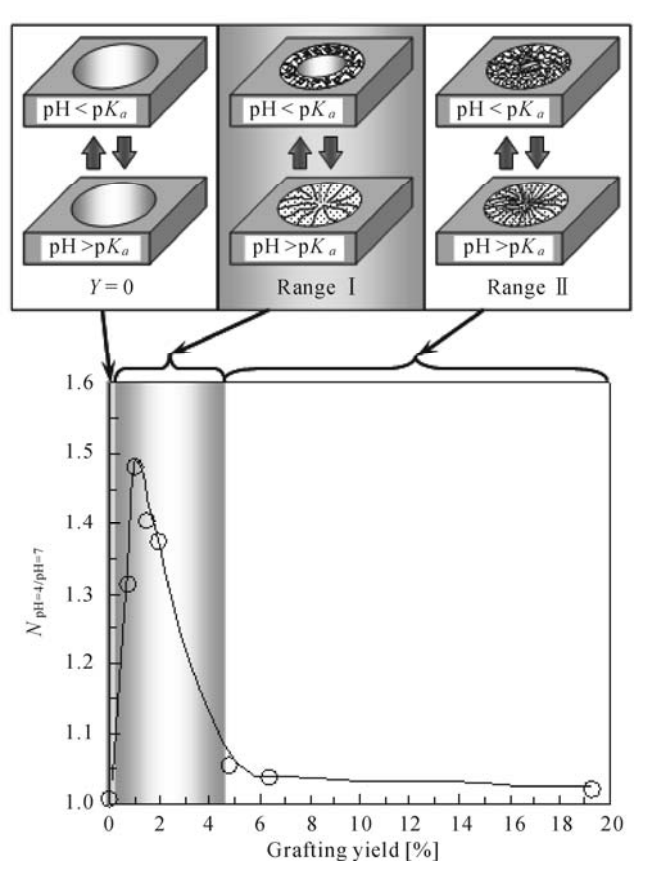


Fig. 9.5. Effect of the grafting yield on the pH-responsive gating factor of membrane pore size and schematic illustration of the pH-responsive control of pore size (Reproduced with permission from Ref. [20]). Copyright (2004), Elsevier

When the grafting yield was too small, the grafted PAAC chains were too short, resulting in small responsivity of the membrane pore size. With an increase in the grafting yield, the length and density of grafted PAAC chains increased, consequently the pH-responsive gating factor of the membrane pore size also increased. However, when the grafting yield increased too much, the grafted PAAC chains became too long and/or too dense and the conformational change in the PAAC chains could not bring any obvious change in the pore size any more. That means the membrane pores had been "choked" by the grafted polymers. The influence of the behavior of the grafting yield on flux responsiveness and on the pH-responsive gating factor of the membrane pore size was similar. This verified again that the pH-responsive flux change in the PAAC-grafted membranes was governed by the pH-responsive gating factor of the membrane pore size. For the environmental stimuli-responsive gating membrane, the larger the responsive gating factor of the membrane pore size, the better the gating property. Therefore, it is very important to design a proper grafting yield to obtain an ideal gating response. In the aforementioned case, it was suggested setting the grafting yield in the range from 0.5% to 3.0% for the membrane to obtain a satisfactory pHresponsive gating property.

9.2.4 Glucose-Responsive Controlled-Release Characteristics

The diffusional permeability experiments of membranes with grafted PAAC and immobilized GOD were carried out using a standard side-by-side diffusion cell. [20] The diffusion cell was located in a constant-temperature water-bath to keep the diffusional temperature constant (30 °C) and the solutions in both the donor and the receptor compartments were magnetically stirred. Each test membrane was immersed in the permeant solution overnight before starting the diffusion experiments. When the solute was sodium chloride, the initial NaCl concentration on the donor side was 0.2 mol·L⁻¹ and well-deionized water was used as the liquid in the receptor cell. The concentration increase in NaCl in the receptor was determined by measuring the electrical conductance with an electrical conductivity meter. When bovine pancreas insulin (28.5 USP units·mg⁻¹) was used as the solute, a 0.1 mol·L⁻¹ Tris-HCl aqueous solution was used as the buffer solution, the initial insulin concentration on the donor side was 0.1 mg mg⁻¹, and pure 0.1 mol·L⁻¹ Tris-HCl-buffered solution was used in the receptor compartment. The concentration increase in insulin in the receptor was measured using a UV-visible recording spectrophotometer at a wavelength of λ =274 nm. The diffusion coefficient of the solute across the membrane can be calculated by Eq.(2.17).

Fig.9.6 shows the effect of the environmental glucose concentration on the diffusional permeation of NaCl through PAAC-grafted and GOD-immobilized PVDF gating membranes with different PAAC grafting yields. [20] When the grafting yield was zero (*i.e.*, the substrate membrane), the environmental glucose concentration almost did not affect the diffusional permeability of solute molecules across the membrane. When the PAAC grafting yield was 1.5%, the diffusional

permeability of NaCl molecules across the membrane was low in the absence of glucose; however, it increased dramatically when the environmental glucose concentration was changed from 0 mol·L⁻¹ to 0.2 mol·L⁻¹. On the other hand, when the grafting yield was as large as 7.5%, the diffusional permeability of NaCl solute across the membrane only increased a little with a change in the environmental glucose concentration from 0 mol·L⁻¹ to 0.2 mol·L⁻¹. From **Fig.9.6** it can be also found that the diffusional permeability of solute across the gating membrane generally decreases with an increase in the PAAC grafting yield.

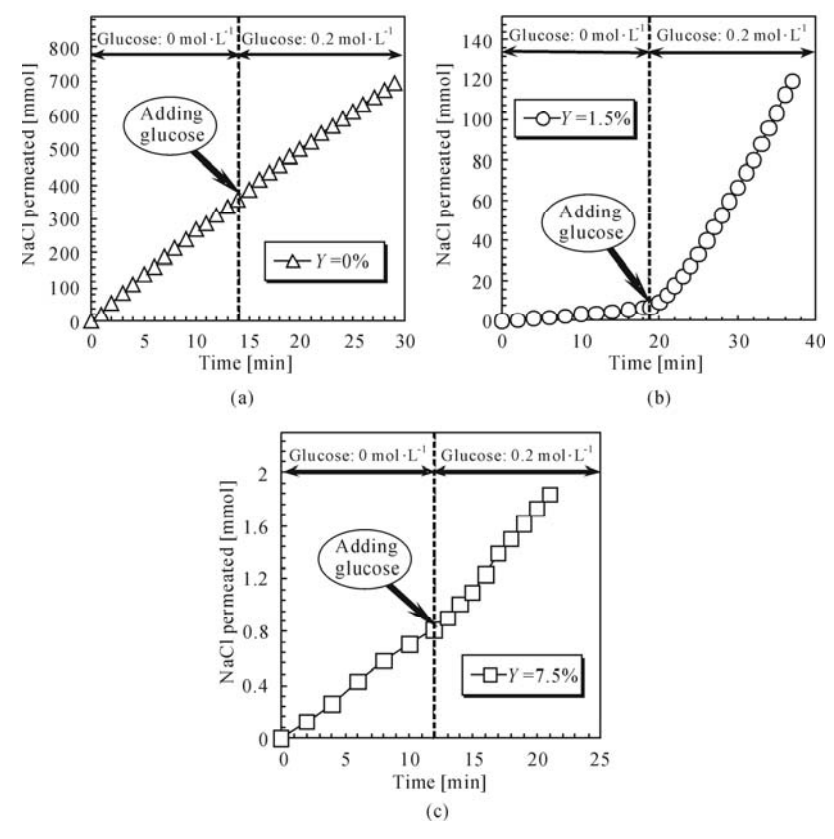


Fig.9.6. Effect of environmental glucose concentration on the diffusional permeation of NaCl through the gating membranes with different PAAC grafting yields: (a) substrate; (b) PAAC grafting yield is 1.5%; (c) PAAC grafting yield is 7.5% (Reproduced with permission from Ref. [20]). Copyright (2004), Elsevier

The prepared glucose-responsive gating membrane was composed of porous PVDF substrate, linear grafted PAAC chains in the pores and covalently bound GOD. The immobilized GOD acted as the glucose sensor and catalyzer; it was sensitive to glucose and catalyzed the glucose conversion to gluconic acid. The stoichiometry of the reaction is described as follows: [3,4,19,22]

Glucose +
$$O_2$$
 + $H_2O \xrightarrow{GOD}$ Gluconic acid + H_2O_2 (9.4)

Because of the appearance of gluconic acid, the local pH decreased in the microenvironment as a result. The linear grafted PAAC chains in the membrane pores acted as the pH-responsive gates or actuators. At neutral pH in the absence of glucose, the carboxyl groups of the grafted PAAC chains were dissociated and negatively charged. Therefore, the membrane gates "closed" because the repulsion between negative charges made the PAAC chains extended. On the other hand, when the glucose concentration increased, GOD catalyzed the oxidation of glucose into gluconic acid, thereby lowering the local pH in the microenvironment, protonating the carboxylate groups of the grafted PAAC chains. Therefore, the gates "opened" because of the shrinkage in the chains resulting from the reduced electrostatic repulsion between the grafted PAAC chains in the pores. Because of the glucose-responsivity of the membrane pore size, the above-mentioned experimental phenomena concerning the glucose-responsive diffusional permeability of solute across the membrane resulted. The results showed that the glucoseresponsivity of the solute diffusional permeability was heavily dependent on the PAAC grafting yield, i.e. the above-mentioned pH-responsive change in the pore size governed the glucose-responsive diffusional permeability.

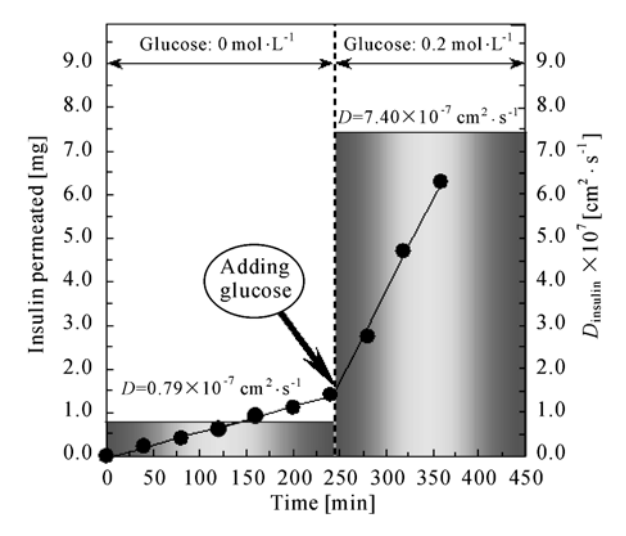


Fig.9.7. Glucose-responsive diffusional permeation of insulin through the proposed gating membrane with PAAC grafting yield of 1.55% (Reproduced with permission from Ref. [20]). Copyright (2004), Elsevier

Fig.9.7 shows the glucose-responsive diffusional permeability of insulin through the proposed gating membrane with PAAC grafting yield of 1.55% caused by glucose addition. [20] In the absence of glucose, the diffusional permeation coefficient of insulin molecules across the membrane was as low as $0.79\times10^{-7}~\rm cm^2\cdot s^{-1}$, and the amount of insulin permeated increased linearly with time. When the environmental glucose concentration was changed from $0~\rm mol\cdot L^{-1}$ to $0.2~\rm mol\cdot L^{-1}$ by adding glucose, the insulin permeation coefficient increased to $7.40\times10^{-7}~\rm cm^2\cdot s^{-1}$ dramatically. The

permeation coefficient after the glucose addition was about 9.37 times that before the addition of glucose. The results presented an exciting glucose-responsive selfregulated permeation of insulin molecules.

9.3 Glucose-Responsive Microcapsule Membranes

In this section, glucose-responsive microcapsule membranes will be introduced.

9.3.1 Design of Glucose-Responsive Microcapsule Membranes

On the basis of the above-mentioned results, the author's group developed a glucose-responsive microcapsule with a porous membrane and glucose-responsive functional gates. The concept of the developed microcapsule is schematically illustrated in **Fig.9.8**. The microcapsule is composed of a porous membrane and linear grafted poly(acrylic acid) (PAAC) chains in the membrane pores and covalently bound glucose oxidase (GOD) enzymes. The linear grafted PAAC chains in the membrane pores act as the pH-responsive gates and the immobilized GOD enzymes act as glucose sensors and catalyzer. At neutral pH in the absence of glucose, the pores in the microcapsule membrane are closed because the repulsion between negative charges makes the PAAC chains extended. On the other hand, when the environmental glucose concentration increases, GOD catalyzes the oxidation of glucose into gluconic acid. As a result the grafted PAAC chains shrink because of the reduced electrostatic repulsion and then the pores open.

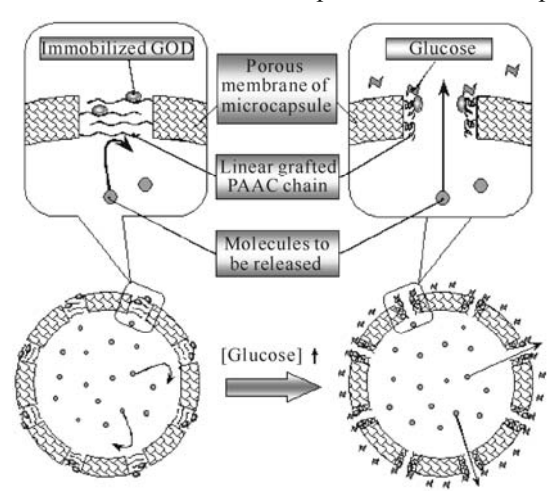


Fig.9.8. Schematic representation of the glucose-responsive release principle of microcapsules with a porous membrane and functional gates (Reproduced with permission from Ref. [21]). Copyright (2004), Elsevier

9.3.2 Preparation of Glucose-Responsive Microcapsule Membranes

The preparation of glucose-responsive microcapsule membranes includes two steps. The first step is to prepare microcapsules with a porous membrane, and the second step is to prepare glucose-responsive gates in the membrane pores.

9.3.2.1 Preparation of Microcapsules with a Porous Membrane

The fabrication of hollow microcapsules with a porous membrane was carried out using the interfacial polymerization method, as described in earlier publications. [23,24] Firstly, 10 ml of the organic solvent mixture of benzene/xylene (2:1 [v·v⁻¹]), containing 0.5 mol·L⁻¹ terephthaloyl dichloride, was added to 160 ml of the water phase containing 1.0 wt% sodium dodecyl sulfate as an emulsifier. Then, the mixture was mechanically agitated for 10 min with a stirring speed of 800 r·min⁻¹ to yield an oil-in-water emulsion. The stirring speed was then reduced to 200 r·min⁻¹ and both the buffer (20 ml water containing 1.18 mol·L⁻¹ sodium carbonate) and 15 ml of monomer ethylene diamine were added to the emulsion and the mixture stirred for a further 5 min. During emulsification and interfacial polymerization, the temperature was kept at a constant 10 °C using a thermostatic unit. The microcapsules were separated by centrifugation and washed three times using deionized water to remove any emulsifier and remnants of the monomer. These were then dialyzed against deionized water and freeze-dried.

9.3.2.2 Grafting PAAC Gates in the Membrane Pores of Microcapsules

Plasma-graft pore-filling polymerization was employed to graft linear PAAC chains into the pores of the microcapsule membranes according to the method described in Section 2.2.1.1. Briefly, the freeze-dried microcapsules were put into a transparent glass tube, which was then filled with argon gas. The tube was then evacuated to a pressure of 10 Pa and the microcapsules were subjected to radio-frequency plasma operating at 13.56 MHz, delivering 30 W for 60 s. Next, under inert atmosphere conditions, the microcapsules were immersed into the AAC monomer solution and the graft polymerization was carried out under vibration in a constant-temperature bath (30 °C) for a fixed period. The PAAC-grafted microcapsules were separated centrifugally, washed three times with deionized water, dialyzed against deionized water and then freeze-dried.

9.3.2.3 Preparation of Glucose-Responsive Microcapsules by Immobilizing GOD

The immobilization of GOD enzymes onto the PAAC-grafted microcapsule

membranes was carried out according to the above-mentioned carbodiimide method. [12] Briefly, the PAAC-grafted microcapsules were immersed in a 10 wt% aqueous solution of 1-(3-dimethyl-aminopropyl)-3-ethylcarbodiimide hydrochloride, which is a water-soluble carbodiimide (WSC), for 1 h at 4 °C. This WSC solution was buffered at pH 4.75 with 0.1 mol·L⁻¹ MES. After being activated, the microcapsules were rapidly washed three times with the MES buffer solution. Then, the activated microcapsules were immediately immersed in a 1 wt% aqueous solution of GOD, buffered at pH 4.75 with 0.1 mol·L⁻¹ MES, for 24 h at 4 °C. After the immobilization of GOD onto the PAAC-grafted microcapsules, the microcapsules were washed repeatedly with deionized water to remove any non-covalently bound GOD enzymes, until no further release of free GOD into the washings was detectable by UV measurement. Then, the validity of the GOD immobilization onto the PAAC-grafted microcapsule membranes was verified by using a fluorescamine method as described by Ito et al.[12] The GOD-immobilized microcapsules were washed in 6 mol·L⁻¹ hydrochloric acid for 12 h and then the resulting acidic solution containing degraded GOD was neutralized with 6-mol·L⁻¹ NaOH. After dilution, the solution was buffered to pH 9.25. Under vigorous stirring with a vortex mixer, a fluorescamine solution (5.2 mg dissolved in 25 ml of acetone) was added and the fluorescence intensity was measured. A stock solution of GOD was prepared and measured to establish the calibration curve. The wavelengths of excitation and emission were 390 and 490 nm, respectively.

9.3.3 Characterization of Glucose-Responsive Microcapsule Membranes

In order to observe the microscopic configuration of microcapsules, a scanning electron microscope (SEM, JSM-5900LV) was used. Fourier transform infrared (FT-IR) spectra of the ungrafted and PAAC-grafted microcapsules were measured on a spectro-photometer (Spectrum one), to ascertain the grafted PAAC formation.

Fig.9.9 shows SEM micrographs of the outer surface and cross-sectional view of microcapsules.^[21] The polyamide microcapsules were shown to have asymmetrical and porous membrane structures; the outer surface (the water side in the interfacial polymerization) was smooth and the inner surface (the organic side) was rough. This reflects the fact that the interfacial polymerization proceeds by the diffusion of the amine compounds from the aqueous to the organic phase. Because of the porous membrane and the smooth outer surface, the microcapsule was suitable for use as the substrate for preparing the glucose-responsive microcapsule by fabricating functional gates in the membrane pores.

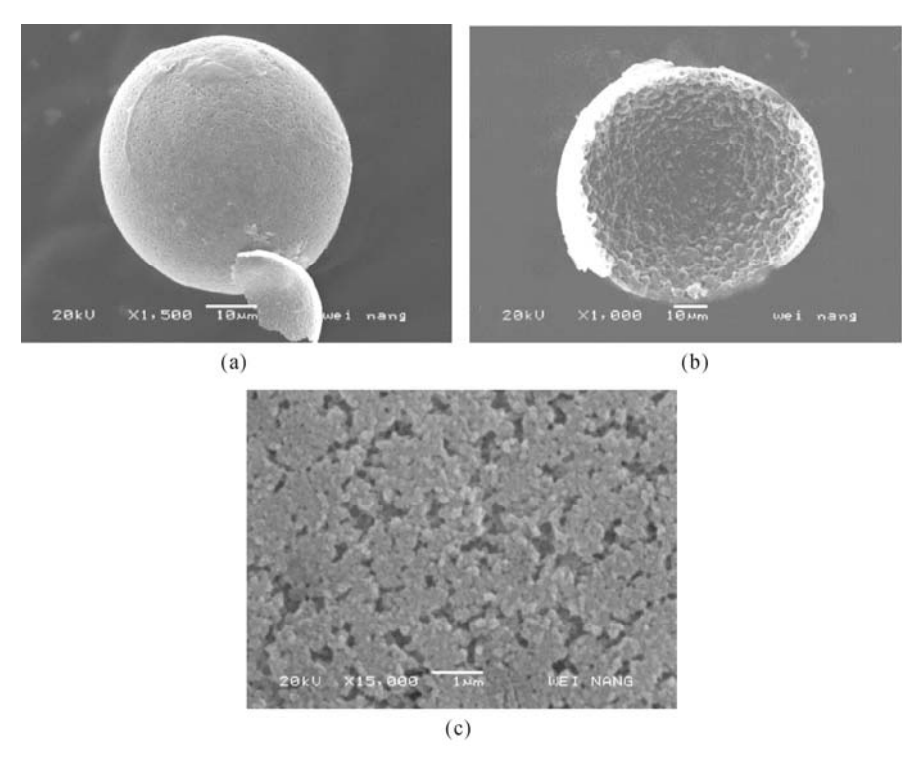


Fig. 9.9. SEM micrographs of microcapsules. (a) Outer surface; (b) Cross-section; (c) Enlarged image of outer surface (Reproduced with permission from Ref. [21]). Copyright (2004), Elsevier

Fig.9.10 shows the KBr FT-IR spectra of the ungrafted and PAAC-grafted microcapsules. ^[21] Compared to the FT-IR spectrum of the ungrafted microcapsules, the spectra of the PAAC-grafted microcapsules show two fresh peaks at 1,715 cm⁻¹ and 1,453 cm⁻¹, in which the absorption peak at 1,715 cm⁻¹ belongs to the carboxyl groups of PAAC. These experimental observations confirm the graft polymerization of PAAC onto the porous microcapsule membranes by plasma- graft pore-filling polymerization.

9.3.4 Glucose-Responsive Controlled-Release Characteristics of Microcapsules

The microcapsule release experiments were carried out using a previously published method as described in Section 3.2.3. [23,24] Sodium chloride and vitamin B_{12} were selected as the model drug solutes to be released. [21] The freeze-dried microcapsules were dialyzed against aqueous NaCl or VB_{12} with a known concentration for more than 3 d to load the solute inside the microcapsules. The dialysis was carried out in a shaking constant-temperature bath kept at 30 °C. The release of the solute from

the microcapsules was measured by determining the increase in the solute concentration of the surrounding medium with time, after mixing a known volume of microcapsule dispersion, with a known solute concentration, with the same volume of deionized water. After a certain period of time, glucose was added to the surrounding solution at a concentration of 0.2 mol·L⁻¹. During the measurements, the temperature of the liquids was kept constant at 30 °C using a thermostatic unit. The concentration of sodium chloride was determined by measuring the electrical conductance with an electrical conductivity meter and the concentrations of VB $_{\rm 12}$ were determined using a UV-visible recording spectrophotometer at wavelengths of $\lambda = 361$ nm.

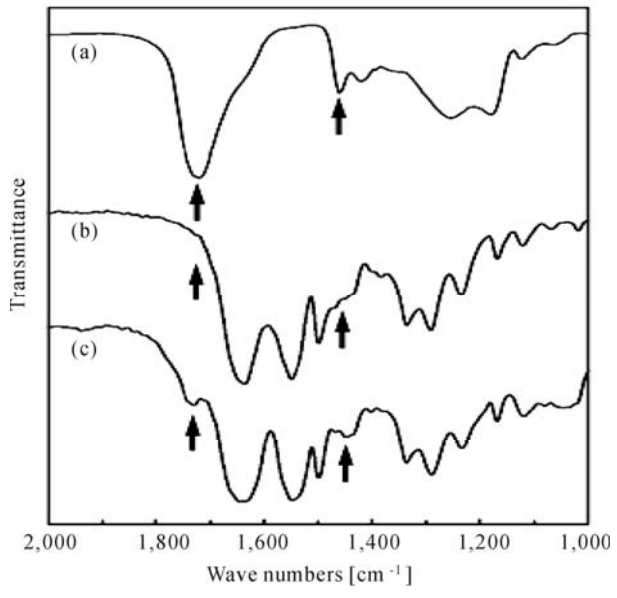


Fig. 9.10. KBr FT-IR spectra of (a) PAAC, (b) ungrafted microcapsules, (c) PAAC-grafted microcapsules (Reproduced with permission from Ref. [21]). Copyright (2004), Elsevier

Fig.9.11 shows the glucose-responsive release results of sodium chloride from the ungrafted and the PAAC-grafted and GOD-immobilized microcapsules. [21] For the fabricated microcapsules with a porous membrane and linear grafted PAAC chains in the membrane pores and covalently bound GOD enzymes, when deionized water was used as the environmental solution, *i.e.* in the absence of glucose, the release of sodium chloride molecules from the microcapsules was slow. In contrast, when the environmental glucose concentration was changed from 0 mol·L⁻¹ to 0.2 mol·L⁻¹ by adding glucose in the surrounding solution, the release rate suddenly increased significantly. The diffusional permeation coefficient after the glucose addition was about 7.9 times that before the addition of glucose. On the other hand, the ungrafted microcapsules did not show such a sharp transition in the release rate during the same change in the chemical environments. This is because the immobilized GOD was sensitive to glucose and

catalyzed the glucose conversion to gluconic acid, and the appearance of gluconic acid resulted in the decrease in pH in the microenvironment, thus causing the grafted PAAC gates to shrink. Consequently, before adding glucose to the environmental solution, the pores of the PAAC-grafted and GOD-immobilized microcapsule membrane were closed, because the carboxyl groups of the grafted PAAC chains were dissociated and negatively charged. Therefore, the repulsion between negative charges made the PAAC chains extended, resulting in a low release rate. In contrast, after adding glucose to the surrounding solution, the pores of the PAAC-grafted and GOD-immobilized microcapsule membrane were suddenly open, because GOD catalyzed the oxidation of glucose into gluconic acid, thereby lowering the pH in the microenvironment, protonating the carboxylate groups of the grafted PAAC chains. Therefore, the grafted PAAC chains in the pores shrunk, owing to the reduced electrostatic repulsion, and then a high release rate resulted (as illustrated in Fig.9.8).

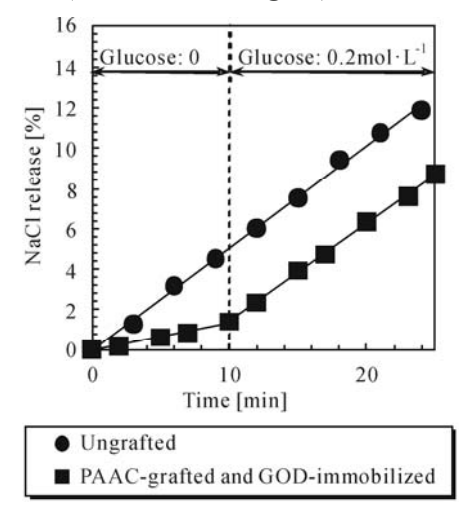


Fig.9.11. Glucose-responsive release of sodium chloride from different microcapsules (Reproduced with permission from Ref. [21]). Copyright (2004), Elsevier

To verify the reversibility of the functional gates in the pores of the microcapsule membrane, release experiments of VB₁₂ were also carried out by using the same microcapsules repeatedly.^[21] The microcapsules were washed with, and dialyzed against, deionized water after the first run, *i.e.*, the release experiments of NaCl. Then, the solute VB₁₂ was reloaded into the inner space of the microcapsules before the second run of release experiments. The glucoseresponsive release characteristics of VB₁₂ from the ungrafted and the PAAC-grafted and GOD-immobilized microcapsules are illustrated in **Fig.9.12**.^[21] For VB₁₂, the same glucose-responsive release property of the microcapsules was also observed as the above-mentioned one for the NaCl release. For the PAAC-grafted and GOD-immobilized microcapsules, when deionized water was the environmental solution, the release of VB₁₂ molecules from the microcapsules was slow; when

the environmental glucose concentration was increased from 0 mol·L⁻¹ to 0.2 mol·L⁻¹, the release rate suddenly increased significantly and the diffusional permeability was about 6.0 times that before the addition of glucose. However, the ungrafted microcapsules did not show such a sharp transition in the release rate under the same experimental conditions. The results indicated that the glucose-responsive release from the fabricated microcapsules was reversible, suggesting that the functional gates retained their gel properties intact, even though they underwent repeated changes in the environmental chemical signal.

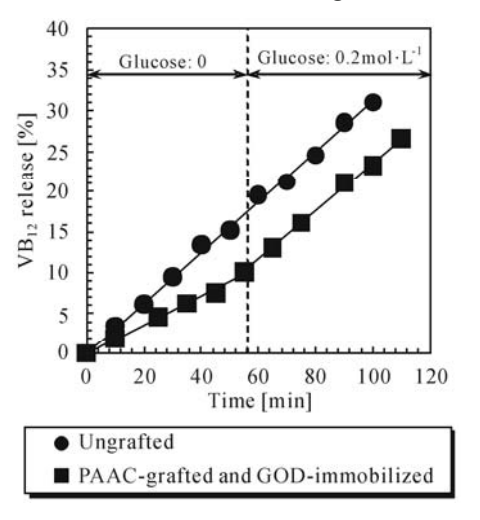


Fig. 9.12. Glucose-responsive release of Vitamin B₁₂ from different microcapsules (Reproduced with permission from Ref. [21]). Copyright (2004), Elsevier

9.4 Summary

In summary, glucose-responsive flat and microcapsule membranes with plasmagrafted PAAC gates and immobilized GOD are described in this chapter. The glucose-responsivity of the solute diffusional permeability through the proposed membranes was heavily dependent on the PAAC grafting yield, because the pH-responsive change in pore size governed the glucose-responsive diffusional permeability. It is very important to design a proper grafting yield to obtain a satisfactory gating response. The prepared PAAC-grafted and GOD-immobilized membranes showed reversible glucose-responsive release characteristics. On the one hand, such membranes provide promising candidates for self-regulated drug delivery systems having the capability of adapting the release rate of drugs such as insulin in response to changes in glucose concentration in order to keep the blood glucose levels within the normal range, which is highly attractive for diabetes therapy. On the other hand, it is still difficult to maintain the activity of GOD enzymes for a long time. Therefore, non-enzyme-based glucose-responsive materials [25,26]

are being considered as alternative promising material candidates for fabricating glucose-responsive gates in membrane pores.

References

- [1] Langer R. Drug delivery and targeting. *Nature*, **1998**, *392*: 5-10.
- [2] Chu L Y. Controlled release systems for insulin delivery. *Expert Opinion on Therapeutic Patents*, **2005**, *15*: 1147-1155.
- [3] Zhang K, Wu X Y. Modulated insulin permeation across a glucose-sensitive polymeric composite membrane. *Journal of Controlled Release*, **2002**, *80*: 169-178.
- [4] Traitel T, Cohen Y, Kost J. Characterization of glucose sensitive insulin release systems in simulated *in vivo* conditions. *Biomaterials*, **2000**, *21*: 1679-1687.
- [5] Brownlee M, Cerami A. A glucose-controlled insulin delivery system: semisynthetic insulin bound to lectin. *Science*, **1979**, *206*: 1190-1191.
- [6] Brownlee M, Cerami A. Glycosylated insulin complexed to concanavalin A. Biochemical basis for a closed-loop insulin delivery system. *Diabetes*, **1983**, *32*: 499-504.
- [7] Jeong S Y, Kim S W, Eenink M J D, Feijen J. Self-regulating insulin delivery systems. I. Synthesis and characterization of glycosylated insulin. *Journal of Controlled Release*, **1984**, *1*: 57-66.
- [8] Sato S, Jeong S Y, McRea J C, Kim S W. Self-regulating insulin delivery systems. II. In vitro studies. *Journal of Controlled Release*, **1984**, *1*: 67-77.
- [9] Jeong S Y, Kim S W, Holemberg D, McRea J C. Self-regulating insulin delivery systems. III. In vivo studies. *Journal of Controlled Release*, **1985**, *2*: 143-152.
- [10] Albin G, Horbett T A, Ratner B D. Glucose sensitive membranes for controlled delivery of insulin: insulin transport studies. *Journal of Controlled Release*, **1985**, *2*: 153-164.
- [11] Kost J, Horbett T A, Ratner B D, Singh M. Glucose sensitive membranes containing glucose oxidase: activity, swelling and permeability studies. *Journal of Biomedical Materials Research*, **1985**, *19*: 1117-1133.
- [12] Ito Y, Casolaro M, Kono K, Imanishi Y. An insulin-releasing system that is responsive to glucose. *Journal of Controlled Release*, **1989**, *10*: 195-203.
- [13] Siegel R A, Firestone B A. Mechanochemical approaches to self-regulating insulin pump design. *Journal of Controlled Release*, **1989**, *11*: 181-192.
- [14] Albin G, Horbett T A, Ratner B D. Glucose-sensitive membranes for controlled release of insulin. In: J. Kost (Ed.), *Pulsed and Self-regulated Drug Delivery*. CRC Press, Boca Raton, FL, **1990**.
- [15] Makino M, Mack E J, Okano T, Kim S W. A microcapsule self-regulating delivery system for insulin. *Journal of Controlled Release*, 1990, 12: 235-239.

- [16] Kitano S, Koyama Y, Kataoka K, Okano T, Sakurai Y. A novel drug delivery system utilizing a glucose responsive polymer complex between poly(vinyl alcohol) and poly(*N*-vinyl-2-pyrrolidone) with a phenylboronic acid moiety. *Journal of Controlled Release*, **1992**, *19*: 162-170.
- [17] Imanishi Y, Ito Y. Glucose-sensitive insulin-releasing molecular systems. *Pure & Applied Chemistry*, **1995**, *67*: 2015-2021.
- [18] Cartier S, Horbett T, Ratner B D. Glucose-sensitive membrane coated porous filters for control of hydraulic permeability and insulin delivery from a pressurized reservoir. *Journal of Membrane Science*, **1995**, *106*: 17-24.
- [19] Kang S I, Bae Y H. A sulfonamide based glucose-responsive hydrogel with covalently immobilized glucose oxidase and catalase. *Journal of Controlled Release*, **2003**, *86*: 115-121.
- [20] Chu L Y, Li Y, Zhu J H, Wang H D, Liang Y J. Control of pore size and permeability of a glucose-responsive gating membrane for insulin delivery. *Journal of Controlled Release*, **2004**, *97*: 43-53.
- [21] Chu L Y, Liang Y J, Chen W M, Ju X J, Wang H D. Preparation of glucose-sensitive microcapsules with a porous membrane and functional gates. *Colloids and Surfaces B: Biointerfaces*, **2004**, *37*: 9-14.
- [22] Podual K, Doyle III F J, Peppas N A. Preparation and dynamic response of cationic copolymer hydrogels containing glucose oxidase. *Polymer*, **2000**, *41*: 3975-3983.
- [23] Chu L Y, Park S H, Yamaguchi T, Nakao S. Preparation of thermoresponsive core-shell microcapsules with a porous membrane and poly(N-isopropylacrylamide) gates. *Journal of Membrane Science*, **2001**, *192*: 27-39.
- [24] Chu L Y, Park S H, Yamaguchi T, Nakao S. Preparation of small-sized monodispersed thermo-responsive core-shell microcapsules. *Langmuir*, **2002**, *18*: 1856-1864.
- [25] Zhang S B, Chu L Y, Xu D, Zhang J, Ju X J, Xie R. Poly(*N*-isopropylacrylamide)-based comb-type grafted hydrogel with rapid response to blood glucose concentration change at physiological temperature. *Polymers for Advanced Technologies*, **2008**, *19*: 937-743.
- [26] Samoei G K, Wang W H, Escobedo J O, Xu X Y, Schneider H J, Cook R L, Strongin R M. A chemomechanical polymer that functions in blood plasma with high glucose selectivity. *Angewandte Chemie-International Edition*, **2006**, *45*: 5319-5322.

Molecular-Recognizable Smart Membranes

In this chapter, the design, fabrication and performance of molecular-recognizable smart membranes with either β -cyclodextrin (CD) or crown ether as molecular recognizing receptor and with poly(N-isopropylacrylamide) (PNIPAM) as actuator are introduced. Both flat and microcapsule membranes with molecular-recognizable smart gates and microcapsules with molecular-recognizable smart hydrogel membranes are developed for different purposes. For the membranes with molecular-recognizable smart gates, the gates in the membrane pores can open or close by recognizing specific molecules or ions; for the microcapsules with crosslinked hydrogel membranes, the membranes swell or shrink isothermally by recognizing specific molecules or ions.

10.1 Introduction

As described in Section 1.3.4, molecular-recognizable smart materials can be designed with poly(N-isopropylacrylamide) (PNIPAM) as actuator and crown ether or cyclodextrin as molecular recognizing receptor. By using such molecularrecognizable smart materials, molecular-recognition gating membranes can be achieved, which are usually fabricated by suspending molecular-recognizable host molecules onto the freely mobile ends of grafted PNIPAM polymers in the membrane pores. The molecular-recognizable molecules acting as sensors can recognize special guest molecules, while the linear grafted thermo-responsive PNIPAM polymers acting as actuators can transform their conformation after the sensors recognize the guest molecules. As a result, the cooperation between the sensors and the actuators achieves the switching function of molecular-recognizable gating membranes. Recently, the author's group developed molecular-recognizable smart membranes with either β -cyclodextrins (CD) or crown ethers as host molecules. [1-3] In this chapter, molecular-recognizable smart membranes with PNIPAM as actuator and with CD or crown ether as host molecule will be introduced respectively, and the membrane form goes from a flat membrane to microcapsule membrane.

10.2 Molecular-Recognizable Smart Membranes with β -CDs as Host Molecules

In this section, molecular-recognizable smart membranes with β -CDs as host molecules will be introduced.

10.2.1 Design of Molecular-Recognizable Gating Membranes with β-CDs as Host Molecules

The concept of the molecular-recognizable gating membrane with β -CD as molecular recognizing receptor and PNIPAM as actuator is schematically illustrated in Fig.10.1.[1] PNIPAM is a thermo-responsive polymer with an LCST around 32 °C. [4] When the temperature is below the LCST, PNIPAM is in a swollen and hydrophilic state in water, while it is in a shrunken and hydrophobic state when the temperature is above the LCST. β -CD molecules possess hydrophobic cavities and hydrophilic external surfaces. Through a series of weak intermolecular forces, such as hydrophobic, electrostatic and hydrogen-bonding interactions, β -CD is capable of selectively associating with a guest molecule having a similar size to its cavity. [5] Due to both the thermo-responsive phase transition of PNIPAM and the molecularrecognition of β -CD, the designed functional gate can achieve gating functions as follows. (1) Thermo-responsive gating function: When the temperature is below the LCST of the grafted copolymer in water (LCST_a), the grafted chains are in a swollen state, while they turn to a shrunken state when the temperature is above the LCST_a. As a result, the membrane shows reversible thermo-responsive gating characteristics when the temperature changes across the LCST_a (2) Molecularrecognition "open" function: When guest molecules with a hydrophobic side group (e.g., 8-anilino-1-naphthalenesulfonic acid ammonium salt (ANS)) are present, β -CD moieties recognize and form complexes with guest ANS molecules and, as a result, the LCST of grafted copolymers in ANS aqueous solution shifts to a lower value (LCST_b) due to the hydrophobic phenyl group of ANS outside the β -CD cavity after forming β -CD/ANS complexation. [6,7] Therefore, because of molecular recognition of ANS, the phase transition of the grafted chains can occur isothermally at a temperature between the LCST_a and LCST_b (e.g., T_1). As a result, the membrane gates switch from a "closed" state in water to an "open" state in ANS aqueous solution isothermally at T_1 . (3) Molecular-recognition "closed" function: When different guest molecules with a hydrophilic side group or without side group (e.g., 2-naphthalenesulfonic acid (NS)) are present in the environmental solution, the LCST of grafted copolymers shifts to a higher temperature (LCST_c). This is because the complexation between β -CD and NS slightly enlarges the hydrophilic moiety of copolymers due to the dissociation of NS molecules in the water. [7] Therefore, because of molecular recognition of NS, the phase transition of grafted

chains can occur isothermally at a temperature between the LCST_a and LCST_c (e.g., T_2). As a result, the membrane gates switch from "open" state in water to "closed" state in NS aqueous solution isothermally at T_2 .

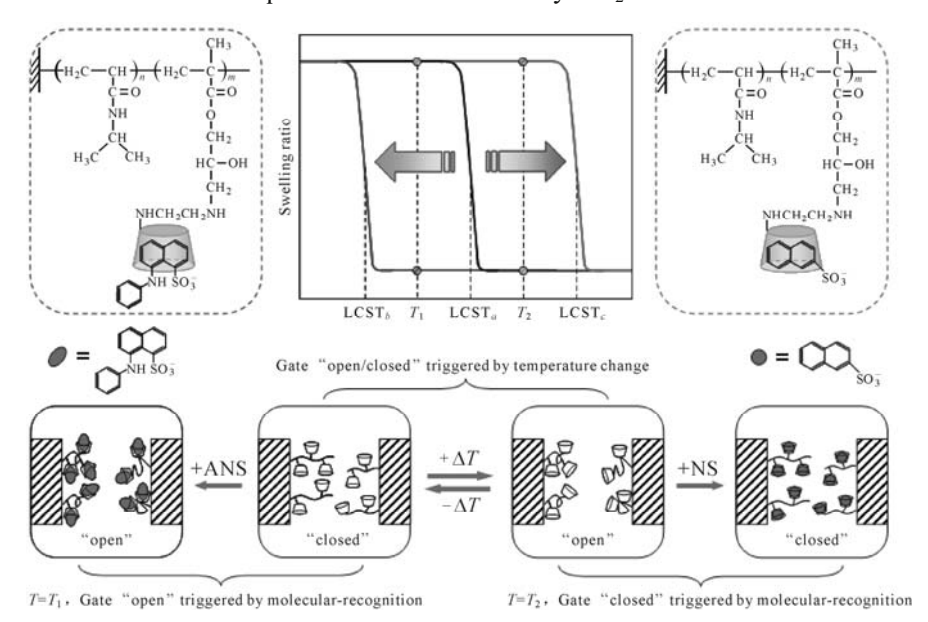


Fig.10.1. Schematic illustration of the molecular-recognizable gating membrane with β -CD as molecular recognizing receptor and PNIPAM as actuator (Reproduced with permission from Ref. [1]). Copyright (2010), Elsevier

10.2.2 Fabrication of Molecular-Recognizable Gating Membranes with β-CDs as Host Molecules

Fabrication of molecular-recognizable gating membranes with β -CDs as host molecules includes the preparation of modified β -CD moieties and the preparation of molecular-recognizable gating membranes.

10.2.2.1 Preparation of Modified β-CD Moieties

Mono-6-Ots- β -CD was synthesized according to a published method.^[8] The melting point of obtained Mono-6-Ots- β -CD was 178~179 °C; ¹H NMR (300 MHz, DMSO-d₆): δ =7.75 (d, H²), δ =7.43 (d, H²), δ =5.87~5.65 (m, H¹⁴), δ =4.84~4.77 (d, H⁶), δ =2.43 (s, H³) ppm.

Synthesis of Mono-6-deoxy-6-ethylene diamino- β -CD (ECD) was carried out according to a reported method. ^[9] The melting point of obtained ECD was 248~249 °C; ¹H NMR (300 MHz, D₂O): δ =5.01 (s, H⁷), δ =3.99~3.88 (m, H²⁸),

 δ =3.67~3.45 (m, H¹⁴), δ =2.83~2.78 (m, H²) ppm; IR (KBr): 3381 cm⁻¹ (s, OH), 2927 cm⁻¹ (w, CH₂), 1030 cm⁻¹(s, C-OH).

10.2.2.2 Preparation of Molecular-Recognizable Gating Membranes

Preparation of molecular-recognizable gating membranes was carried out in two steps. [1] Firstly, plasma-graft pore-filling polymerization was employed to graft linear poly(NIPAM-co-glycidyl methacrylate) (poly(NIPAM-co-GMA), PNG) chains onto inner surfaces of membrane pores in Nylon-6 membrane substrates (with an average pore size of 0.22 µm) according to the method described in Section 2.2.1.1. Then, modified β -CD moieties (Mono-6-deoxy-6-ethylene diamino- β -CD, ECD) were appended onto the grafted PNG copolymer chains by chemical reaction. The reaction was conducted in 1,4-dioxane/water (1:1 v/v) solution mixture. Due to the shielding effect of macromolecular chains on epoxy groups and the steric hindrance of β -CD, the grafting was performed in the presence of an excess amount of ECD (2:1, β -CD/epoxy groups). [10] According to the grafting yield of the first step, a fixed amount of ECD was dissolved in the 1,4-dioxane/water solution mixture and then PNG-grafted membranes were immersed in the solution. Consequently, the grafting polymerization took place in a shaking constant-temperature bath at 60 °C for 48 h. The grafted membrane was also rinsed with deionized water under vibration in a constant-temperature bath (30 °C) for 24 h to remove any non-reacted monomer, and then was dried in an oven at 50 °C overnight.

In the plasma-graft pore-filling polymerization, NIPAM and GMA were used as monomers and the grafted copolymer was PNG. The grafting yield (*Y*) of the membrane was defined as the weight increase of the membrane after grafting and was calculated according to the following equation:

$$Y_{\rm PNG} = \frac{W_1 - W_0}{4} \tag{10.1}$$

where Y_{PNG} stands for the grafting yield of PNG on the membrane substrate [mg·cm⁻²], A for the area of the membrane [cm²] and W_1 and W_0 for the mass of the membrane after and before grafting respectively [mg].

The relationship of Y_{PNIPAM} , Y_{PGMA} and Y_{PNG} could be expressed as follows:

$$Y_{\text{PNIPAM}} + Y_{\text{PGMA}} = Y_{\text{PNG}} \tag{10.2}$$

$$\frac{Y_{\text{PNIPAM}}}{Y_{\text{PGMA}}} = \frac{M_{\text{NIPAM}} \times N_{\text{PNIPAM}}}{M_{\text{GMA}} \times N_{\text{PGMA}}}$$
(10.3)

where $Y_{\rm PNIPAM}$ and $Y_{\rm PGMA}$ stand for the grafting yields of PNIPAM and poly (glycidyl methacrylate) (PGMA) on the membrane substrates respectively [mg·cm⁻²], $M_{\rm NIPAM}$ and $M_{\rm GMA}$ for the molecular weights of NIPAM and GMA [g/mol] and $N_{\rm PNIPAM}$ and $N_{\rm PGMA}$ for the masses of PNIPAM and PGMA in the grafted copolymer PNG [mol].

According to the results of X-ray photoelectron spectroscopy (XPS) spectra, it was found that the molar ratio of PNIPAM and PGMA in PNG was approximately

consistent with that of the feed molar ratio, *i.e.*, $N_{\text{PNIPAM}}/N_{\text{PGMA}}$ were almost equal to a fixed α value. Thus, Y_{PNIPAM} could be calculated as follows:

$$\alpha = \frac{N_{\text{PNIPAM}}}{N_{\text{PGMA}}} \tag{10.4}$$

$$Y_{\text{PNIPAM}} = \frac{Y_{\text{PNG}}}{1 + M_{\text{GMA}} / \alpha M_{\text{NIPAM}}}$$
(10.5)

In the chemical grafting polymerization, the grafting yield of CD was also defined as the weight increase of the membrane after grafting of CD and was calculated by the following equation:

$$Y_{\rm CD} = \frac{W_2 - W_1}{A} \tag{10.6}$$

where $Y_{\rm CD}$ stands for the grafting yield of CD on the membrane substrate [mg·cm⁻²], A for the area of the membrane [cm²] and W_2 and W_1 for the mass of the membrane after and before CD grafting respectively [mg].

A series of membranes with different grafting yields and different α values could be prepared by adjusting the monomer concentration, the polymerization time and the feed molar ratio of $N_{\text{NIPAM}}/N_{\text{GMA}}$ during the membrane fabrication.

10.2.3 Componential and Morphological Characterization of Membranes

Cross-sectional structures of ungrafted and grafted membranes were characterized using a scanning electron microscope (SEM, JSM-5900LV, JEOL, Japan) operated at an accelerating voltage of 20 kV. SEM samples were prepared by freezing the membranes in liquid nitrogen for enough time, fracturing them mechanically and then sticking them into the sample holder. The FT-IR spectra of membranes were measured with a Fourier transform infrared spectrometer (FT-IR, IR Prestige-21, Shimadzu) using the attenuated total reflection (ATR) method.

Fig.10.2 shows SEM images of cross-sectional views of an ungrafted porous Nylon-6 substrate membrane and a PNG-CD grafted Nylon-6 membrane with grafting yields of $Y_{\rm PNIPAM}=131~{\rm mg\cdot cm^{-2}}/Y_{\rm CD}=62~{\rm mg\cdot cm^{-2}}.^{[1]}$ From the cross-sections of ungrafted (**Fig.10.2a**) and PNG-CD-grafted (**Fig.10.2b**) membranes, we can see that their structures are quite different. The ungrafted Nylon-6 membrane is constructed with a thin functional porous top layer, and the honeycombed pores can be clearly seen (**Fig.10.2a**). After grafting of PNG-CD onto the inner pore surfaces of the porous Nylon-6 membrane, the membrane pore size decreases (**Fig.10.2b**). The grafted polymers are obviously formed inside the pores throughout the entire membrane thickness. That means the functional polymer chains have been grafted onto the porous membrane substrates as expected.

Fig.10.3 shows the FT-IR spectra of both an ungrafted Nylon-6 substrate membrane and PNG-CD grafted Nylon-6 membrane with grafting yields of

 $Y_{\rm PNIPAM}$ =220 mg·cm⁻²/ $Y_{\rm CD}$ =37 mg·cm⁻². [1] Curve a) clearly shows a strong C=O stretching vibration around 1,650 cm⁻¹ and a N-H deformation vibration around 1,550 cm⁻¹, which are characteristic of ungrafted Nylon-6 substrate membranes. However, in the IR characteristic absorptions of the PNG-CD grafted membrane (curve b)), we clearly observe a strong C=O stretching vibration at a wave number of 1720 cm⁻¹, characteristic of the carbonyl group of GMA, and double peaks at 1,388 and 1,366 cm⁻¹, characteristic of the isopropyl group of NIPAM. In addition, there is a strong C-O-C characteristic stretching vibration around 1,030 cm⁻¹, characteristic of CD units. These results demonstrate that the designed PNG-CD functional polymer has been successfully grafted onto the porous Nylon-6 substrate membrane.

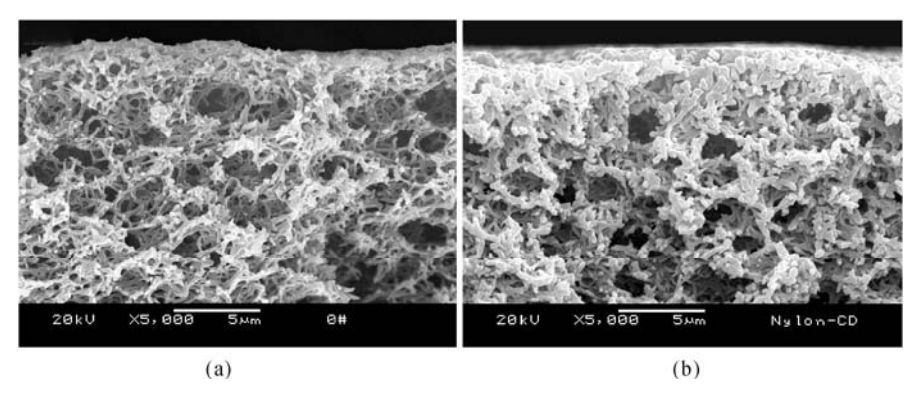


Fig.10.2. SEM images of the cross-sectional views of (a) ungrafted porous Nylon-6 substrate membrane; (b) PNG-CD-grafted Nylon-6 membrane with $Y_{\text{PNIPAM}}=131 \text{ mg} \cdot \text{cm}^{-2}/Y_{\text{CD}}=62 \text{ mg} \cdot \text{cm}^{-2}$ (Reproduced with permission from Ref. [1]). Copyright (2010), Elsevier

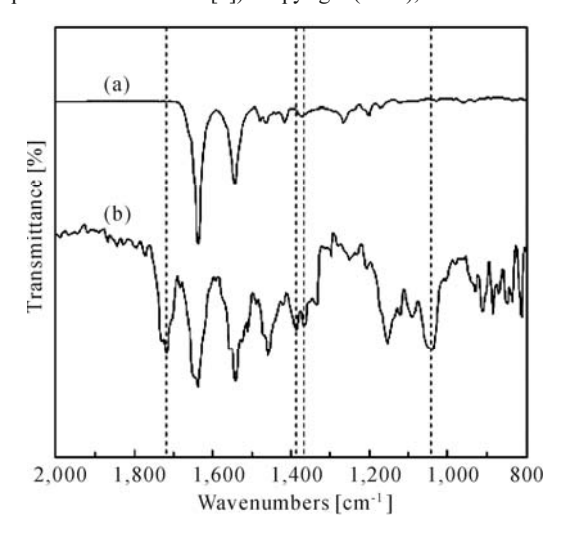


Fig.10.3. FT-IR spectra of (a) ungrafted porous Nylon-6 substrate membrane; (b) PNG-CD-grafted Nylon-6 membrane with $Y_{\text{PNIPAM}} = 220 \text{ mg} \cdot \text{cm}^2/Y_{\text{CD}} = 37 \text{ mg} \cdot \text{cm}^2$ (Reproduced with permission from Ref. [1]). Copyright (2010), Elsevier

10.2.4 Molecular-Recognizable Diffusional Permeability and Gating Characteristics

The permeation experiments of VB_{12} molecules diffusing through membranes were carried out using a standard side-by-side diffusion cell. The diffusion cell was located in a water bath to keep the temperature constant. Each tested membrane was kept in an experimental blank solution (including well-deionized water, 1.0 mmol·L⁻¹ ANS solution and 1.0 mmol·L⁻¹ NS solution) overnight before being loaded into the cell. According to the thermo-sensitive phase-transitions of PNG-CD polymer in pure water and aqueous solutions with ANS and NS molecules, ^[7] the operating temperatures for the diffusional permeability experiments of ungrafted and PNG-CD-grafted membranes in different solutions were chosen as 37 °C (T_1 in Fig.10.1) and 50 °C (T_2 in Fig.10.1) respectively. ^[1]

After checking for leakage, VB_{12} solution and blank solution were added simultaneously to the receptor and donator compartments, respectively, and stirred with a pair of magnetic stirrers. The solutions in receptor and donator compartments were sampled at a fixed time interval and the concentration of VB_{12} was determined by measuring UV absorbance. The wavelength of maximum absorbance determined for VB_{12} was 361 nm. The relationship between concentration and absorbance was calibrated by taking spectra of known concentrations.

The diffusion coefficient of the solute VB_{12} across the flat membrane can be calculated using the following equation, derived from Fick's first law of diffusion:

$$D = \frac{\delta}{A} \frac{V_1 V_2}{V_1 + V_2} \frac{1}{t} \ln \frac{(C_1)_0 V_1}{(C_1)_0 V_1 - (C_2)_t (V_1 + V_2)}$$
(10.7)

where D is the diffusional coefficient $[\text{cm}^2 \cdot \text{s}^{-1}]$, $(C_1)_0$ and $(C_2)_t$ are the initial and intermediate concentrations (at time t) of the solute in the donor and receptor compartments, respectively $[\text{mol} \cdot \text{L}^{-1}]$, V_1 and V_2 show the volume of the liquid in the donor compartment and the volume in the receptor compartment, respectively $[\text{cm}^3]$, δ is the thickness of the membrane [cm] and A is the effective diffusion area of the membrane $[\text{cm}^2]$.

Figs.10.4 and **10.5** show the molecular-recognition gating characteristics of the membranes. ^[1] **Fig.10.4** shows the ANS-recognition gating characteristics of membranes in terms of the diffusional permeability of solute VB_{12} molecules passing through PNG-CD-g-Nylon-6 membranes with different grafting yields. The ANS-recognition gating coefficient (at 37 °C) in **Fig.10.4b**, $R_{D,\text{ANS/H}_2\text{O}(37)}$, is defined as the ratio of the diffusional coefficient of VB_{12} passing through membranes at 37 °C in 1.0 mmol·L⁻¹ ANS solution to that in pure water, which can be calculated by the following equation

$$R_{D,\text{ANS/H}_2\text{O(37)}} = \frac{D_{\text{ANS(37)}}}{D_{\text{H,O(37)}}}$$
(10.8)

where $D_{\rm H_2O}$ and $D_{\rm ANS}$ show the measured diffusional coefficient of VB₁₂ through membranes in pure water and ANS solution, respectively [cm²·s⁻¹] and the subscript "(37)" stands for the diffusion at an environmental temperature of 37 °C.

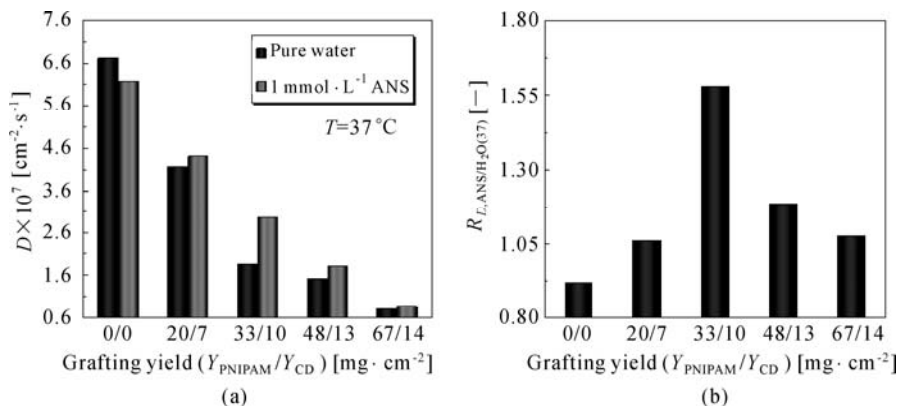


Fig.10.4. ANS-recognition gating characteristics of membranes in terms of diffusional permeability of solute VB₁₂ molecules passing through PNG-CD-*g*-Nylon-6 membranes with different grafting yields. (a) Diffusional coefficient; (b) ANS-recognition gating coefficient (Reproduced with permission from Ref. [1]). Copyright (2010), Elsevier

At 37 °C, when the environmental solution changes from pure water to 1.0 mmol·L⁻¹ ANS solution, the diffusional coefficient (Fig.10.4a) for the ungrafted membrane decreases slightly, due to the effect of adsorbed ANS molecules on the diffusion of VB₁₂ molecules and the ANS-recognition gating coefficient $R_{D,ANS/H,O(37)}$ (Fig.10.4b) is slightly smaller than 1.0. However, for the PNG-CD-grafted membrane, the diffusional coefficient increases significantly and the ANS-recognition gating coefficient $R_{D,ANS/H,O(37)}$ increases to as high as 1.6. The significant increase in the ANS-recognition gating coefficient $R_{D,\text{ANS/H},\text{O(37)}}$ demonstrates that the membrane pores switch from "closed" state to "open" state to some extent, due to the ANS-recognition shrinking conformational change in the polymer chains grafted in the membrane pores. The effects of grafting yields on the ANS-recognition gating coefficient of membranes are shown in Fig.10.4b. The amount of CD/ANS complex increases with the increase in the grafting yield, due to more and more ECD attached to PNG chains when the grafting yields increase. As a result, the membrane pores open to a larger extent and the ANS-recognition gating coefficient increases. However, it decreases when the grafting yield continuously increases, because the pores are finally choked by the over-grafted polymers. In Fig.10.4b, the ANS-recognition gating coefficient $R_{D,\text{ANS/H},O(37)}$ is at its largest value when the grafting yield is $Y_{\text{PNIPAM}} = 33 \text{ mg} \cdot \text{cm}^{-2} / Y_{\text{CD}} = 10 \text{ mg} \cdot \text{cm}^{-2}$.

Fig.10.5 shows the NS-recognition gating characteristics of membranes in terms of diffusional permeability of solute VB_{12} molecules passing through PNG-CD-g-Nylon-6 membranes with different grafting yields. ^[1] The NS-recognition gating coefficient (at 50 °C) in **Fig.10.5b**, $R_{D, NS/H_2O(50)}$, is defined as the ratio of the diffusional coefficient of VB_{12} passing through membranes at 50 °C in 1.0 mmol·L⁻¹ NS solution to that in pure water, which can be calculated by the following equation.

$$R_{D,\text{NS/H}_2\text{O(50)}} = \frac{D_{\text{NS(50)}}}{D_{\text{H,O(50)}}}$$
(10.9)

where $D_{\rm H_2O}$ and $D_{\rm NS}$ show the measured diffusional coefficient of VB₁₂ passing through membranes in pure water and NS solution respectively [cm²·s⁻¹] and the subscript "(50)" stands for the diffusion at an environmental temperature of 50 °C.

At 50 °C, when the environmental solution changes from pure water to 1.0 mmol·L⁻¹ NS solution, the diffusional coefficient (Fig.10.5a) for the ungrafted membrane decreases slightly, due to the adsorbed NS molecules on the membrane substrates slightly hindering the diffusion of VB₁₂ molecules across the membranes. As a result, the NS-recognition gating coefficient $R_{D,NS/H,O(50)}$ (Fig.10.5b) for the ungrafted membrane is slightly smaller than 1.0. On the other hand, for the PNG-CD-grafted membrane, the diffusional coefficient of VB₁₂ molecules through the membrane obviously decreases and the NS-recognition gating coefficient $R_{D,NS/H,O(50)}$ reduces to 0.85. The significant decrease in the NS-recognition gating coefficient $R_{D,NS/H,O(50)}$ indicates that the membrane pores switch from "open" state to "closed" state to some extent due to the NS-recognition swelling conformational change in the grafted polymer chains in membrane pores. The effects of grafting yields on NS-recognition gating coefficient of membranes are shown in Fig.10.5b. The amount of CD/NS complex increases with the increase in the grafting yield, due to more and more ECD attached to PNG chains with an increase in the grafting yields. As a result, the membrane pores close to a larger extent and the NS-recognition gating coefficient decreases. There is also an optimum grafting yield for obtaining an optimum NS-recognition gating coefficient. In **Fig.10.5b**, the NS-recognition gating coefficient $R_{D,NS/H,O(50)}$ is also at its largest value when the grafting yield is $Y_{PNIPAM} = 33 \text{ mg} \cdot \text{cm}^{-2} / Y_{CD} = 10 \text{ mg} \cdot \text{cm}^{-2}$.

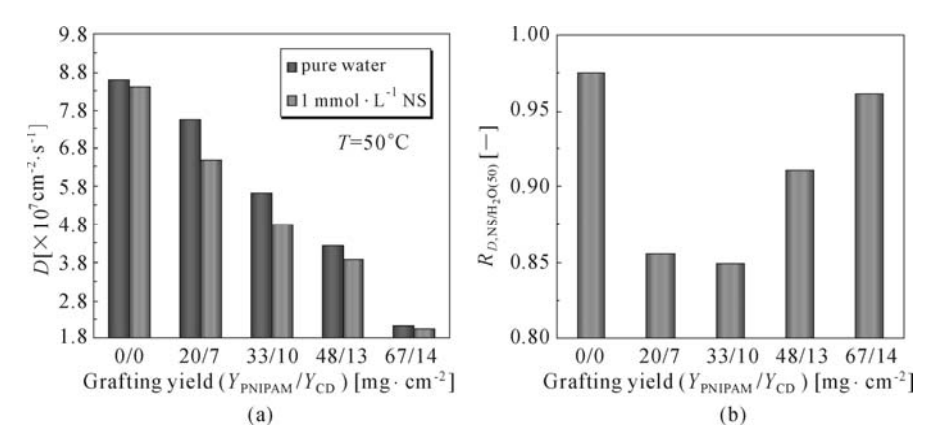


Fig.10.5. NS-recognition gating characteristics of membranes in terms of diffusional permeability of solute VB₁₂ molecules passing through PNG-CD-*g*-Nylon-6 membranes with different grafting yields. (a) Diffusional coefficient; (b) NS-recognition gating coefficient (Reproduced with permission from Ref. [1]). Copyright (2010), Elsevier

PNIPAM behaves as the actuator for the membrane pore gating, so the gating characteristics of the as-prepared membranes should be able to be adjusted by controlling the molar ratio of PNIPAM in the grafted gates. In order to adjust the molecular-recognizable gating characteristics of PNG-CD-g-Nylon-6 membranes, a series of membranes with a similar amount of CD but different ratios of N_{PNIPAM} $N_{\rm PGMA}$ (defined as the coefficient " α ") in the grafted chains are prepared and the effects of α values on thermo-responsive and molecular-recognizable gating characteristics are investigated experimentally. Fig.10.6 shows the comparison of diffusion coefficients of VB₁₂ passing through the membranes and the ANSrecognition gating characteristics of PNG-CD-grafted membranes with different ratios of $N_{\text{PNIPAM}}/N_{\text{PGMA}}$. [1] As shown in **Fig.10.6**, the α value affects the ANSrecognition gating characteristics significantly. When the α value is 4.0, the ANS-recognition gating coefficient is improved to about 2.0. The reason can be explained as follows. The molecular-recognizable gating function of membranes with a similar amount of CD but different ratios of N_{PNIPAM}/N_{PGMA} is achieved by the cooperation between PNIPAM and CD. When the PNIPAM component in grafted chains increases, the swelling/shrinking volume phase transition of the grafted PNG-CD gates in the membranes becomes more significant and the above-mentioned cooperation is enhanced. However, the steric hindrance caused by the significant phase transition of grafted chains could affect the association constant of CD toward guest molecules ANS. As a result, when the α value increases further to 8.0, the ANS-recognition gating coefficient decreases to a certain degree. Therefore, there are optimum ratios of N_{PNIPAM}/N_{PGMA} for the molecular-recognizable gating characteristics of the membranes.

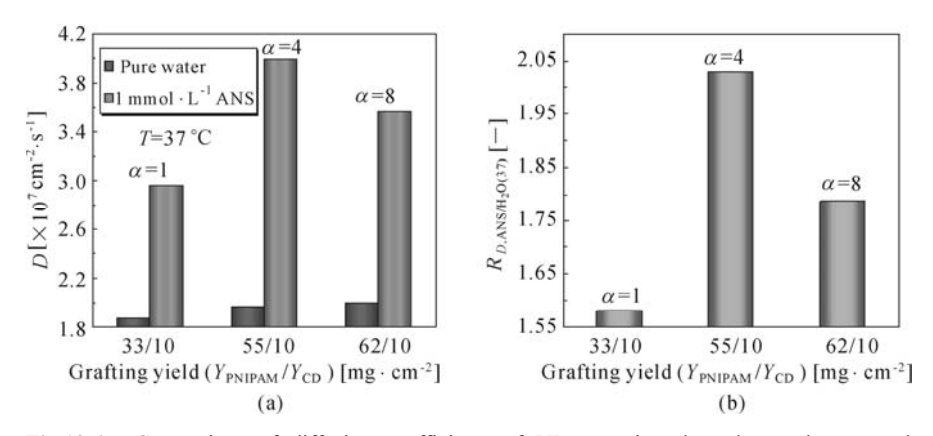


Fig.10.6. Comparison of diffusion coefficients of VB₁₂ passing through membranes and ANS-recognition gating characteristics of PNG-CD-grafted membranes with different ratios of $N_{\text{PNIPAM}}/N_{\text{PGMA}}$ (α) in the grafted gates. (a) Diffusional coefficient; (b) ANS-recognition gating coefficient (Reproduced with permission from Ref. [1]). Copyright (2010), Elsevier

10.3 Molecular-Recognizable Smart Membranes with Crown Ethers as Host Molecules

In this section, molecular-recognizable smart membranes with crown ethers as host molecules will be introduced.

10.3.1 Smart Microcapsules with Molecular-Recognizable Gating Membranes

Microcapsules can encapsulate various substances in their inner spaces, and it is thus possible to achieve a controlled permeation of substances through microcapsule membranes by adopting appropriate materials. Because of their characteristics, such as small size, huge total surface area, large inner volume and stable membrane, microcapsules have found many applications in various fields from drug delivery to the textile, petroleum and pesticide industries. Recently, the author's group developed a smart microcapsule with a molecular-recognizable gating membrane by employing crown ether as host molecule and PNIPAM as actuator. [2]

10.3.1.1 Design of Microcapsules with Molecular-Recognizable Gating Membranes

The concept of the microcapsule with a molecular-recognizable gating membrane is schematically illustrated in **Fig.10.7**.^[2] The molecular recognition microcapsule is composed of a porous membrane and linear-grafted poly(N-isopropylacrylamideco-benzo-18-crown-6-acrylamide) (poly(NIPAM-co-BCAm)) chains in the pores, acting as molecular recognition gates. PNIPAM, a thermo-responsive polymer, exhibits a dramatic conformational change due to gel swelling/shrinking. Benzo-18-crown-6-acrylamide (BCAm), a crown ether receptor, allows ionic molecular recognition. PNIPAM has an LCST, and when the receptor BCAm captures a specific metal ion, the LCST can be shifted. [11,12] Therefore, the phase transition of the grafted gel gates can occur isothermally as the result of a specific metal ion signal at a temperature between the two LCSTs. The linear-grafted PNIPAM polymer with pendant crown ether was fixed on the pore surfaces of the porous microcapsule membrane. When there exist specific molecules in the environmental solution, the pores in the microcapsule membrane are closed by the swelling of the gel gates, resulting in a low release rate of solute from the microcapsule; on the other hand, when the recognizable specific molecules do not exist in the environmental solution, the pores open due to the shrinking of the gel gates and then a high release rate results. That means the encapsulated solutes can be controlled to release only in those situations when the recognizable molecules do not exist in the surrounding solution.

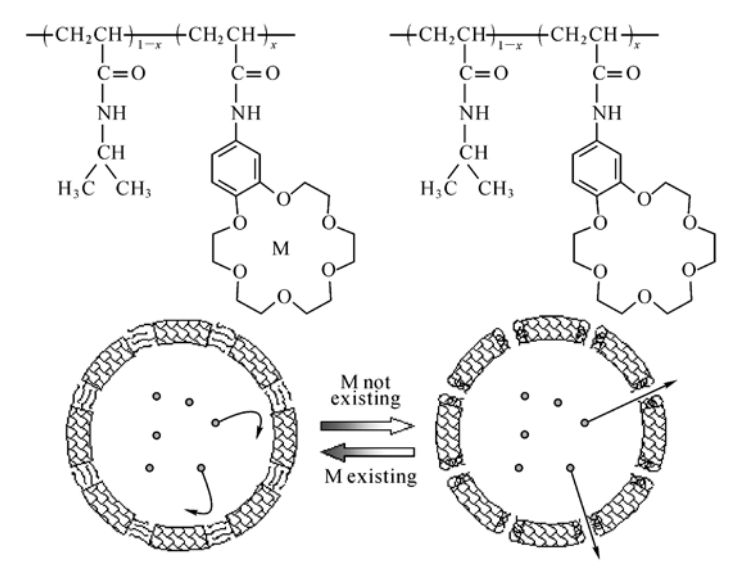


Fig.10.7. Schematic representation of the smart microcapsule with molecular-recognizable gating membrane by using crown ether as molecular sensor and PNIPAM as actuator (Reproduced with permission from Ref. [2]). Copyright (2002), Wiley-VCH Verlag GmbH & Co. KGaA

10.3.1.2 Preparation of Microcapsules with Molecular-Recognizable Gating Membranes

BCAm was synthesized according to a published method. [13,14] The microcapsules were prepared by the interfacial polymerization method as described in Section 3.2.1.1. Plasma-graft pore-filling polymerization was employed to graft linear poly(NIPAM-co-BCAm) chains into the pores of the microcapsule membranes according to the method described in Section 3.2.2.1. [2] Briefly, the freeze-dried microcapsules were put into a transparent glass tube, which was then filled with argon gas. The tube was then evacuated to a pressure of 10 Pa and the microcapsules were subjected to a radio-frequency plasma operating at 13.56 MHz and delivering at 30 W for 60 s. Then, plasma treated microcapsules were in contact with air for 60 s. Next, the tube was filled with argon gas, then evacuated again to 10 Pa and then the microcapsules were immersed into monomer solution under inert atmosphere conditions. For the monomer solution, a mixture of NIPAM, BCAm and water solution was emulsified with SDS. The SDS and total monomer concentrations in solution were 4 wt% and 5 wt% respectively. The weight percentage ratio of NIPAM to BCAm in the monomer solution was 85:15. The graft polymerization was carried out under vibration in a constant-temperature bath (80 °C) for a fixed period. The grafted microcapsules were separated centrifugally, washed three times with deionized water, and then dialyzed against deionized water and freeze-dried.

Fig.10.8 shows FE-SEM micrographs of the outer surface and cross-sectional

views of the ungrafted and poly(NIPAM-co-BCAm)-grafted microcapsules.^[2] Comparing **Fig.10.8c** with **Fig.10.8d**, the cross-sections of the un-grafted and poly(NIPAM-co-BCAm)-grafted microcapsules are seen to have significantly different structures. After grafting poly(NIPAM-co-BCAm) onto the inner pore surface in the porous membrane of the microcapsule, the pore size became smaller. The porous structure across the cross-section of the microcapsule was homogeneously covered by the grafted polymer throughout the entire membrane thickness.

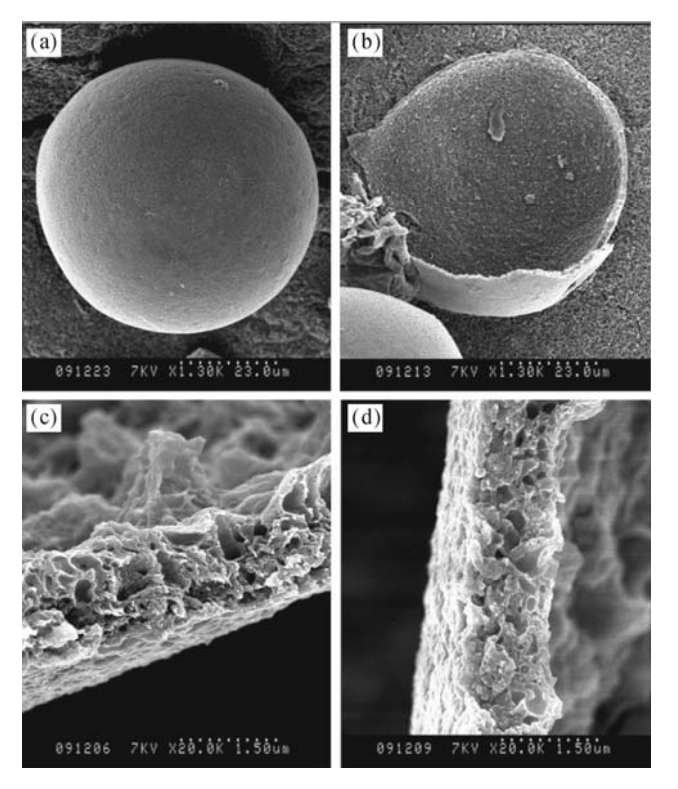


Fig.10.8. FE-SEM micrographs of microcapsules. (a) Outer surface; (b) Cross-section; (c) Cross-section of ungrafted microcapsule; (d) Cross-section of poly(NIPAM-*co*-BCAm)-grafted microcapsule (Reproduced with permission from Ref. [2]). Copyright (2002), Wiley-VCH Verlag GmbH & Co. KGaA

10.3.1.3 Molecular-Recognizable Controlled Release and Gating Characteristics

 Na^+ and Ba^{2^+} metal ions were chosen as the guest substance in the environment because metal ions are important for chemical signals in biomembranes and the signal-receptive characteristics of the release of VB_{12} were investigated. The release of the solute from the microcapsules was measured by determining the increase in the solute concentration of the surrounding medium with time, after

mixing a known volume of microcapsule dispersion with a known solute (VB $_{12}$) concentration with the same volume of deionized water. After 20 min, sodium chloride was added to the surrounding solution to let the surrounding NaCl concentration be 0.2 mol·L $^{-1}$. More than 20 min later, barium chloride was also added to the surrounding solution to let the surrounding NaCl and BaCl $_2$ concentrations be 0.18 mol·L $^{-1}$ and 0.02 mol·L $^{-1}$, respectively. During the measurements, the liquid's temperature was kept at a constant 38 °C using a thermostatic unit. The concentration of VB $_{12}$ was determined using a UV-visible recording spectrophotometer at a wavelength of 361 nm.

Fig.10.9 shows the release results of VB₁₂ from the microcapsules in different chemical environments. [2] For the poly(NIPAM-co-BCAm)-grafted microcapsules, when pure water or 0.2 mol·L⁻¹ NaCl aqueous solution was used as the environmental solution, the release of VB₁₂ from the microcapsules was fast; in contrast, when 0.02 mol·L⁻¹ BaCl₂ existed in the surrounding solution, the release rate suddenly dropped significantly. On the other hand, the ungrafted microcapsule did not show such a sharp transition in the release rate under the same experimental conditions. Because the crown ether has a high stability constant for complexing with Ba²⁺ ions, the Ba²⁺ ions are selectively trapped in the crown ether and thus cause the grafted gel gates to swell. Consequently, before adding BaCl2 to the environmental solution, the pores of the poly(NIPAM-co-BCAm)-grafted microcapsule membrane were open because of the shrunken state of the polymeric gates, then resulting in a high release rate; in contrast, after adding BaCl₂ to the surrounding solution, the pores of the poly(NIPAM-co-BCAm)-grafted microcapsule membrane were suddenly closed due to the swelling of the grafted polymeric gates and a very low release rate resulted (as illustrated in Fig.10.7). The release of solute from the microcapsules was significantly sensitive to the existence of Ba²⁺ ions in the environmental solution.

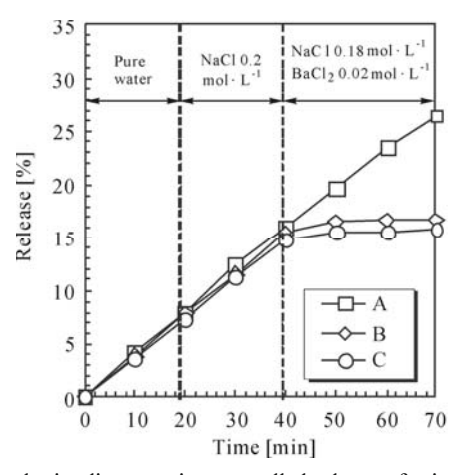


Fig.10.9. Environmental stimuli-responsive controlled-release of microcapsules by molecular recognition. (A) Ungrafted microcapsules; (B, C) Poly(NIPAM-*co*-BCAm)-grafted microcapsules. *T*=38 °C (Reproduced with permission from Ref. [2]). Copyright (2002), Wiley-VCH Verlag GmbH & Co. KGaA

To verify the reversibility of the poly(NIPAM-co-BCAm) gates grafted on the surface of the pores in the microcapsule membrane, release experiments were carried out repeatedly by using the same microcapsules. [2] The microcapsules were washed with, and dialyzed against, deionized water after each run, to remove the Ba2+ ions from the crown ether. Furthermore, to ensure that there was enough solute inside the microcapsules for release during the entire release experiment, solute VB₁₂ was reloaded into the inner space of the microcapsules before each run. The reversible environmental stimuli-responsive release characteristics of the poly(NIPAM-co-BCAm)-grafted microcapsules are shown in Fig.10.10.[2] The molecular recognition release of the poly(NIPAM-co-BCAm)-grafted microcapsules was found to be satisfactorily reversible and reproducible, suggesting that the Ba2+ ions could be easily removed from the crown ether and that the grafted poly(NIPAM-co-BCAm) gates retained their gel properties intact, even though they underwent repeated changes in the environmental chemical signal. That is to say, a repeatable molecular recognition stimuli-responsive release was effectively achieved.

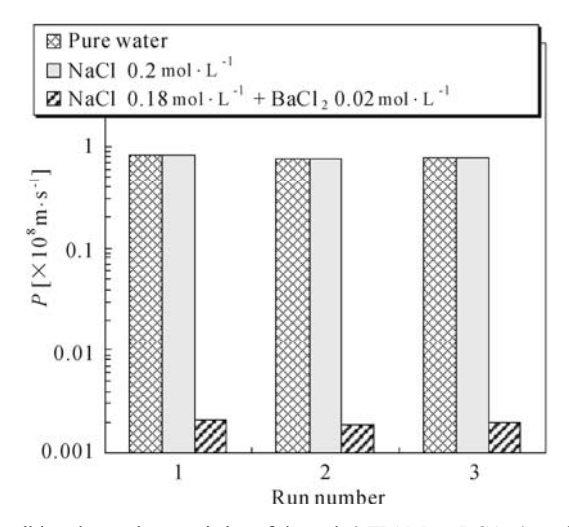


Fig.10.10. Reversible release characteristics of the poly(NIPAM-*co*-BCAm)-grafted microcapsules. (Reproduced with permission from Ref. [2]). Copyright (2002), Wiley-VCH Verlag GmbH & Co. KGaA

10.3.2 Smart Microcapsules with Molecular-Recognizable Hydrogel Membranes

In this section, smart microcapsules with molecular-recognizable hydrogel membranes will be introduced.

10.3.2.1 Design of Microcapsules with Molecular-Recognizable Hydrogel Membranes

By using the above-mentioned poly(NIPAM-co-BCAm) materials, microcapsules with molecular-recognizable hydrogel membranes can be designed as in **Fig.10.11**, ^[3] in which the ion-recognizable crown ether 18-crown-6 is used as an ion-signal sensing receptor and thermo-responsive PNIPAM acts as an actuator. When the BCAm receptors in the crosslinked poly(NIPAM-co-BCAm) hydrogels capture specific ions, the volume phase transition temperature (VPTT) of crosslinked poly(NIPAM-co-BCAm) hydrogels shifts from a lower value (VPTT_a in **Fig.10.11**) to a higher one (VPTT_b in **Fig.10.11**). ^[15,16] As a result, when the environmental temperature (T_c in **Fig.10.11**) is located between VPTT_a and VPTT_b, the designed microcapsules can exhibit an isothermal and significant swelling by recognizing special metal ions, *i.e.*, the crosslinked polymeric network of the microcapsule membrane changes from a shrunken state to a swollen state isothermally and there is a reversible shrinking by removing the metal ions from the crown ethers.

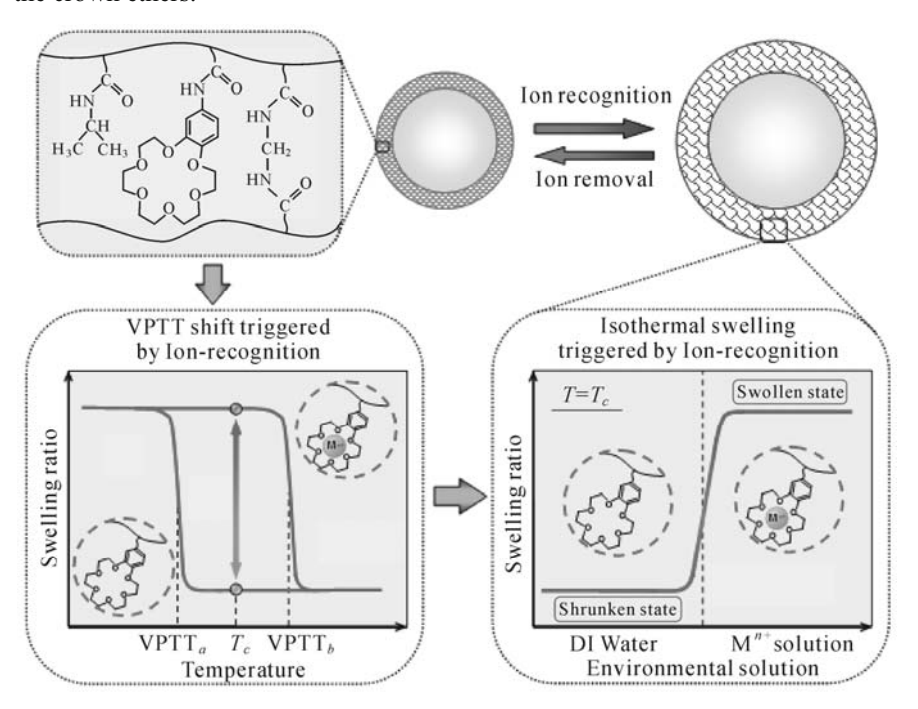


Fig.10.11. Schematic illustration of the ion-recognizable smart microcapsule with crosslinked poly(NIPAM-*co*-BCAm) hydrogel membrane (Reproduced with permission from Ref. [3]). Copyright (2010), Elsevier

10.3.2.2 Preparation of Microcapsules with Molecular-Recognizable Hydrogel Membranes

The microcapsules were prepared by using oil-in-water-in-oil (O/W/O) double emulsions as the polymerization templates and the O/W/O double emulsions were generated by a microfluidic method. The coaxial flow focusing microfluidic device for the generation of monodisperse O/W/O double emulsions was fabricated according to our published method. [17,18] In the microfluidic preparation of O/W/O double emulsions, soybean oil containing 3% (w/v) polyglycerol polyricinoleate (PGPR) was used as the innermost oil phase and soybean oil containing 5% (w/v) PGPR was used as the outer oil phase. For the middle aqueous phase, 5ml deionized (DI) water containing monomers NIPAM (0.452 g) and benzo-18-crown-6-acrylamide (BCAm) (0.15 g), crosslinker N,N-methylene-bis-acrylamide (MBA) (0.006 g), initiator 2,2'-azobis(2-amidinopropane dihydrochloride) (V50) (0.01 g), glycerin (0.35 g) and emulsifier Pluronic F127 (0.04 g) was used typically. The content of the crosslinker MBA was also changed for comparison. The generated O/W/O double emulsions were collected in a beaker containing excess soybean oil with another initiator 2,2-diethoxyacetophenone (DEAP). The microcapsules with crosslinked poly(NIPAM-co-BCAm) membranes were polymerized via UV-initiated polymerization in an ice-bath for 10 min. After UV-initiated polymerization, the microcapsules were isolated from surrounding oil by adding benzyl benzoate and DI water. The microcapsules were then washed with DI water several times.

10.3.2.3 Molecular-Recognizable Swelling/Shrinking Characteristics

Temperature-dependent and ion-recognizable phase transition behavior of the prepared microcapsules was studied by optical microscope equipped with a thermostatic stage system and a CCD camera within the temperature range from 22 °C to 46 °C. Briefly, the ion-recognition properties of the prepared microcapsules were investigated by evaluating their temperature-induced volume phase transitions in DI water and different metal ion solutions. Firstly, by changing the temperature step by step, the microcapsules were kept in the DI water for 15 min at every determined temperature to reach the swelling/shrinking equilibrium state and then micrographs of the microcapsules were taken by the optical microscope. Next, the same batch of microcapsules was put into predetermined metal ion solutions for 48 h to ensure that the BCAm receptors had fully captured the ions and the PNIPAM actuators had responded thoroughly. Then, the temperature-dependent volume changes in the microcapsules in different metal ionic solutions were measured, with the same procedure as mentioned above in DI water. To minimize the salting-out effects, nitrates were chosen for all the metal ion salts. [19]

Fig.10.12 shows the temperature-dependent size-changes in microcapsules with crosslinked poly(NIPAM-*co*-BCAm) membranes in DI water and different metal ion solutions, in which all the crosslinking degrees of poly(NIPAM-*co*-BCAm) membranes are 1%. [3] All the poly(NIPAM-*co*-BCAm) microcapsules

exhibit excellent thermo-responsive characteristics and their diameters decrease dramatically as the ambient temperature increases across a corresponding temperature range. It is obvious that the diameter change of the microcapsule in 0.1mol·L⁻¹ Ba²⁺ solution is significantly different compared with that in DI water and other ion solutions. The VPTT of poly(NIPAM-*co*-BCAm) microcapsules in DI water is about 32 °C; however, in 0.1 mol·L⁻¹ Ba²⁺ solution, the VPTT increases by about 7 °C and shifts to about 39 °C. The VPTT in 0.1 mol·L⁻¹ Na⁺ solution is almost the same as that in DI water, the VPTT in 0.1 mol·L⁻¹ K⁺ solution is only a little bit higher than that in DI water and the VPTT in 0.1 mol·L⁻¹ Ca²⁺ solution is only a little bit lower than that in DI water.

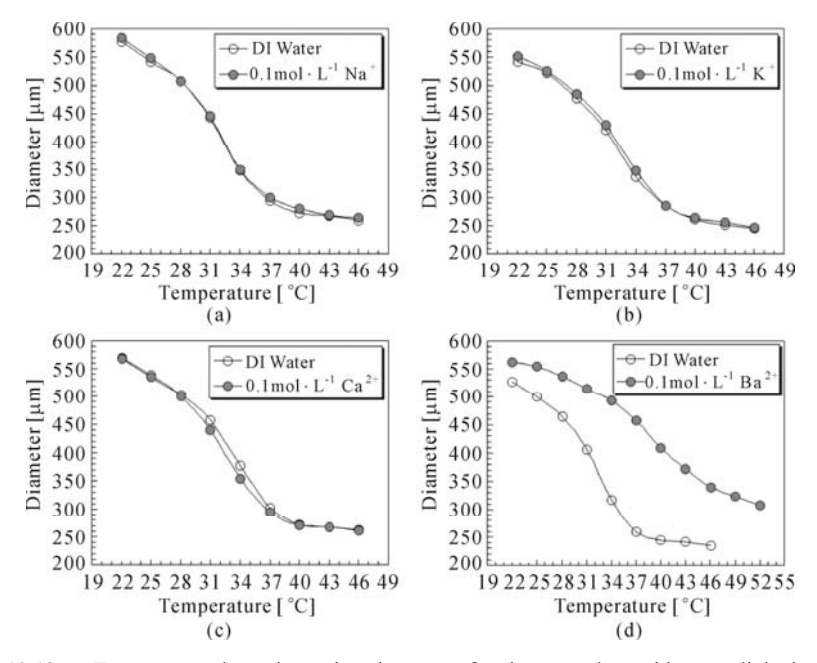


Fig.10.12. Temperature-dependent size-changes of microcapsules with crosslinked poly (NIPAM-*co*-BCAm) membranes in DI water and different metal ion solutions. For each figure, the diameter of the same microcapsule was measured in DI water first and then in the metal ion solution (Reproduced with permission from Ref. [3]). Copyright (2010), Elsevier

The reason for the above-mentioned phenomena is the effect of the formation of crown ether/metal-ion complexes. BCAm receptors in the crosslinked poly (NIPAM-co-BCAm) membranes recognize specific ions and form "host-guest" complexes. The order of the formation constant, $\log K$, of benzo-18-crown-6 with metal ions in water is Ba²⁺ > K⁺ > Na⁺ > Ca²⁺. [15] This order shows a good correlation with the VPTT shift in different ion solutions. The $\log K$ of benzo-18-crown-6 with K⁺ or Na⁺ is smaller and the polymeric network of the poly(NIPAM-co-BCAm) membrane is crosslinked, so there is no significant VPTT change in Na⁺ or K⁺ solution (**Figs.10.12a** and **10.12b**). Because the $\log K$ of benzo-18-crown-6 with Ca²⁺ is the smallest and the concentration of NO₃⁻ is 0.2 mol·L⁻¹, the VPTT in

0.1 mol·L⁻¹ Ca²⁺ is a little bit lower than that in DI water (**Fig.10.12c**) due to slight salting-out effects. [19] The log K of benzo-18-crown-6 with Ba²⁺ is the largest, thus BCAm can recognize Ba2+ best and form most stable "host-guest" complexes with Ba²⁺ ions. When the poly(NIPAM-co-BCAm) microcapsules are put into Ba²⁺ solution, very stable BCAm/Ba²⁺ complexes are formed. Therefore, the side chains bearing pendent BCAm/Ba²⁺ complexes in the poly(NIPAM-co-BCAm) polymeric network would be charged. The electrostatic repulsion among the charged BCAm/Ba²⁺ groups would make the side chains exclude each other and hinder the shrinking of the poly(NIPAM-co-BCAm) membranes induced by the temperature increase. In addition, the osmotic pressure within the polymeric network of the poly(NIPAM-co-BCAm) membrane due to a Donnan potential also makes the poly(NIPAM-co-BCAm) membrane swell more. [20,21] As a result, the VPTT in Ba2+ solutions shifts to a higher temperature than that in DI water (Fig.10.12d). Furthermore, the poly(NIPAM-co-BCAm) microcapsule in Ba²⁺ solution has a larger degree of swelling, and the diameter of the poly(NIPAMco-BCAm) microcapsule in Ba²⁺ solution is always larger than that in DI water at any temperature throughout the experiments (Fig.10.12d).

Fig.10.13 shows the isothermal swelling behavior of the prepared microcapsules with poly(NIPAM-co-BCAm) membranes by recognizing barium ions at 37 °C, which are selected between the VPTT in DI water and that in Ba²⁺ solution. ^[3] To characterize the isothermal swelling behavior quantitatively, three parameters called the swelling ratios of inner diameter (ID) ($R_{\rm ID}$), outer diameter (OD) ($R_{\rm OD}$) and membrane thickness ($R_{\rm Thickness}$) of microcapsules caused by ion-recognition, are defined as follows:

$$R_{\rm ID} = \frac{\rm ID_{Ba^{2+}}}{\rm ID_{H_2O}} \tag{10.10}$$

$$R_{\rm OD} = \frac{\rm OD_{Ba^{2+}}}{\rm OD_{H,O}}$$
 (10.11)

$$R_{\text{Thickness}} = \frac{\text{OD}_{\text{Ba}^{2+}} - \text{ID}_{\text{Ba}^{2+}}}{\text{OD}_{\text{H}_2\text{O}} - \text{ID}_{\text{H}_2\text{O}}}$$
(10.12)

No matter how large is the concentration of Ba^{2+} solution (0.1 mol·L⁻¹ or 0.2 mol·L⁻¹), the isothermal swelling behavior of the prepared microcapsules with poly(NIPAM-co-BCAm) membranes triggered by recognizing barium ions at 37 °C is significant. The microcapsule membranes are in a shrunken state and the polymeric network structure in the membrane is compacted in DI water (**Figs.10.13a** and **10.13b**); however, after the microcapsules recognize the Ba^{2+} ions, the microcapsule membranes automatically switch to a swollen state with the polymeric network structure being loosened (**Figs.10.13a** and **10.13b**). When the concentration of Ba^{2+} solution increases to 0.2 mol·L⁻¹, the values of $R_{\rm OD}$, $R_{\rm ID}$ and $R_{\rm Thickness}$ are slightly smaller than the corresponding values in 0.1 mol·L⁻¹ Ba^{2+} solution (**Fig.10.13c**), which might be caused by the following reasons. Because the quantity of BCAm units in the poly(NIPAM-co-BCAm) membranes is limited,

both the 0.1 mol·L⁻¹ and 0.2 mol·L⁻¹ Ba²⁺ concentrations might provide excessive Ba²⁺ ions for the BCAm units in the poly(NIPAM-*co*-BCAm) membranes to form "host-guest" complexes.

On the other hand, the above-mentioned salting-out effect of the increased amount of anions NO_3^- in solutions would counteract the swelling of the poly (NIPAM-co-BCAm) membranes to some extent. When the concentration of Ba²⁺ solution is 0.1 mol·L⁻¹, the inner diameter of the prepared microcapsule is 1.67 times larger than that in DI water ($R_{\rm ID} = 1.67$), the outer diameter increases isothermally 1.77 times ($R_{\rm OD} = 1.77$) and the thickness of the microcapsule membrane increases 2.26 times ($R_{\rm Thickness} = 2.26$) (**Fig.10.13c**).

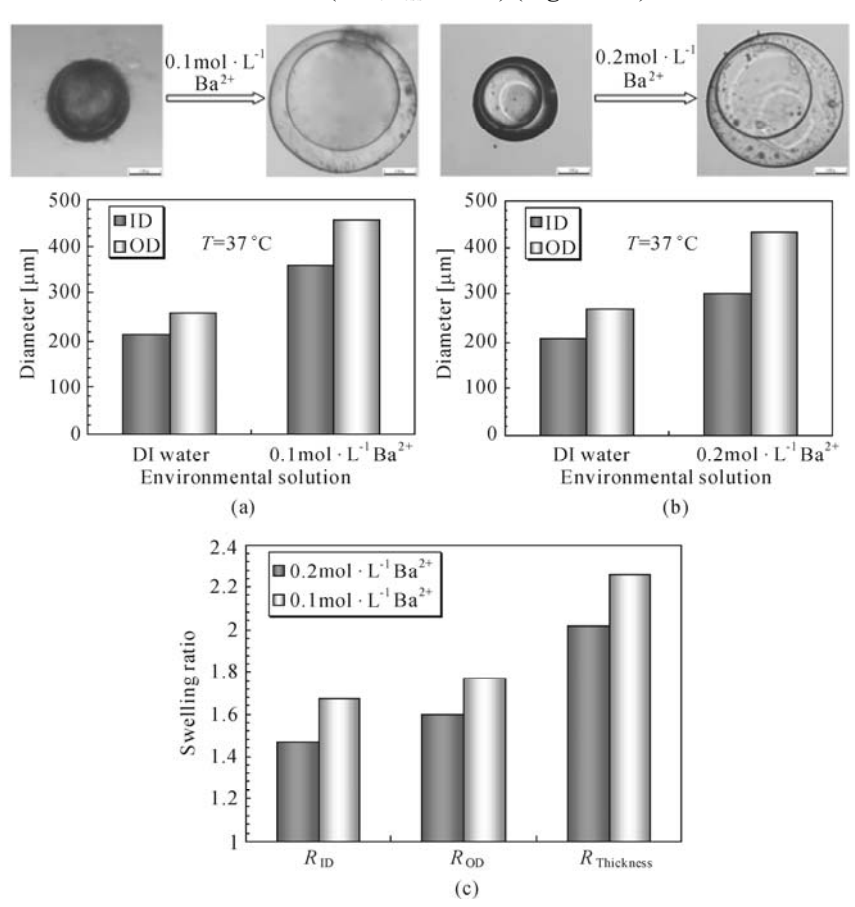


Fig.10.13. The isothermal swelling behavior of the prepared microcapsules with poly(NIPAM-co-BCAm) membranes triggered by recognizing barium ions at 37 °C. (a) The increase in the inner diameter (ID) and outer diameter (OD) of the microcapsule by transferring it from DI water into 0.1 mol·L⁻¹ Ba²⁺ solution, (b) the diameter change by transferring the microcapsule from DI water into 0.2 mol·L⁻¹ Ba²⁺ solution; (c) the swelling ratios of ID ($R_{\rm ID}$), OD ($R_{\rm OD}$) and membrane thickness ($R_{\rm Thickness}$) of microcapsules caused by ion-recognition (Reproduced with permission from Ref. [3]). Copyright (2010), Elsevier

Fig.10.14 shows the swelling ratios of the inner and outer diameters and the thickness of the prepared microcapsules with P(NIPAM-co-BCAm) membranes by recognizing lead(II) ions at 37 °C. [3] The concentration of environmental Pb2+ ions is 0.01 mol·L⁻¹. When the microcapsule recognizes the Pb²⁺, all of the inner and outer diameters and the thickness increase. The reason is that P(NIPAM-co-BCAm) microcapsules can recognize Pb2+ and form BCAm/Pb2+ complexes just like Ba2+ as explained before. [22, 23] When the crosslinking degree is 1%, the inner diameter of the microcapsule in 0.01 mol·L⁻¹ Pb²⁺ solution is about 2.02 times larger than that in DI water ($R_{\rm ID} = 2.02$), the outer diameter and thickness of the microcapsule membrane in 0.01 mol·L⁻¹ Pb²⁺ solution become 2.16 and 2.6 times respectively larger than those in DI water ($R_{\rm OD} = 2.16$ and $R_{\rm Thickness} = 2.6$). When the crosslinking degree increases to 5%, all these three swelling ratios decrease to some extents due to the highly crosslinked networks restrict the swelling of microcapsule to some degrees. A lower crosslinking degree is better for achieving a more significant isothermal swelling of the polymeric network in the P(NIPAM-co-BCAm) membrane triggered by recognizing heavy metal ions. Such a significant isothermal swelling of the polymeric network in the poly(NIPAM-co-BCAm) membrane triggered by recognizing specific metal ions enables the microcapsules to dramatically increase their permeability across the membrane.

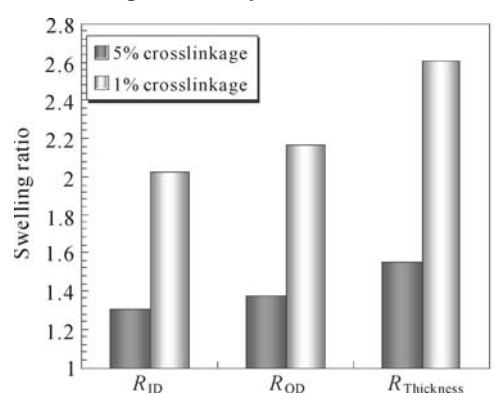


Fig.10.14. The isothermal swelling behaviors of the prepared microcapsules with P(NIPAM-co-BCAm) membranes triggered by recognizing lead(II) ions at 37 °C. The concentration of lead(II) ions is 0.01 mol·L⁻¹. (Reproduced with permission from Ref. [3]). Copyright (2010), Elsevier

10.4 Summary

In summary, molecular-recognizable gating membranes are developed on the basis of the cooperative function of PNIPAM and CD or crown ether. For the PNG-CD-grafted gating membranes, the membrane gates can not only switch from "closed" to "open" state by recognizing certain guest molecules with a hydrophobic side group at temperatures below the LCST of grafted PNG-CD chains in water, but

also can switch from "open" to "closed" state by recognizing different guest molecules with a hydrophilic side group or without a side group in different cases at temperatures above the LCST of PNG-CD in water. The molecular-recognizable gating characteristics of the membranes can be adjusted by changing the grafting yields of both PNIPAM and CD on the membranes as well as the molar ratio of PNIPAM in the grafted chains. Microcapsules with porous membranes and linear-grafted poly(NIPAM-co-BCAm) chains in the pores, acting as molecular recognition gates, can achieve reversible and reproducible molecular recognition stimuli-responsive controlled-release performance. Microcapsules with crosslinked poly (NIPAM-co-BCAm) hydrogel membranes exhibit isothermal and significant swelling not only in outer and inner diameters but also in the membrane thickness by recognizing special metal ions. Molecular-recognizable smart membranes have great potential in the fields of chemical valves, chemical sensors and actuators, drug carriers and so on.

References

- [1] Yang M, Xie R, Wang J Y, Ju X J, Yang L, Chu L Y. Gating characteristics of thermo-responsive and molecular-recognizable membranes based on poly(N-isopropylacrylamide) and β -cyclodextrin. *Journal of Membrane Science*, **2010**, *355*: 142-150.
- [2] Chu L Y, Yamaguchi T, Nakao S. A molecular recognition microcapsule for environmental stimuli-responsive controlled-release. *Advanced Materials*, **2002**, *14*: 386-389.
- [3] Pi S W, Ju X J, Wu H G, Xie R, Chu L Y. Smart responsive microcapsules capable of recognizing heavy metal ions. *Journal of Colloid and Interface Science*, **2010**, *349*: 512-518.
- [4] Heskins M, Guilleit J E. Solution properties of poly(*N*-isopropylacrylamide). *Journal of Macromolecular Science: Part A–Chemistry*, **1968**, *2*: 1441-1455.
- [5] Kusumocahyo S P, Sumaru K, Kanamori T, Iwatsubo T, Shinbo T. Synthesis and characterization of an ultrathin polyion complex membrane containing beta-cyclodextrin for separation of organic isomers. *Journal of Membrane Science*, **2004**, *230*: 171-174.
- [6] Ohashi H, Hiraoka Y, Yamaguchi T. An autonomous phase transition-complexation/decomplexation polymer system with a molecular recognition property. *Macromolecules*, **2006**, *39*: 2614-2620.
- [7] Yang M, Chu L Y, Xie R, Wang C. Molecular-recognition induced phase-transition of two thermo-responsive polymers with pendent beta-cyclodextrin groups. *Macromolecular Chemistry & Physics*, **2008**, *209*: 204-211.
- [8] Petter R C, Salek J S, Sikorski C T, Kumaravel G, Lin F T. Cooperative binding by aggregated mono-6-(alkylamino)-beta-cyclodextrins. *Journal of American Chemical Society*, **1990**, *112*: 3860-3868.
- [9] Bonomo R P, Cucinotta V, D'Allessandro F, Impellizzeri G, Maccarrone G,

- Rizzarelli E. Coordiation properties of 6-deoxy-6-[1-(2-amino)ethylamino]-beta-cyclodextrin and the ability of its copper(II) complex to recognize and separate amino acid enantiomeric pairs. *Journal of Inclusion Phenomena and Molecular Recognition in Chemistry*, **1993**, *15*: 167-180.
- [10] Virtanen J, Baron C, Tenhu H. Grafting of poly(*N*-isopropylacrylamide) with poly(ethylene oxide) under various reaction conditions. *Macromolecules*, **2000**, *33*: 336-341.
- [11] Irie M, Misumi Y, Tanaka T. Stimuli-responsive polymers: chemical induced reversible phase separation of an aqueous solution of poly(*N*-isopropylacrylamide) with pendent crown ether groups. *Polymer*, **1993**, *34*: 4531-4535.
- [12] Yamaguchi T, Ito T, Sato T, Shinbo T, Nakao S. Development of a fast response molecular recognition ion gating membrane. *Journal of American Chemical Society*, **1999**, *121*: 4078-4079.
- [13] Ungrao R, El H B, Smid J. Substituent effects on the stability of cation complexes of 4'-substituted monobenzo crown ethers. *Journal of American Chemical Society*, **1976**, *98*: 5198-5202.
- [14] Yagi K, Ruiz J A, Sanchez M C. Cation binding properties of polymethacrylamide derivatives of crown ethers. *Die Makromolekulare Chemie, Rapid Communications*, **1980**, *1*: 263-268.
- [15] Ju X J, Chu L Y, Liu L, Mi P, Lee Y M. A novel thermo-responsive hydrogel with ion-recognition property through supramolecular host-guest complexation. *The Journal of Physical Chemistry B*, **2008**, *112*: 1112-1118.
- [16] Ju X J, Liu L, Xie R, Niu C H, Chu L Y. Dual thermo-responsive and ion-recognizable monodisperse microspheres. *Polymer*, **2009**, *50*: 922-929.
- [17] Chu L Y, Utada A S, Shah R K, Kim J W, Weitz D A. Controllable monodisperse multiple emulsions. *Angewandte Chemie International Edition*, **2007**, *46*: 8970-8974.
- [18] Wang W, Liu L, Ju X J, Zerrouki D, Xie R, Yang L H, Chu L Y. A novel thermo-induced self-bursting microcapsule with magnetic-targeting property. *ChemPhysChem*, **2009**, *10*: 2405-2409.
- [19] Inomata H, Goto S, Otake S, Saito S. Effect of additives on phase transition of N-isopropylacrylamide gels. *Langmuir*, **1992**, *8*: 687-690.
- [20] Hirotsu S, Hirokawa Y, Tanaka T. Volume-phase transitions of ionized *N*-isopropylacrylamide gels. *Journal of Chemical Physics*, **1987**, 87: 1392-1395.
- [21] Wang K L, Burban J H, Cussler E L. Hydrogels as separation agents. *Advances in Polymer Science*, **1993**, *110*: 67-69.
- [22] Ito T, Hioki T, Yamaguchi T, Shinbo T, Nakao S, Kimura S. Development of a molecular recognition ion gating membrane and estimation of its pore size control. *Journal of American Chemical Society*, **2002**, *124*: 7840-7846.
- [23] Ju X J, Zhang S B, Zhou M Y, Xie R, Yang L, Chu L Y. Novel heavy-metal adsorption material: ion-recognition P(NIPAM-co-BCAm) hydrogels for removal of lead(II) ions. *Journal of Hazardous Materials*, **2009**, *167*: 114-118.

Dual-/Multi-Stimuli-Responsive Smart Membranes

In this chapter, dual-/multi-stimuli-responsive smart membranes are described for more applicable purposes. Dual stimuli-responsive microcapsules with a superparamagnetic porous membrane and thermo-responsive gates, superparamagnetic and thermo-responsive microcapsules with hydrogel membranes, dual thermo-responsive and molecular-recognizable membranes and multi-stimuli-responsive membrane gates with hierarchical structures are introduced. The content in this chapter provides a more open mind for designing and fabricating stimuli-responsive smart membranes.

11.1 Introduction

From the applications' point of view, smart membranes would be more favorable if they could respond to dual or even several stimuli simultaneously. Along these lines, dual/multi stimuli-responsive smart membranes have been designed and developed. According to Section 1.4, artificial environmental stimuli-responsive smart membranes can be designed as smart membranes with porous substrates and stimuli-responsive gates, smart membranes with grafted stimuli-responsive surfaces and stimuli-responsive smart hydrogel membranes. Therefore, dual/multi stimuliresponsive smart membranes can be designed by introducing dual/multi stimuliresponsive functions into the grafted polymers and the substrates respectively, or by introducing dual/multi stimuli-responsive functions into the grafted gates or surfaces, or by introducing dual/multi stimuli-responsive functions into the smart hydrogel membranes. In this chapter, dual stimuli-responsive microcapsules with a superparamagnetic porous membrane and thermo-responsive gates, superparamagnetic and thermo-responsive microcapsules with hydrogel membranes, dual thermoresponsive and molecular-recognizable membranes, and multi-stimuli-responsive membrane gates with hierarchical structures will be described.

11.2 Dual Stimuli-Responsive Microcapsules with Superparamagnetic Porous Membrane and Thermo-Responsive Gates

Superparamagnetic and thermo-responsive microcapsules possessing both magnetic field and temperature dual stimuli-responsive properties, which exhibit magnetic properties only when an external magnetic field is added, can be guided and aggregated more conveniently with the help of an external magnetic field and change the release rate of their contents following the change of temperature. Recently, the author's group developed a type of dual stimuli-responsive microcapsule that has a superparamagnetic porous membrane and thermo-responsive gates. [1]

11.2.1 Strategy for Fabricating Microcapsules with Superparamagnetic Porous Membrane and Thermo-Responsive Gates

The strategy for fabricating microcapsules with a superparamagnetic porous membrane and thermo-responsive gates is illustrated in **Fig.11.1**.^[1] Before preparing the microcapsule, oleic acid (OA) modified superparamagnetic Fe₃O₄ nanoparticles are synthesized using a chemical coprecipitation route followed by coating with OA. Subsequently, the modified Fe₃O₄ nanoparticles are introduced, to prepare the polyamide microcapsules with magnetic porous membranes by using the interfacial polymerization method, and then the microcapsule membranes are grafted with thermo-responsive poly(*N*-isopropylacrylamide) (PNIPAM) chains by employing plasma-induced grafting polymerization. When the temperature is below the lower critical solution temperature (LCST), the grafted PNIPAM chains in the magnetic thermo-responsive microcapsule membranes are in a swollen state and the gates of membrane pores show the "closed" situation; on the other hand, when the temperature is above the LCST, the PNIPAM chains are in a shrunken state and the gates of the membrane pores show the "open" situation. Thus, the release of substance from the microcapsules is controlled by changing the environmental temperature.

11.2.2 Preparation of Microcapsules with a Superparamagnetic Porous Membrane and Thermo-Responsive Gates

Fabrication of microcapsules with a superparamagnetic porous membrane and thermo-responsive gates includes the synthesis of OA modified Fe_3O_4 nanoparticles, the preparation of microcapsule membranes embedded with Fe_3O_4 nanoparticles by interfacial polymerization, and the fabrication of PNIPAM gates into the pores of microcapsule membranes by plasma-induced grafting polymerization.

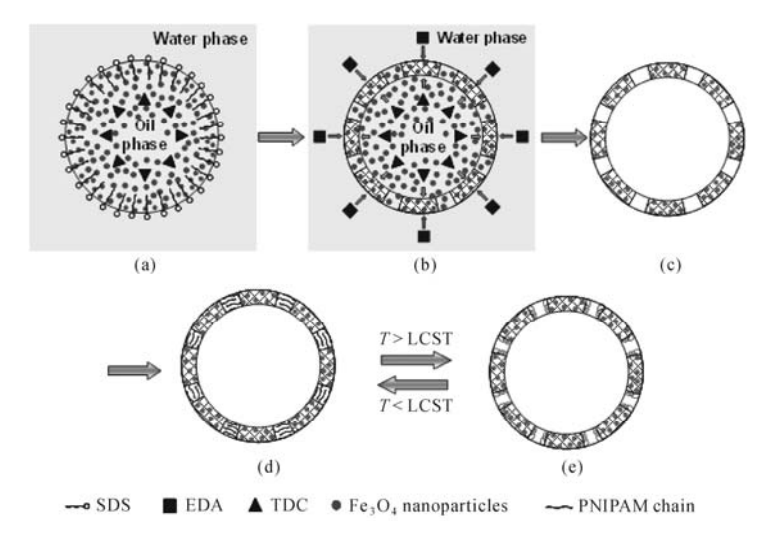


Fig.11.1. Strategy for fabricating microcapsules with superparamagnetic porous membrane and thermo-responsive gates. (a) Oil-in-water emulsion prepared by emulsification; (b) Core-membrane superparamagnetic microcapsule with a porous membrane prepared by interfacial polymerization; (c) Spherical hollow microcapsule with a superparamagnetic porous membrane prepared by freeze-drying the microcapsules; (d) Microcapsule with PNIPAM gates prepared using a plasma-induced grafting polymerization to graft linear PNIPAM chains into the pores of the membrane. The grafted PNIPAM chains are swollen and the gates "closed" at temperatures below the LCST (d) while they are shrunken and the gates "open" above the LCST (e). (Reproduced with permission from Ref. [1]). Copyright (2008), Elsevier

11.2.2.1 Synthesis and Characterization of OA Modified Fe₃O₄ Nanoparticles

Fe₃O₄ nanoparticles are synthesized using a chemical coprecipitation route. [2] 10 g of FeSO₄·7H₂O and 18 g of FeCl₃·6H₂O are dissolved into 142 ml of deionized water, followed by the rapid addition of 47 ml of NH₃·H₂O, and the solution is stirred vigorously for 3 min. The resulting magnetic nanoparticles are washed with deionized water repeatedly and finally diluted to 100 ml. The pH of aqueous solution suspended with nanoparticles is adjusted to 9~10 by the addition of NH₃·H₂O. To obtain OA modified Fe₃O₄ nanoparticles, OA is coated on the surface of Fe₃O₄ nanoparticles. Under stirring at 300 rpm, 4.3 ml of OA is slowly dropped into the dispersion at 80 °C over the course of 60 min. The whole process is carried out under a nitrogen atmosphere. After modification, these magnetic nanoparticles are extracted into xylene by simply adding NaCl as inducer. This xylene-based dispersion of OA modified magnetic nanoparticles is refluxed to remove most of the water under a nitrogen atmosphere and the concentration of magnetic nanoparticles is diluted with xylene to 40 mg·ml⁻¹ for further use. X-ray diffraction (XRD) patterns of Fe₃O₄ particles are recorded using an X-ray diffractometer (D/max-rA, Rigaku, Japan) with a CuKα radiation at 42 kV and 109 mA. The magnetic properties of Fe₃O₄ particles are measured by a Lakeshore

7,400 vibrating-sample magnetometer (VSM) at room temperature. The OA modified Fe_3O_4 particles are measured by Fourier transform infrared (FT-IR) with KBr on a Nicolet-560 spectrometer. A transmission electron microscope (TEM, JEM-100CX, JEOL, Japan) is used to observe the morphology and size of OA modified Fe_3O_4 particles with an acceleration voltage of 80 kV. TEM specimens are prepared by aspirating a xylene based dispersion sample onto a copper grid.

Fig.11.2 shows the XRD patterns of the obtained Fe_3O_4 particles.^[1] The presented XRD pattern features six strong Bragg diffraction peaks when 2θ is between 20° and 70° , which can be easily indexed as (220), (311), (400), (422), (511) and (440) planes of Fe_3O_4 in a cubic phase.^[3] The results confirm the successful synthesis of Fe_3O_4 crystals.

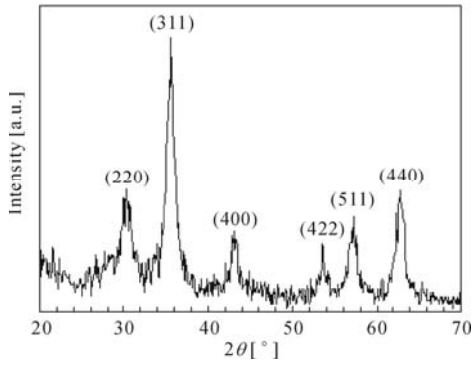


Fig.11.2. X-ray diffraction pattern of Fe₃O₄ nanoparticles (Reproduced with permission from Ref. [1]). Copyright (2008), Elsevier

The magnetization vs. field plots of Fe_3O_4 particles at room temperature are given in **Fig.11.3**.^[1] The saturation magnetization (M_s) of Fe_3O_4 particles is 61.42 emu·g⁻¹ and the hysteresis and coercivity are almost undetectable, suggesting that the superparamagnetic property of the Fe_3O_4 nanoparticles is satisfactory. Superparamagnetic particles are of great interest because they do not retain any magnetism after removal of the external magnetic field.

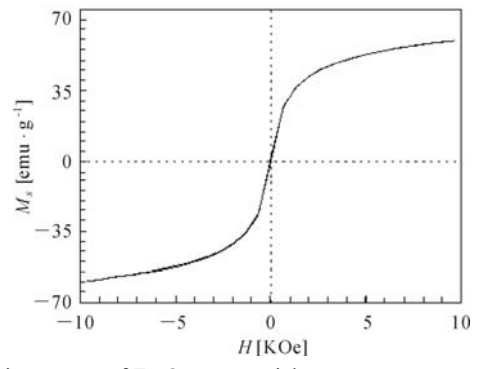


Fig.11.3. Magnetization curves of Fe₃O₄ nanoparticles at room temperature (Reproduced with permission from Ref. [1]). Copyright (2008), Elsevier

FT-IR analysis is performed to determine the surface composition of the OA modified Fe₃O₄ nanoparticles, as illustrated in **Fig.11.4.**^[1] In **Figs.11.4b** and **11.4c**, the 570.20 cm⁻¹ band belongs to Fe₃O₄.^[2] Compared with **Figs.11.4a** and **11.4b**, **Fig.11.4c** shows OA modified Fe₃O₄ nanoparticles obtain characteristic absorption bands of OA. The 2,918.90 cm⁻¹ and 2,849.30 cm⁻¹ bands in the spectrum of OA modified Fe₃O₄ nanoparticles (**Fig.11.4c**) belong to the asymmetric CH₂ stretch and the symmetric CH₂ stretch of OA.^[4,5] It is worth noting that the C=O stretch band of the carboxyl group, which is present at 1,706.31 cm⁻¹ in the FT-IR spectrum of pure OA (**Fig.11.4a**),^[4,5] is absent in the spectrum of the OA modified Fe₃O₄ nanoparticles (**Fig.11.4c**). Instead, two new bands at 1,518.65 cm⁻¹ and 1,403.62 cm⁻¹ appear in **Fig.11.4c**, which is a characteristic peak of the asymmetric COO⁻ and the symmetric COO⁻ stretch. This result confirms that OA is chemisorbed as a carboxylate onto the surface of Fe₃O₄ nanoparticles.^[2,4]

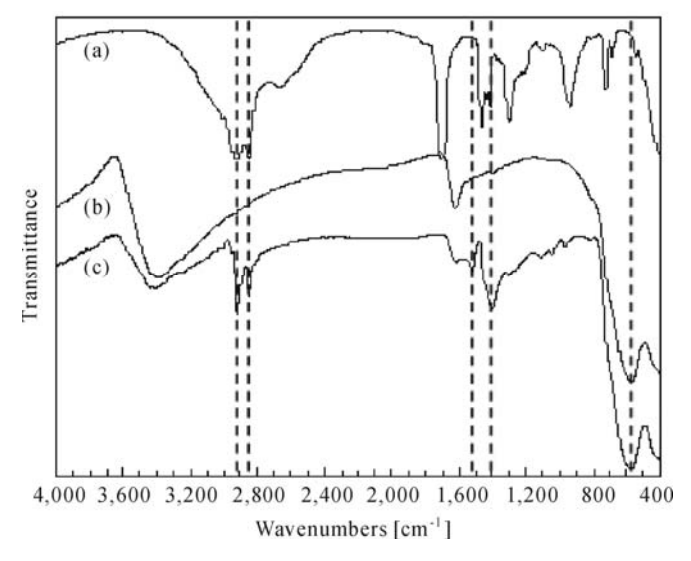


Fig.11.4. FT-IR spectra of pure OA (a), Fe₃O₄ nanoparticles (b) and OA modified Fe₃O₄ nanoparticles (c) (Reproduced with permission from Ref. [1]). Copyright (2008), Elsevier

TEM observation is introduced to characterize the morphology and distribution of the OA modified Fe_3O_4 nanoparticles in xylene. The representative TEM micrograph is shown in Fig.11.5, which clearly shows that the mean diameter of OA modified Fe_3O_4 particles is about 10 nm. Each particle is separated from its neighbors by the OA absorbed on the particles. It can be seen that Fe_3O_4 nanoparticles disperse quite well in xylene, which is essential for embedding them homogeneously inside the microcapsule membranes.

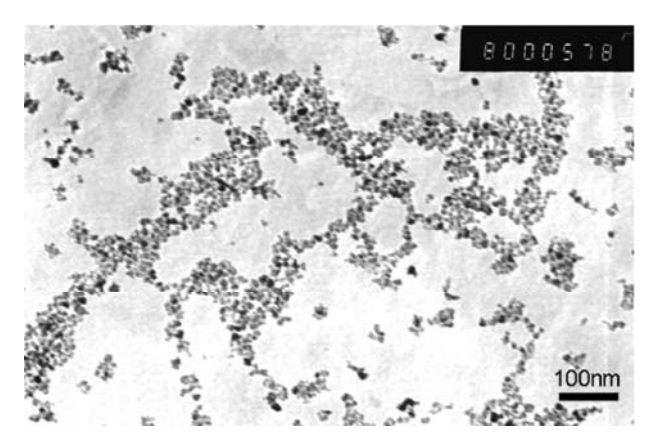


Fig.11.5. TEM photograph of OA modified Fe₃O₄ nanoparticles (Reproduced with permission from Ref. [1]). Copyright (2008), Elsevier

11.2.2.2 Preparation of Microcapsule Membranes Embedded with Fe_3O_4 Nanoparticles by Interfacial Polymerization

The microcapsule membranes embedded with Fe₃O₄ nanoparticles are prepared from monomers terephthalyl chloride (TDC) and ethylenediamine (EDA) by interfacial polymerization with OA modified Fe₃O₄ nanoparticles in the oil phase.^[1] Firstly, 10 ml of the organic solvent mixture of benzene/xylene (2:1 (v/v)), containing both 0.5 mol·L⁻¹ TDC and 2 ml of xylene-based dispersion of OA modified Fe₃O₄ nanoparticles, is added to 160 ml of the water phase containing 1.0 wt% of sodium dodecyl sulfate (SDS) as an emulsifier. Next, the mixture is stirred for 10 min at a stirring speed of 800 r min⁻¹ to yield an oil-in-water emulsion. The stirring speed is then reduced to 150 r·min⁻¹ and both 15 ml of EDA and the buffer (i.e., 20 ml of water containing 1.18 mol·L⁻¹ sodium carbonate) are added into the emulsion and the mixture is further stirred. During emulsification and interfacial polymerization, the temperature is kept at 10 °C using a thermostatic unit and the polymerization time is 30 min. The magnetic microcapsules are separated by magnetic and gravitational fields alternately and washed ten times using deionized water in order to remove emulsifier and remnant monomers. These microcapsules are then freeze-dried. Polyamide microcapsules without any Fe₃O₄ nanoparticles in the membranes are also prepared as references.

11.2.2.3 Grafting PNIPAM into the Pores of Microcapsule Membranes by Plasma-Induced Grafting Polymerization

Plasma-induced grafting polymerization is used to graft linear PNIPAM chains into the pores of the microcapsule membrane according to the steps described in Section 2.2.1.1.^[1] Briefly, the freeze-dried magnetic microcapsules are placed in a

transparent glass tube which is then filled with argon gas. The tube is then evacuated to a pressure of 10 Pa and the microcapsules are subjected to a radio frequency plasma operating at 13.56 MHz, 30 W, sustained for 60 s. Subsequently, under inert atmosphere conditions, the microcapsules are immersed in 80 ml of 1.0 wt% NIPAM monomer solution and the graft polymerization takes place in a shaking constant-temperature bath at 30 °C for 60 min. The experimental parameters of the plasma-induced grafting polymerization used in this study are chosen in order to obtain a low graft yield of PNIPAM in the membrane pores. The PNIPAM-grafted microcapsules are separated using a magnetic field and washed five times with deionized water.

11.2.3 Morphology and Composition Characterization of the Microcapsules

The surface and cross-sectional morphologies of magnetic microcapsules are observed using a scanning electron microscope (SEM, JSM-5900LV, JEOL, Japan). Like modified Fe₃O₄ particles, the chemical composition of PNIPAM-grafted magnetic microcapsules is also confirmed by FT-IR with KBr. An energy dispersive X-ray spectrometer (EDX) in conjunction with a field emission scanning electron microscope (FE-SEM, S-4800, Hitachi, Japan) is employed to confirm the embedding of Fe₃O₄ nanoparticles in the magnetic microcapsule membrane. Thermogravimetric analysis (TGA) measurement is performed with a thermal analyzer (Q500, TA Instruments, USA) with a heating rate at 10 °C·min⁻¹ from room temperature up to 800 °C under a nitrogen atmosphere, in order to confirm the mass content of Fe₃O₄ nanoparticles inside the microcapsule membrane. The mean diameter of grafted magnetic microcapsules is measured using an optical microscope (BX 61, Olympus, Japan).

Fig.11.6 shows representative SEM micrographs of the external surface and cross-sectional views of magnetic microcapsules.^[1] The microcapsules show a satisfactorily spherical appearance and their mean diameter is about 70 μm. They have asymmetrical and porous membrane structures whose outer surface (the water phase side in the interfacial polymerization) is smooth and the inner surface (the oil phase side) rough. This reflects the fact that the interfacial polymerization proceeds by the diffusion of the amine monomers from the aqueous to the oil phase.^[6] Because of the porous structure of the membrane, these microcapsules are suitable for use as the substrate for preparing thermo-sensitive microcapsules by fabricating thermo-responsive gates in the membrane pores.

Fig.11.7 shows the FT-IR spectra of pure polyamide microcapsules, magnetic microcapsules and PNIPAM-grafted magnetic microcapsules. ^[1] In **Fig.11.7a**, all the peaks are the characteristic peaks of polyamide. Comparing **Figs.11.7b** and **11.7c** with **Fig.11.7a**, the peaks are almost the same except the one around 570 cm⁻¹ which belongs to the Fe₃O₄ nanoparticles as mentioned above. To further confirm

the Fe_3O_4 nanoparticles are embedded into the membrane of magnetic microcapsules, EDX line scan analysis is employed. **Fig.11.8** shows an FE-SEM micrograph and EDX line scan results of the cross-section of the magnetic microcapsule. ^[1] The Fe and O elements are distributed throughout the cross-section of the microcapsule membrane. The results reveal that the Fe_3O_4 nanoparticles are embedded in the membrane of microcapsules successfully and homogeneously during the interfacial polymerization process.

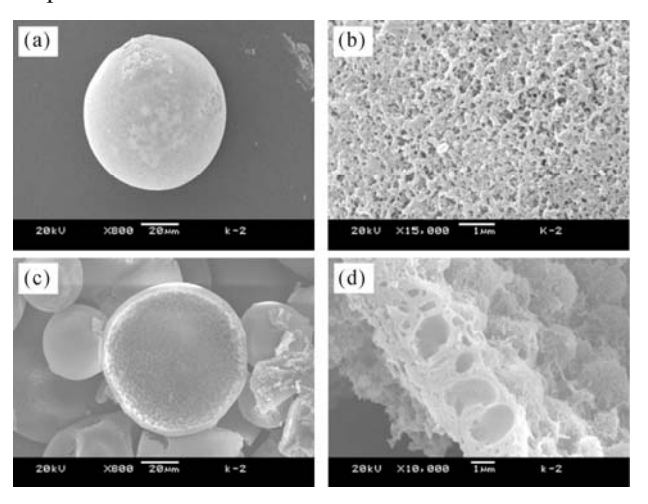


Fig.11.6. SEM micrographs of the magnetic microcapsules. (a) (b) Outer surface; (c) (d) Cross-section (Reproduced with permission from Ref. [1]). Copyright (2008), Elsevier

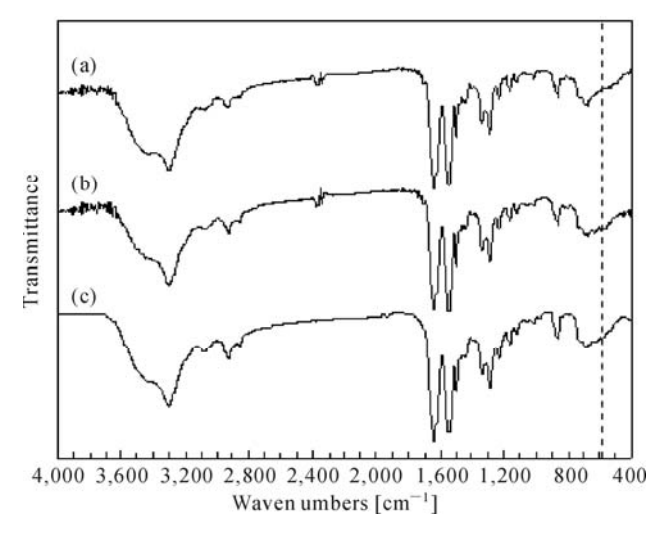


Fig.11.7. FT-IR spectra of pure polyamide microcapsules (a), magnetic microcapsules (b) and PNIPAM-grafted magnetic microcapsules (c) (Reproduced with permission from Ref. [1]). Copyright (2008), Elsevier

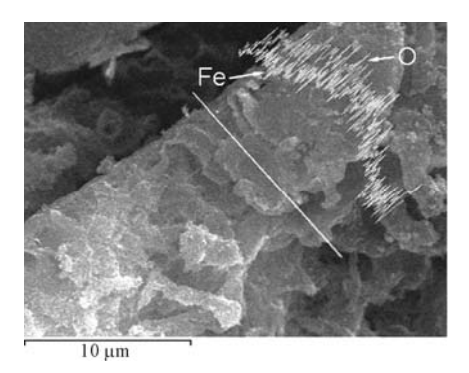


Fig.11.8. FE-SEM micrograph and EDX scan of the cross-section of magnetic microcapsule, the local line scan curves of Fe and O elements (Reproduced with permission from Ref. [1]). Copyright (2008), Elsevier

Fe $_3O_4$ nanoparticles, magnetic microcapsules and pure polyamide microcapsules are characterized with TGA carried out in a nitrogen environment, as shown in Fig.11.9. For Fe $_3O_4$ nanoparticles, at temperatures below 300 °C, the loss of weight is attributed to the gasification of water while, above 300 °C, the mass almost remains constant and the residual mass percentage is 94.02 wt% at 800 °C. The pure polyamide microcapsule references start decomposing to a great extent at 400 °C and the residual mass percentage is 3.63 wt% at 800 °C, while the residual mass percentage of the magnetic microcapsule is 14.38 wt% at 800 °C. This verifies that the embedded content of Fe $_3O_4$ nanoparticles in the magnetic microcapsule is about 10.75 wt%.

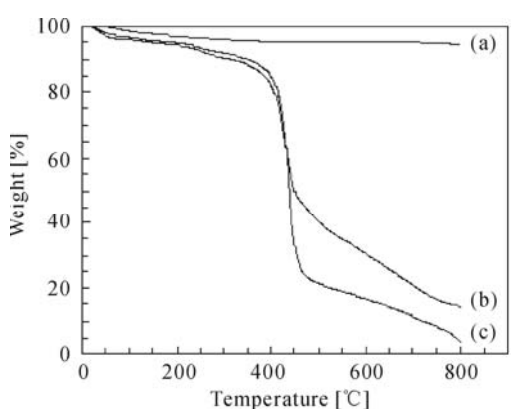


Fig.11.9. Thermogravimetric curves of Fe_3O_4 nanoparticles (a), magnetic microcapsules (b) and pure polyamide microcapsules (c) in N_2 atmosphere (Reproduced with permission from Ref. [1]). Copyright (2008), Elsevier

Comparing **Fig.11.7b** with **Fig.11.7c**, the peaks are almost the same as each other. Because PNIPAM is also a kind of polyamide, its characteristic peaks could be covered by the peaks of polyamide magnetic microcapsules. That means the

PNIPAM grafting cannot be confirmed from the FT-IR spectra in **Fig.11.7**. In order to verify the grafting of PNIPAM in the pores of PNIPAM-grafted magnetic microcapsule membranes, a SEM micrograph of the cross-section of the PNIPAM-grafted magnetic microcapsule membrane is illustrated in **Fig.11.10**. Comparing the microstructure in **Fig.11.10** with that of ungrafted magnetic microcapsule membrane shown in **Fig.11.6d**, it is found that the cross-sections of ungrafted and PNIPAM-grafted magnetic microcapsules have significantly different structures. After grafting PNIPAM onto the inner pore surface in the porous membrane of the magnetic microcapsules, the pore size becomes smaller. The porous structure across the cross-section of the microcapsule is covered by PNIPAM throughout the entire membrane thickness. This reveals that PNIPAM is grafted onto the inner pore surface in the porous membrane of the magnetic microcapsules.

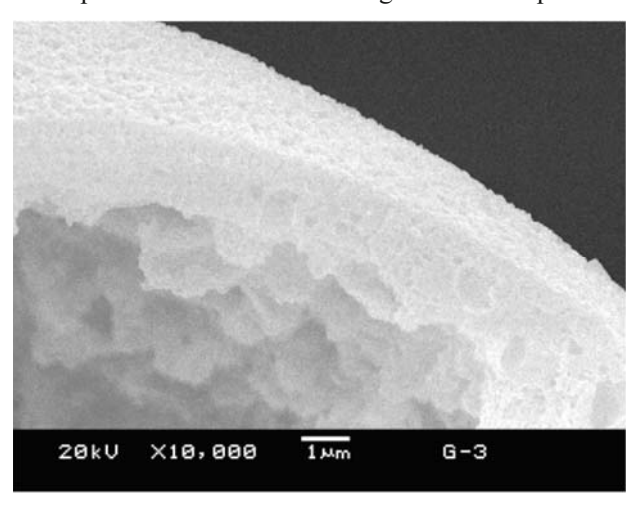


Fig.11.10. SEM micrograph of the cross-section of PNIPAM-grafted magnetic microcapsule (Reproduced with permission from Ref. [1]). Copyright (2008), Elsevier

11.2.4 Magnetic Properties of PNIPAM-Grafted Magnetic Microcapsules

A vibrating-sample magnetometer (VSM, 7400, Lakeshore, USA) is used to study the magnetic properties of the PNIPAM-grafted magnetic microcapsules. The typical magnetization curves of PNIPAM-grafted magnetic microcapsules and those that have been used 30 times are displayed in **Fig.11.11**.^[1] It can be seen that the hysteresis and coercivity are almost undetectable, suggesting that the grafted microcapsules retain a satisfactory superparamagnetic property at room temperature resulting from Fe₃O₄ nanoparticles. The superparamagnetic property of the microcapsules is critical for their application in biomedical and bioengineering fields, which prevents them from aggregation and enables them to redisperse

rapidly when the magnetic field is removed. [7] The M_s of the PNIPAM-grafted magnetic microcapsule is 6.31 emu·g⁻¹, which is much lower than that of Fe₃O₄ nanoparticles (61.42 emu·g⁻¹). The reduced M_s can be attributed to the low content of Fe₃O₄ nanoparticles in the magnetic microcapsule membranes. The M_s value of the microcapsules represents a magnetic content of about 10.3 wt% of the Fe₃O₄ nanoparticles. This result is very close to the result from the thermogravimetric analysis. Although the PNIPAM-grafted magnetic microcapsules exhibit relatively low M_s , they show a satisfactory magnetic-responsive aggregation and redispersion property in deionized water by adding and removing the magnetic field, respectively (Fig.11.12).[1] As shown in Fig.11.11, after having been used or operated with magnetic stimuli 30 times (the microcapsules are washed with deionized water after each operation), the M_s of PNIPAM-grafted magnetic microcapsules is almost the same as that of the fresh PNIPAM-grafted magnetic microcapsules. The results reveal that the superparamagnetic property of the PNIPAM-grafted magnetic microcapsules does not reduce with time. That is to say, the magnetic nanoparticles embedded into the membrane of microcapsules do not leach out with time. Owing to van der Waals attractive forces between the OA modified Fe₃O₄ nanoparticles and polyamide polymers and the embedment function of polyamide polymer surrounding the Fe₃O₄ nanoparticles, the Fe₃O₄ nanoparticles are kept tightly in the microcapsule membrane. That means the prepared microcapsules possess satisfactory time-independent magnetic responsive ability and can be readily guided and collected with the help of an external magnetic field.

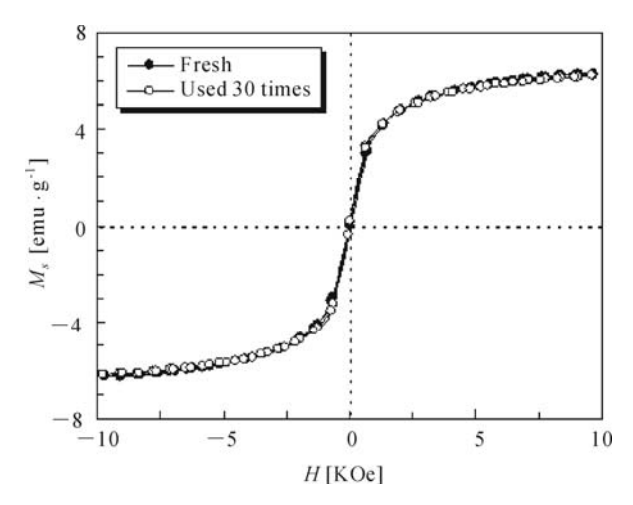


Fig.11.11. Magnetization curves of fresh PNIPAM-grafted magnetic microcapsules and those that have been used 30 times. The magnetization curves are measured at room temperature (Reproduced with permission from Ref. [1]). Copyright (2008), Elsevier

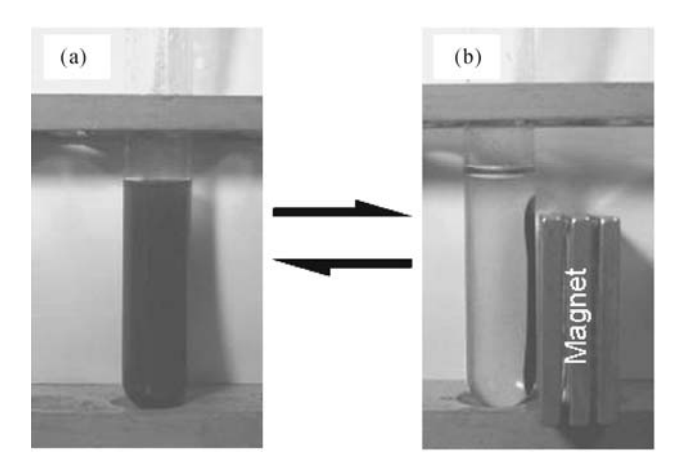


Fig.11.12. Photos of the magnetic-responsive aggregation (a \rightarrow b) and redispersion (b \rightarrow a) of PNIPAM-grafted magnetic microcapsules in deionized water by adding and removing external magnetic field. (a) Without external magnetic field; (b) With external magnetic field (the magnetic field strength of the magnet is 3 T). (Reproduced with permission from Ref. [1]). Copyright (2008), Elsevier

11.2.5 Thermo-Responsive Controlled-Release Properties of PNIPAM-Grafted Magnetic Microcapsules

The controlled release experiment is carried out according to the method described in Section 3.2.3. The freeze-dried ungrafted magnetic microcapsules and PNIPAMgrafted magnetic microcapsules are dialyzed against VB₁₂ aqueous solution with a concentration of 4×10⁻⁵ mol·L⁻¹ for more than 72 h. The dialysis is carried out in shaking constant-temperature baths kept at 25 and 40 °C alternately. The permeability of the solute across the microcapsule membranes is measured by determining the increase in the solute concentration of the surrounding medium with time, after mixing a known volume of microcapsule dispersion with a known solute concentration having the same volume of deionized water. During the measurements, the temperature of the liquid is kept constant using a thermostatic unit. The VB12 concentration at regular intervals is measured using a UV-vis spectrophotometer at a wavelength of 361 nm. The release experiments are carried out by changing the environmental temperature across the LCST of PNIPAM. The chosen route is: 40 °C \rightarrow 25 °C \rightarrow 37 °C \rightarrow 28 °C \rightarrow 34 °C \rightarrow 31 °C. To ensure that there is enough solute inside the microcapsules for release during the entire release experiment, solute (VB₁₂) is reloaded into the inner space of the microcapsules after each run. For each data, the measurement is repeated at least 3 times to analyze the experimental error. The permeability coefficient of the solute across the microcapsule membranes is calculated using Eqs.(3.1) and (3.2).

The permeability coefficients of VB₁₂ releasing from ungrafted and PNIPAM-

grafted magnetic microcapsule membranes are shown in Fig.11.13 as a function of temperature. [1] For the PNIPAM-grafted magnetic microcapsule membranes, the values of permeability P are low when the environmental temperature is below 31 °C, while they increase little between 25 °C and 31 °C; on the other hand, the values of P are much higher when the environmental temperature is above 34 °C, while the P values increase little when the temperature increases from 34 °C to 40 °C. A sharp transition in the permeability coefficient occurs on going from 31 °C to 34 °C, which corresponds to the LCST of PNIPAM (around 32 °C). On the contrary, the P of ungrafted magnetic microcapsule membranes does not show such a sharp transition between 31 °C and 34 °C under the same experimental conditions. That means the PNIPAM-grafted magnetic microcapsules show a thermo-responsive release characteristic. At temperatures below the LCST, the linear grafted PNIPAM chains in the pores of the microcapsule membranes are swollen and the pores of the membranes are "closed" by the PNIPAM gates. As a result, the release of VB₁₂ molecules across the microcapsule membranes is slow. In contrast, at temperatures above the LCST, the grafted PNIPAM chains in the membrane pores are shrunken and therefore the pores of the microcapsule membranes are "open", which results in a faster release rate of the VB₁₂ molecules across the microcapsule membranes. [6,8] Consequently, the release rate of the solute molecules from the NIPAM-grafted magnetic microcapsules is much larger at temperatures above the LCST than that below the LCST. This temperaturedependent "ON/OFF" characteristic of PNIPAM-grafted magnetic microcapsules enables the release of their contents in a controlled way by simply adjusting the environmental temperature.

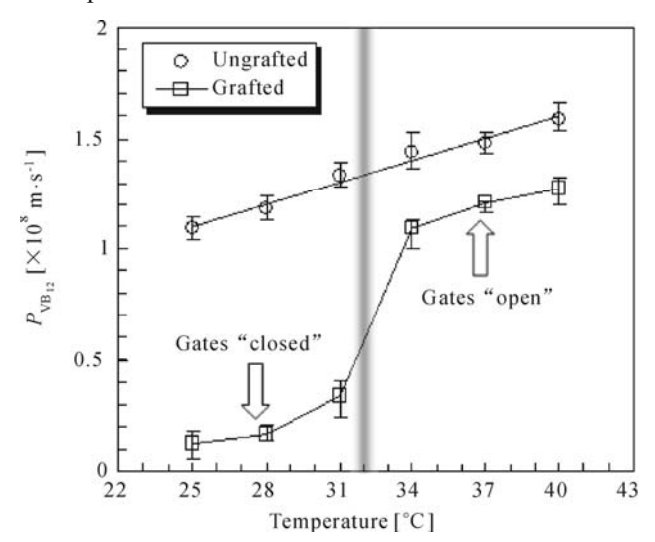


Fig.11.13. Thermo-responsive release of VB₁₂ from ungrafted and PNIPAM-grafted magnetic microcapsules (Reproduced with permission from Ref. [1]). Copyright (2008), Elsevier

11.3 Superparamagnetic and Thermo-Responsive Microcapsules with Hydrogel Membranes

In **Section 4.3**, a thermo-induced self-bursting microcapsule with magnetic-targeting property has been introduced, and the prepareation of this microcapsule is schematically shown in **Fig.4.5**.^[9] In the microcapsule membrane, the embedded Fe₃O₄ nanoparticles contribute a magnetic-response property to the microcapsule^[1] and the PNIPAM network makes the membrane thermo-responsive. As a result, the Fe₃O₄/PNIPAM membrane enables the microcapsule to undergo magnetic-guided targeting delivery, have no unintended drug leakage during microcapsule transport and exhibit thermo-triggered drug release. In Section **4.3.2**, thermo-responsive controlled-release characteristics of the microcapsules have been demonstrated.

Fig.11.14 is a series of snapshots showing the magnetic-guided targeting performance of Sudan III-loaded microcapsules from site A to site B.^[9] The microcapsules are randomly dispersed in deionized water at 20 °C at the beginning (**Fig.11.14a**). When a magnet is placed under the Petri dish, the microcapsules are attracted together in site A (**Fig.11.14b**). After that, the aggregated microcapsules as a whole are moved quickly following the arrows from site A to site B under the magnetic guide and finally trapped in the targeted site B (**Figs.11.14b** to **11.14f**). Such a magnetic-responsive property can make the microcapsules achieve the purpose of site-and/or route-specific targeting drug delivery. Once the microcapsules are specifically delivered to the desired site, the release of the encapsulated chemicals can be triggered by local heating or by applying a high frequency alternating magnetic field locally, because the superparamagnetic nanoparticles can transform the energy of an alternating magnetic field into heat.^[10]

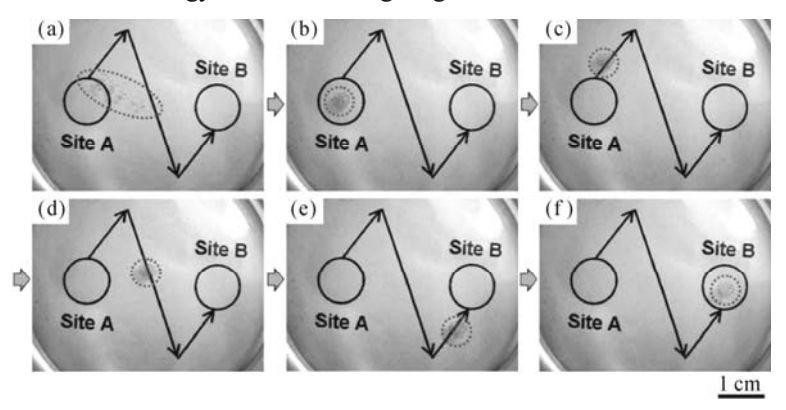


Fig.11.14. Snapshots of the magnetic-guided targeting behavior of microcapsules loaded with Sudan III in water at 20 $^{\circ}$ C. A cylindrate NdFeB magnet with size of Ø12 mm×8 mm was placed under the Petri dish to guide the microcapsules. The magnetic field strength of the magnet is 0.3 T. (Reproduced with permission from Ref. [9]). Copyright (2009), Wiley-VCH Verlag GmbH & Co. KGaA

11.4 Dual Thermo-Responsive and Molecular-Recognizable Membranes

In fact, the thermo-responsive membranes for chiral resolution described in Chapter 5, the temperature-dependent molecular-recognizable membranes for affinity separation described in Section 6.3 and the molecular-recognizable smart membranes described in Chapter 10 all show dual thermo-responsive and molecularrecognizable characteristics. As mentioned in Section 1.3.4, molecular-recognizable smart materials are usually designed with either β -cyclodextrin (CD) or crown ether as molecular recognizing receptor and with poly(*N*-isopropylacrylamide) (PNIPAM) as actuator. Consequently, besides the molecular-recognition property, such smart materials are also featured with a thermo-responsive property. Therefore, when the smart membranes are fabricated with such materials, the smart membranes are also featured with dual thermo-responsive and molecular-recognizable properties. For example, when poly(NIPAM-co-CD) chains (Figs.1.14 and 1.15) are grafted into the membrane pores as functional gates, the membranes show dual thermo-responsive and molecular-recognizable gating characteristics due to both thermo-responsive phase transition of PNIPAM and molecular-recognition of β-CD.^[11] As illustrated in **Fig.10.1**, the poly(NIPAM-co-CD) functional gate can achieve triple signal-responsive gating functions as follows (Fig.11.15): (1) Gate "open/closed" function triggered by temperature change. (2) Gate "open" function isothermally triggered by recognition of certain guest molecules with a hydrophobic side group (e.g., 8-anilino-1-naphthalenesulfonic acid ammonium salt (ANS)) at a lower temperature. (3) Gate "closed" function isothermally triggered by recognition of different guest molecules with a hydrophilic side group or without side group (e.g., 2-naphthalenesulfonic acid (NS)) at a higher temperature. [11]

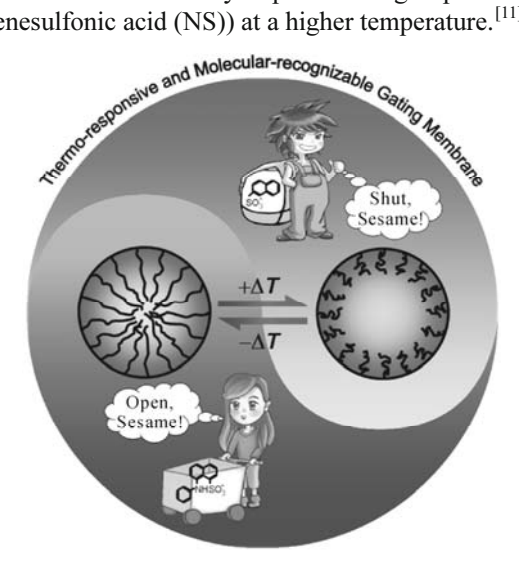


Fig.11.15. Schematic illustration of the pore "open/closed" gating function of poly(NIPAM-co-CD)-grafted dual thermo-responsive and molecular-recognizable membrane

11.5 Multi-Stimuli-Responsive Membrane Gates with Hierarchical Structures

By using the atom-transfer radical polymerization (ATRP) method described in Section 2.2.2.1, it is possible to fabricate multi-stimuli-responsive membrane gates with hierarchical structures. For example, by using the surface-initiated ATRP method, gating membranes with grafted diblock poly(methacrylic acid)-block-poly(N-isopropylacylamide) (PMAA-b-PNIPAM) or poly(N-isopropylacylamide)-block-poly(methacrylic acid) (PNIPAM-b-PMAA) chains in the membrane pores can be prepared (Fig.11.16). Such gating membranes show a multi-response to temperature, pH, salt concentration and ionic species due to the individual or cooperative function of PNIPAM and PMAA segments (Fig.11.16), in which the thermo-response is contributed by the grafted PNIPAM segments, the pH-response is contributed by the grafted PMAA segments, the salt concentration response and the ion-response are contributed by the cooperative function of grafted PNIPAM and PMAA segments. Along these lines, other multi-stimuli-responsive membranes or even more complicated multi-stimuli-responsive membranes can be designed and fabricated.

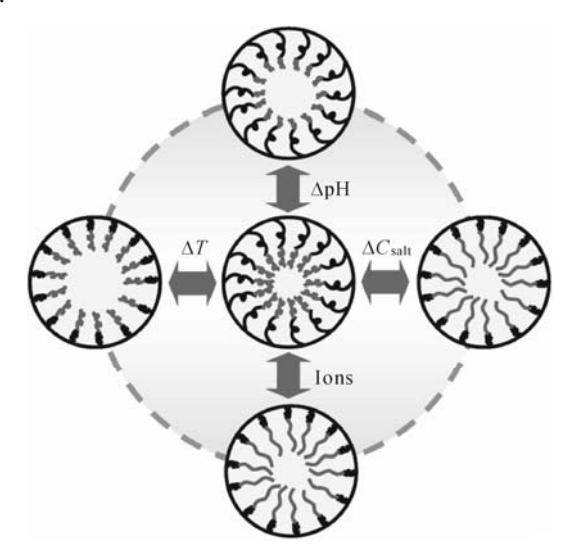


Fig.11.16. Schematic illustration of the pore "open/closed" function of a multi-stimuli-responsive membrane with PNIPAM-*b*-PMAA-grafted hierarchical gates

11.6 Summary

In summary, smart membranes would be more favorable if they could respond to dual or even several stimuli simultaneously from an applications' point of view. Dual/multi stimuli-responsive smart membranes can be designed by introducing dual/multi stimuli-responsive functions into the grafted polymers and the substrates respectively, or by introducing dual/multi stimuli-responsive functions into the grafted gates or surfaces, or by introducing dual/multi stimuli-responsive functions into the smart hydrogel membranes. The content in this chapter provides a more open mind for designing and fabricating dual/multi stimuli-responsive smart membranes.

References

- [1] Yang W C, Xie R, Pang X Q, Ju X J, Chu L Y. Preparation and characterization of dual stimuli-responsive microcapsules with a superparamagnetic porous membrane and thermo-responsive gates. *Journal of Membrane Science*, **2008**, *321*: 324-330.
- [2] Sun Y B, Ding X B, Zheng Z H, Cheng X, Hu X H, Peng Y X. Magnetic separation of polymer hybrid iron oxide nanoparticles triggered by temperature. *Chemical Communication*, **2006**, *26*: 2765-2767.
- [3] Fang H, Ma C Y, Wan T L, Zhang M, Shi W H. Fabrication of monodisperse magnetic Fe₃O₄-SiO₂ nanocomposites with core-shell structures. *Journal of Physical Chemistry C*, **2007**, *111*: 1065-1070.
- [4] Wu N Q, Fu L, Su M, Aslam M, Wong K C, Dravid V P. Interaction of fatty acid monolayers with cobalt nanoparticles. *Nano Letters*, **2004**, *4*: 383-386.
- [5] Zhang L, He R, Gu H C. Oleic acid coating on the monodisperse magnetite nanoparticles. *Applied Surface Science*, **2006**, 253: 2611-2617.
- [6] Chu L Y, Park S H, Yamaguchi T, Nakao S. Preparation of thermo-responsive coreshell microcapsules with a porous membrane and poly(*N*-isopropylacrylamide) gates. *Journal of Membrane Science*, **2001**, *192*: 27-39.
- [7] Hafeli U, Schutt W, Teller J, Zborowski M. *Scientific and clinical applications of magnetic carriers*. Plenum Press, New York, **1997**.
- [8] Chu L Y, Park S H, Yamaguchi T, Nakao S. Preparation of small-sized monodispersed thermo-responsive core-shell microcapsules. *Langmuir*, **2002**, *18*: 1856-1864.
- [9] Wang W, Liu L, Ju X J, Zerrouki D, Xie R, Yang L, Chu L Y. A novel thermo-induced self-bursting microcapsule with magnetic-targeting property. *ChemPhysChem*, **2009**, *10*: 2405-2409.
- [10] Satarkar N S, Hilt J Z. Magnetic hydrogel nanocomposites for remote controlled pulsatile drug release. *Journal of Controlled Release*, **2008**, 130:246-251.
- [11] Yang M, Xie R, Wang J Y, Ju X J, Yang L, Chu L Y. Gating characteristics of thermo-responsive and molecular-recognizable membranes based on poly(N-isopropylacrylamide) and β -cyclodextrin. *Journal of Membrane Science*, **2010**, *355*: 142-150.
- [12] Chen Y C. *Stimuli-responsive membranes with hierarchical gating structures*. M.S. Thesis, Sichuan University, **2010** (in Chinese).

Perspectives on Smart Membrane Materials and Systems

In this chapter, the development trend of smart membrane materials and systems and the potential applications of smart membranes are introduced and discussed briefly.

12.1 Development Trend of Smart Membrane Materials and Systems

Nowadays, stimuli-responsive smart materials are attracting ever-increasing attention from all over the world. In 2007, Langmuir published its first issue of the year as a special themed issue "Stimuli-Responsive Materials: Polymers, Colloids and Multicomponent Systems", and the editors mentioned that this issue "focuses on an area of intensive current study that has emerged from the application of bioinspired mechanisms to create functional systems using traditional materials". In February 2010, Soft Matter published its issue No. 4 of this year as a special themed issue "Emerging Themes in Soft Matter: Responsive and Active Soft Materials", and the editors mentioned that "the general theme of this issue is the design and fabrication of 'smart' materials that are capable of producing a global behavior in response to a local signal". In August 2010, Advanced Materials published its issue No. 31 of this year as a special themed issue "Stimuli-Sensitive Polymers", and the editors mentioned that "the field of stimuli-sensitive polymers is presently progressing rapidly" and "applications are being realized based on stimuli-sensitive polymers for various areas including aerospace, packaging, textiles, microfluidics, sensors and actuators as well as bioengineering". Novel and efficient artificial smart materials are being developed and reported continuously, which are certainly promoting the development of smart membrane materials and systems.

Up to now, various stimuli-responsive smart membrane materials and systems

have been designed and developed. Worldwide, considerable effort is being deployed to develop smart membrane materials and systems. The technological benefits of such membrane materials and systems have begun to be identified and demonstrators are under construction for a wide range of applications from controlled drug delivery, to chemical separation, to water treatment, to bioseparation, to chemical sensors, to chemical valves, to tissue engineering, etc.

In the field of smart membrane materials and systems, the following two topics will be the main focus of research in the future. One is the development of novel and efficient smart membrane materials and the other is the enhancement of smart membrane processes. For the first topic, the process-oriented design of efficient smart membrane materials, the concept design of smart membrane materials and systems with novel functions, the micro/nano-structure-controllable fabrication of smart membrane materials and the stability and large-scale production of smart membrane materials and systems are some foreseeably important themes. For the second topic, the improvement in the response rate of smart membranes, the improvement in the sensitivity of smart membranes and the development of multi-stimuli-responsive complex smart membrane processes are some important themes that should be involved.

"To Innovate, Learn from Nature!" This is definitely the right way for scientists and technologists in the field of smart membrane materials and systems to develop novel smart membrane materials and to improve smart membrane processes. Nature is demonstrating numerous original models for achieving efficient artificial biomimetic smart membrane materials and systems.

12.2 Potential Applications of Smart Membranes

Artificial smart membranes are considered as one of the most important and promising topics in the field of membrane science and technology in the 21st century, although they are still in their initial development stage now. The potential applications of smart membranes are listed as, but not limited to, the following fields:

- Controlled release: *e.g.*, environmental signal-responsive controlled release of substances, self-regulated controlled release, etc.
- Targeted or self-regulated drug delivery: *e.g.*, site-targeted, time-programmed, or self-regulated delivery of drugs or chemicals or DNA, etc.
- Bio/chemical separation: *e.g.*, stimuli-responsive surface-regulated separation, self-regulated adsorption/desorption separation with thermo-responsive membranes, molecular-recognition separation, etc.
- Bio/chemical sensors/actuators: *e.g.*, potassium ion sensors/actuators, heavy metal ion sensors/actuators, glucose concentration sensors/actuators, specific molecule sensors/actuators, etc.
- Bio/chemical valves: e.g., heavy metal ion valves, self-regulated insulin valves,

thermo-responsive gates, molecular-recognition valves, etc.

- Artificial cells: e.g., artificial cells with environmental response properties, etc.
- Tissue engineering: *e.g.*, dead-cell-signal (*e.g.*, abnormal potassium ion concentration) recognizable cell culturing systems, etc.
- Water treatment: e.g., self-regulated removal of heavy metal ions, pollutant-recognizable filtration and separation, etc.
- Smart removers: *e.g.*, microcapsule membrane containers that can recognize and suck in heavy metal ions, thermo-responsive micro-grabbers, etc.
-and more.

With more and more smart membranes being developed and better and better performances being achieved, it is definitely to be expected that smart membrane materials and systems will be applied more and more widely. I believe that smart membranes might be applied in some cases in the future that we cannot even imagine today.

The author sincerely hopes that the content of this book will initiate new endeavors and discussions among scientists and technologists working with continued inspiration and enthusiasm toward the design and fabrication of novel stimuli-responsive smart membrane materials and systems.

Index

A Acidic hydrolysis of Schiff base, 8-186	Benzo-15-crown-5-acrylamide (B15C5Am), 1-10
Acrylamide (AAM), 2-61	Beta-cyclodextrin (β -CD), 1-12
3-Acrylamidophenylboronic acid	Bio/chemical sensors/actuators, 12-260
(AAPBA), 1-8	Bio/chemical sensors/actuators, 12-260
Actuator, 10-217	Bio/chemical valves, 12-260
*	· · · · · · · · · · · · · · · · · · ·
Adsorption-enantioselective membrane, 5-122	Biomembranes, 1-1
	Bionic technology, 1-2
Adsorption-selective membranes, 5-122	Bovine serum albumin, 6-145
	2-Bromoisobutyryl bromide (BIBB), 2-27
Affinity separation, 6-145	
Aggregation, 3-87	Bubble-point experiments, 2-35
3-Aminopropyl trimethoxysilane (ATMS),	Burst release, 4-104
2-27	Butyl methacrylate (BMA), 2-61
8-Anilino-1-naphthalenesulfonic acid	~
ammonium salt (ANS), 1-12	C
Anionic surfactant, 3-87	Cancer, 4-103
Anodic aluminum oxide (AAO) membranes,	Capillary microfluidic device, 4-115
2-27	Carbodiimide, 9-198
ANS-recognition gating coefficient,	CCD camera, 4-101
10-233	Cell membrane, 1-2
Anticancer drugs, 4-103	Chain-chain zipper effect, 2-64
Artificial cells, 12-260	Chemical coprecipitation, 11-242
Artificial smart membranes, 1-1	Chemical grafting, 2-20
Association constant, 5-123	Chiral recognition, 5-121
Atomic force microscope (AFM), 2-26	Chiral resolution, 5-121
Atom-transfer radical polymerization	Chiral selectivity, 5-121
(ATRP), 2-27	Chiral selectors, 5-121
	Chitosan, 8-185
В	Chitosan hydrogel membranes, 8-185
Benzo-18-crown-6-acrylamide	Coefficient of variation (CV), 8-189
(BCAm), 1-10	Concanavalin A, 1-8

Concentration-driven diffusion, 7-169 Concentration-driven molecular diffusion,	Drug release kinetics, 3-82 Dual-/multi-stimuli-responsive smart
2-21	membranes, 11-241
Confocal laser scanning microscope	Dual stimuli-responsive microcapsules,
(CLSM), 4-100	11-241
Contact angle (θ) , 2-61	Dual thermo-responsive and molecular-
Contact angle instrument, 6-150	recognizable membranes, 11-241,
Continuous phase, 3-83	255
Controlled factor (<i>CF</i>), 7-180	Dynamic atomic force microscopy
Controlled release, 12-260	(DFM), 2-26
Core/shell microparticles, 4-103	(D1 W1), 2-20
Corrosion inhibitors, 4-117	Е
Crosslinked chitosan membranes,	Ecballium elaterium, 4-108
8-185	
Crosslinked grafted PNIPAM gates,	Effective dissociation constant (pKa), 1-7
2-52	
Crosslinked PNIPAM hydrogel	Emulsification, 3-71
membrane, 4-97	Emulsifier, 3-72
Crosslinker, 4-98	Emulsions, 3-71
Crown ethers, 1-9	Enantiomer, 5-121
Cylindrical capillary tubes, 8-188	Enantiomeric excess (e.e., %), 5-134
	Enantioselective solid membranes, 5-122
D	Enantioseparation, 5-122
Decomplexation ratio, 5-121	Energy dispersive X-ray spectrometer
Diabetes, 1-8	(EDX), 11-247
Diabetes therapy, 9-197	Environmental stimuli-responsive
2,2-Diethoxyacetophenone (DEAP),	channels, 1-2
10-233	Environmental stimuli-responsive
Diffusion coefficient (D), 2-48	controlled-release systems, 3-69
Diffusion driving force, 2-48	Environmental stimuli-responsive smar
Diffusion-enantioselective membranes,	membranes, 1-2
5-122	Environment-responsive membranes,
Diffusion-selective membranes, 5-122	2-20
Diffusional permeability, 2-21	Equilibrium swelling/shrinking states.
Diffusional permeability coefficient (<i>P</i>),	4-103
2-48	Equilibrium volume-change, 4-102
2,2-Dimethoxy-2-phenylacetopheno	Ethylenediamine (EDA), 3-72
ne (BDK), 4-100	Exploding cucumber, 4-108
1-(3-Dimethyl-aminopropyl)-3-ethylc	External stimuli, 1-3
arbodiimide hydrochloride, 9-210	
Disperse phase, 3-83	F
D,L-tryptophan, 5-131	Fick's first law of diffusion, 2-47
Donor side, 2-46	Field Emission Scanning Electron
Drug delivery carriers, 4-103	Microscope (FE-SEM), 11-247
Drug delivery systems (DDS), 3-82	Flat membranes 1-14

Fluorescence intensity, 4-112 Fourier transform infrared (FT-IR), 2-22 Free-radical polymerization, 4-99 Free radicals, 4-100 Freeze-drying, 3-71 G Gating membrane, 2-19 Glucose-responsive gating membranes, 9-197 Glucose-responsive insulin delivery systems, 9-197 Glucose-responsive microcapsule, 9-198 Glucose-responsive self-regulated insulin release systems, 9-197 L Glucose-responsive smart materials, 1-8 Glucose-responsivity, 9-197

Glucose-responsive self-regulated insulin release systems, 9-197 Glucose-responsive smart materials, 1-8 Glucose-responsivity, 9-197 Glucose oxide, 1-8 Glucose oxidase (GOD), 1-8 Glucose sensor, 9-206 Gluconic acid, 1-8, 9-197 Glycidyl methacrylate (GMA), 5-126 Grafted membrane, 2-22 Grafted stimuli-responsive surfaces, 1-15 Grafting yield (*Y*), 2-29, 2-39 Guest molecules, 1-12

H

Hagen-Poiseuille equation, 2-37 Harmful side effects, 4-103 High-speed video camera, 6-150 Hollow microcapsules, 3-70 Homogenizer, 4-109 Homopolymer, 2-22 Host-guest complexes, 1-9, 10-235 Host molecules, 1-12, 5-124 HPLC system, 5-134 Hydraulic permeability, 2-21 Hydrogels, 1-4 Hydrogen bonding, 1-5 Hydrophobic adsorption, 6-145 Hydrophobic-adsorption/hydrophilicdesorption, 6-155 Hydrophilicity, 6-146

Hydrophobicity, 6-146 Hydroxyethylcellulose, 8-188

I Ice-water bath, 4-110 Intelligent materials, 1-3 Interfacial crosslinking reaction, 8-185 Interfacial polymerization, 3-71 Intermolecular complexes, 2-65 Interpenetrating polymer networks (IPNs), 1-5, 2-64 Ion channels, 1-2 Ion-recognition, 1-10 Ion-signal sensing receptor, 1-10

Large-scale production, 12-260
Linear grafted chains, 2-21
Liquid membranes, 5-122
Liquid surface tension, 2-61
Lipophilic drugs, 4-103
Liposomes, 4-108
Lower critical solution temperature
(LCST), 1-4
L-phenylalanine (L-Phe), 5-134

M

Magnetic nanoparticles, 4-103 Magnetic-guided targeting, 11-254 Mass change ratio of membranes, 2-29 Membrane, 1-1 Membrane emulsification, 3-83 Membrane regeneration, 5-121 Mercury intrusion method, 6-150 Methylenebisacrylamide (MBA), 2-65 Micelles, 4-108 Microcapsule membranes, 1-14, 3-2 Microfiltration, 1-1 Microfluidic approach, 8-185 Microfluidic device, 4-109 Microfluidic preparation, 4-109 Microfluidic technique, 4-115 Microforge, 8-188 Microgel-coated gating membrane, 2-20

Microgels, 2-20	0
Micropuller, 8-188	Oil-in-water (O/W) emulsions, 3-71
Molecular recognition, 5-121	Oil-in-water-in-oil (O/W/O) double
Molecular recognition microcapsule,	emulsions, 4-97
10-228	Oil/water (O/W) interface, 4-100
Molecular-recognizable gating membranes,	Oleic acid (OA), 11-242
6-158	On-off switching, 3-70
Molecular-recognizable hydrogel membranes,	Operation pressure, 2-53
10-232	Optical microscope, 4-100
Molecular-recognizable smart materials,	
1-4	P
Molecular-recognizable smart membranes, 10-217	Particle size dispersal coefficient (δ), 3-84
Molecular recognizing receptor, 10-217	1,1,4,7,7-Pentamethyl diethylenetriamine
Molecular-responsive copolymer, 1-10	(PMDTA), 2-29
Mono-6-deoxy-6-ethylene	Permeability, 1-2
diamino- β -CD (ECD), 10-219	Phase transition, 1-4
Monodispersed microcapsules, 3-82	Phenylboronic acid (PBA), 1-8
Monodispersity, 3-84	Photo-initiated polymerization, 4-104
Monomer, 2-22	Photo-initiator, 4-99
Multi-stimuli-responsive membrane gates, 11-242	pH-responsive gating factor of the membrane pore size, 7-174
Multi-stimuli-responsive membrane	pH-responsive gating membrane, 7-169
gates with hierarchical structures,	pH-responsive hydrogel, 7-169
11-256	pH-responsive microcapsules, 8-185
	pH-responsive smart materials, 1-6
N	pH-sensitivity, 8-190
Nanofiltration, 1-1	Plasma-graft pore-filling polymerization,
Nanoparticles, 4-103	2-21
Nano-structured pores, 6-146	Plasma-induced grafting, 2-20
Negatively thermo-responsive gating	Plasma-induced pore-filling graft
characteristics, 2-63	polymerization, 2-21
N-isopropylacrylamide (NIPAM), 1-8	Plasma treatment, 2-21
2-Naphthalenesulfonic acid (NS), 1-12	Pluronic F127, 4-109
2-(<i>N</i> -morpholino)ethanesulfonic acid (MES), 9-200	PMAA-grafted PVDF (PMAA-g-PVDF) membrane, 7-172
<i>N,N</i> -dimethylaminoethyl methacrylate (DM), 7-170	PNIPAM-grafted anodic aluminum oxide (PNIPAM-g-AAO) membranes,
Non-enzyme-based glucose-responsive	2-27
materials, 9-214	PNIPAM-grafted Nylon6 (PNIPAM-
Normal tissues, 4-103	g-Nylon6) membranes, 2-40
NS-recognition gating coefficient,	PNIPAM-grafted PCTE (PNIPAM-g-
10-225	PCTE) membranes, 2-25
Nylon-6 (N6) substrates, 2-40, 2-65	PNIPAM-grafted polyethylene (PNIPAM-
	g-PF) membrane 2-22

PNIPAM-grafted PVDF (PNIPAM-g-	Pressure-tight vessel, 3-83
PVDF) membranes, 2-41	Process-oriented design, 12-260
Poly(acrylamide) (PAAM), 1-5, 2-45	Protein nanoparticles, 4-108
Poly(acrylic acid) (PAAC), 1-6, 2-64	Pulsated release systems, 3-69
Polyamide, 3-72	Pumping effects, 7-169
Polycarbonate track-etched (PCTE)	
membranes, 2-24	R
Polycomplexes, 1-5	Racemates, 5-124
Poly(<i>N</i> , <i>N</i> -dimethylaminoethyl meth	Radiation-induced grafting, 2-20
acrylate) (PDM), 1-7, 7-170	Radio-frequency plasma, 2-22
Polyethylene (PE), 2-22	Receptor side, 2-47
Polyethylene terephthalate (PET) track-	Response kinetics, 4-101
etched membranes, 6-159	Response temperature, 2-62
Polyglycerol polyricinoleate (PGPR),	Reverse osmosis, 1-1
4-99	Rhodamine B (Rd B), 4-100
Poly(glycidyl methacrylate) (PGMA),	~
5-127	S
Poly(N-isopropylacrylamide)	Salting-out effects, 10-234
(PNIPAM), 1-4	Saturation magnetization (M _s), 11-244
Poly(N-isopropylacrylamide-co-	Scanning electron microscope (SEM),
benzo-18-crown-6-acrylamide)	2-251
(poly(NIPAM-co-BCAm)), 10-228	Schiff base, 8-186
Poly(N-isopropylacrylamide-co-glycidyl	Self-healing agents, 4-117 Self-regulated drug delivery, 12-260
methacrylate) (poly(NIPAM-co-GMA),	Self-regulated insulin release systems,
PNG), 5-124	1-8
Poly(methacrylic acid) (PMAA), 1-7,	Shirasu porous glass (SPG), 3-83
7-170	Side-by-side diffusion cell, 2-47
Polymethylsilsesquioxane (GRT-350),	Size distribution, 3-83
4-99	SiO ₂ nano-particles, 6-147
polyoxyethylene (20) sorbitan monooleate	Smart hydrogels, 4-97
(Tween 80), 3-83	Smart materials, 1-3
Polyvinyl alcohol (PVA), 3-83	Smart microcapsules, 3-69
Poly(vinylidene fluoride) (PVDF), 2-39	Smart removers, 12-261
Pore-covering model, 2-20	Smart valves, 1-13
Pore diameter ratio, 2-36	Sodium dodecyl sulfate (SDS), 3-72
Pore-filling model, 2-20	Square capillary tubes, 8-188
Pore-filling ratio (<i>F</i>), 2-35, 2-38	Squirting cucumber, 4-108
Pore size thermo-responsivity ($N_{d,40/25}$),	Stabilizer, 3-83
2-46	Steric hindrance, 5-123
Porous membrane substrates, 1-13, 2-19	Stimuli-responsive controlled-release
Positively thermo-responsive gating	systems, 3-69
characteristics, 2-63	Stimuli-responsive gates, 1-13
Potassium persulfate (KPS), 2-65	Stimuli-responsive polymeric hydrogels,
Pressure-driven convective flow, 2-21	7-170

Thermo-responsive Trojan-horse-like Stimuli-responsive smart hydrogel membranes, 1-15 microcapsules, 4-115 Thermo-sensitivity, 5-121 Stokes-Einstein equation, 2-51, 5-133 Thermostatic stage system, 8-190 Sudan III, 4-105 Thermo-triggered squirting capsule Superhydrophobicity, 6-146 for nanoparticle delivery, 4-108 Superparamagnetic and thermoresponsive microcapsules, 11-241 Time-dependent volume-change, 4-102 Tissue engineering, 12-260 Superparamagnetic Fe₃O₄ nanoparticles, Transmembrane pressures, 3-83 Transmission electron microscope Superparamagnetic porous membrane, (TEM), 11-243 11 - 241Tryptophan enantiomers, 5-131 Surfactant, 3-86 Ultrafiltration, 1-1 Targeted drug delivery, 4-103, 12-260 Ultrasonification, 3-87 Templates, 3-71 Upper critical solution temperature Terephthalaldehyde, 8-185 (UCST), 1-6, 2-64 Terephthaloyl dichloride (TDC), 3-72 UV absorbance measurement, 5-139 Thermogravimetric analysis (TGA), UV-initiated polymerization, 4-98 11-247 UV irradiation, 4-99 Thermo-induced self-bursting release, UV radiation-induced grafting 4-106 polymerization, 2-20 Thermo-induced self-bursting UV-visible spectrophotometer, 6-155 microcapsules, 4-103 Thermo-responsive affinity membrane, 6-146 Venus flytraps, 1-10 Thermo-responsive burst squirting, Vibrating-sample magnetometer (VSM), 11-243 Thermo-responsive factor (R_D) , 2-51 Vitamin B_{12} (VB₁₂), 3-77 Thermo-responsive gates, 11-242 Volume phase transition temperature Thermo-responsive gating coefficient (VPTT), 10-238 (R_J) , 2-43 Thermo-responsive gating membranes, 2 - 19Water flux, 2-36 Thermo-responsive hydrophilic/ Water-in-oil-in-water-in-oil hydrophobic surface wettability, (W/O/W/O) triple emulsions, 4-97 Water treatment, 12-260 Thermo-responsive membranes, 5-121 Wettability, 2-61 Thermo-responsive polymers, 2-19 Thermo-responsive smart materials, X X-ray diffraction (XRD), 11-243 Thermo-responsive squirting X-ray photoelectron spectroscopy microcapsules, 4-108 (XPS), 5-127